

**Postoperative skeletal pain**  
Development of non-opioid treatment  
strategies

Jasper Gerard Steverink

Copyright 2023 © **J.G. Steverink**

The Netherlands. All rights reserved. No parts of this thesis may be reproduced, stored in a retrieval system or transmitted in any form or by any means without permission of the author.

Printing: Gildeprint Enschede, [gildeprint.nl](http://gildeprint.nl)

Cover Design: Jasper Steverink

Layout and design: Eduard Boxem, [persoonlijkproefschrift.nl](http://persoonlijkproefschrift.nl)

# **Postoperative skeletal pain**

## Development of non-opioid treatment strategies

### **Postoperatieve skeletpijn**

Ontwikkeling van opiaatvrije behandelstrategieën  
(met een samenvatting in het Nederlands)

Proefschrift

ter verkrijging van de graad van doctor aan de Universiteit Utrecht op gezag van de rector magnificus, prof.dr. H.R.B.M. Kummeling, ingevolge het besluit van het college voor promoties in het openbaar te verdedigen op

woensdag 19 april 2023 des middags te 4.15 uur

door

Jasper Gerard Steverink

geboren op 26 oktober 1993 te Zwijndrecht

Promotoren:

Prof. dr. J. Malda

Prof. dr. J.J. Verlaan

Copromotor:

Dr. S. Piluso

Beoordelingscommissie:

Prof. dr. P.A.J.T. Robe

Prof. dr. M.R. van Dijk (voorzitter)

Prof. dr. R.M. Schiffelers

Prof. dr. A. Dahan

Prof. dr. F.C. Oner

Dit proefschrift werd (mede) mogelijk gemaakt met financiële steun van SentryX B.V.

## TABLE OF CONTENTS

<b>General Introduction</b>	7
<b>Part I. The origins and severity of postoperative skeletal pain</b>	
Chapter 1 Balancing postoperative pain relief with the risk of developing ORADEs in patients undergoing major spine surgery	22
Chapter 2 Sensory innervation of human bone: an immunohistochemical study to further understand bone pain	36
Chapter 3 An Understanding of Bone Pain: A Narrative Review	58
<b>Part II. Bupivacaine for musculoskeletal applications</b>	
Chapter 4 Comparison of <i>in vitro</i> and <i>in vivo</i> toxicity of bupivacaine in musculoskeletal applications	76
Chapter 5 Lack of concentration-dependent local toxicity of highly concentrated (5%) versus conventional 0.5% bupivacaine following musculoskeletal surgery in a rat model	90
Chapter 6 Exploratory study into the <i>ex vivo</i> conduction properties and local anesthetic susceptibility of nervous tissues	108
<b>Part III. Robust hydrogel formulation for sustained local release of bupivacaine</b>	
Chapter 7 Robust gelatin hydrogels for local sustained release of bupivacaine following spinal surgery	126
Chapter 8 Testing a new sustained-release local anesthetic formulation specifically designed for spine surgery in a sheep model	160
Chapter 9 Preclinical safety and feasibility of a bupivacaine-loaded hydrogel for drug delivery in spinal surgery	182
<b>Part IV. Directions for clinical application</b>	
Chapter 10 Designing a phase Ib clinical trial to assess the safety and preliminary efficacy of a robust hydrogel for sustained bupivacaine release in patients undergoing instrumented spine surgery	206
<b>Summary, General Discussion and Summary in Dutch</b>	
Summary	226
General Discussion	230
Nederlandse Samenvatting	244
<b>References</b>	250
<b>List of Publications, Manuscripts, Acknowledgements and Curriculum Vitae</b>	
List of Publications and Manuscripts	274
Acknowledgements - Dankwoord	276
Curriculum Vitae	279



## GENERAL INTRODUCTION

### Nociception and pain

Every day, thousands of surgical interventions are performed worldwide. Almost all of the patients undergoing these surgeries will experience some degree of postoperative pain.<sup>1,2</sup> Despite everyone knowing what pain is, it can be difficult to describe, quantify and / or standardize pain. Pain is defined by the International Association for the Study of Pain (IASP) as "An unpleasant sensory and emotional experience associated with, or resembling that associated with, actual or potential tissue damage".<sup>3</sup> Nociception on the other hand, is defined as "the neural process of encoding noxious stimuli".<sup>3</sup> These stimuli are picked up by a nociceptor, which is a high-threshold sensory receptor located in the peripheral somatosensory nervous system. The noxious stimulus is converted to an action potential, which is conducted by sensory nerve fibers towards the dorsal horn in the spinal cord. Nociceptive signals are sent towards the thalamus and subsequently to the sensory cortex, undergoing modulation throughout the central nervous system. Modulation serves as the translation from a noxious stimulus to pain. It incorporates the social, biological and psychological factors that influence pain perception.<sup>3,4</sup> Upon arrival of the modulated noxious stimulus in the sensory cortex, patients experience pain and may change or adjust their behavior accordingly. The IASP further states that pain is a personal experience and is influenced by social, biological and psychological factors, and that pain is different to nociception. Although pain usually serves an adaptive role, it may have adverse effects on function and social and psychological well-being of the patient. If a patient were to fracture a bone, loading that bone would *increase* the pain experienced. Increased pain will then lead to the patient *decreasing* the load on the affected bone, decreasing pain and accelerating the regenerative process. Pain is thus part of a negative feedback loop and has an important protective function.

Notwithstanding the difficulties in quantifying pain, it is generally accepted that pain negatively affects the perceived quality of life through multiple mechanisms. This also holds true for postoperative pain.<sup>5</sup> To a certain degree, postoperative pain can be useful to guide a patient's level of activity, but unbearable postoperative pain serves no physiological role and can slow the recovery process. Early ambulation after orthopedic surgery is linked to better postoperative outcomes.<sup>6</sup> However, both severe postoperative pain and excessive analgesic treatment, leading to drowsiness or motor-blocks that accompany sensory blocks, can inhibit early ambulation.<sup>7</sup> In addition, severe acute postoperative pain can precede the development of chronic pain through a series of neuroplastic and maladaptive processes, clouding the adequate perception of future pain.<sup>8,9</sup> Taken together, it would be desirable to *control*, rather than *eliminate*, acute

postoperative pain. However, safe and effective postoperative pain management remains challenging.<sup>10</sup>

### **Postoperative analgesia: A contemporary clinical challenge**

Postoperative pain management is a major determinant of surgical outcomes and patient satisfaction.<sup>11</sup> Patients experiencing insufficiently controlled postoperative pain take longer to start mobilizing after surgery and are discharged home later. Furthermore, they are more likely to develop complications such as decubitus and respiratory/urinary tract infections. In general, patients with insufficiently controlled postoperative pain are less satisfied with surgical treatment, negatively influencing their perceived quality of life. In contrast, optimal analgesia following skeletal surgery can lead to an early discharge home.<sup>6,7</sup> These patients have lower risks of developing complications after interventions. Skeletal surgery, and spine surgery in particular, ranks amongst the most painful interventions overall. In fact, three out of the seven most painful surgical interventions are performed on the spinal column.<sup>12</sup> In the aging population, the prevalence of degenerative spine disease grows concomitantly. Therefore, instrumented spinal surgery is a frequently and increasingly performed procedure.<sup>13</sup> In the United States alone, 450.000 procedures are performed annually.<sup>14</sup> Severe postoperative pain is reported by nearly all patients, leading to a large population whose perceived quality of life is at risk.<sup>15,16</sup> Moreover, the severity of acute pain is one of the major predictors for the development of chronic pain.<sup>9</sup> The reason why skeletal surgery is so painful remains unclear. Exploratory animal experiments point towards the characteristics of bone innervation as potential explanation, revealing a high density of sensory nerve fibers in skeletal tissues.<sup>17–20</sup> More specifically, subanalysis was performed in bone marrow, cortical bone and periosteum, a thin layer of tough connective tissue enveloping bone. As the highest innervation density was found in the periosteum, it might be a major contributor to postoperative pain. The periosteum has important mechanosensory functions to detect bone loading.<sup>21</sup> In the example of a fractured bone, the periosteum would experience excessive stretching following fractured bone loading, leading to nociception that urges the patient to decrease the load on the affected bone. Conversely, it could also be an attractive new target for analgesic therapies, as it is easily accessible during surgery.

Currently, postoperative skeletal pain is treated using a multimodal analgesic regime that includes non-steroidal anti-inflammatory drugs and acetaminophen, but mostly relies on potent opioids. Opioids are effective analgesic drugs, but come with serious potential side effects. The balance between analgesic effect and side effects in patients undergoing spine surgery has not been studied. However, it is important to understand the benefits and costs of opioid use in spine surgery, as the use of opioids has considerable impact not only on the individual patient, but also on hospitals and society.



## Opioid Crisis

Opioids have been used for the treatment of pain since the beginning of history, when the opium poppy plant (*Papaver somniferum*) was cultivated in Mesopotamia around 3400 BC. Its sap was named opion by the ancient Greeks, from which opium and opioids now derive their name. In 1805, the principal alkaloid in opium was isolated by Friedrich Sertürner. He named it morphium (now morphine), after the Greek god of dreams Morpheus.<sup>22</sup> Hippocrates recognized the analgesic potential of opium, but was also convinced that it should be used sparingly.<sup>23</sup> Indeed, the analgesic effect of opioids is undisputed, but so are their side effects.<sup>24</sup> Common opioid-related adverse drug events (ORADEs) are decreased consciousness (*somniferum* translates to 'bringing sleep'), nausea, dizziness, reduction of gastrointestinal motility and ileus, respiratory suppression and, in the longer term, dependence and addiction. These side effects, in turn, can delay mobilization after surgery and prolong the time to discharge, mirroring the adverse events due to postoperative pain.<sup>24</sup> Synthetic opioid use as analgesics has been increasing since the 1990's.<sup>25</sup> Due to large-scale marketing campaigns, opioids became more easily accessible, were prescribed more frequently and large numbers of patients started using (and misusing) opioids for acute and chronic pain relief.<sup>26,27</sup> The damaging addictive potential of opioids only became evident later. In the year 2019 almost 50.000 Americans died from opioid overdose, and 1.7 million suffered from prescription opioid-substance use disorders. Opioid-related deaths have increased over 400% since 1999.<sup>28</sup> It is estimated that one in four patients on prescribed opioids for chronic pain misuses opioids, and one in ten develops an opioid use disorder.<sup>29</sup> Alarmingly, approximately one in twenty people misusing opioids starts using heroin, and, conversely, the majority of people using heroin first misused prescription opioids.<sup>30,31</sup>

The risk of developing ORADEs is especially relevant for patients suffering from musculoskeletal disease, as orthopedic surgeons are amongst the caregivers who most frequently prescribe opioids. Despite opioid use, the majority of patients still experiences insufficiently controlled postoperative pain.<sup>1,2</sup> However, simply increasing the dose is not always an option. A delicate balance between analgesia and side effects seems present in modern-day multimodal analgesic regimens.<sup>32</sup> The substance that provides analgesia is the same that induces harmful effects at higher doses. As Paracelsus put it: '*Sola dosis facit venenum*'.<sup>33</sup> The addictive potential and high incidence of ORADEs after opioid use, combined with insufficient pain relief demonstrate a clear unmet clinical need for better analgesic treatment with an improved balance between analgesic effects and side effects.

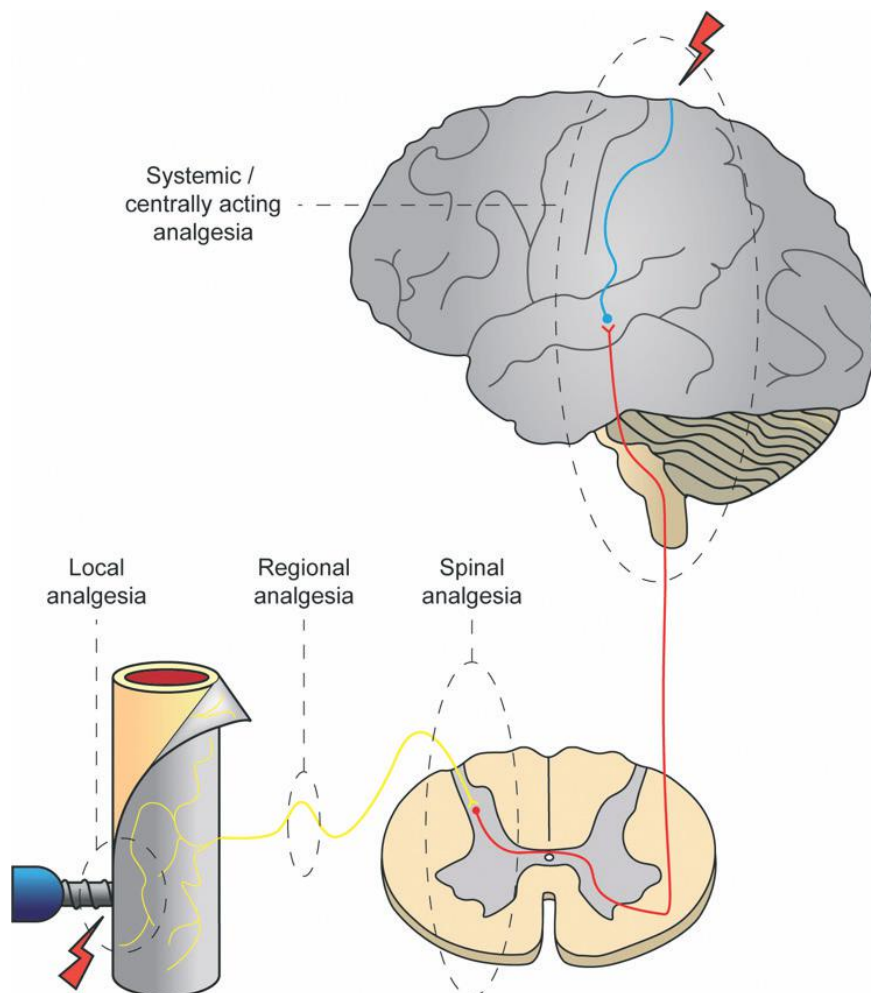


**Figure 1.** Nociceptive signal conduction and targets for analgesia.

### Reducing opioid consumption

Opioids act at the level of the central nervous system, which they reach directly through intrathecal administration or *via* the circulation after oral or parenteral administration. However, the circulation distributes opioids *systemically*. As opioid receptors are also present in other anatomical locations, *e.g.*, the gastrointestinal tract, ORADEs, including constipation and ileus occur. Opioid receptors in brain regions involved in breathing explain respiratory depression as side effect of opioids. The nociceptive pathway provides several targets for signal inhibition or modulation beyond opioid receptors. Locoregional analgesic treatment acts on the nerves that conduct nociceptive signals to the central

nervous system. Its use could prevent the occurrence of serious systemic side effects without compromising on analgesic efficacy.

Local anesthetics, such as lidocaine and bupivacaine are increasingly being used to speed up recovery after various orthopedic interventions, such as total knee replacement. Moreover, a number of exploratory studies have applied local anesthetics directly onto the previously discussed periosteum, with favorable results.<sup>34,35</sup> Their well-known safety profile makes local anesthetics attractive candidates for use in postoperative analgesic treatment. However, their duration of effect is relatively short (up to eight hours for bupivacaine) in relation to the multiple days of severe pain after musculoskeletal surgery.<sup>16,36</sup> The challenge is therefore to extend the duration of effect of current local anesthetics. In an effort to extend pain relief after surgery, continuous wound infusion (CWI) has been tested in a variety of interventions.<sup>37</sup> This technique employs a cannula dwelling in the surgical wound, over which local anesthetics are continually infused. Despite the practical downsides of a patient being continuously connected to a cannula and external pump, and uncertainties about the increased risk of infection, the efficacy of CWI shows that sustained presence of local anesthetics in the surgical site can improve the postoperative pain experience.

To obtain sustained local drug levels without the use of an externally connected cannula, various drug delivery formulations incorporating local anesthetics have been developed in the past decade (figure 2).<sup>38</sup>

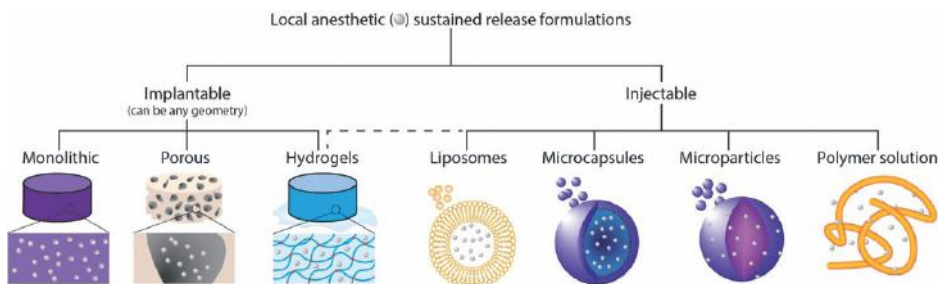


**Figure 2.** Variety of local anesthetic sustained release formulations. The formulations are split up into injectables and implantables. Drug molecules are represented by the small silver spheres.

Bupivacaine is most frequently selected as the active agent in such formulations, as it has the longest duration of action of all amide-type local anesthetics. Examples of sustained delivery formulations include injectables, such as hydrogels, polymer solutions, liposome emulsions and microparticle or -capsule suspensions. In addition, multiple implantable formulations have been developed, which can vary greatly in shape and size, including

monolithic synthetic polymer constructs, porous collagen meshes and hydrogels.<sup>39–42</sup> For example, liposomal bupivacaine, (Exparel, Pacira) which obtained FDA approval for single-dose infiltration to produce postsurgical local analgesia, has been tested for various interventions including hemorrhoidectomy, inguinal hernia repair, bunionectomy and total knee arthroplasty.<sup>43–45</sup> Additionally, a collagen mesh loaded with bupivacaine for use in incisional wounds (Xaracoll, Innocoll) has been approved for use in open inguinal hernia repair by the FDA.<sup>46</sup> Each of these formulations suffers from its own shortcomings; solutions and dispersions of local anesthetics can leak from wounds, or can be rapidly absorbed and diffuse away in multiple directions from the target site. Liposomes readily fuse with cell membranes, which might explain the limited duration of effect of liposomal bupivacaine. In clinical practice, the duration of analgesic effects is limited to 24 hours and the effectiveness of liposome formulations has not been demonstrated in spinal surgery.<sup>47</sup> Macroscopic implants can interfere with wound healing when interposed between tissues, are prone to fibrous encapsulation, and leave debris at the surgical site that can persist for months.<sup>41</sup> Moreover, all formulations encapsulate bupivacaine at concentrations higher than clinically used. The local tissue effects of such concentrations have not extensively been studied. The main challenge is to find a solution that locally releases local anesthetics and stays at the target site for a clinically relevant duration, after which it is absorbed by the body.

Clearance from the surgical site can be influenced by selecting an appropriate biodegradable material in the delivery formulation. Biodegradability is an important requirement, as later surgical removal of the formulation following drug release is undesirable. In addition, extensive degradation time leads to accumulation of degradation products at the implantation site.<sup>41</sup> Degradation rates vary greatly between materials. Biopolymers, such as chitosan, hyaluronic acid and gelatin are derived from natural sources and are generally well-tolerated and degraded by the body. Synthetic polymers, such as polycaprolactone and poly-lactic-co-glycolic acid, have the advantage that they can be synthesized in a highly controlled fashion. However, application of synthetic polymers for local anesthetic release can lead to toxic tissue effects or extensive host reactions.<sup>41,48</sup> Moreover, synthetic polymers degrade at a much slower rate in the body, if degradable at all.<sup>49</sup> Examples of formulations constructed from polymers are microspheres, monolithic macroscopic implants, injectable liquid polymers and hydrogels.<sup>42</sup> The versatility and tunability of hydrogels makes them attractive candidates for use in drug delivery.

### **Hydrogels for drug delivery**

Hydrogels are three-dimensional hydrophilic polymer networks that are chemically or physically crosslinked, and provide a means for spatial and temporal control over the release of various therapeutic agents.<sup>50–52</sup> They can be formed in almost any size

and shape. An important feature of hydrogels is the high water-absorption capacity which allows water-soluble drug loading. Desirable features for local anesthetic delivery formulations, such as hydrogels, include a simple method of administration, a favorable ratio of sensory and motor blockade, a prolonged duration of action, absence of (or extremely low) systemic toxicity, acceptable local tissue response and biodegradability.<sup>42</sup> A specific requirement for effective application in musculoskeletal applications (*e.g.*, in orthopedic/trauma surgery) is a high degree of mechanical robustness to be able to withstand co-implantation with metallic implants. To fulfil these requirements, both the material choice and cross-link chemistry used are important. Selecting the right combination of materials and cross-linking agents allows tuning of drug release rates, hydrogel mechanical properties, degradation rates, and determines the chemicals that can leach from the hydrogel. Moreover, varying cross-link density and polymer concentration allows tuning of mechanical and drug-releasing properties.<sup>53</sup>

Increased cross-link density or polymer concentration both decrease the mesh size of the hydrogel, which is the linear distance between two adjacent cross-links. The mesh size can, based on its size relative to the therapeutic agent, lead to steric hindrance in diffusion processes. This way, drug release rates can be influenced. When the therapeutic agent is larger than the mesh size, it relies on the hydrogel's swelling or degradation of the matrix for its release.<sup>53</sup> Conversely, smaller mesh sizes inhibit influx of degrading enzymes into the hydrogel, slowing down the hydrogel degradation rate. Hydrogels can be administered to the target site *via* injection, or implantation. Their tunability, degradability, and biocompatibility make hydrogels attractive for use as local anesthetic delivery formulation. However, considerable mechanical resilience is required for successful application in the orthopedic/trauma environment, where large forces and non-yielding materials are at play. As of yet, no hydrogels that are robust, biocompatible and biodegradable are available for use as a local anesthetic delivery formulation.

### **Aims and thesis outline**

The goal of the work included in this thesis is to gain insight in the severity and etiology of bone pain, and to develop a novel solution for the improved management of pain following skeletal surgery. Its specific aims are:

- 1) to understand the origins and severity of postoperative skeletal pain;
- 2) to assess the safety of a local anesthetic (bupivacaine) when applied in high concentrations in tissues of interest;
- 3) to develop a clinically relevant hydrogel formulation for sustained local release of bupivacaine for use in musculoskeletal surgery; and

4) to provide directions for clinical trials, assessing safety and feasibility of the hydrogel for sustained local release of bupivacaine.

The relation of the various chapters in this thesis to the research aims, and the research questions they try to answer are described in more detail below. Chapters 1, 2 and 3 correspond to specific research aim 1: to understand the origins and severity of (postoperative) bone pain.

In *Chapter 1*, pain experienced and opioids consumed by patients following instrumented spinal surgery are studied in a retrospective cohort design. The balance between beneficial and side effects of opioids is critically assessed, to answer the question:

*What is the prevalence and severity of postoperative pain, consumption of opioids and occurrence of opioid-related side effects in a spine surgery patient cohort?*

*Chapter 2* aims to better understand the severity of bone pain via immunohistochemical analysis of the sensory innervation of human bone. Fiber types and density, as well as the effect of sex and age were studied for each bone location and compartment, providing an answer to the questions:

*Can bone innervation density provide an explanation of the severity of bone pain? How are nerve fibers distributed across the various bone compartments?*

*Chapter 3* reviews the etiology and underlying pathways leading to the sensation of bone pain. Four mechanistic causes of bone pain are identified and suggestions for future targets to alleviate bone pain are provided, to form an answer to:

*What are the main underlying pathways leading to the sensation of bone pain?*

Chapters 4, 5 and 6 provide insight in specific aim 2: To assess the safety and efficacy of bupivacaine when applied in high concentrations in musculoskeletal tissues.

In *Chapter 4*, the toxic effect of bupivacaine in musculoskeletal applications is reviewed from multiple perspectives on the translational path. The effects of clinically used concentrations of bupivacaine on relevant tissues are appraised from *in vitro* experiments, via animal testing, to clinical situations. A paucity of literature on toxic effects of bupivacaine concentrations higher than used clinically is identified.

*What are the effects of bupivacaine on musculoskeletal tissue types, and how do in vitro toxic effects translate to clinical findings?*

In *Chapter 5*, the *in vivo* toxicity of bupivacaine at increasing concentrations is tested in a rat model for skeletal surgery and compared to the clinically used bupivacaine solution. Histological assessment of the administration site is performed to answer the question:

*What are the local tissue effects of high bupivacaine concentrations when applied in instrumented skeletal surgery?*

*Chapter 6* explores the concentrations of local anesthetics needed to obtain analgesia at the surgical site. Freshly excised human and ovine nervous tissue was placed in an electrophysiological setup able to generate action potentials in the sensory nerve fibers. Local anesthetics were then applied in increasing concentrations to achieve action potential amplitude reduction or extinction, raising the question:

*Which concentration of local anesthetic is needed to obtain analgesia at the musculoskeletal surgical site?*

Chapters 7, 8 and 9 correspond to specific aim 3: to develop a clinically relevant hydrogel formulation for sustained local release of bupivacaine.

In *Chapter 7*, the development of a robust hydrogel for sustained local release of bupivacaine for use in instrumented spinal surgery is described. Its feasibility as a drug delivery formulation for orthopedic applications is assessed and optimized *in vitro*. This chapter studies the research questions:

*What are requirements for feasible application of a bupivacaine sustained delivery hydrogel formulation in spinal surgery? Does the hydrogel fulfill these requirements in vitro?*

In *Chapter 8*, the hydrogel developed in *Chapter 7* is applied in a sheep model for instrumented spinal surgery. The *in vivo* mechanical performance and rate of drug release of the hydrogel, as well as wound and plasma drug levels resulting from drug release are quantified. Moreover, the *in vivo* degradation of hydrogels and subsequent local foreign body response is studied. This chapter provides an answer to:

*Does the previously developed hydrogel formulation provide sustained release of bupivacaine in vivo? Are the hydrogel and incorporated drug dose safe, and is the hydrogel biodegradable?*

*Chapter 9* describes the toxicological assessment of the bupivacaine sustained release hydrogel formulation in sheep as developed in *Chapter 7* and tested in *Chapter 8*, according to Good Laboratory Practice (GLP) guidelines. Following a 6- or 56-day follow-up, histological analysis of implant sites containing a clinical control (screw-only), placebo (screw and hydrogel) and treatment (screw and bupivacaine-loaded hydrogel) was performed. Pharmacokinetic properties of the hydrogel formulation were compared to reference use of bupivacaine hydrochloride infiltration. This study provides insight in the local tissue response elicited by the hydrogel material and the drug-loaded hydrogel in comparison to the clinical reference situation.

*What are the local and systemic toxicological effects of the bupivacaine sustained release hydrogel formulation compared to the clinical reference situation of screw implantation?*

*Chapter 10* addresses specific aim 4: To provide directions for clinical trials, assessing safety and feasibility of the hydrogel for sustained local release of bupivacaine. The chapter consists of a clinical trial protocol for a phase 1B study, which will answer the research question:

*What are the safety and preliminary efficacy of the bupivacaine-loaded hydrogel in the spine surgery target population?*



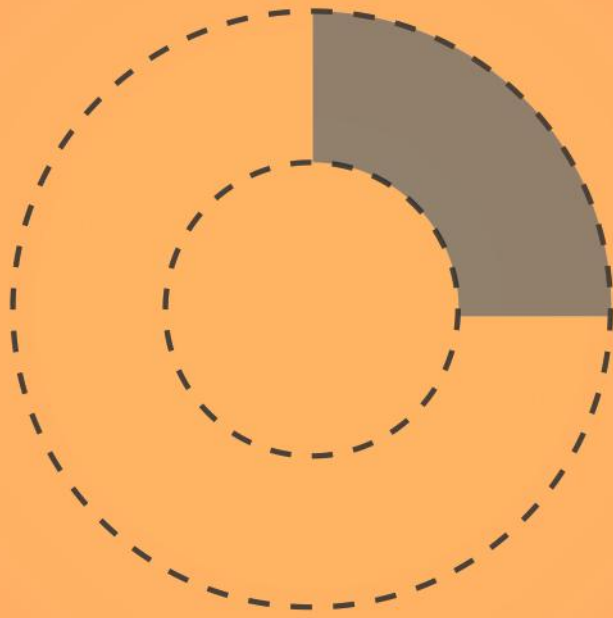




# PART I



The origins and severity of  
postoperative skeletal pain



# CHAPTER 1

## Balancing postoperative pain relief with the risk of developing ORADEs in patients undergoing major spine surgery

D. Oostinga, J.G. Steverink, J.F.M. van Dijk, A.J.M. van Wijck, J.J. Verlaan

*Submitted*

## ABSTRACT

**Study design:** Ambispective cohort study

**Objectives:** Patients undergoing major spine surgery often experience severe postoperative pain, which negatively affects postoperative recovery. Although opioids are effective in reducing postoperative pain, opioid-related adverse drug events (ORADEs) are common and have been associated with worse patient outcomes. The objective of this study was to report on daily practice regarding postoperative pain severity, and opioid use with its potential side effects after surgical stabilization of the spine.

**Methods:** An ambispective cohort study was conducted, including a single-center subcohort of patients enrolled in the Pain Out Study (NCT02083835), undergoing surgical stabilization of the spine. Indications for surgery included spinal trauma, metastatic spinal disease or degenerative spinal disease. Demographic data, surgical details, and preoperative analgesics use were prospectively collected as Pain Out study data. Pain scores, postoperative analgesics use, the incidence of ORADEs, and patient outcomes were retrospectively collected from electronic medical records. Opioid dosages were converted into oral morphine milligram equivalents (MME). ORADEs were classified as mild, moderate, or severe based on potential harm for patients.

**Results:** A total of 64 patients were included for analysis. All patients required opioids during hospitalization, and the median postoperative opioid use was 73.50 oral MME per 24 hours (IQR, 37.5-140.25). On the first postoperative day patients reported pain scores of NRS 5 in rest (IQR, 3-6) and NRS 6.5 with movement (IQR, 5-8). During hospitalization, 60 patients (93.8%) developed adverse events most likely caused by opioid use. Thirty-six patients (56.3%) developed mild ORADEs (e.g. constipation), 50 patients (78.1%) developed moderate ORADEs (e.g. confusion), and 17 patients (28.3%) developed severe ORADEs (e.g. acute respiratory depression). The median time needed before independent mobilization was 48 hours (IQR, 24-72), and the median length of hospital stay was 7 days (IQR, 4-9).

**Conclusions:** Patients who undergo major spine surgery experience moderate to severe postoperative pain and use high doses of opioids and various other analgesics. The high incidence of postoperative ORADEs illustrates the delicate balance between sufficient pain relief and risk of developing ORADEs. Implementation of opioid-sparing strategies and opioid-replacing techniques might aid in improving postoperative recovery.

## 1. INTRODUCTION

The prevalence of musculoskeletal diseases is increasing, with low back problems as the leading cause of disabled life years<sup>54</sup>. Spinal diseases and trauma can lead to spinal instability, spinal cord or cauda equina compression, and neurological deficits, often necessitating surgical intervention<sup>55,56</sup>. Although spinal stabilization (sometimes combined with decompression of neural tissues) can be a successful treatment for spinal injury or disease, patients frequently report severe and difficult to control postoperative pain, despite state of the art analgesic therapy<sup>12,57</sup>. Moreover, postoperative pain is associated with delayed postoperative ambulation, prolonged hospitalization, development of chronic postoperative pain, decreased quality of life, and increased risks of pulmonary, cardiac, gastrointestinal and renal complications<sup>9,11,15,58-63</sup>. In fact, the combination of severe postoperative pain and spine surgery is a major predictor for the development of chronic postoperative pain<sup>64</sup>. Adequate pain management is therefore imperative in the postoperative care following major spine surgery.

Currently, opioids fulfill a central role in multimodal pain treatment protocols following major spine surgery. Although these analgesics are effective in reducing acute postoperative pain, its utilization might induce potentially harmful opioid-related adverse drug events (ORADEs). The severity of ORADEs ranges from mild pruritus to acute respiratory depression requiring antidote administration<sup>65-74</sup>. Patients suffering from ORADEs have higher risks of prolonged postoperative recovery and hospital stay, as well as higher rates of 30-day readmission and inpatient mortality<sup>24,75,76</sup>. In addition, preoperative use of opioids increases the risk for developing ORADEs after surgery<sup>76,77</sup>. The high occurrence rates of ORADEs following orthopedic surgery puts many patients at risk of prolonged recovery and mortality<sup>78</sup>. In The Netherlands, opioid prescription increased 24% from 2013 to 2017, and is believed to increase further in the coming years<sup>79</sup>. The expanded prescription of opioids has led to a simultaneous increase in the number of opioid overdose hospital admissions, addictions, and overdose deaths<sup>79</sup>. In the United States, increased opioid prescriptions created an epidemic of opioid misuse and opioid-related deaths<sup>80-83</sup>. These examples illustrate the growing medical and societal concerns regarding hospital-based opioid use<sup>84</sup>.

The objective of this study was to report on daily practice regarding postoperative pain severity, and opioid use with its potential side effects after surgical stabilization of the spine. This study might provide insights in the trade-off between sufficient postoperative pain relief and the risk of developing ORADEs; a dilemma that patients and their surgeons are facing in daily medical practice.

## **2. METHODS**

### **2.1 Patient population**

This ambispective study was conducted at a single tertiary spine center. A subcohort of eligible patients was included from the Pain Out study, a European project aiming to improve the quality of postoperative pain management after surgery (clinicaltrials.gov; NCT02083835). The original follow-up of only one day postoperatively from the Pain-Out study was extended to include the entire duration of hospital stay by review of patient records. Adult patients who suffered from spinal trauma, metastatic spinal disease or degenerative spinal disease requiring surgical stabilization of the spine were considered eligible. Inclusion of patients in the Pain Out study and this study was performed between January 2018 and March 2019. During this period, surgical stabilization of the spine was performed, and patients were subsequently hospitalized in the ward where the Pain Out questionnaire was presented. If patients were unable to fill out the questionnaire independently (e.g., due to severe illness), they were not considered eligible for inclusion. Additional data (as described in the next section) were retrospectively collected between August 2019 and November 2019. The local institutional ethical review board approved the research protocol (number 17/253) and all patients provided written informed consent.

### **2.2 Data collection**

Prospectively collected data for the Pain Out study database, including demographics, surgical indication, surgical details and preoperative analgesics consumption, were used in this study. Intraoperative analgesics administration, pain scores, postoperative analgesics use, the incidence of ORADEs, and patient outcomes including length of hospital stay and time to mobilization were retrospectively collected from electronic medical records. Retrospective data were retrieved for the duration of hospital stay starting at the day of surgery (annotated as day 0). As follow-up data beyond the first postoperative day required access to patient records, only the portion of patients from the Pain-OUT study treated in our tertiary center was included.

### **2.3 Pain scores**

Pain severity was quantified using the numeric rating scale (NRS), which is an eleven-point scale for patient self-reporting of pain in rest and with movement (0 indicates no pain, 10 indicates worst imaginable pain)<sup>85,86</sup>. Pain scores were collected and recorded in electronic medical files on a daily basis by the nursing staff during clinical rounds.

### **2.4 Pain treatment protocol**

All patients received a multimodal pain treatment regime postoperatively based on the World Health Organization analgesic ladder and local institutional guidelines<sup>87</sup>.



This protocol included a PCA pump with opioids (e.g. morphine) if necessary, oral (e.g. oxycodone) or transdermal opioids (e.g. fentanyl patch), a non-steroid anti-inflammatory drug (NSAID) (e.g. celecoxib), and acetaminophen. Additional dosages of opioids (e.g., the amount of bolus on PCA) were either prescribed by the APS (Acute Pain Service) team, or the treating physician. Oral and transdermal opioids were not prescribed when patients were using a PCA pump. After discontinuation of the PCA pump patients were rotated to oral or transdermal opioids. In the case of neuropathic pain, patients were also prescribed antidepressants (e.g., amitriptyline) or anticonvulsants (e.g., gabapentin). Furthermore, NMDA-receptor antagonists (e.g., esketamine) and invasive analgesia techniques (e.g., epidural analgesia) were applied when high levels of postoperative pain were anticipated, or if pain was insufficiently managed. When patients reported pain scores of NRS  $\geq 4$ , the analgesic dosage was increased or a more potent type of analgesic prescribed (i.e., a PCA pump with IV morphine instead of oral oxycodone) after consultation of a physician or a nurse practitioner. If patients considered pain to be bearable, regardless of pain score, no changes in pain treatment regimens were made.

### **2.5 Oral morphine milligram equivalents**

Opioid doses were converted into oral morphine milligram equivalents (MME) to calculate a comparable daily median dosage for each patient. The following conversion factors were used: oral oxycodone (mg)\*1.5; IV morphine/piritramide/oxycodone (mg)\*3; IV sufentanil ( $\mu\text{g}$ )\*1000; fentanyl skin patch ( $\mu\text{g}$ )\*2.5<sup>88</sup>.

### **2.6 Opioid-related adverse drug events**

ORADEs were defined as the occurrence of adverse events most likely caused by opioid use<sup>78</sup>. ORADEs were classified as mild, moderate, or severe based on potential harm for patients as previously described<sup>24</sup>. Mild ORADEs included constipation and pruritis. Moderate ORADEs included nausea, accidental fall, confusion, and urinary retention. Severe ORADEs included sedation, acute respiratory depression (including the need for antidote administration), and severe gastro-intestinal adverse events (e.g., ileus).

### **2.7 Statistical analysis**

Given the descriptive goal of this study, mainly descriptive statistics were used (mean and standard deviation (SD) or median and interquartile range (IQR) for continuous variables, absolute number and frequency for categorical variables). Data were assessed for normality by eye and Shapiro-Wilk testing. The Spearman's rank-order correlation coefficient was calculated to assess the relationship between opioid use and the development of ORADEs. Kruskal-Wallis testing was used to assess subgroup differences between indication groups. The percent change in pain scores between postoperative day one and the day of discharge was calculated. No missing data were observed. The sample

size was not precalculated; all eligible patients during the study period were included. A p-value <0.05 was considered significant. Statistical analyses were performed using IBM SPSS statistics version 26.0 (IBM Corporation, Armonk, NY, USA) and RStudio version 1.2.5033 (RStudio Inc., Boston, MA, USA).

### 3. RESULTS

#### 3.1 Demographics and surgical details

A total of 64 patients who underwent surgical stabilization of the spine were included for analysis. Baseline characteristics of the study population are listed in Table 1. The mean age was 54.5 years (SD±16.5), and 34 patients were female (53.1%). Most patients had a degenerative condition (n=25 (39.1%)) requiring spinal stabilization, followed by patients who suffered from traumatic injury (n=21 (32.8%)), and patients suffering from metastatic spinal disease (n=18 (28.1%)). Thirty-one patients (48.4%) used opioids preoperatively. This group included 10 patients (32.3%) with a degenerative condition, 10 trauma patients (32.3%), and 11 patients (35.4%) with metastatic spinal disease.

Surgical stabilization of the spine was performed with an open posterior approach in 39 patients (60.9%) and a percutaneous posterior approach in 25 patients (39.1%). Surgery on the thoracolumbar spine was most often performed (n=20 (31.3%)), and in most patients (n=22 (34.4%)) four spinal levels were bridged. The mean total operating time was 189.8 minutes (SD±101.9), and the mean intraoperative blood loss was 367.3 milliliters (SD±412.7). Intraoperatively, a median of 72.5 oral MME (IQR, 55.6-105) were administered.

**Table 1.** Baseline values. SD, standard deviation; BMI, body-mass index; VBS, vertebral body stenting; NRS, numeric rating scale.

Characteristic	Value
<b>Age at surgery, mean (±SD) (years)</b>	54.5 (±16.5)
<b>Gender, n (%)</b>	
Female	34 (53.1%)
<b>BMI, mean (±SD) (kg/m<sup>2</sup>)</b>	26.5 (±5.1)
<b>Surgical indication, n (%)</b>	
Trauma	21 (32.8%)
Degenerative	25 (39.1%)
Metastatic	18 (28.1%)
<b>Surgical treatment, n (%)</b>	
Open fixation	10 (15.6%)

**Table 1.** Continued.

<b>Characteristic</b>	<b>Value</b>
Open refixation	11 (17.2%)
Open fixation + decompression	18 (28.1%)
Open fixation + VBS	3 (4.7%)
Percutaneous fixation	10 (15.6%)
Percutaneous fixation + VBS	12 (18.8%)
<b>Treated level, n (%)</b>	
Cervical	4 (6.3%)
Cervicothoracic	5 (7.8%)
Thoracic	13 (20.3%)
Thoracolumbar	20 (31.3%)
Lumbar	15 (23.4%)
Lumbosacral	3 (4.7%)
Thoracolumbosacral	4 (6.3%)
<b>Pedicle screws, n (%)</b>	
2	1 (1.6%)
4	22 (34.4%)
6	5 (7.8%)
8	22 (34.4%)
10	5 (7.8%)
12	4 (6.3%)
>12	5 (7.8%)
<b>Instrumented vertebrae, n (%)</b>	
1	1 (1.6%)
2	21 (32.8%)
3	5 (7.8%)
4	22 (34.4%)
5	5 (7.8%)
6	5 (7.8%)
>6	5 (7.8%)
<b>Operating time, mean (<math>\pm</math>SD) (min)</b>	189.8 ( $\pm$ 101.9)
<b>Intraoperative blood loss, mean (<math>\pm</math>SD) (mL)</b>	367.3 ( $\pm$ 412.7)

### 3.2 Pain scores, opioid use and ORADEs

On the first day after surgery patients reported median pain scores of NRS 5 in rest (IQR, 3-6) and NRS 6.5 with movement (IQR, 5-8) (Figure 1, overall), and opioid use was 73.50 oral MME per 24 hours (IQR, 37.5-140.25) (Figure 2, overall). Subgroup pain scores and

opioid use were comparable between indication groups (i.e., degenerative, metastatic and trauma), and are displayed in figure 1 and 2. Forty patients (62.5%) reported pain scores of NRS  $\geq 4$  in rest on postoperative day one leading to the initiation of additional analgesic treatment.

During the postoperative hospital stay, median pain scores were NRS 4 in rest (IQR, 3-6) and NRS 6 with movement (IQR, 4-7) (Figure 1, overall). All patients used opioids, and the median dosage was 75.0 oral MME per 24 hours (IQR, 37.5-129.4) (Figure 2, overall). Sixty-three patients (98.4%) used oral or transdermal opioids, and in 47 patients (73.4%) IV opioids were prescribed. Thirteen patients (20.3%) were readmitted to the recovery room to receive a new loading dosage of IV opioids.

Patients who were prescribed opioids preoperatively used a median dosage of 82.5 oral MME per 24 hours (IQR, 45.0-175.5) after surgery. Postoperative opioid use by patients who did not use opioids before surgery was a median dosage of 60.0 oral MME per 24 hours (IQR, 37.50-97.50).

During the postoperative hospitalization period, 60 patients (93.8%) developed adverse events most likely caused by opioid use (Table 2). Of this group, 36 patients (56.3%) suffered from at least one mild ORADE, 50 patients (78.1%) from at least one moderate ORADE, and 17 patients (26.6%) from at least one severe ORADE. The most common adverse events were mild and moderate gastro-intestinal ORADEs, including constipation (54.7%) and nausea (56.3%). Acute respiratory depression was the most frequently reported (15.6%) severe ORADE, and four patients (6.3%) necessitated an antidote (e.g., naloxone) to antagonize intoxication. One patient suffered from a paralytic ileus requiring treatment. ORADEs are further specified in supplementary Table 1. Spearman's rho was 0.434 ( $p < 0.001$ ) indicating a moderate positive correlation between opioid use and the development of ORADEs<sup>89</sup>.

**Table 2.** Opioid-Related Adverse Drug Events.

	<b>Overall (n=64)</b>	<b>Degenerative (n=25)</b>	<b>Metastatic (n=18)</b>	<b>Trauma (n=21)</b>
<b>Any ORADE, n (%)</b>	60 (94%)	24 (96%)	16 (89%)	20 (95%)
<b>Any mild ORADE, n (%)</b>	36 (56%)	14 (56%)	11 (61%)	11 (52%)
<b>Any moderate ORADE, n (%)</b>	50 (78%)	22 (84%)	13 (72%)	16 (76%)
<b>Any severe ORADE, n (%)</b>	17 (27%)	5 (20%)	5 (28%)	7 (33%)

At discharge, patients reported median pain scores of NRS 4 in rest (IQR, 2-6), and NRS 5 with movement (IQR, 4-7). In 33 cases (51.6%) a pain score of NRS  $\geq 4$  in rest was reported at the time of discharge. A total of 54 patients (84.4%) were prescribed opioids at discharge.

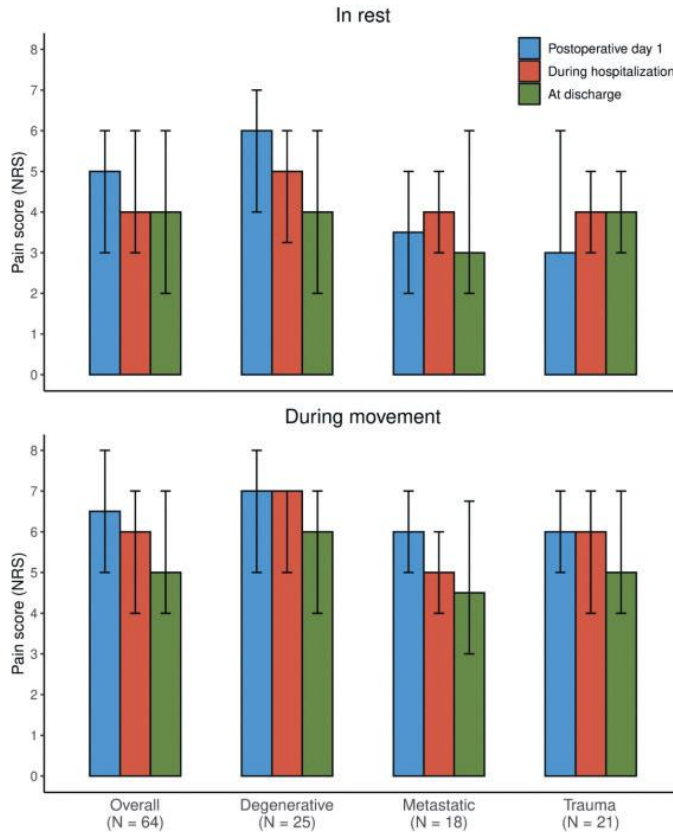


**Figure 1.** Boxplots displaying pain scores (NRS) in rest (top) and with movement (bottom) on postoperative day 1 (blue), during hospitalization (red), and at discharge (green). Pain scores are displayed for the overall group and the subgroups. The boxes indicate the median, and the whiskers indicate the interquartile range (IQR).

### 3.3 Postoperative recovery outcomes

The median time needed before patients were able to mobilize independently from bed to chair was 48 hours (IQR, 24-72). Patients were hospitalized for a median of 7 days (IQR, 4-9) after surgery. Subgroup time to mobilization and postoperative admittance were similar between indication groups, as assessed by Kruskal-Wallis testing.

Pain scores reported at discharge were compared with pain scores reported at the first day after surgery. This comparison demonstrated that in 35 patients (54.7%) pain scores in rest had decreased at discharge, while in 11 patients (17.2%) and in 18 patients (28.1%) pain scores were similar or had increased, respectively (Table 3). The similar comparison of pain scores with movement showed that in 33 patients (51.6%) pain scores had decreased at discharge, but in 18 patients (28.1%) and in 13 patients (20.3%) pain scores were similar or had increased, respectively.

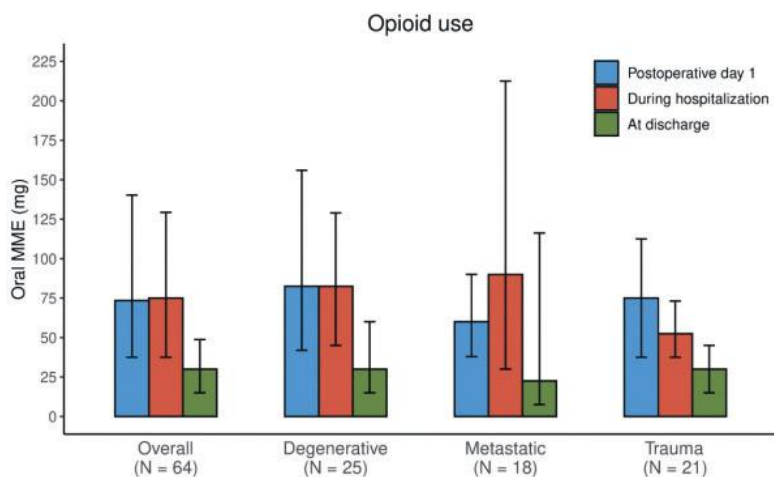


**Figure 2.** Boxplots displaying opioid use (oral MME (mg)) on postoperative day 1 (blue), during hospitalization (red), and at discharge (green). Opioid use is displayed for the overall group and the subgroups. The boxes indicate the median, and the whiskers indicate the interquartile range (IQR).

**Table 3.** Percent change in pain scores at discharge compared to postoperative day 1. NRS, numeric rating scale; POD, postoperative day.

Percent change compared to POD 1	NRS in rest, n (%)	NRS with movement, n (%)
<b>Reduction &gt; 50%</b>	17 (27%)	9 (14%)
<b>Reduction &lt; 50%</b>	18 (28%)	24 (38%)
<b>No change</b>	11 (17%)	18 (28%)
<b>Increase &lt; 50%</b>	8 (13%)	10 (16%)
<b>Increase &gt; 50%</b>	10 (16%)	3 (5%)

## 4. DISCUSSION

The objectives of this study were to evaluate postoperative pain severity, analgesics use (with a focus on opioids), and the incidence of adverse events likely caused by opioid use (i.e., ORADEs) in patients who underwent surgical stabilization of the spine. Patients experienced moderate to severe pain during the postoperative hospitalization period. Despite the use of high doses of opioids and various other analgesics (e.g., NSAID, NMDA-receptor antagonist) through both parenteral and enteral administration routes, postoperative pain had not declined at discharge from the hospital for a large group of patients. Several patients had to be readmitted to the recovery room to receive a new loading dose of IV opioids on top of their regular pain treatment to achieve adequate pain control. We illustrated that ORADEs are common in patients after surgical stabilization of the spine. Almost all patients suffered from ORADEs, and most patients were affected by multiple ORADEs. As a consequence, patients frequently suffer from both inadequately managed pain *and* the adverse events associated with opioid use.

Opioids are the cornerstone of current postoperative pain management, yet patients are, sometimes severely, affected by the adverse events associated with opioid use. In particular, patients suffering from ORADEs have an increased likelihood of inpatient mortality, prolonged length of hospital stay, higher cost of hospitalization, and higher readmission rates<sup>24,75,90</sup>. As opioid consumption is generally higher in the United States compared to the Netherlands, the adverse events associated with opioids could have even more impact on patients in such countries<sup>91</sup>. In the present study we did not investigate a causal relationship between opioid use and the development of ORADEs due to a lack of information on the timing of ORADEs relative to the administration of opioids. The monitored adverse events could have been caused by the surgical procedure (e.g., paralytic ileus is a known complication after spine surgery), or administration of general anesthesia, and not directly because of opioid use<sup>92</sup>. This possible downside might have increased the heterogeneity of the study population. Nevertheless, the reported adverse events are described as being an ORADE in the literature with similar incidences as found in this study<sup>78,93</sup>. Assuming that adverse events are frequently caused by opioids, one may advocate opioid reduction to try to lower the incidence of ORADEs. However, reducing the use of opioids could lead to an even larger portion of patients experiencing insufficiently controlled pain, which in turn also increases the risk for prolonged hospital stay and readmissions but, potentially at least, with fewer ORADEs<sup>9,11,15,62</sup>. Previous research has shown that patients would rather experience more pain, than suffer from ORADEs<sup>93,94</sup>. Although classified in this study as a moderate ORADE, patients were willing to give up most pain relief to prevent experiencing nausea and vomiting<sup>93</sup>. This tradeoff illustrates

the challenge and unmet clinical need of adequately treating postoperative pain while preventing the development of ORADEs.

Reducing the use of opioids while adequately treating pain requires analgesic interventions able to substitute the analgesic effects of opioids. Examples of such interventions are opioid-sparing and opioid-replacing techniques, in which opioids are combined with or substituted by alternative analgesics, respectively<sup>95-98</sup>. Examples of rising opioid-replacing techniques are the (continuous) infusion of local anesthetics into the surgical field, and locoregional blocks such as the erector spinae plane (ESP) block. Continuous wound infiltration has proven to be effective in reducing postoperative pain in total knee and total hip replacement, and might be suitable for surgical stabilization of the spine as well<sup>99-101</sup>. Although a novel technique, ESP blocks have shown reduction of pain and opioid consumption following instrumented spine surgery<sup>102,103</sup>. Utilization of opioid-replacing techniques and opioid-sparing strategies as part of multimodal pain treatment regimens may reduce the frequency and/or impact of ORADEs, and could help shorten length of hospital stay and reduce readmission rates, which will eventually increase patient satisfaction and decrease overall costs<sup>90,104</sup>. Future studies should focus on the timing of implementation and feasibility of opioid-sparing strategies and opioid-replacing techniques.

The present study has several limitations. Similar to previous literature, in the descriptive analysis it was assumed that documented adverse events were most likely caused by opioid use<sup>78</sup>. However, causality between opioid use and development of ORADEs could not be established as the documented ORADEs were not linked to a hospitalization day. Hence, it was not possible to determine if adverse events were a consequence of opioid use or due to other causes. Ascribing all adverse events to opioid use might have overestimated the frequency of ORADEs. On the other hand, due to the retrospective nature of this study in which data were obtained from medical records, not all ORADEs may have been recorded. Common mild and moderate adverse drug events, such as nausea, pruritus, and constipation, were possibly not identified as ORADEs, lowering their incidence.<sup>93</sup> Secondly, the small sample size of this study did not allow for comprehensive statistical analysis. However, given the explorative goal of this study, a descriptive approach was used rather than a sample size calculation. Moreover, the study population underwent spinal stabilization for a variety of indications such as degenerative or metastatic spinal disease, or spinal trauma. Pain is a multidimensional phenomenon that is influenced not only by the extent of tissue damage, but also by patient expectations, coping strategies and many other factors.<sup>105,106</sup> The underlying disease of the patients might influence their psychological well-being and so influence their pain perception, leading to differences



between the patients included<sup>106,107</sup>. To this end, NRS scores were displayed separately per indication group.

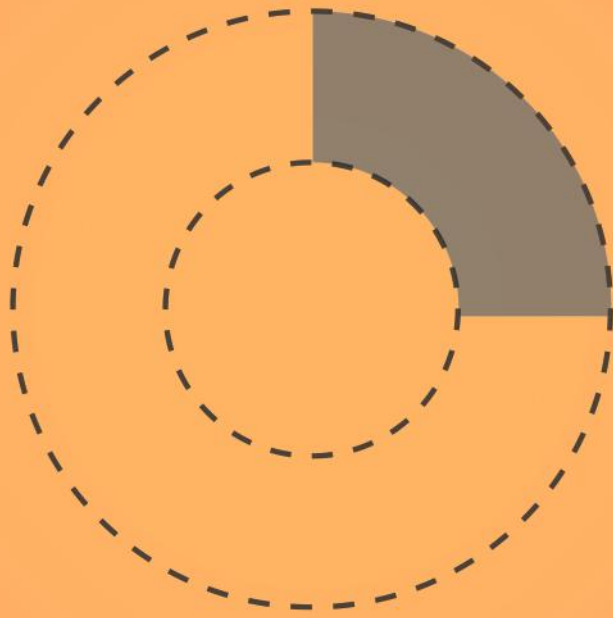
Lastly, this study was conducted in a single academic medical center limiting the generalizability of the results to other hospitals and health care systems. However, given the general trend that patients frequently report severe postoperative pain after major spine surgery, and require high doses of opioids, the results from this study might be translatable to other hospitals offering similar healthcare.

## 5. CONCLUSIONS

This study demonstrated that patients who undergo surgical stabilization of the spine experience moderate to severe postoperative pain despite the use of high doses of opioids supplemented with various other analgesics. Almost all patients suffered from opioid-related adverse drug events, illustrating the delicate balance between sufficient pain relief and risk of developing these events. The results of this study stress the necessity for more research on implementation of opioid-sparing strategies and opioid-replacing techniques as integral parts of multimodal pain treatment regimens following major spine surgery.

**Supplementary table 1.** *Specification of Opioid-Related Drug Events.*

ORADE	Classification	Overall (n=64)	Degenerative (n=25)	Metastatic (n=18)	Trauma (n=21)
<b>Constipation</b>	Mild	35 (55%)	14 (56%)	11 (61%)	10 (48%)
<b>Pruritus</b>	Mild	9 (14%)	5 (20%)	1 (6%)	3 (14%)
<b>Accidental fall</b>	Moderate	6 (9%)	3 (12%)	2 (11%)	1 (5%)
<b>Confusion</b>	Moderate	16 (25%)	9 (36%)	5 (28%)	2 (10%)
<b>Nausea</b>	Moderate	36 (56%)	18 (72%)	9 (50%)	9 (43%)
<b>Urinary retention</b>	Moderate	22 (34%)	6 (24%)	6 (33%)	10 (48%)
<b>Acute respiratory depression</b>	Severe	10 (16%)	5 (20%)	2 (11%)	3 (14%)
<b>Sedation</b>	Severe	8 (13%)	2 (8%)	3 (17%)	3 (14%)
<b>Severe gastro-intestinal events</b>	Severe	1 (2%)	0 (0%)	0 (0%)	1 (5%)



# CHAPTER 2

## Sensory innervation of human bone: an immunohistochemical study to further understand bone pain

Jasper G. Steverink, Douwe Oostinga, Floris R. van Tol, Mattie H.P. van Rijen, Claire Mackaaij, Suzanne A.M.W. Verlinde-Schellekens, Bas J. Oosterman, Albert J.M. Van Wijck, Tom A.P. Roeling, Jorrit-Jan Verlaan

## **ABSTRACT**

Skeletal diseases and their surgical treatment induce severe pain. The innervation density of bone potentially explains the severe pain reported. Animal studies concluded that sensory myelinated A $\delta$ -fibers and unmyelinated C-fibers are mainly responsible for conducting bone pain, and that the innervation density of these nerve fibers was highest in periosteum. However, literature regarding sensory innervation of human bone is scarce. This observational study aimed to quantify sensory nerve fiber density in periosteum, cortical bone, and bone marrow of axial and appendicular human bones using immunohistochemistry and confocal microscopy. Multivariate Poisson regression analysis demonstrated that the total number of sensory and sympathetic nerve fibers was highest in periosteum, followed by bone marrow, and cortical bone for all bones studied. Bone from thoracic vertebral bodies contained most sensory nerve fibers, followed by the upper extremity, lower extremity, and parietal neurocranium. The number of nerve fibers declined with age and did not differ between male and female specimens. Sensory nerve fibers were organized as a branched network throughout the periosteum. The current results provide an explanation for the severe pain accompanying skeletal disease, fracture, or surgery. Further, the results could provide more insight into mechanisms that generate and maintain skeletal pain and might aid in developing new treatment strategies.

## 1. INTRODUCTION

Musculoskeletal diseases are highly prevalent in the general population and are a leading cause of disability among patients and medical costs every year.<sup>108–113</sup> Diseases affecting bone and their (surgical) treatment can lead to considerable pain.<sup>12</sup> Bone pain negatively affects mobility, inhibits rehabilitation, and can lead to long-term disabilities.<sup>55,56,114–118</sup> The complex underlying mechanisms and multiple possible etiologies of bone pain, make this pain difficult to attenuate.<sup>20,119,120</sup>

A deeper understanding of sensory innervation of human bones could aid in improved treatment of bone pain. Recent reports have shown innervation density to correlate with the presence of pain, for example regarding intervertebral disc innervation in low back pain.<sup>121,122</sup> However, literature on human bone innervation is scarce. Some early reports on human bone innervation exist, but these studies did not yet have access to current advanced imaging techniques.<sup>123,124</sup> Previous studies in rodents demonstrated that periosteum, cortical bone and bone marrow are all innervated with afferent sensory nerve fibers and post-ganglionic sympathetic neurons.<sup>17,18,125–128</sup> The main function of sensory nerve fibers is conduction of sensory stimuli from the bone, however, together with sympathetic fibers, they also play a role in bone healing and remodeling.<sup>129–136</sup> Several mammalian studies identified two important types of sensory nerve fibers performing these functions: myelinated A $\delta$ -fibers and smaller diameter, unmyelinated C-fibers.<sup>18,126,137–140</sup> A $\delta$ -fibers are mainly responsible for conducting sharp, localized pain, while C-fibers transmit dull, diffuse pain.<sup>19</sup> Earlier mammalian studies concluded that innervation density of sensory nerve fibers is highest in the periosteum, followed by bone marrow and cortical bone.<sup>17,126</sup> The periosteum is therefore suggested to be a major contributor to pain arising from musculoskeletal diseases, but data in humans are lacking.

The aim of the present study was to quantitatively explore the number and distribution of A $\delta$ -fibers, C-fibers, and sympathetic fibers in axial and appendicular human bones using immunohistochemistry, and fluorescent and confocal microscopy. Furthermore, this study set out to assess the distribution of nerve fibers between different bone-related compartments (i.e. periosteum, bone marrow, and cortical bone), between different anatomical locations (i.e. neurocranium, thoracic spine, upper extremity and lower extremity), and between genders. Lastly, the effect of age on bone innervation in the elderly population included in this study was determined.

## 2. METHODS

### 2.1 Tissue Collection

In order to represent the human skeleton as completely as possible, experiments were performed on available anatomical specimens from parietal bones of the neurocranium, thoracic vertebral bodies, midshaft humeri, midshaft radii, midshaft femora, and midshaft tibiae. Of all bones, a cross-section containing periosteum, cortical bone and bone marrow was retrieved (figure 1). To prevent interference of joint disease in innervation density, midshaft portions of long bones were used.<sup>141,142</sup> No approval was needed from the medical research ethics committee for this study. Tissues were collected from bodies that entered the department of anatomy of our institution through a donation program. These persons provided written consent during life, that allowed the use of their entire bodies for educational and research purposes and therefore, samples were collected based on availability.

Bodies were previously fixated in 4% formaldehyde for varying durations (6 months – 4 years). Age and sex of the bodies was known. From the long bones, 0.5 cm transversal sections of the diaphysis were gently cut using a saw (Dremel 3000, Racine, WI, USA), and from the thoracic vertebrae 0.5 cm sagittal sections of the vertebral body. Sections measuring 1x1cm from the parietal bone of the neurocranium were obtained using a saw. The anatomical specimens were stored until further processing in 4% buffered formaldehyde to preserve tissue characteristics and prevent decay.

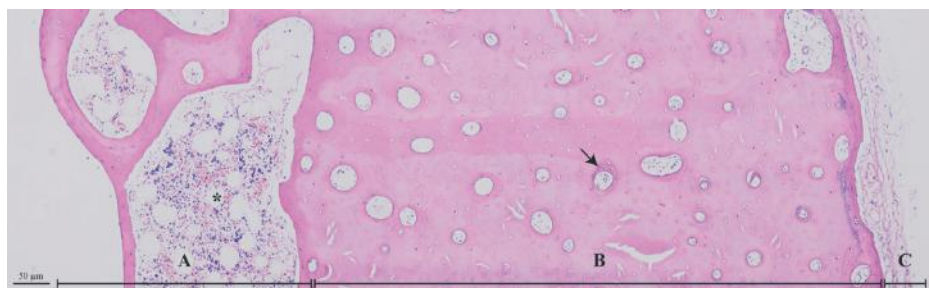


**Figure 1.** A cross-section of a radius stained with hematoxylin and eosin (H&E) displays the three bone-related compartments: bone marrow/trabecular bone (A), cortical bone (B) and periosteum (C) (50x magnification). The bone marrow consists of hematopoietic stem cells and adipose tissue (asterisk). In the cortical bone, Haversian canals run parallel to the longitudinal axis of the bone as part of an osteon and contain blood vessels and/or nerve fibers (arrow). The periosteum is a thin sheath of connective tissue that surrounds the outer surface of the cortical bone and consists of a cellular rich layer and a fibrous layer.

## 2.2 Tissue Processing

The collected anatomical specimens were decalcified using 0.5M ethylenediaminetetraacetic acid (EDTA). Every seven days the decalcification progress was radiographically monitored using a  $\mu$ -CT scanner (PerkinElmer Quantum FX, Waltham, MA, USA). After each cycle of seven days, anatomical specimens were again fixated with 4% formaldehyde overnight, and placed in fresh EDTA the next day. Upon complete decalcification, anatomical specimens were stored in 15% sucrose in 0.1M phosphate-buffered saline (PBS) (pH 7.4) at 4 °C for further processing.

Anatomical specimens were dehydrated in graded ethanol series, cleared in xylene and embedded in paraffin. 5 mm thick sections were cut and mounted on clean, positively charged microscopic slides (VWR Premium Printer Slides, Radnor, PA, USA). Cross-sections were dried overnight at room temperature (RT), placed for five hours on a 60 °C plate, and subsequently incubated at 60 °C overnight to improve microscopic slide attachment.

## 2.3 Immunohistochemistry on bone cross-sections

With immunohistochemistry, distinctive molecular markers can be used to label and visualize specific sensory and sympathetic nerve fibers. A $\delta$ -fibers were labeled with anti-neurofilament 200 kD (NF-200) antibodies (Developmental Studies Hybridoma Bank, Iowa City, IA, USA). NF-200 is an intermediate filament part of the cytoskeleton of A $\delta$ -fibers.<sup>140,143</sup> C-fibers express calcitonin gene-related peptide (CGRP), a neurotransmitter involved in nociception and nerve injury, and were labeled with anti-CGRP (Sigma-Aldrich, St. Louis, MO, USA).<sup>140,144,145</sup> Anti-tyrosine hydroxylase (TH) antibodies (Pel-Freez, Rogers, AR, USA), an enzyme part of the catecholamine synthesis, were used to label sympathetic fibers.<sup>146</sup> Anti-Protein gene product 9.5 (PGP9.5) (Dako, Carpinteria, CA, USA) antibodies were used as a pan-neuronal marker.<sup>147-149</sup> As positive controls, a human vagus nerve for NF-200, CGRP, PGP9.5 antibodies, and a human sympathetic trunk for TH and PGP9.5 antibodies were used. Primary antibodies were omitted in the negative controls. Details of the primary antibodies, including references to antibody characterization, are presented in Table 1.

Bone cross-sections were deparaffinized in xylene (3 x 5 minutes), stepwise hydrated in an ethanol gradient (3 x 5 minutes in 100% and in 96%, 3 min in 80%, 70%, and 50%), and subsequently washed in de-ionized water. For antigen retrieval, cross-sections were incubated in 0.01M citrate buffer (pH 6.0) for five minutes at RT. Samples were then transferred to an 80 °C citrate buffer for 40 minutes, and subsequently cooled down to RT. Bone cross-sections were rinsed with wash buffer (0.05M tris-buffered saline (TBS) (pH 7.6) and 0.05% Tween), and blocked with 5% normal human serum (NHS) (Jackson ImmunoResearch, West Grove, PA, USA) in 0.05M TBS (pH 7.6) for ten minutes at RT. The

blocking buffer was removed, and primary antibodies were added in TBS with 3% bovine serum albumin (BSA) (GERBU Biotechnik GmbH, Heidelberg, BW, DE), and incubated overnight at 4 °C, except for the PGP9.5 antibodies, which were applied for 48 hours.

**Table 1.** Background information on primary and secondary antibodies

Primary / secondary antibody	Immunogen	Manufacturer, species raised in, mono/ polyclonal, catalogue and lot number	Dilution	Reference
<b>PGP9.5</b>	Purified PGP9.5 isolated from bovine brain	Dako, rabbit, polyclonal, Cat# Z5116, Lot# 20043529	Cross-sections: 1:2000 Whole-mount: 1:100	Manufacturer's information (Bernal Sierra et al., 2017) <sup>150</sup> (Cleypool et al., 2020) <sup>151</sup> (Rots et al., 2019) <sup>152</sup>
<b>NF-200</b>	Semi-purified neurofilament 200 kD from rat brain homogenate	Developmental Studies Hybridoma Bank (DSHB), mouse, monoclonal, Cat# RT97	Cross-sections: 1:1000	Manufacturer's information (Haskins et al., 2017) <sup>153</sup> (Lawson et al., 1993) <sup>154</sup> (Viehöfer et al., 2015) <sup>155</sup>
<b>CGRP</b>	Purified rat $\alpha$ -CGRP peptide. The epitope recognized by the antibody resides within the C-terminal ten amino acids of rat $\alpha$ -CGRP	Sigma-Aldrich, mouse, monoclonal, Cat# C7113, Lot# 106M4836V	Cross-sections: 1:500	Manufacturer's information (Yen et al., 2006) <sup>156</sup>
<b>TH</b>	SDS-denatured rat tyrosine hydroxylase purified from pheochromocytoma	Pel-Freez, rabbit, polyclonal, Cat# P40101, Lot# AJO3190	Cross-sections: 1:500 Whole-mount: 1:100	Manufacturer's information (Cleypool et al., 2020) <sup>151</sup> (Rots et al., 2019) <sup>152</sup>
<b>BrightVision Poly-AP Anti-rabbit</b>		ImmunoLogic (VWR), goat, Cat# VWRKDPVM110AP, Lot# 191217	Used for cross-sections	
<b>BrightVision Poly-AP Anti-mouse</b>		ImmunoLogic (VWR), goat, Cat# VWRKDPVR110AP, Lot# 251018	Used for cross-sections	
<b>Alexa Fluor 594 Goat Anti-rabbit</b>		Jackson ImmunoResearch, goat, polyclonal, Cat# 111-586-045, Lot# 112163	Whole-mount: 1:200	



After incubation in primary antiserum, bone cross-sections were washed with wash buffer, followed by incubation in secondary antibodies for 30 minutes at RT. BrightVision Poly AP-anti-Rabbit (ImmunoLogic VWR, Amsterdam, NH, NL) was used for TH and PGP 9.5 antibodies, and Poly AP-anti-Mouse for NF-200 and CGRP antibodies. Bone cross-sections were then rinsed with wash buffer, followed by 10 minutes incubation in Liquid Permanent Red (LPR) (Dako, Carpinteria, CA, USA). LPR was washed away with TBS and de-ionized water. To obtain sufficient contrast for tissue examinations, bone cross-sections were counterstained with hematoxylin. Finally, a cover slip with Entellan (Merck KGaA, Darmstadt, HE, DE) was applied, and bone cross-sections were air dried for 12 hours at RT before imaging.

#### **2.4 Immunohistochemistry on whole-mount preparations of periosteum**

Whole-mount preparations of periosteum were harvested from midshaft radii. Excess muscle was removed using a carbon steel surgical blade No. 20 (Swan-Morton, Sheffield, YSS, ENG). Sharpey's fibers were gently cut, and periosteum was taken off the bone by careful elevation. The periosteum was constantly irrigated with TBS during dissection to prevent tissue dehydration. Whole-mount samples were then frozen and thawed twice in TBS, and washed in whole-mount wash buffer (0.05M TBS (pH 7.6) and 0.1% Saponin). Subsequently, whole-mount samples were incubated for 90 minutes at 37 °C in blocking solution containing 5% NHS and whole-mount wash buffer. Primary antibodies TH and PGP9.5 were applied for 12 hours and 48 hours, respectively, in whole-mount wash buffer with 3% BSA at RT. Primary antiserum was aspirated and whole-mount samples were rinsed with whole-mount wash buffer. Alexa Fluor 594 goat anti-rabbit secondary antibodies (Jackson ImmunoResearch, West Grove, PA, USA) were applied for 30 minutes at RT in whole-mount wash buffer. BSA (3%) was added to minimize non-specific binding. Finally, samples were washed with whole-mount wash buffer, covered with FluorSave (Sigma-Aldrich, St. Louis, MO, USA), and dried for 12 hours at RT before imaging.

#### **2.5 Microscopy and nerve fiber quantification**

High-power field (HPF, 400x magnification) images of bone cross-sections were captured with a Leica DM6 B (Wetzlar, HE, DE) fluorescent microscope using LAS X imaging software. A 400x magnification (311 x 233 mm in dimension) was used to distinguish between individual axons. The I3 filter cube (excitation range: blue, excitation filter: BP 450 - 490 nm, dichromatic mirror: 510 nm, and suppression filter: LP 515 nm) was set. Three HPFs were obtained per bone compartment per histology slide. The imaging location was chosen so that each set of three HPFs would adequately resemble the overall bone-related compartment. Fluorescent images of bone cross-sections were analyzed, and nerve fibers were quantified manually in ImageJ (NIH, Bethesda, MD, USA) by two observers (J.S. and D.O.). A fiber was counted if it was identifiable as a vividly

fluorescent solid, solitary, round (in case of transverse cross-section) or elongated (in case of longitudinal cross-section) structure. No minimal dimensions were pre-specified. In case one fiber yielded more than one cross-section due to a sinuous course, this was counted as a single fiber. Mean fiber count of the three HPFs and of both observations was used for analysis. Brightness and contrast were adjusted to enhance image quality, no other image corrections or filters were used.

For whole-mount preparations of periosteum, images were captured with a ZEISS LSM 800 (Oberkochen, BW, DE) laser confocal microscope using a 5x objective, a 180  $\mu\text{m}$  pinhole and ZEN imaging software. A 594 nm excitation beam was used, and emission was detected using a 620 nm emission filter. Z-stacks were generated to allow for three-dimensional assessment of nerve fiber distribution through the full-thickness periosteum using a 25  $\mu\text{m}$  step size. Acquired images of whole-mount preparations were displayed as a maximal intensity projection in ImageJ. Background was subtracted using the Subtract Background function in ImageJ, and brightness and contrast were adjusted in Adobe Photoshop (Adobe Systems Incorporated, San Jose, CA, USA).

## 2.6 Statistical analysis

Data was subsequently analyzed in RStudio version 1.2.5033 (RStudio Inc., Boston, MA, USA). Data distribution was checked for normality graphically, using Q-Q plots, and confirmed using Shapiro-Wilk testing. Spearman's Rho and an Intra-Class Correlation coefficient for absolute agreement were calculated to assess inter-observer variation. Comparisons were performed using a Kruskal-Wallis test and a post hoc Wilcoxon rank-sum test. P-values were corrected for multiple testing with a Bonferroni correction. A multivariate regression was performed using a generalized linear model with Poisson residuals and a log link function allowing for identification of interaction effects between variables. Residuals were checked for normality using Q-Q plots. If interaction effects were statistically significant, the effect was embedded into the generalized linear model. Variables studied were age, gender, bone-related compartment (i.e. periosteum, bone marrow, and cortical bone), immunohistochemical staining, anatomical location, and nerve fiber count. As nerve fiber count functioned as the outcome variable, ten unique interaction effects were possible and thus analyzed. Data were presented as median number of nerve fibers with interquartile range (IQR). Results from the multivariate regression were reported as incident rate ratios (IRR) calculated from Poisson coefficients ( $e^{\text{Poisson coefficient}}$ ), and represent a multiplicative factor. In addition, estimated marginal means (EMM) with standard error (SE) were presented. The level of significance was set at  $p < 0.05$ .

### 3. RESULTS

#### 3.1 Demographics of collected tissue

A total of 54 anatomical specimens were harvested from 29 human fixated cadavers. Four parietal bones (7%), six thoracic vertebrae (11%), five midshaft humeri (9%), seven midshaft radii (13%), 17 midshaft femora (32%), and 15 midshaft tibiae (28%) were available and studied after harvesting. Sixteen (55%) cadavers were female, and overall mean age was  $84.0 \pm 8.2$  years (range 66-99). Anatomical specimen characteristics are displayed in Table 2. Complete decalcification of anatomical specimens was achieved after a maximum of 23 days. A total of 3 NF-200, 5 CGRP, 4 TH, and 1 PGP9.5-stained bone cross-sections failed during the immunohistochemical staining process and were thus discarded, despite protocol changes to improve microscopic slide attachment.

**Table 2.** Bone sample characteristics.

Characteristics	Value
<b>Gender, n (%)</b>	
Female	16 (55%)
Male	13 (45%)
<b>Age, mean (SD) (years)</b>	84.0 ( $\pm 8.2$ )
<b>Bones, n (%)</b>	N=54
Neurocranium	4 (7%)
Thoracic vertebra	6 (11%)
Midshaft humerus	5 (9%)
Midshaft radius	7 (13%)
Midshaft femur	17 (32%)
Midshaft tibia	15 (28%)

#### 3.2 Innervation of the periosteum, cortical bone, and bone marrow

Overall, periosteum contained most nerve fibers, as compared to bone marrow, and cortical bone (Figure 2). The amount of A $\delta$ -fibers was largest in the periosteum (median 7 (IQR 4-12) fibers/HPF;  $p < 0.001$  vs. cortical bone,  $p < 0.001$  vs. bone marrow), followed by bone marrow (2 (1-4) fibers/HPF;  $p < 0.001$  vs. cortical bone), and cortical bone (0 (0-1) fibers/HPF) (Figure 2A1-A3, 2E). The number of C-fibers in periosteum was higher (6 (3-10) fibers/HPF;  $p < 0.001$  vs. cortical bone,  $p = 0.075$  vs. bone marrow), compared with bone marrow (5 (2.75-8) fibers/HPF;  $p < 0.001$  vs. cortical bone), and cortical bone (1 (1-2) fibers/HPF) (Figure 2B1-B3, 2E). The number of sympathetic nerve fibers was greatest in periosteum (9 (6-13) fibers/HPF;  $p < 0.001$  vs. cortical bone,  $p < 0.001$  vs. bone marrow), followed by bone marrow (5 (3-9) fibers/HPF;  $p < 0.001$  vs. cortical bone), and

cortical bone (2 (1-4) fibers/HPF) (Figure 2C1-C3, 2E). PGP9.5-positive nerve fibers were mostly present in periosteum (9 (6-16.2) fibers/HPF;  $p < 0.001$  vs. cortical bone,  $p < 0.001$  vs. bone marrow), followed by bone marrow (3 (2-5.75) fibers/HPF;  $p < 0.001$  vs. cortical bone), and cortical bone (1 (1-3) fibers/HPF) (Figure 2D1-D3, 2E). Spearman's Rho was 0.890 and the intra-class correlation coefficient for absolute agreement was 0.851 (0.751-0.904), indicating good to excellent agreement between observers.<sup>89,157</sup>

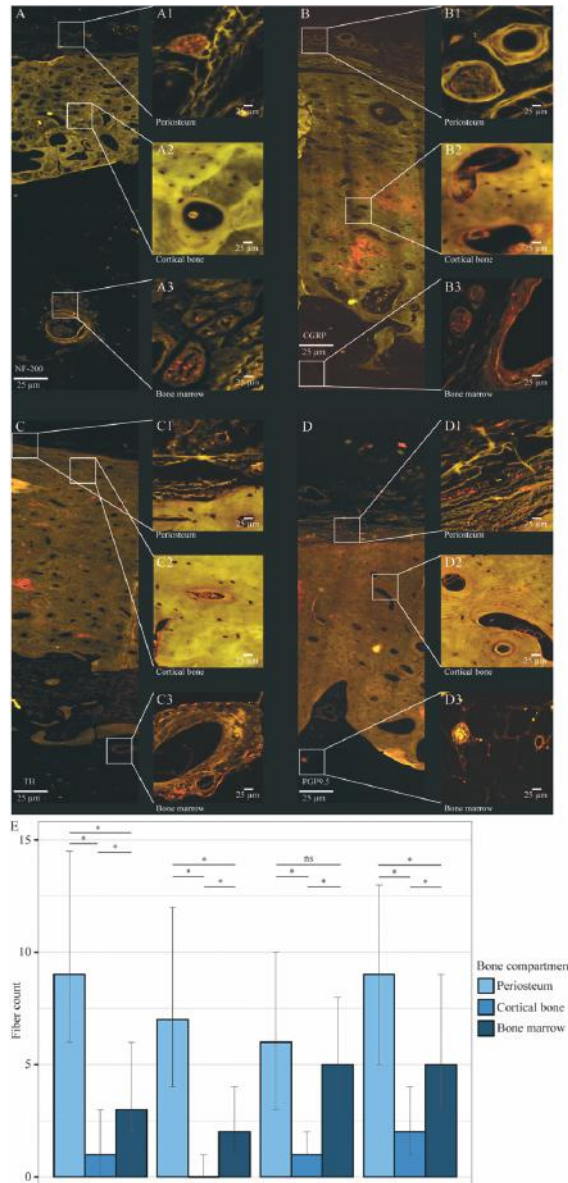


**Figure 2.** Fluorescent images showing NF-200-positive myelinated A $\delta$ -fibers (A, A1-A3), CGRP-positive unmyelinated C-fibers (B, B1-B3), TH-positive sympathetic nerve fibers (C, C1-C3), and PGP9.5-positive nerve fibers (D, D1-D3) in red. In periosteum and bone marrow, sensory nerve fibers were organized in large bundles (A1, A3, B1, B3), or were branched off as single nerve fibers (A3, D1). TH-positive sympathetic nerve fibers were co-localized with blood vessels (C1, C3). Cortical bone only contained sensory and sympathetic nerve fibers in Haversian canals (C2, D2), but not every canal was innervated (A2). Immunohistochemical stains were quantified and presented as median (IQR) number of nerve fibers per HPF for periosteum (light blue), cortical bone (medium blue), and bone marrow (dark blue) (E). Fiber counts from all locations were combined. For every immunohistochemical staining, periosteum contained most nerve fibers, followed by the bone marrow, and cortical bone.

### 3.3 Nerve fiber distribution in bone-related compartments

The periosteum and bone marrow cavity were innervated with large bundles of multiple sensory nerve fibers, while in the cortical bone only single fibers confined to Haversian canals were observed (Figure 2A1, 2A3, 2B1, 2D2, 3A-B). Sympathetic fibers were also present in all three bone-related compartments, but always co-localized with blood vessels (Figure 2C1-C3). Confocal images of periosteal whole-mount samples were prepared to allow assessment of coherence between nerve fibers, and illustrated that PGP9.5-positive nerve fibers (pan-neuronal marker) formed a branched network throughout the periosteum (Figure 3A-B). Periosteal whole-mount preparations confirmed the co-localization of sympathetic fibers and blood vessels, and indirectly illustrated the abundance of blood vessels in the periosteum (Figure 3C).

Differences between A $\delta$ -fibers, C-fibers, and sympathetic nerve fibers within bone-related compartments were analyzed. See previous section and Figure 2E for median nerve fiber count. In periosteum, no difference between the number of A $\delta$ -fibers and C-fibers was observed ( $p=0.71$ ). However, the number of C-fibers was significantly higher compared to the amount of A $\delta$ -fibers in cortical bone, and bone marrow (both  $p<0.001$ ). Nerve fiber count for sympathetic nerve fibers was significantly higher compared with C-fibers in periosteum ( $p<0.001$ ). This difference was not observed in bone marrow or cortical bone ( $p=1.000$  and  $p=0.59$ , respectively). The number of sympathetic nerve fibers was significantly higher compared with A $\delta$ -fibers in cortical bone ( $p<0.001$ ), bone marrow ( $p<0.001$ ), and in periosteum ( $p=0.043$ ). These results indicate that in bone marrow and cortical bone, C-fibers are slightly more abundant than A $\delta$ -fibers, while in periosteum both C-fibers and A $\delta$ -fibers are present to the same extent. In addition, sympathetic fibers are large in number in every bone-related compartment.

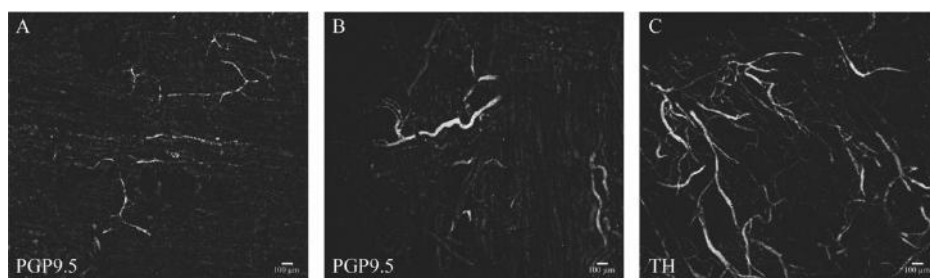


**Figure 3.** Confocal images of whole-mount preparations of periosteum from a radius (female, 83 years) demonstrating PGP9.5-positive nerve fibers (A-B), and TH-positive sympathetic nerve fibers (C) in white. PGP9.5-positive nerve fibers were organized in a branched network throughout the periosteum. TH-positive sympathetic nerve fibers were co-localized with blood vessels, which indirectly showed the abundance of blood vessels in the periosteum.

### 3.4 Multivariate regression

Possible effects of bone-related compartment, gender, age, anatomical location, and immunohistochemical staining on nerve fiber count were analyzed using a Poisson multivariate regression with interaction effects. Interaction tables and estimated marginal means (EMM) are provided in the supplementary information. The multivariate regression model was based on 1836 individual nerve fiber counts. In the elderly individuals studied (age range 66 – 99 years), the number of nerve fibers significantly declined per year of age (IRR=0.985,  $p<0.001$ ), especially in the periosteum (Table 3, S1). No overall effect of sex on innervation density was present (male N = 738 counts, female N = 1098 counts, IRR=1.016,  $p=0.881$ ), however the interaction effect between gender and anatomical location demonstrated higher nerve fiber counts for lower extremity bones of females (Table 3, S3, S8). The overall number of C-fibers was significantly lower compared to PGP9.5-positive nerve fibers (IRR=0.650,  $p=0.003$ ) (Table 3, S2). No differences were observed in the number of A $\delta$ -fibers (IRR=1.225,  $p=0.132$ ) and sympathetic nerve fibers (IRR=1.052,  $p=0.704$ ) compared to PGP9.5-positive nerve fibers (Table 3). The thoracic spine (IRR=2.513,  $p<0.001$ ), upper extremity (IRR=1.595,  $p<0.001$ ), and lower extremity (IRR=1.540,  $p<0.001$ ) contained significantly more nerve fibers compared to neurocranium (Table 3, S5, S8, Figure 4). Nerve fiber count was significantly lower for bone marrow compared to periosteum (IRR=0.189,  $p<0.001$ ), and lowest for cortical bone compared to periosteum (IRR=0.094,  $p<0.001$ ). The low number of nerve fibers in cortical bone was mainly visible in female bones and lower extremity (Table S4, S7, S8).

**Table 3.** Multivariate regression analyzing factors that influence nerve fiber count per high power field. <sup>1</sup> Results are averaged over the levels of other categorical variables. Estimated Marginal Means (EMM) represent the mean fiber count for each factor, adjusted for any other variables in the model. In the GLM Poisson LogLink without interactions, multiplying the factor's reference EMM (e.g., male in Gender) by the incident rate ratio (IRR) of non-reference categories gives the EMM for the non-reference category. Due to the involvement in interactions, this multiplication does not work in the GLM Poisson LogLink with interactions. <sup>2</sup> Results may be misleading due to involvement in interactions.

Fiber count	n=1836	GLM Poisson LogLink with interactions			GLM Poisson LogLink without interactions				
		IRR	EMM <sup>1,2</sup>	EMM SE	IRR	EMM <sup>1,2</sup>	EMM SE	p-value	
<b>Intercept</b>		25.153	4.32	0.080	<0,001	23.871	4.42	0.073	<0,001
<b>Age</b>	Per year	0.985	4.32	0.080	<0,001	0.987	4.42	0.072	<0,001
<b>Gender</b>	Male	Ref	4.32	0.114	N/A	Ref	3.97	0.084	N/A
	Female	1.016	4.33	0.112	0.881	1.240	4.92	0.094	<0,001
<b>Staining</b>	PGP9.5	Ref	4.88	0.151	N/A	Ref	5.47	0.118	N/A
	NF-200	1.225	2.78	0.125	0.132	0.635	3.48	0.089	<0,001
	CGRP	0.650	4.22	0.149	<b>0.003</b>	0.706	3.86	0.097	<0,001
	TH	1.052	6.11	0.181	0.704	0.950	5.20	0.116	<0,001
<b>Location</b>	Neurocranium	Ref	3.32	0.184	N/A	Ref	3.06	0.145	N/A
	Thoracic spine	2.513	5.73	0.191	<0,001	2.057	6.28	0.163	<0,001
	Upper extremity	1.595	4.83	0.123	<0,001	1.567	4.79	0.103	<0,001
	Lower extremity	1.540	3.81	0.072	<0,001	1.359	4.15	0.065	<0,001
<b>Compartment</b>	Periosteum	Ref	9.30	0.188	N/A	Ref	9.90	0.166	N/A
	Cortical bone	0.094	1.76	0.078	<0,001	0.183	1.81	0.057	<0,001
	Bone marrow	0.189	4.95	0.131	<0,001	0.486	4.81	0.101	<0,001



## 4. DISCUSSION

The present study set out to study the sensory innervation of human bone. The results demonstrate that the highest sensory innervation density can be found in the periosteum, followed by bone marrow and cortical bone. Of the locations studied, the thoracic vertebra received most sensory innervation. The neurocranium received the least sensory innervation. Innervation density decreased with age. In the present study, relative differences in innervation between periosteum, cortical bone and bone marrow were smaller compared to earlier mammalian studies.<sup>17,126</sup> One study reported a ratio of summed A $\delta$ -fibers and C-fibers between periosteum, bone marrow and cortical bone of 100:2:0.1, while in the current study a ratio of 100:54:8 was found.<sup>126</sup> The use of a different species and calculations based on medians instead of means might partially account for these differences. Remarkably, not all osteons were innervated, which partially explained the low number of both sensory and sympathetic nerve fibers in cortical bone as presented in section 3.3 (Figure 2A2). The number and distribution of sensory nerve fibers varied between different anatomical locations (i.e. neurocranium, thoracic spine, upper, and lower extremity). Possibly, skeletal injury in more densely innervated locations is more painful than in locations receiving less sensory innervation. Previous reports have shown correlations between innervation of the intervertebral disc and severity of low back pain. However, a causal relationship between innervation density and pain severity cannot be established, as tissue injury (inflicting pain) and the subsequent inflammatory processes have been shown to lead to hyperinnervation.<sup>158</sup> Gerbershagen *et al.* studied pain scores on the first postoperative day for any type of surgery. The top ten of most painful interventions included seven skeletal surgeries, of which three were in the spinal column.<sup>12</sup> Although pain is a multidimensional phenomenon and not necessarily equal to sensory innervation density, the high nerve fiber count in thoracic spine as demonstrated in the current study reflects these clinical findings, supporting a correlation between innervation density and pain severity.

We demonstrated that sensory nerve fibers in periosteum were organized in a network of large bundles or were branched off as single nerve fibers forming a net-like structure. The typical symptom of a bone fracture is acute, stabbing pain localized near or at the fracture site.<sup>159</sup> Mechanical distortion of the periosteum might help explain the severe pain experienced by these patients. In addition, skeletal pain can be caused by pathology in the bone marrow (e.g. in bone tumors), and is typically described as a dull and aching pain.<sup>20,133,160,161</sup> In the present study we demonstrated that the number of C-fibers was slightly higher compared to the number of A $\delta$ -fibers in bone marrow. This finding is in line with the clinical picture of patients experiencing different types of pain in different types of pathology. The here presented data may provide new treatment targets for these various types of pain arising from skeletal pathology.

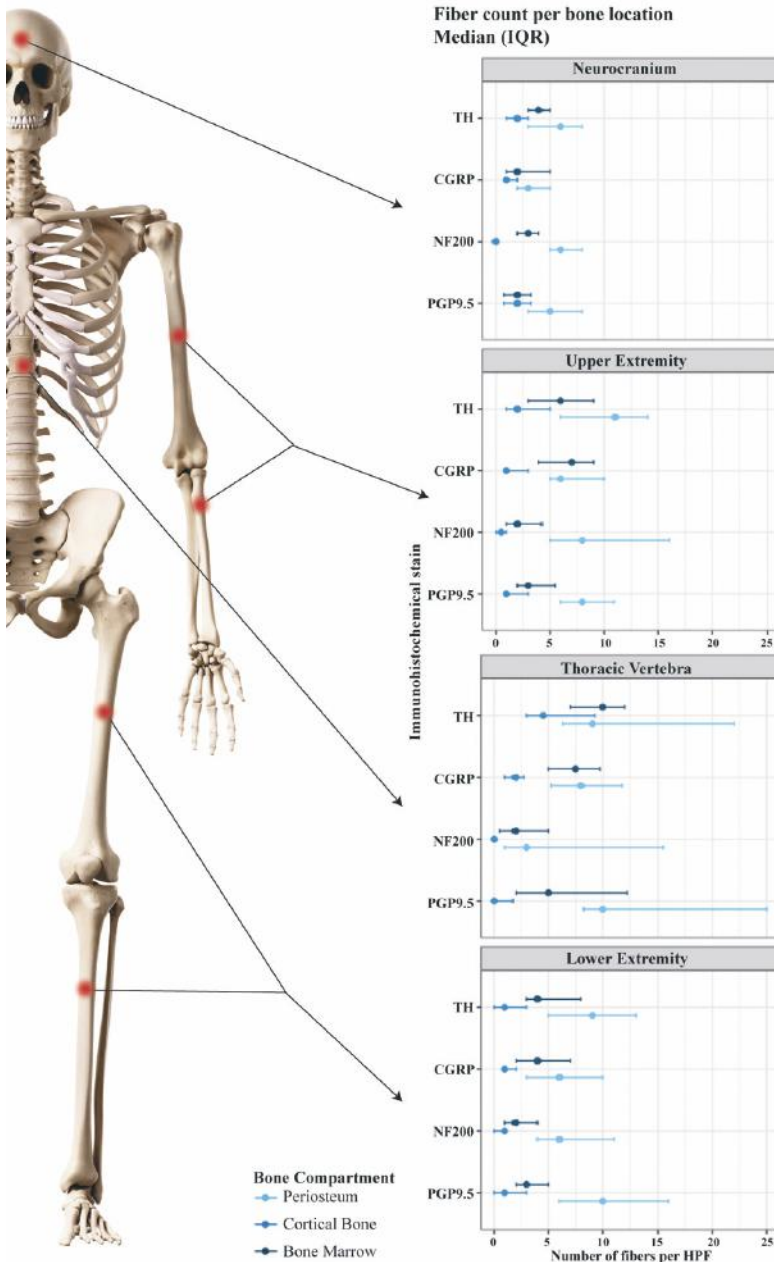


**Figure 4.** The median number (IQR) of CGRP-positive unmyelinated C-fibers, NF-200-positive myelinated A $\beta$ -fibers, TH-positive sympathetic nerve fibers, and PGP9.5-positive nerve fibers separately displayed for the neurocranium, thoracic vertebra, upper extremity, and lower extremity. Compared to the neurocranium, the number of nerve fibers was higher in all three anatomical locations, especially in the thoracic vertebra. Skeleton adjusted from sciepro/shutterstock.com, used under license of Shutterstock.com.

A strength of this study was the use of four immunohistochemical stains to visualize A $\delta$ -fibers, C-fibers, and sympathetic fibers. Subsequently, we were able to draw conclusions about their relative number in different bone-related compartments. It should be noted that the total volume of bone marrow is greater than cortical bone and periosteum.<sup>17</sup> Therefore, the absolute number of sensory and sympathetic nerve fibers might be higher in bone marrow. Use of multivariate regression enabled us to draw conclusions on the complete data set. For example, to analyze the effect of gender on bone innervation, all 1836 observations were taken into account. Another strong element of the present study was the use of bones from multiple anatomical locations, to adequately represent human axial and appendicular innervation. The use of bones from both men and women of ages ranging from 66 to 99 were used to account for potential differences in bone innervation based on sex or age. Our findings demonstrated no overall differences in innervation between female and male bones. Collecting all four bone sites studied from the same individual would have provided paired samples and thus might have further strengthened our conclusions, but was not possible due to incompleteness of the skeletal material available. Furthermore, experiments were performed on macroscopically healthy bones, making the results relevant to the general population. As mentioned, average donor age was relatively high ( $84 \pm 8.2$  years) and ranged from 66 until 99 years. We found that the number of sensory and sympathetic nerve fibers declined with age, which is consistent with a previous animal study.<sup>127</sup> Nevertheless, a wider age range of subjects is necessary to determine whether our findings are applicable for a younger population. A drawback of using anonymous human cadavers, is that the cause of death and its possible effects on bone innervation remains unknown. Previous studies on human innervation have reported on the effects of osteoarthritis and degenerative disc disease on bone innervation. To avoid influence of joint diseases on nerve fiber density, we collected samples from midshaft regions of bone only.<sup>141,142</sup> CGRP-positive fibers have been reported to have a punctuated morphology, while the NF200 signal has a continuous morphology. To avoid overestimation of CGRP-positive fibers due to their morphology, bone cross-sections were used for nerve fiber quantification. As nerve fibers run parallel to the longitudinal axis of long bones, risks of overcounting are minimized. Another possible limitation is the increased EDTA bone decalcification time when compared to previously conducted mammalian studies (>3 weeks vs. 2 weeks).<sup>17,126,127</sup> The extended decalcification was necessary to demineralize cortical bone, which is thicker in humans than in rodents. Literature described that EDTA negatively affects the antigenicity of A $\delta$ -fibers, C-fibers, and sympathetic fibers.<sup>17,127</sup> This might have resulted in a lower nerve fiber count in the present study and thus underestimation of overall innervation density, although this is expected to equally affect all bone compartments and thus does not necessarily impact the here presented ratios. Contradictory reports on the effect of formaldehyde on immunoreactivity of tissue exist.<sup>162,163</sup> The specimens have been fixated in formaldehyde

for various amounts of time, which might have led to variation in immunoreactivity. Our and others' experience is that no large differences regarding immunoreactivity between fresh-frozen samples and formaldehyde-fixated samples were present.<sup>163</sup> Fourth, since PGP9.5 is a pan-neuronal marker, the number of PGP9.5-positive nerve fibers should theoretically equal the sum of A $\delta$ -fibers, C-fibers, and sympathetic fibers. However, in the present study we found that the sum of A $\delta$ -fibers, C-fibers, and sympathetic fibers was approximately 4 times the number of PGP9.5-positive nerve fibers in bone marrow. For periosteum and cortical bone, similar computations resulted in a factorial difference of about 2.4 and 3, respectively. This finding was remarkable as previous studies reported adequate specificity of the immunohistochemical markers used, and showed a lack of other sensory nerve fibers innervating the bone such as A $\beta$ -fibers.<sup>137,150,152-154,156</sup> Although CGRP has been used as a marker for non-myelinated fibers in similar experiments,<sup>17,164</sup> other studies have shown CGRP to be expressed by A $\delta$ -fibers.<sup>165</sup> Further, calculations with median nerve fiber counts and usage of separate microscopic slides for each neuronal marker might have contributed to this discrepancy. These factors might explain the observation that the sum of A $\delta$ -fibers, C-fibers, and sympathetic fibers exceeded PGP9.5 fiber count and highlights the need for a more specific C-fiber marker. However, as these limitations were present in all bones and bone compartments, the authors suggest that these phenomena do not affect the overall trends observed in this study nor the final conclusions.

## 5. CONCLUSION

To our knowledge, the present study is the first to demonstrate the sensory innervation in the human axial and appendicular skeleton. The current results provide an explanation for the severe pain experienced by patients suffering from musculoskeletal diseases or following skeletal surgery. The number of sensory and sympathetic nerve fibers was highest in periosteum, followed by bone marrow and cortical bone. Of all locations studied, bone from thoracic vertebral bodies was most densely innervated. In the periosteum, sensory nerve fibers were organized in a net-like structure that may allow for detection of mechanical distortion such as experienced during traumatic events. The number of nerve fibers declined with age. Since the periosteum is the most densely innervated bone-related compartment in human bones, treatment strategies that locally target the periosteum might aid in attenuating pain after skeletal surgery. Future studies are needed to understand how bone diseases affect density, sensitivity, and morphology of sensory and sympathetic nerve fibers.

## 6 ACKNOWLEDGEMENTS

We would like to thank prof. dr. Ronald Bleys, Simon Plomp, and Marco Rondhuis from the Department of Anatomy (UMC Utrecht) for their help with tissue collection, designing immunohistochemical protocols, and for using their microscope facility. Peter Zuithoff from the Julius Center (Utrecht) is thanked for valuable input on statistical analysis. The Developmental Studies Hybridoma Bank is gratefully acknowledged for supplying the NF-200 antibody.

## 7 SUPPLEMENTARY DATA

Interaction tables from the multivariate regression are presented below. The interaction terms are displayed as Poisson coefficient (IRR). The incident rate ratios (IRR) represent a multiplicative factor. The estimated marginal means (EMM) are presented below and display the mean (SE) number of nerve fibers.

**Table S1.** Interaction term between age and bone-related compartment

	Bone-related compartment		
	Periosteum	Cortical bone	Bone marrow
<b>Age</b>	9,30 (0,188)	1,76 (0,078)	4,95 (0,131)

**Table S2.** Interaction term between gender and immunohistochemical stain

	Immunohistochemical staining				
	TH	PGP9.5	NF-200	CGRP	TH
<b>Gender</b>	Male	4,67 (0,186)	2,61 (0,147)	4,31 (0,184)	6,63 (0,259)
	Female	5,10 (0,196)	2,95 (0,149)	4,14 (0,189)	5,63 (0,206)

**Table S3.** Interaction term between gender and anatomical location

	Anatomical location				
		Neurocranium	Thoracic spine	Upper extremity	Lower extremity
<b>Gender</b>	Male	3,63 (0,268)	5,99 (0,257)	4,93 (0,177)	3,25 (0,097)
	Female	3,04 (0,225)	5,49 (0,252)	4,72 (0,157)	4,46 (0,094)

**Table S4.** Interaction term between gender and bone-related compartment

		<b>Bone-related compartment</b>		
		Periosteum	Cortical bone	Bone marrow
<b>Gender</b>	Male	8,81 (0,252)	1,89 (0,109)	4,83 (0,179)
	Female	9,81 (0,262)	1,63 (0,093)	5,07 (0,176)

**Table S5.** Interaction term between immunohistochemical stain and anatomical location

		<b>Anatomical location</b>			
		Neurocranium	Thoracic spine	Upper extremity	Lower extremity
<b>Staining</b>	PGP9.5	3,21 (0,294)	7,58 (0,375)	4,66 (0,207)	5,01 (0,147)
	NF-200	2,93 (0,309)	2,66 (0,219)	3,41 (0,181)	2,24 (0,101)
	CGRP	3,05 (0,335)	5,48 (0,317)	4,93 (0,228)	3,85 (0,129)
	TH	4,24 (0,405)	9,75 (0,432)	6,93 (0,272)	4,86 (0,139)

**Table S6.** Interaction term between immunohistochemical stain and bone-related compartment

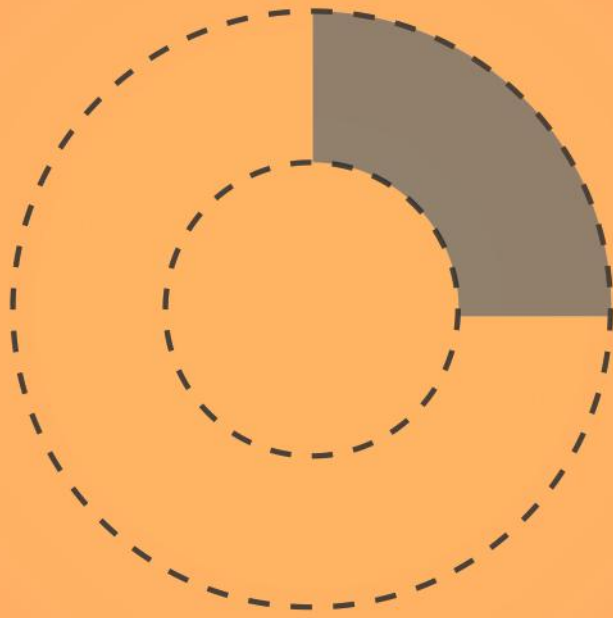
		<b>Bone-related compartment</b>		
		Periosteum	Cortical bone	Bone marrow
<b>Staining</b>	PGP9.5	11,85 (0,370)	2,07 (0,132)	4,75 (0,208)
	NF-200	9,22 (0,339)	0,72 (0,076)	3,21 (0,174)
	CGRP	6,57 (0,277)	2,00 (0,137)	5,72 (0,252)
	TH	10,41 (0,364)	3,19 (0,182)	6,87 (0,278)

**Table S7.** Interaction term between anatomical location and bone-related compartment

		<b>Bone-related compartment</b>		
		Periosteum	Cortical bone	Bone marrow
<b>Location</b>	Neurocranium	6,30 (0,410)	1,51 (0,194)	3,83 (0,316)
	Thoracic vertebra	12,10 (0,429)	2,19 (0,168)	7,11 (0,321)
	Upper extremity	10,74 (0,284)	1,98 (0,120)	5,29 (0,198)
	Lower extremity	9,12 (0,169)	1,45 (0,067)	4,16 (0,112)

**Table S8.** Estimated marginal means (SE)

<b>Anatomical location</b>	<b>IHC stain</b>	<b>Gender</b>	<b>Periosteum</b>	<b>Cortical bone</b>	<b>Bone marrow</b>	
<b>Neuro-cranium</b>	PGP9.5	Male	6,362 (0,7088)	1,540 (0,2558)	3,042 (0,3937)	
		Female	6,759 (0,7376)	1,274 (0,2168)	3,046 (0,3924)	
	NF-200	Male	8,269 (1,0220)	0,889 (0,1761)	3,453 (0,4976)	
		Female	8,821 (0,9300)	0,738 (0,1423)	3,472 (0,4521)	
	CGRP	Male	4,414 (0,5605)	1,892 (0,3179)	4,592 (0,5836)	
		Female	3,985 (0,5667)	1,330 (0,2467)	3,908 (0,5625)	
	TH	Male	7,033 (0,8836)	3,112 (0,5116)	5,594 (0,7384)	
		Female	5,630 (0,6478)	1,939 (0,3158)	4,221 (0,5216)	
	<b>Thoracic spine</b>	PGP9.5	Male	16,280 (0,9566)	2,840 (0,2981)	7,253 (0,5363)
			Female	18,914 (1,1594)	2,568 (0,2801)	7,942 (0,5976)
NF-200		Male	7,917 (0,6923)	0,613 (0,0938)	3,081 (0,3177)	
		Female	9,235 (0,7766)	0,557 (0,0856)	3,387 (0,3380)	
CGRP		Male	8,493 (0,6130)	2,623 (0,2862)	8,233 (0,6169)	
		Female	8,384 (0,6449)	2,016 (0,2326)	7,660 (0,6023)	
TH		Male	17,381 (0,9945)	5,542 (0,5145)	12,883 (0,8325)	
		Female	15,214 (0,9732)	3,777 (0,3802)	10,629 (0,7437)	
<b>Upper extremity</b>		PGP9.5	Male	10,065 (0,5603)	1,909 (0,1851)	3,790 (0,2732)
			Female	11,900 (0,6083)	1,757 (0,1645)	4,223 (0,2827)
	NF-200	Male	10,732 (0,5833)	0,904 (0,1136)	3,529 (0,2644)	
		Female	12,740 (0,6885)	0,835 (0,1047)	3,949 (0,2894)	
	CGRP	Male	8,003 (0,5099)	2,688 (0,2586)	6,556 (0,4513)	
		Female	8,039 (0,4681)	2,102 (0,1955)	6,208 (0,3907)	
	TH	Male	12,540 (0,6902)	4,348 (0,3709)	7,855 (0,5042)	
		Female	11,170 (0,5745)	3,015 (0,2521)	6,595 (0,3968)	
	<b>Lower extremity</b>	PGP9.5	Male	10,044 (0,4186)	1,642 (0,1375)	3,549 (0,2088)
			Female	17,201 (0,4947)	2,189 (0,1484)	5,729 (0,2538)
NF-200		Male	6,258 (0,3154)	0,454 (0,0559)	1,931 (0,1377)	
		Female	10,760 (0,3902)	0,608 (0,0677)	3,130 (0,1776)	
CGRP		Male	5,547 (0,2898)	1,606 (0,1404)	4,265 (0,2522)	
		Female	8,072 (0,3235)	1,819 (0,1332)	5,850 (0,2648)	
TH		Male	8,032 (0,3577)	2,400 (0,1849)	4,722 (0,2599)	
		Female	10,364 (0,3615)	2,411 (0,1537)	5,743 (0,2498)	





# CHAPTER 3

## An Understanding of Bone Pain: A Narrative Review

Douwe Oostinga, Jasper G. Steverink, Albert J.M. van Wijck, Jorrit-Jan Verlaan

## **ABSTRACT**

Skeletal pathologies are often accompanied by bone pain, which has negative effects on the quality of life and functional status of patients. Bone pain can be caused by a wide variety of injuries and diseases including (poorly healed) fractures, bone cancer, osteoarthritis and also iatrogenic by skeletal interventions. Orthopedic interventions are considered to be the most painful surgical procedures overall. Two major groups of medication currently used to attenuate bone pain are NSAIDs and opioids. However, these systemic drugs frequently introduce adverse events, emphasizing the need for alternative therapies, which are directed at the pathophysiological mechanisms underlying bone pain. The periosteum, cortical bone and bone marrow are mainly innervated by sensory A-delta fibers and C-fibers. These fibers are mostly present in the periosteum rendering this structure most sensitive to nociceptive stimuli. A-delta fibers and C-fibers can be activated upon mechanical distortion, acidic environment and increased intramedullary pressure. After activation, these fibers can be sensitized by inflammatory mediators, phosphorylation of acid-sensing ion channels and cytokine receptors, or by upregulation of transcription factors. This can result in a change of pain perception such that normally non-noxious stimuli are now perceived as noxious. Pathological conditions in the bone can produce neurotrophic factors, which bind to receptors on A-delta fibers and C-fibers. These fibers then start to sprout and increase the innervation density of the bone, making them more sensitive to nociceptive stimuli. In addition, repetitive painful stimuli cause neurochemical and electrophysiological alterations in afferent sensory neurons in the spinal cord, which leads to central sensitization and can contribute to chronic bone pain. Understanding the pathophysiological mechanisms underlying bone pain in different skeletal injuries and diseases is important for the development of alternative, targeted pain treatments. These pain mechanism-based alternatives have the potential to improve the quality of life of patients suffering from bone pain without introducing undesirable systemic effects.

## 1. INTRODUCTION

Skeletal diseases accompanied by pain are highly prevalent and have an extensive impact on physical ability, quality of life and medical costs<sup>56,109,111,166</sup>. One of the most reported outcomes caused by bone pain is physical dysfunction, which has secondary effects including decreased mobility, bone mass loss, muscle mass loss and reduction in cognitive and cardiovascular health, all of which lower quality of life<sup>114–116</sup>. Due to these negative effects, skeletal pathologies and their associated pain are considered a major health burden. This burden is expected to increase as the average life expectancy rises and the world population grows<sup>56,109,111</sup>. In addition, risk factors such as decreased physical activity, sedentary behavior and obesity become more prevalent<sup>167</sup>. All these factors can reduce musculoskeletal health, thereby increasing the risk of developing skeletal pathologies with associated pain<sup>167,168</sup>. Examples of skeletal conditions leading to bone pain include inflammation, trauma, infection, autoimmune diseases, cancer, genetic disorders and degenerative diseases<sup>56,109,111</sup>. More specific, 60% – 84% of the patients with skeletal metastatic disease experience severe bone pain<sup>169</sup>. These patients report persistent background pain and breakthrough pain, which is poorly managed by current medications<sup>170</sup>. Not only patients with bone cancer experience pain, 9,6% of men and 18,0% of women older than 60 years worldwide suffer from bone pain caused by symptomatic osteoarthritis<sup>112</sup>. In addition, up to 30% of postmenopausal Caucasian women in the USA have osteoporosis, increasing the risk of painful osteoporotic fractures<sup>56</sup>. These fractures are associated with reduced functional status and more nursing home and rehabilitation hospital admissions<sup>171,172</sup>. Thus, skeletal pathologies and the risk of developing pain will continue to put an increasing medical and economic load on both individuals and society.

One of the treatment options for skeletal conditions is surgery, however, this type of treatment regularly causes more pain in the short term<sup>12</sup>. A cohort study that analyzed and ranked postoperative pain after different types of surgery, reported that out of 40 procedures with the highest pain scores, 22 were orthopedic or traumatologic interventions<sup>12</sup>. The results from this study suggest that surgery to the musculoskeletal apparatus is very painful, which is not only associated with postoperative discomfort, but also with increased risks for postoperative complications (e.g. pneumonia and thrombosis) and chronic pain afterwards<sup>9,173</sup>. In current practice, postoperative pain treatment strategies after musculoskeletal interventions are often inadequate and leave room for improvement.

Nowadays, acute, recurrent and chronic bone pain is mainly attenuated with non-steroid anti-inflammatory drugs (NSAIDs) and opioids<sup>174</sup>. However, the choice for this class of

analgesics is based on the assumption that bone pain pathophysiology is broadly similar to mechanisms that cause pain in other tissues. In addition, short-term use (< 3 months) of NSAIDs can generate nausea, dyspepsia and pyrosis and short-term use of opioids can induce nausea, constipation, urinary retention, cognitive impairment and respiratory distress<sup>66,175–178</sup>. Long term use (> 3 months) of NSAIDs can induce liver, renal and gastrointestinal toxicity and long term use of opioids is correlated with a decreased prospect of returning to work, risk of addiction and renal toxicity<sup>66,175–178</sup>. Furthermore, the use of NSAIDs and opioids in the treatment of skeletal pain could complicate the treatment of the underlying bone pathology, as these drugs might interfere with bone remodeling and healing<sup>179,180</sup>. These problems suggest a need for different treatment strategies aiming more at the pathophysiological mechanisms that generate and maintain skeletal pain. Before such mechanism-based alternatives can be developed, a thorough understanding of the pathophysiology of bone pain is necessary.

In this review, pathophysiological mechanisms of bone pain are discussed in terms of the different types of afferent sensory nerve fibers that innervate the periosteum, bone marrow and cortical bone. These fibers are responsible for the initial sensation of bone pain and the quality of this pain (i.e. sharp pain and dull pain). The activation and organization of afferent sensory nerve fibers able to detect mechanical distortion, acid and pressure is described with respect to their critical role in disease and injury of the bone. The mechanism of peripheral sensitization of afferent sensory nerve fibers caused by inflammatory cytokines, the phosphorylation of ion channels and receptors and by transcriptional changes is evaluated and the induction of sprouting of sensory neurons due to pathological conditions is also described. This review finally concludes with explaining molecular processes that are involved in central sensitization, which plays a role in chronic bone pain.

## **2. TYPES OF SENSORY NERVE FIBERS**

Bone pain can be perceived if the periosteum, cortical bone or bone marrow are disturbed, injured or affected by pathological processes<sup>17</sup>. For example, patients with a fracture involving the cortical bone and periosteum, often experience a sharp and localized pain, while patients with a bone marrow tumor experience a constantly present dull pain, which increases as the disease progresses<sup>159,169</sup>. The latter group of patients also describe breakthrough pain, which is less dull and more intense, like the pain caused by a fracture<sup>170</sup>. These findings suggest that the type of pain (i.e. sharp, diffuse or dull) is predominantly determined by the type of pathology located in the bone. Furthermore, this indicates that afferent sensory nerve fibers, which are sensitive for nociceptive

information, innervate all structural compartments of the bone (i.e. bone marrow cavity, cortical bone and periosteum).

Several studies reported a diversity of afferent sensory nerve fibers in the bone, each with its own conduction velocity, neurotransmitters, receptor characterizations, innervation pattern and function<sup>17,18,137-139</sup>. A rat model with fracture-induced bone pain showed that nociceptive information is largely conducted by A-delta fibers and C-fibers<sup>140</sup>. Studies performed on femora of mice and humeri of cats revealed that there is little innervation of other afferent sensory nerve fibers, such as A-alpha fibers and A-beta fibers<sup>18,126,137,139</sup>. Both A-delta fibers and C-fibers exhibit specific characteristics. A-delta fibers are myelinated and express tropomyosin receptor kinase A (TrkA), which is a nerve growth factor (NGF) receptor and neurofilament 200 kDa (NF200), an intermediate neurofilament part of the cytoskeleton<sup>18,126</sup>. C-fibers are not myelinated and express TrkA, substance P (SP), which is a neurotransmitter involved in nociceptive transport from the peripheral nervous system to the central nervous system, and calcitonin gene-related peptide (CGRP), a peptide playing a role in nociception and nerve injury<sup>18,126</sup>. Both C-fibers and A-delta fibers innervate the bone marrow cavity, cortical bone and periosteum<sup>18</sup>.

The periosteum covers most of the bone surface with the exception of the articular surface in joints. It consists of an outer fibrous layer, which contains fibroblasts, and an inner cambium layer, which consists of progenitor cells that mature into osteoblasts during bone remodeling or fracture healing<sup>125,181,182</sup>. A-delta fibers and C-fibers are mostly located (> 90%) in the cambium layer and are organized as a mesh network<sup>125,140</sup>. Therefore, these fibers are capable of detecting mechanical disturbance, such as stretching or pressure, which can be caused by a fracture. The cortical bone is innervated by A-delta fibers and C-fibers that run through Haversian and Volkmann canals together with blood vessels<sup>17</sup>. In the bone marrow these fibers also colocalize with blood vessels<sup>17</sup>. Castañeda-Corral *et al.* performed a study on the mouse femur and showed that the ratio of relative densities of the sum of A-delta fibers and C-fibers in the periosteum, bone marrow and cortical bone is 100, 2 and 0.1, respectively (with 100 set as reference and measured as length of A-delta fibers and C-fibers per volume tissue)<sup>126</sup>. This indicates that the periosteum is innervated by the highest number of A-delta fibers and C-fibers and is therefore most sensitive to nociceptive stimuli. Literature on sensory innervation of human bone is limited. Sayilekshmy *et al.* reported that the sensory innervation of human bone was highest in cortical pores, followed by periosteum and bone marrow, but did not separately identify A-delta and C-fibers<sup>129</sup>. Furthermore, the tissue was obtained from patients suffering from hyperparathyroidism and therefore these results might not translate to the healthy population.

Although it is clear that C-fibers and A-delta fibers process nociceptive stimuli from the periosteum, cortical bone and bone marrow, Bataille *et al.* suggested that the skeleton is also innervated by cholinergic and adrenergic sympathetic fibers of the autonomic nervous system<sup>130</sup>. Indeed, several mouse and rat studies showed that sympathetic fibers play a role in bone remodeling and skeletal pain<sup>130–132,134</sup>. These fibers are also involved in vasodilation, vasoconstriction, macrophage infiltration and bone progenitor cell function<sup>130,131</sup>. Taken together, these studies present that sympathetic fibers are involved in skeletal health and might contribute to the progression of skeletal disease. However, to what extent sympathetic fibers interact with A-delta fibers and C-fibers, thereby effecting skeletal disease progression and pain, is unknown.

In summation, A-delta fibers and C-fibers are the most important sensory fibers that innervate the periosteum, cortical bone and bone marrow and conduct most nociceptive information. Therefore, this review will continue with how these fibers play a role in four pathophysiological mechanisms that underlie bone pain.

### **3. MECHANISMS UNDERLYING BONE PAIN**

#### **3.1 Activation of A-delta fibers and C-fibers**

Normally, A-delta fibers and C-fibers are silent and only activated upon noxious stimulation including mechanical distortion, local acidosis or an increase in intramedullary pressure (Figure 1). For example, A-delta fibers process nociceptive stimuli such as a pinch or a prick, but also noxious stimuli caused by mechanical deformation, such as a fracture. These stimuli are processed from the bone to the dorsal horn of the spinal cord and to particular regions of the brain resulting in a sensation of pain<sup>183</sup>.

Mechanical distortion is well-studied in mouse models with fracture-induced bone pain (Figure 1, A). These models showed that myelinated A-delta fibers have a higher conduction velocity (10 – 20 m/s, measured in rats) compared to non-myelinated C-fibers (1 m/s, measured in rats)<sup>139,143,184</sup>. This characteristic can be attributed to their difference in myelination. Due to the high conduction velocity of A-delta fibers, it is thought that they are involved in the acute sensation of sharp pain, which occurs after a fracture<sup>139,159</sup>. This pain is short lasting and restricted to a small surface area<sup>159</sup>. Mechanosensitive A-delta fibers and C-fibers continue to discharge after a fracture, until they are spatially relocated into their original position<sup>159,185</sup>. Martin *et al.* demonstrated that A-delta and C-fibers fibers are organized as a mesh network in the periosteum of mice<sup>125</sup>. Such a network is optimally positioned to detect stretching of the periosteum. Relocating the fractured bone with an external cast or interval rod reduces mechanical distortion (i.e. stretching of the periosteum) and, consequently, reduces the discharge frequency of A-delta fibers and

thereby the associated pain. After stabilization, a duller or burning pain is perceived, which lasts longer and is conducted by non-myelinated C-fibers, as their conduction velocity is lower compared to A-delta fibers<sup>139,159</sup>. Furthermore, within hours of the initial fracture, the dull pain conducted by C-fibers is probably maintained by inflammatory mediators released from osteoblasts, osteoclasts and immune cells creating an inflammatory soup near the fracture site<sup>184,186</sup>. These factors include bradykinin, prostaglandin E2, serotonin, TNF- $\alpha$ , colony stimulating factors, NGF and protease-activated receptor 2<sup>187-190</sup>. This implies that the generation of pain after a fracture is a dynamic process of mechanical and chemical stimuli.

While bone pain caused by trauma (i.e. a bone fracture) is initiated by the mechanical distortion of mechanosensitive A-delta fibers and C-fibers, in diseases with increased bone turnover or multiple myeloma, osteoclasts can create a local acidosis, which also activates these sensory fibers (Figure 1, B)<sup>191-196</sup>. Studies performed on mice and rats demonstrated that A-delta fibers and C-fibers in the bone express acid-sensing ion channels, including acid-sensing ion channel-1 (ASIC1) and ASIC3<sup>196-199</sup>. In addition, a rat study showed the expression of the transient receptor potential vanilloid receptor-1 (TrpV1) on A-delta fibers and C-fibers, which is also an acid-sensing ion channel<sup>200</sup>. These ion channels are activated when the pH drops to approximately 4 locally<sup>201</sup>. The acidic environment is created by overactivity of osteoclasts. These cells have a critical role in the regulation of skeletal mass and are responsible for bone resorption. Osteoclasts produce protons after resorbing bone, thereby lowering the pH and activating acid-sensing ion channels on A-delta fibers and C-fibers, which results in bone pain. A commonly used therapy in the treatment of bone cancer, osteogenesis imperfecta and osteoporosis, are bisphosphonates<sup>194,195,202,203</sup>. Bisphosphonates inhibit osteoclast activity and consequently reduce bone resorption, thereby raising the pH and relieving bone pain<sup>194,195,202,203</sup>. Thus, similar to stabilizing a fracture, activation of A-delta fibers and C-fibers can be reduced by normalizing the pH.

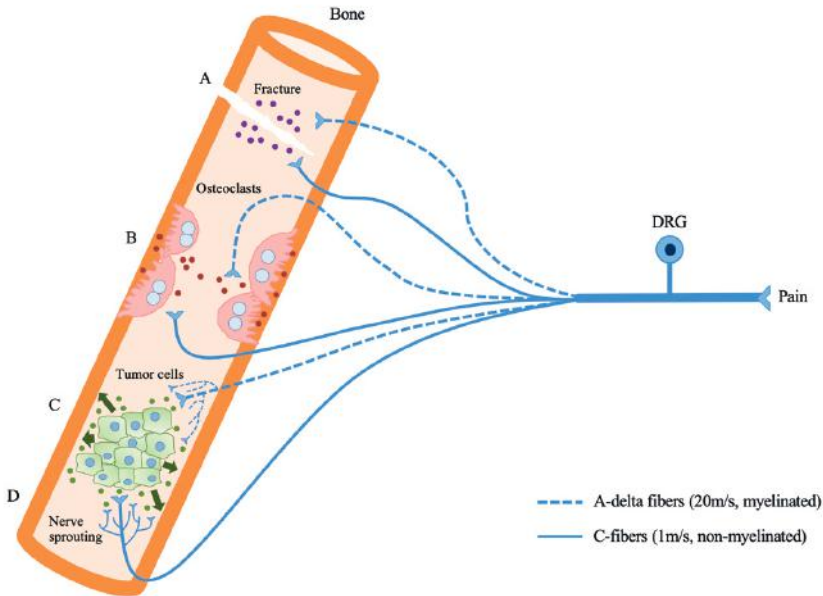


**Figure 1.** A schematic overview of the activation of A-delta fibers (dashed blue lines, myelinated) and C-fibers (blue lines, non-myelinated). (A) A-delta fibers are activated due to mechanical distortion (e.g. a fracture) and conduct sharp and localized pain. C-fibers are also activated upon mechanical distortion and process a more dull and deeper pain. In addition, due to mechanical distortion, osteoblasts, osteoclasts and immune cells produce inflammatory mediators (purple dots), such as bradykinin and prostaglandin E2. This also activates C-fibers, thereby maintaining the dull pain. (B) Acid-sensing ion channels on A-delta fibers and C-fibers are activated due to a local acidosis created by an abundance of protons (red dots), which are produced by overactive osteoclasts in skeletal diseases (e.g. multiple myeloma). This results in dull bone pain. (C) An increase in medullary pressure activates the mechanoreceptors on A-delta fibers and C-fibers, thereby causing pain. (D) Sprouting of A-delta fibers and C-fibers is promoted after secretion of NGF and glial cell line-derived neurotrophic factor (green dots) by immune cells, tumor cells and stromal cells due to pathology in the bone (e.g. bone marrow tumor). Sprouting of sensory neurons results in a higher innervation density localized near the pathology site, which makes the bone highly sensitive to mechanical distortion. Abbreviations: DRG, dorsal root ganglion.

The second pathophysiological mechanism underlying bone pain is peripheral sensitization. This mechanism is triggered by lowering of the resting membrane potential closer to the depolarization threshold and by the upregulation of ion channels. The result is that A-delta fibers and C-fibers become highly sensitive to nociceptive stimuli. Sensitization of A-delta fibers and C-fibers is caused by three different pathways (Figure 2). The first pathway involves sensitization by inflammatory mediators secreted during bone injury<sup>135</sup>. As mentioned before, A-delta fibers and C-fibers can be activated by inflammatory mediators, which are produced in response to bone fracture. In addition to this finding, several studies showed that C-fibers and A-delta fibers located in the periosteum, cortical



bone and bone marrow can be sensitized by similar mediators<sup>184,204–207</sup>. The application of histamine, serotonin, bradykinin and prostaglandin E2 caused an easier depolarization of the mechanosensitive A-delta fibers and C-fibers<sup>184</sup>. This suggests that these fibers can be sensitized during inflammatory diseases or even due to inflammatory mediators released by hematopoietic stem cells located in the bone marrow, thereby lowering the threshold for discharge in reaction to a mechanical stimulus.

The second pathway inducing sensitization is the phosphorylation of ion channels and receptors located on A-delta fibers and C-fibers. In particular, NGF plays a major role in this mechanism. Similar to inflammatory cytokines, NGF is released by immune cells after bone injury or by tumor cells and subsequently binds to nociceptors that exhibit TrkA, which both A-delta fibers and C-fibers do<sup>126,135,208</sup>. This results in the phosphorylation of ion channels and receptors<sup>135,209–211</sup>. Especially, binding of NGF causes phosphorylation the TrpV1 and ASIC3 ion channels, making A-delta fibers and C-fibers more sensitive to pH alterations<sup>209–211</sup>. This finding can be related to the first pathophysiological mechanism of bone pain, involving the activation of A-delta fibers and C-fibers due to an acidic environment (section 3.1). The discharge frequency of A-delta fibers and C-fibers might increase if NGF release is combined with a local acidosis. In addition, NGF also causes phosphorylation of bradykinin-receptors (BR) and prostaglandin E2-receptors (PR), making A-delta fibers and C-fibers more sensitive to these cytokines<sup>210,212</sup>. Therefore, a high local concentration of NGF causes an increased sensitivity of A-delta fibers and C-fibers in response to protons released by osteoclasts and in response to bradykinin and prostaglandin E2 released during inflammation. In line with this finding, a study performed in humans showed that treatment with NGF induces sensitization of nociceptors in the skin, thereby increasing the signaling of noxious stimuli to the brain<sup>213</sup>. This suggests that blocking NGF might be a novel target for treating bone pain.

The third pathway that induces sensitization of A-delta fibers and C-fibers is an increase in transcription of genes involved in nociception. A study performed in rats showed that after binding of NGF to TrkA, NGF and TrkA form a complex, which is transported into the nucleus of A-delta fibers and C-fibers<sup>214</sup>. In the nucleus, this complex alters the activity of transcriptional factors such that genes involved in the processing of nociceptive stimuli are more frequently transcribed<sup>208,212,215–219</sup>. In particular, these genes encode for neurotransmitters including SP, CGRP, brain-derived neurotrophic factor (BDNF) and sodium and calcium channels<sup>208,212,215–219</sup>. Higher concentrations of the aforementioned factors cause a change in membrane potentials of A-delta fibers and C-fibers resulting in easier depolarizations and an increased sensitivity to painful stimuli. Remarkably, a study performed in humans showed that after intracutaneous injection of NGF, the increase of transcription factors involved in mechanical nociception is not likely to normalize in short

term (i.e. weeks)<sup>213</sup>. This might help explain the long-lasting duration of pain syndromes, which are sometimes developed after bone pathology.

For clarity, the three aforementioned pathways have been described separately, but in reality, are interconnected rather than self-contained. In bone pathology they form a dynamic pathophysiological mechanism sensitizing A-delta fibers and C-fibers, thereby modulating pain.

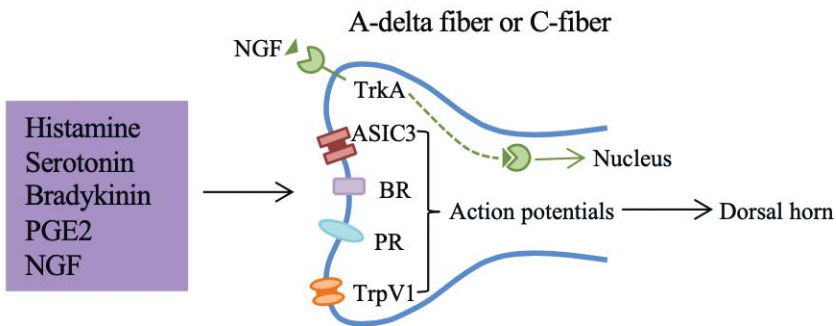


**Figure 2.** A schematic overview of the three pathways involved in sensitization of A-delta fibers and C-fibers presented in one sensory nerve. The first pathway involves the release of inflammatory mediators (purple box) after bone injury. These mediators can sensitize A-delta fibers and C-fibers when they are excessively present. The second pathway includes the phosphorylation of ASIC3 and TrpV1 due to binding of NGF (green triangle) on TrkA. This results in an increased sensitivity to pH alterations. In addition, binding of NGF on TrkA also causes phosphorylation of bradykinin-receptors (BR) and prostaglandin-receptors (PR), making A-delta fibers and C-fibers more sensitive to these cytokines. The third pathway involves the increase in transcription of genes that play a role in nociception. Binding of NGF to TrkA results in a TrkA-NGF-complex, which is retrogradely transported into the nucleus of a sensory neuron. In the nucleus, this complex increases the activity of transcription factors, such that neurotransmitters involved in nociception are more frequently transcribed. Notably, the three aforementioned pathways are not self-contained, but rather interconnected and mutually influenced after skeletal injury.

### 3.3 Sprouting of A-delta fibers and C-fibers

The third pathophysiological mechanism contributing to the maintenance of bone pain is the new formation of A-delta fibers and C-fibers, termed nerve sprouting (Figure 1, D). This phenomenon also occurs in physiological conditions, for example during fracture healing<sup>220–223</sup>. In this case, callus formation is accompanied by nerve sprouting, making the fracture site more sensitive to mechanical loading preventing excessive use of the fractured bone until it is sufficiently healed. Fracture-induced pain models in mice and rats showed that after callus resorption and fracture healing, newly formed A-delta fibers and C-fibers are withdrawn and innervation of the bone returned to normal<sup>220–222</sup>. Another physiological example is the new formation of bone by an increase in mechanical load (i.e.

Wolff's law). Mechanical signals upregulate the expression of NGF in osteoblasts, which causes activation and sprouting of sensory nerves that exhibit TrkA<sup>224</sup>. Subsequently, this leads to the release of osteogenic factors that modulate bone formation<sup>224</sup>.

On the contrary, in pathological conditions such as osteosarcoma, non-fused fractures, degenerated vertebral discs and osteoarthritis, newly formed A-delta fibers and C-fibers have a deviant morphology and a different organization, and the innervation density of these fibers is higher in the bone marrow cavity, cortical bone and periosteum compared to healthy bone<sup>129,132,134,141,225-229</sup>. Human, mouse and rat studies reported that immune cells, stromal cells and tumor cells produce chemical mediators (including endothelin, epidermal growth factor, glial cell line-derived neurotrophic factor, vascular endothelial growth factor, TNF- $\alpha$ , and NGF), causing activation, sensitization and sprouting of sensory neurons<sup>132,134,141,225-229</sup>. Newly formed A-delta fibers and C-fibers remain to exist resulting in a highly innervated periosteum, cortical bone or bone marrow<sup>132,134,225-228</sup>. Consequently, mechanical stimuli which are not perceived as painful under physiological conditions, are now experienced as noxious. This means that mechanical disturbances are easily detected, because the bone is now weaker due to underlying pathology and is more innervated due to sprouting.

Tumor cells located in the bone marrow are able to secrete chemical mediators such as NGF, inducing pathological growth of A-delta fibers and C-fibers into the direction of the tumor<sup>160,225,226,228,230</sup>. Together with tumor (in-)growth itself, tumor cells can damage sensory neurons (e.g. due to an ischemic tumor microenvironment) causing subsequent pain that might lead to chronic neuropathic pain states, suggesting that skeletal pain can have a neuropathic component. These findings, in combination with the effects of NGF in peripheral sensitization, highlight anti-NGF as an interesting new agent for the treatment of bone pain. Indeed, a mouse model of bone cancer pain showed that administration of anti-NGF reduced skeletal pain by approximately 40% - 60%<sup>228</sup>. Similar results were obtained in two mouse models of fracture pain<sup>231,232</sup>. Furthermore, a clinical trial demonstrated that pain resulting from osteoarthritis in the knee can be relieved by 45% - 60% after treatment with anti-NGF<sup>233</sup>. Unfortunately, such treatment induced significant amounts of adverse effects including hypoesthesia, hyperesthesia, paresthesia, headaches, arthralgia, peripheral edema, upper respiratory tract infections and increased risks of rapidly progressive osteoarthritis<sup>233,234</sup>. Therefore, before anti-NGF treatment in humans can be used safely, more research is necessary.

Thus, novel A-delta fibers and C-fibers formed by sprouting increase the innervation of the periosteum, cortical bone and bone marrow, thereby increasing the sensitivity to

mechanical stimuli. This phenomenon can be considered as the third pathophysiological mechanism underlying bone pain.

### 3.4 Central sensitization

The fourth pathophysiological mechanism playing a modulating role in bone pain is central sensitization (Figure 3). Similar to afferent sensory neurons in the periphery, central sensitization is caused by lowering of resting membrane potentials such that sensory neurons depolarize more easily in response to mechanical stimuli. More specific, after applying repetitive noxious stimuli to the bone, pain transmitting neurons in the dorsal horn become sensitized, thereby amplifying the perception and intensity of pain<sup>208,235-241</sup>. Clinical manifestations of central sensitization include hyperalgesia (the amplification of painful stimuli), allodynia (the perception of pain following non-noxious stimuli) and temporal summation of pain (increased perception of pain to repetitive stimuli).

Several studies demonstrated central sensitization using the expression of c-Fos in afferent sensory neurons in a rat<sup>208,235,236,240</sup>. C-Fos is a proto-oncogene that is expressed when neurons repetitively discharge after processing multiple noxious stimuli and can therefore be used as a marker for neuronal activity. These studies showed that, after applying noxious mechanical stimuli to the bone, the expression of c-Fos increases in the ipsilateral dorsal horn<sup>208,235,236,240</sup>. Strikingly, after applying such painful stimuli, innocuous mechanical stimuli also induced an increase in c-Fos expression<sup>236,241</sup>. This implicates that the resting membrane potential of pain transmitting neurons in central nervous system shifts more closely to the depolarization threshold. Such electrophysiological change is observed in animals with bone cancer pain, fracture pain or pain caused by inflammatory diseases<sup>208,236,238,239,241,242</sup>.

While c-Fos expression demonstrates electrophysiological changes in the central nervous system due to persistent bone pain, two neurochemical changes also play an important role in facilitating central sensitization. The first process is the upregulation of dynorphin<sup>208,236,241</sup>. Dynorphin is a class of opioid peptides, which has multiple downstream effects, but in particular is involved as a modulator of pain response (i.e. causes neural excitation)<sup>243</sup>. Lai *et al.* performed an in vitro study in sensory neurons of the dorsal horn demonstrating that dynorphin activates the bradykinin-receptor<sup>244</sup>. This results in an increase in calcium influx via voltage-sensitive calcium channels causing hyperalgesia<sup>244</sup>. In addition, a rat study showed that allodynia induced by dynorphin is mediated by the N-methyl-D-aspartic-receptor (NMDA-R)<sup>243</sup>. Several studies demonstrated that dynorphin is upregulated in the dorsal horn of the spinal cord in mice with osteosarcoma<sup>208,236,241</sup>. The pain caused by the tumor cells is persistently processed to the spinal cord resulting

in central sensitization. However, to what extent dynorphin regulates central sensitization and acts on the NMDA-R, needs to be studied more extensively.

The second neurochemical process which facilitates central sensitization as a result from nociceptive stimulation of bone is microglial activation and astrocyte hypertrophy in the spinal cord<sup>236,241,245</sup>. Several studies demonstrated that purinergic receptors (P2X-R) displayed on microglia are upregulated after repetitive noxious stimulation<sup>246–250</sup>. These receptors can bind adenosine triphosphate (ATP), which is released from afferent sensory neurons upon activation<sup>246–250</sup>. Binding of ATP to P2X-R results in the production of BDNF, a neurotrophic factor involved in short-term promotion of pain sensitivity<sup>249–252</sup>. Consequently, BDNF binds to a variety of receptors on afferent sensory neurons in the spinal cord, thereby lowering the resting membrane potential such that these neurons become sensitized<sup>251</sup>. This results in hyperalgesia, allodynia and temporal summation.

Thus, electrophysiological and neurochemical changes induced by different (molecular) pathways cause sensitization of the central nervous system. These alterations can influence the perception of pain and therefore might be involved in patients with chronic bone pain.

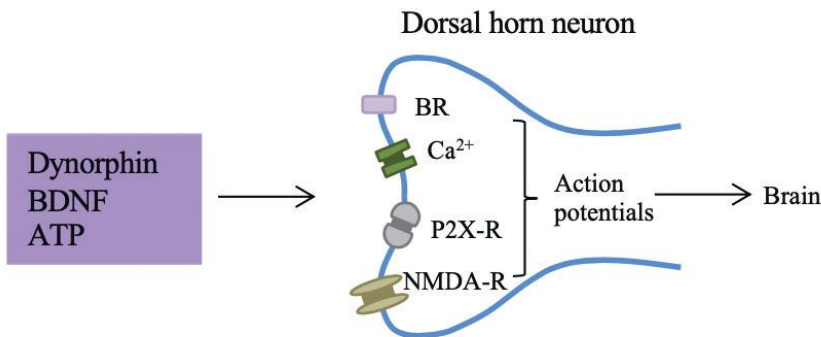


**Figure 3.** A schematic overview of the involved factors in central sensitization presented in one sensory nerve. Repetitive processing of noxious stimuli originating from the bone cause sensory nerve fibers in the spinal cord to undergo electrophysiological and neurochemical changes. This results in central sensitization, which amplifies and intensifies the perception of bone pain. One important neurochemical change is the upregulation of dynorphin activating the NMDA-R and the bradykinin-receptor (BR), thereby increasing the calcium ( $Ca^{2+}$ ) influx in sensory neurons, resulting in hyperalgesia. The second neurochemical change is the upregulation of P2X-Rs. These receptors can bind ATP, resulting in the production of BDNF, which subsequently binds to a variety of receptors on sensory neurons in the spinal cord, resulting in central sensitization.

## 4. FUTURE DIRECTIONS

Bone pain affects millions of individuals suffering from skeletal pathology worldwide and has a negative effect on quality of life. In the last decade, more research on skeletal pathologies has been performed in order to increase knowledge in the mechanisms that generate, facilitate and modulate bone pain. This review discusses the fibers that innervate the skeleton and describes four pathophysiological mechanisms underlying bone pain. These mechanisms include activation of A-delta fibers and C-fibers due to mechanical distortion, a local acidosis or an increase in medullary pressure. Activation can lead to sensitization by inflammatory mediators, by phosphorylation of acid-sensing ion channels and cytokine receptors, or by upregulation of transcription factors. Neurotrophic factors induce sprouting of A-delta fibers and C-fibers. These newly formed fibers have a deviant morphology, thereby increasing the sensitivity for noxious stimuli exerted on the bone. Neurochemical and electrophysiological changes in the dorsal horn of the spinal cord can lead to central sensitization, which might, partially, be the cause of chronic bone pain.

The identification of multiple key processes involved in skeletal health and disease can be considered successful, however, a full understanding of the whole concept of bone pain remains problematic. In particular, the interaction between sympathetic fibers and afferent sensory nerve fibers in the bone should be studied further in order to grasp how these fibers influence skeletal disease progression and pain. Furthermore, the described pathophysiological mechanisms are not self-contained, it is more likely that they are interconnected, suggesting that the generation and continuation of bone pain is a dynamic process. Lastly, some of the molecules involved in peripheral and central sensitization are well studied, however there are several studies proposing additional molecular pathways that have not yet been validated. Combining the individual mechanisms and further elucidating additional molecular pathways for a comprehensive understanding of bone pain form the basis for developing pain mechanism-based therapies.

Several studies attempted to block specific molecular mechanisms to attenuate bone pain. For example, blocking NGF reduces peripheral sensitization and nerve sprouting, resulting in a reduction of bone pain. Whether anti-NGF can be successfully used in humans depends on how the reported side effects can be eliminated or minimized. Other novel therapies involve the blocking of NMDA-receptors and P2X-receptors. These interventions reduce central sensitization and consequently reduce hyperalgesia, allodynia and temporal summation of pain. Another way would be to intensify the research of local therapies instead of systemic therapies to avoid side effects and still effectively attenuate bone pain.

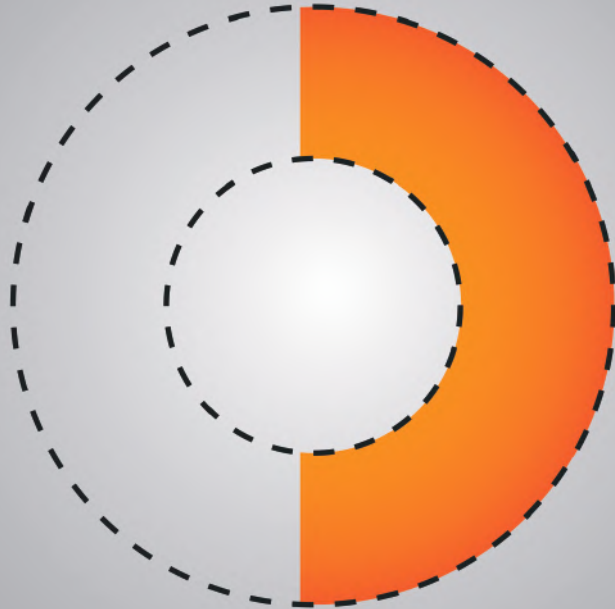
A strong element of this review is the step-by-step explanation of different pathophysiological mechanisms underlying bone pain. This approach resulted in a clear overview of the involved dynamic processes. The neuropathic component of bone pain is not in-depth described in this review. Clinical studies show analgesic effects of anti-neuropathic drugs following skeletal surgery. However, insufficient experimental data exist on the contribution of a neuropathic component to bone pain and the mode of action of anti-neuropathic drugs in attenuating bone pain. Further research might clarify the role of a neuropathic component in generating and maintaining bone pain.

In conclusion, this review highlights the dynamic concepts of bone pain and the need for mechanism-based therapies to treat bone pain and improve the functional status of patients.

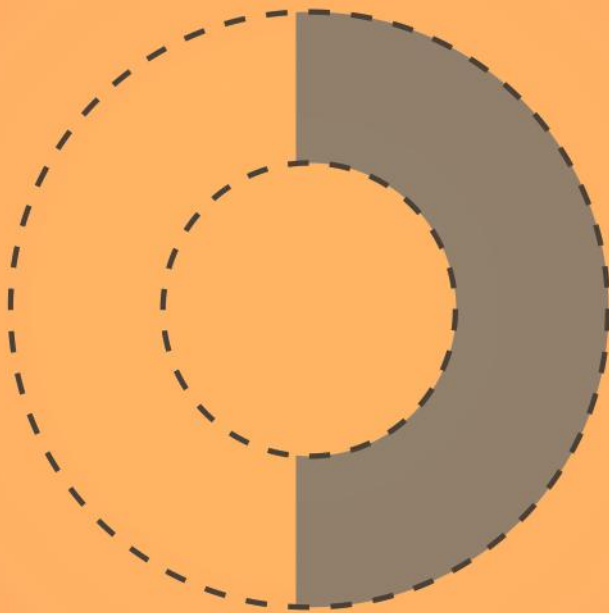




# PART II



Bupivacaine for  
musculoskeletal applications



# CHAPTER 4

## Comparison of in vitro and in vivo toxicity of bupivacaine in musculoskeletal applications

Jasper G. Steverink, Susanna Piluso, Jos Malda, Jorrit-Jan Verlaan

## **ABSTRACT**

The recent societal debate on opioid use in treating postoperative pain has sparked the development of long-acting, opioid-free analgesic alternatives, often using the amino-amide local anesthetic bupivacaine as active pharmaceutical ingredient. A potential application is musculoskeletal surgeries, as these interventions rank amongst the most painful overall. Current literature showed that bupivacaine induced dose-dependent myo-, chondro-, and neurotoxicity, as well as delayed osteogenesis and disturbed wound healing *in vitro*. These observations did not translate to animal and clinical research, where toxic phenomena were seldom reported. An exception was bupivacaine-induced chondrotoxicity, which can mainly occur during continuous joint infusion.

To decrease opioid consumption and provide sustained pain relief following musculoskeletal surgery, new strategies incorporating high concentrations of bupivacaine in drug delivery carriers are currently being developed. Local toxicity of these high concentrations is an area of further research. This review appraises relevant *in vitro*, animal and clinical studies on musculoskeletal local toxicity of bupivacaine.

## INTRODUCTION

Musculoskeletal surgeries rank amongst the most painful surgical interventions overall<sup>12</sup>. The debilitating effects of postoperative pain include delayed mobilization and complications, such as pneumonia and decubitus, which in turn can lead to increased hospital stay and re-admissions<sup>11</sup>. Pain resulting from musculoskeletal surgery is usually treated with multimodal pain regimens in which opioids often fulfill an important role. Opioids have, however, well-known side effects such as nausea, respiratory depression and drowsiness, and can lead to dependence and addiction. Of all patients enrolling in opioid-abuse treatment programs, almost half were first exposed to opioids through prescription from their physician<sup>253,254</sup>. Currently, an estimated two million American citizens are addicted to prescription pain killers, such as opioids<sup>255</sup>. The risks of dependence and abuse are especially relevant for patients undergoing musculoskeletal surgery<sup>27</sup>. Despite administration of opioids, poorly controlled postoperative pain is reported by 75% of patients<sup>11</sup>. Therefore, the interest in alternative pain treatments not displaying the systemic side effects of current opioid-based regimes is increasing. The use of local anesthetics (LAs) has the potential to accelerate postoperative recovery and reduce opioid consumption in musculoskeletal surgery. To this end, bupivacaine is especially popular as it displays the longest duration of action of all LAs (up to 8 hours)<sup>256</sup>. In comparison, the effects of lidocaine last up to two hours in soft tissue<sup>257</sup>. Because of its extensive clinical use and the highest potency compared to other long-acting amino-amide LAs such as ropivacaine and levobupivacaine, this review focuses on bupivacaine<sup>258</sup>. However, eight hours of analgesia is likely insufficient for postoperative pain control and therefore novel formulations aim to further extend the duration of action of LAs. In fact, bupivacaine is the main LA that has been incorporated in recent opioid-free inventions for postsurgical pain relief<sup>39,259–262</sup>.

Recent studies have expressed concerns regarding the *local* toxic effects of bupivacaine infiltration when used for musculoskeletal applications. This review aims to assess i) the *in vitro*, *in vivo* and clinical effects of bupivacaine on various musculoskeletal tissues, cell types and relevant environments (including cartilage, bone, muscle, nerves, intervertebral disc, and surgical wounds) and ii) and the clinical translatability and real-world relevance of these effects. Furthermore, recent approaches and developments to decrease the toxic profile and increase the duration of action of bupivacaine are discussed. Studies providing data on *in vitro*, animal model or clinical local toxicity of bupivacaine were manually selected. References of selected papers were checked for relevant literature. In addition, separate searches were performed for studies comparing free bupivacaine with novel formulations of bupivacaine (*e.g.*, liposomal bupivacaine). Articles published in languages other than English and case reports were excluded from review. Studies

describing systemic toxicity following administration of bupivacaine were outside the scope of this review. This literature review did not require an ethical board approval because no patients or patient data were involved in the review, and only publicly available data was used.

### **Bupivacaine**

After its discovery in 1957, bupivacaine (1-Butyl-N-(2,6-dimethylphenyl)-2-piperidinecarboxamide) has become one of the most widely and frequently used LAs, and is listed as a World Health Organization Essential Drug <sup>263,264</sup>. Bupivacaine belongs to the class of amino-amide LAs, exerting their anesthetic action through binding to the intracellular portion of voltage-gated sodium channels, more specifically the alpha subunit. By inhibiting sodium influx into axons, depolarization and, therefore, pain signal transduction is inhibited <sup>264</sup>. Examples of LA application in musculoskeletal surgery are local infiltration anesthesia (LIA) after total hip and total knee arthroplasty (THA and TKA, respectively). These local applications are associated with low rates of *systemic* toxicity and adverse effects, providing a favorable comparison with opioids <sup>265-268</sup>. Besides therapeutic applications, LA infiltrations also serve as diagnostic tool in a variety of joint disorders, such as hip or shoulder osteoarthritis <sup>269</sup>.

The class of amino-amide LAs has been derived from amino-ester LAs, such as cocaine. All amino-amide LAs have a similar molecular structure, with an aromatic lipophilic portion linked with an amide-containing intermediate chain to an amine hydrophilic portion <sup>270</sup>. Bupivacaine has the longest duration of action (up to 8 hours) of all amino-amide LAs due to its butyl group attached to the tertiary amine. The lipophilic butyl group allows for easy membrane-crossing resulting in high anesthetic potency and prolonged duration of action. In plasma, 95% of bupivacaine is protein-bound, mainly to albumin. Bupivacaine is metabolized in the liver by conjugation with glucuronic acid and excreted renally <sup>271</sup>. Elimination half-life is approximately 2.7 hours in adults and 8.1 hours in neonates <sup>272</sup>. The recommended maximum doses are 2 mg/kg body weight or a maximum of 400 mg per day. The dose can be increased to 2,5 mg/kg body weight with addition of epinephrine, by virtue of decreased systemic uptake resulting from local vasoconstriction <sup>273</sup>. The left-isomer-only formulation of bupivacaine, levobupivacaine, is commercially available separately and has been associated with decreased systemic toxicity, predominantly cardiotoxicity <sup>258</sup>. In *in vitro* studies, the concentration of bupivacaine is often reported in mM or uM. To help comparison between studies presented in this review, it should be noted that a clinically used concentration of 0.5% Bupivacaine HCl solution equals a molarity of 15.4 mM. Bupivacaine HCl solutions are registered for use in spinal, epidural, regional or local infiltrative anesthesia. In all cases the solution is administered by injection.

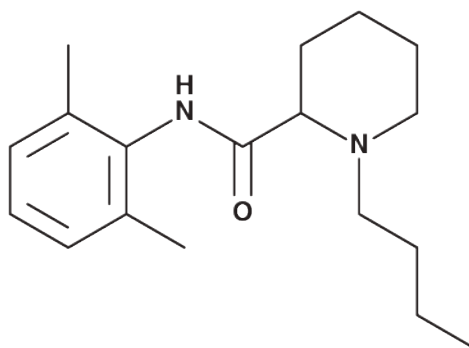


**Figure 1.** Bupivacaine structure formula.

### Effects of Bupivacaine on Skeletal Muscle

In musculoskeletal surgery, exposing osseous structure(s) often requires cutting through or releasing muscle tissue. Muscle recovery after surgery is of paramount importance, since it is essential for wound healing, and facilitates quick mobilization and uneventful return to preoperative function.

It is known that LAs are myotoxic *in vitro*. Bupivacaine is reported to lead to 60-100% *in vitro* myocyte toxicity in concentrations >1 mM (*i.e.* in clinically used concentrations)<sup>274</sup>. Previous studies have described histopathological changes at the injection site of LAs<sup>275-278</sup>. Within minutes, hypercontraction of fiber bundles and myofibrils occurs. Within hours, a degenerative phase is observed, with disruption and condensation of myofilaments, lytic degeneration of the sarcoplasmic reticulum and mitochondria, and pathologic condensation of chromatin, which are signs of early necrosis and apoptosis. The sarcolemmal structure remains intact, potentially indicating that fiber degeneration occurs mainly intracellularly and does not affect the macroscopic structure of the muscle. This degenerative phase lasts for 24-48 hours, after which phagocyte infiltration of the application site occurs. Debris is cleared without damage to basal laminae and satellite cells. As these cells remain largely intact, complete muscular regeneration can occur within three to four weeks.

It is hypothesized that the myotoxic effects of bupivacaine are induced by calcium influx in muscle cells. This is supported by the finding that bupivacaine in concentrations >>1 mM leads to activation of the Ca-release channel-ryanodine receptor in the sarcoplasmic reticulum<sup>275,279</sup>. Interestingly, levobupivacaine has been shown to have stronger effects on Ca-uptake in muscle cells compared with racemic bupivacaine, theoretically potentiating its myotoxicity<sup>279,280</sup>. Another factor that might play a key role in myotoxicity is pH. Indeed, the free base form of LAs reaching the sarcoplasmic reticulum is thought to be

responsible for myocyte injury. At higher pH (*i.e.* closer to and beyond the drug's pKa), the free base fraction increases, potentiating bupivacaine's capacity to damage muscle <sup>281</sup>.

Bupivacaine displays considerable myotoxicity *in vitro*, leading to apoptosis and (myo-) necrosis (Figure 2) <sup>282–284</sup>. Bupivacaine-induced myotoxicity is dose and time dependent <sup>285</sup>, with the myotoxic effects being reversible within three weeks <sup>286</sup>. Animal models have been established to study muscle damage using bupivacaine as an agent to induce myotoxicity <sup>287</sup>. A recent systematic review summarized the *in vivo* myotoxicity of bupivacaine and its effect on muscle recovery. Myotoxicity was defined as the presence of (a combination of) muscle weakness or paralysis, or enzymatic changes indicative of muscle damage (*e.g.*, elevated creatine phosphokinase serum levels). Muscle tissue recovery time was defined as regeneration of muscle fibers, normalization of myofibril diameters, and resolution of inflammation and was doubled after LA administration (up to 30 days, versus normal regeneration time of 14 days) <sup>274,288</sup>. Full recovery to preoperative function was reported in 21 studies, partial recovery in 17 studies and minimal recovery in four studies <sup>274</sup>. Notably, myotoxicity also occurred after administration of liposomal bupivacaine <sup>274,289</sup>. The authors remarked that myotoxicity was correlated with increased concentrations of and exposure time to bupivacaine. The occurrence of myotoxicity can be explained by the fact that liposomal bupivacaine uses relatively high bupivacaine concentrations and sustained release leads to increased exposure time.



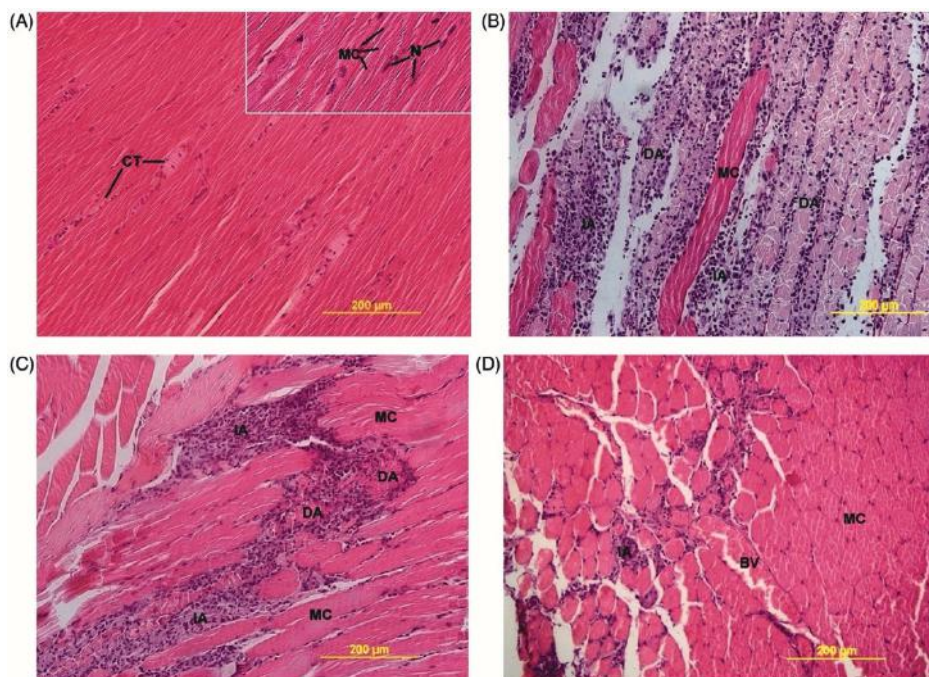


**Figure 2.** Light microscopy images of LA-induced myotoxicity. (A) Skeletal muscle two days after 0.9% saline injection, showing connective tissue (CT) between normal muscle fibers (MC) (20x magnification, insert 40x). (B) Skeletal muscle two days after 0.5% bupivacaine injection, showing degenerative (DA) and inflammatory areas (IA) alternated with MC (20x magnification). (C) Skeletal muscle two days after 0.5% ropivacaine injection, also displaying DA and IA (20x magnification). (D) Skeletal muscle two days after 0.5% levobupivacaine injection, showing incidental IA and blood vessels (BV) between MC (20x magnification). Öz Gergin et al. Comparison of the Myotoxic Effects of Levobupivacaine, Bupivacaine, and Ropivacaine: An Electron Microscopic Study. *Ultrastructural Pathology*, May 2015. Reprinted by permission of the publisher (Taylor & Francis Ltd)<sup>284</sup>

Clinically, effects of muscle damage appear negligible except in muscles of the eye, where temporary diplopia after local anesthesia has been reported<sup>290</sup>. Continuous infusion of LAs after rotator cuff surgical repair did not lead to worse clinical outcomes. The authors concluded that myotoxicity may be reversible or is not severe enough to affect tissue healing and postoperative outcomes<sup>291</sup>. In orthopedic surgery about 0.14% of patients experienced clinical symptoms of LA-induced myotoxicity, which included significant loss of muscle contraction force and tenderness of the operated extremity. Recovery times ranged from four days up to one year<sup>274</sup>. However, clinical symptoms of muscle damage after LA infiltration are prone to be under-reported. Pain and dysfunction after injections administered for post-surgical analgesia can easily be attributed to- or masked by postsurgical pain<sup>281</sup>. Furthermore, a variable degree of damage to muscle (and the associated elevated serum creatine phosphokinase levels) will be caused by muscle

dissection during the surgical intervention, complicating isolation of myotoxicity induced specifically by bupivacaine.

### **Effects of Bupivacaine on Articular Cartilage**

Bupivacaine ranks amongst the most chondrotoxic LAs<sup>292</sup>. Levobupivacaine (the S-enantiomer of bupivacaine) induces similar chondrotoxicity when compared to racemic bupivacaine, with some studies also reporting increased *in vitro* chondrocyte mortality after one hour of exposure to levobupivacaine, when compared to the racemic mixture<sup>293,294</sup>. The cytotoxicity of LAs might be due to lipophilicity rather than stereoisomers, possibly explaining these differences<sup>295</sup>. The *in vitro* chondrotoxicity has been thoroughly reviewed and is dependent on exposure time, dose and concentration, and occurs at clinically used concentrations<sup>292,296–298</sup>. Interestingly, osteoarthritic joints appear more susceptible to LA-induced damage compared with joints with healthy cartilage. Management of osteoarthritis-associated pain with LA injections can, therefore, lead to increased cartilage damage, potentially resulting in more pain<sup>296</sup>. Exposure of cultured chondrocytes to LAs in *in vitro* studies is often limited to one hour<sup>296</sup>. As the elimination half-life of bupivacaine is approximately 2.7 hours, the limited *in vitro* exposure time could hamper translatability of laboratory findings to the clinic<sup>272</sup>.

The chondrotoxic effects of bupivacaine solutions and liposomal bupivacaine were studied in a porcine model. The bupivacaine solution (0.5% w/v) was injected in the stifle joint, leading to significant chondrocyte death *in vivo* (33% nonviable cells), when assessing full-thickness cartilage biopsies with live/dead staining one week after administration<sup>299</sup>. The use of liposomal bupivacaine formulation (1.3% w/v) resulted in a higher chondrocyte viability when compared to bupivacaine HCl (6.2% nonviable cells for liposomal bupivacaine vs 33% nonviable cells for bupivacaine HCl) and was therefore considered safer for intra-articular use. However, histological changes regarding surface integrity, fibrillation and chondrocyte viability did not show significant differences between bupivacaine solutions and liposomal bupivacaine formulation one week after injection in a porcine model. The synovial membrane was not assessed<sup>299</sup>.

In another study, the long-term effects of bupivacaine during 48 hours of continuous infusion were studied in a rabbit shoulder model<sup>300</sup>. No macroscopic or radiological differences were observed between infused glenohumeral joints and controls after three months. Cartilage metabolism assessed with sulfate uptake increased after bupivacaine infusion, potentially indicating a regenerative response. No difference in cell density, percentage of live cells, macroscopic or radiographic changes were observed. Therefore, in the model used, articular cartilage has the potential to recover from chondrotoxic effects induced by bupivacaine. However, other animal studies conclude that chondrocyte

homeostasis does not fully recover following intra-articular bupivacaine administration. Rats received a 0.5% bupivacaine injection into the stifle joint. The contralateral joint received 0.9% saline with the same volume. Cartilage was assessed histologically after 1, 4, 12 weeks and 6 months. Bupivacaine did not lead to damage to the chondral surface, or superficial chondrocyte viability up to 12 weeks after injection. After six months, chondrocyte density had significantly decreased when compared with the control joint, despite cell viability remaining constant <sup>301</sup>.

Clinically, chondrolysis following a single intra-articular LA administration has seldom been reported. This phenomenon is characterized by increasing pain and stiffness in the treated joint, with radiological signs of cartilage breakdown and reduced joint space width. A 2015 systematic review discussed reports of four clinical cases. The rate of chondrolysis when studying continuous infusion was considerably higher compared with single injections, and 97.7% (163 out of 167) of chondrolysis cases reported occurred after continuous infusion and the majority of cases occurred in the glenohumeral joint. It should be noted that in most studies adrenaline was co-administered with bupivacaine <sup>302</sup>.

### **Effects of Bupivacaine on the Intervertebral Disc**

Bupivacaine is a commonly used LA for both diagnosis and treatment of discogenic back pain. However, various *in vitro* studies have shown toxic effects of bupivacaine on intervertebral disc (IVD) cells. Bupivacaine appears to lead to both concentration- and exposure time-dependent necrosis and apoptosis of IVD cells, and decreased matrix synthesis <sup>303–308</sup>.

As with osteoarthritic synovial joints, attempts to relieve pain from degenerative disc disease using LAs could lead to an increase of symptoms due to the cytotoxic effects of these LAs. Interestingly, these findings only partially correlate with data from *in vivo* and clinical studies. For instance, increased rates of apoptosis were observed seven days after bupivacaine (0.5%) injection into intervertebral discs of a rabbit model when compared to saline controls, which are in agreement with previous *in vitro* studies <sup>309,310</sup>. However, no significant differences in IVD degeneration as scored on MRI, histological scoring using safranin-O staining, or amount of viable IVD cells between saline and bupivacaine injection were observed after 6 and 12 months. The main cause of damage appeared to be insertion of the needle into the annulus fibrosus <sup>309</sup>. When comparing bupivacaine-treated (discography or disc-block, both single injection) IVDs with control discs five years after treatment, no significant radiological differences were observed between groups regarding disc height, pain, disability scores or range of motion <sup>311</sup>. Accelerated disc degeneration 10 years after discography has been reported, but this study did not specify the injection fluid used <sup>312</sup>. Therefore, the observed degeneration following diagnostic or

therapeutic disc injections appears to be induced mainly by damage caused by insertion of the needle and/or by the use of a contrast agent <sup>309,313</sup>. A potential explanation for the discrepancies between *in vitro* and *in vivo* or clinical observations might be cell proliferation reported *in vivo* after bupivacaine injection into the IVD, which is potentially associated with a regenerative response <sup>314</sup>.

### **Effects of Bupivacaine on Bone Repair / Regeneration**

Bone (re)generation and formation are essential processes in the recovery period following musculoskeletal interventions. Impaired bone healing can have severe clinical consequences, such as mal- or non-union of fractures or reduced osteointegration of implants. Lucchinetti *et al.* reported a dose-dependent reduction of mineralized matrix deposition by MSCs during LA exposure, with bupivacaine being the most inhibitory. At bupivacaine concentrations of 250  $\mu\text{M}$  (= 0.008%) no osteogenesis was observed *in vitro* <sup>315</sup>. These findings are in contrast to studies in animal models assessing bone healing in the presence of bupivacaine. Fourteen and thirty-five days after hematoma infiltration with 0.25% bupivacaine following a closed diaphysis fracture in rat femora, no difference in callus composition, bone tensile strength or histological appearance was observed between bupivacaine-treated and control groups <sup>316,317</sup>. Similar results were reported in dogs for 0.5% bupivacaine infiltration <sup>318</sup>. Clinical studies describing effects of bupivacaine on bone healing is limited. Results of the few studies available seem to agree with findings from the animal studies mentioned. A retrospective cohort study assessing feasibility of hematoma block following femoral fracture in 35 children did not report delayed bone healing <sup>319</sup>. The effect of liposomal bupivacaine (120 mg) on bone healing was assessed on X-ray images taken 4-6 weeks after bunionectomy. None of the 158 patients showed evidence of impaired bone healing. However, whether the surgery included any correction osteotomy was not specified. In the case of bunionectomy only, no bone fragments would have to fuse <sup>320</sup>.

### **Effects of Bupivacaine on Wound Healing**

Wound healing is an important regenerative process following surgery. Various drugs are known to be associated with delayed or disturbed wound healing <sup>321</sup>. In an *in vitro* wound healing scratch assay, MSCs were cultured using medium supplemented with 20 ng/mL TNF-alpha and exposed to bupivacaine 100  $\mu\text{M}$  (=0.00325%). Following three and six hours of bupivacaine exposure, delayed migration of MSCs and delayed repopulation of the *in vitro* defect size compared with controls were observed <sup>315</sup>. Population doubling time increased significantly from 40 hours to 93 hours at these concentrations. At higher concentrations of bupivacaine, a decrease in cell count was observed. This phenomenon was accompanied by LDH release, a marker for cytotoxicity and increased membrane permeability <sup>315</sup>. However, in a rat model of wound healing, no differences regarding

amount of collagen fibers, wound tensile strength and inflammatory parameters were observed between the intervention and control group after 14 days, indicating that bupivacaine did not negatively affect wound healing<sup>322</sup>. Similar studies have been performed in mice<sup>323</sup>. After three days, no differences regarding wound surface, re-epithelialization or neutrophil numbers were observed compared to controls in both the healthy and impaired healing groups. In contrast to results from the rat model, a non-significant trend towards decreased collagen accumulation in wounds following LA administration was found in mice. However, this study did not objectify wound tensile strength and used a shorter follow-up period (3 vs 14 days)<sup>322,323</sup>.

Furthermore, results of clinical studies showed no significant differences in wound healing or scar formation in later phases when using liposome bupivacaine or conventional bupivacaine HCl. Overall, satisfactory wound healing in both interventional groups was reported across various surgical models<sup>324</sup>. A randomized clinical trial reported no wound healing complications of bupivacaine infiltration compared to control group in human breast surgery<sup>325</sup>.

### **Effects of Bupivacaine on Neural Tissue**

The musculoskeletal system, especially the spinal column, is in close relationship with the central and peripheral nervous system. To obtain anesthesia during orthopedic interventions, administering regional or spinal blocks with bupivacaine are common in the perioperative pain management.

Bupivacaine can lead to significant neuronal cell death *in vitro*. In experiment using human SH-SY5Y neuroblastoma cells, a concentration-dependent decrease in cell viability after exposure to various LAs was observed in 10 minutes. Bupivacaine had the highest toxic potency of all LAs included in the study. Cell death was primarily due to necrosis, but bupivacaine also led to apoptosis when concentration or exposure time increased<sup>326</sup>. These results are in agreement with other reports<sup>327</sup>.

*In vivo*, the effect of intraneural injection of both plain bupivacaine solution and liposomal bupivacaine was studied at clinically used concentrations in a porcine model. No persistent neurological deficits were observed 12 hours after treatment. The sciatic nerve was excised two weeks after injection and assessed for histological nerve injury. Immune cell count, cytokine mRNA and axonal density did not differ significantly in both groups when compared to controls<sup>328</sup>. In rabbits, bupivacaine led to moderate neurotoxicity (regarding CSF glutamate concentrations and vacuolation of the dorsal funiculus) of the spinal cord one week after intrathecal administration. However, the LA concentrations used in the study were higher than those used clinically<sup>329</sup>.

From a clinical perspective, persisting neurological damage from LAs is rare, with risks of neurological injury after *peripheral* nerve blocks estimated to be around 0.04%<sup>330</sup>. The risk of lasting damage is lower in *central* nerve blocks (*i.e.* spinal and epidural applications), with estimates between 1 and 4 in 100.000 cases<sup>331</sup>. The incidence of anesthesia-related neurologic complications varies, however, both over time and between studies<sup>331,332</sup>. For example, neurological deficits have been reported in 3-5% of patients two weeks after undergoing a brachial plexus block. After 4 weeks, 0.4% of patients still experienced deficits<sup>333</sup>. These numbers, apart from being at risk for publication bias, might overestimate the actual damage done by LAs, as injection pressure, needle trauma and patient positioning during surgery can also account for (persisting) neurological damage<sup>331</sup>.

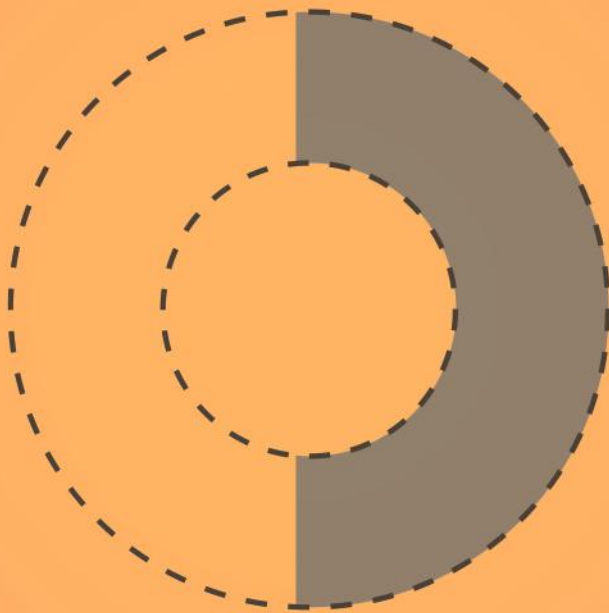
### Recent Developments

To both extend duration of action and minimize toxicity, alternative formulations of bupivacaine have been developed. Examples are liposomal formulations and biodegradable polymer matrices, with liposome bupivacaine being the only formulation to have reached market approval presently<sup>39,259–262</sup>. A hydrogel formulation of bupivacaine, liposome bupivacaine and a conventional bupivacaine solution have been tested *in vivo* in direct comparison<sup>262</sup>. Following plantar incision, rats were administered 0.1 mL near the sciatic nerve of either liposome bupivacaine (13,3 mg/mL), hydrogel matrix containing bupivacaine HCl (105 mg/mL), or the hydrogel matrix without any bupivacaine. An irritant rank score was calculated based on histological analysis, grading the presence of inflammatory cells, fibroblasts, neovascularization, fibrosis, necrosis, hemorrhage, and tissue ingrowth into the material. Mechanical pain sensitivity threshold was tested using Von Frey ligaments. Rats treated with the bupivacaine-containing hydrogel matrix tolerated higher mechanical forces on the injured paw compared to the liposomal bupivacaine group and the empty hydrogel matrix group. However, this group also displayed the highest irritant ranking scores after 5 (moderate score) and 42 (slight score) days. The empty hydrogel matrix also displayed moderate and slight irritant rank scores at 5 and 42 days, respectively, indicating local toxic effects of the matrix itself. It is pointed out that only the cumulative score was reported, preventing evaluation of specific local effects on inflammation, vascularization, necrosis and other factors. Furthermore, not only the concentration but also the cumulative dose of bupivacaine differed between the intervention and control group, hampering their comparability. No clinical trials of the hydrogel bupivacaine formulation are available yet. Liposomal bupivacaine formulations have been tested clinically; however, the analgesic advantages compared with plain bupivacaine solutions appear limited<sup>334</sup>. *In vivo*, the myotoxic effects of liposomal bupivacaine (13,3 mg/mL bupivacaine HCl) were comparable to 5 mg/mL plain bupivacaine HCl solution after 5 days, and significantly less than a 13,3 mg/mL plain bupivacaine HCl solution. However,

the degree of inflammation after two weeks was comparable between the 13,3 mg/mL bupivacaine HCl solution and liposomal bupivacaine <sup>289</sup>.

## CONCLUSIONS AND OUTLOOK

Bupivacaine is extensively used in (surgical) treatment of musculoskeletal diseases since its discovery in 1957. In bone regeneration, muscle repair, nerve damage, wound healing, and intervertebral disc damage, the *in vitro* effects of bupivacaine point towards an inhibitory effect, even at concentrations lower and exposure times shorter than those used clinically. Racemic mixtures of bupivacaine enantiomers and levobupivacaine lead to similar degrees of *in vitro* toxicity. However, in both animal and clinical studies, these effects are rarely reproduced and, if they are, appear largely reversible. In IVD, neural and muscle applications, the local toxic effects of bupivacaine displayed reversibility, albeit delayed compared to controls. Clinically observed adverse events following local toxicity of bupivacaine have seldom been reported. The local toxic effects of bupivacaine, when used as perioperative anesthetic, may have minimal impact compared to the extensive tissue damage and systemic response elicited by the surgery itself. Bupivacaine seems to induce chondrotoxicity *in vitro* and up to a certain extent also in *in vivo* and in clinical studies. Therefore, the use of bupivacaine in synovial joints might best be avoided. Recently developed liposomal and polymer matrix formulations of bupivacaine provide a longer duration of action, but with similar degrees of local toxicity. This leaves an unmet need for a LA-formulation that increases the duration of pain blockage without increasing local toxicity. As described in this review, the *in vitro* toxic effects of bupivacaine are rare in *in vivo* studies. Interestingly, if adverse effects are observed *in vivo* or clinically, they appear to be reversible. A possible explanation for the discrepancies observed between *in vitro* and *in vivo* data might be the models used to study *in vitro* toxicity of bupivacaine. Indeed, most of the *in vitro* tests are performed in two-dimensional cell cultures, which are not representative of the complex architecture and systemic absorption and metabolism of the human body. Furthermore, the inflammatory, high-perfusion, regenerative phase taking place after both bupivacaine injection and surgery is overlooked *in vitro*. In summary, this review revealed that current literature report low levels of bupivacaine local toxicity in clinically used concentrations for the majority of musculoskeletal applications.





# CHAPTER 5

## Lack of concentration-dependent local toxicity of highly concentrated (5%) versus conventional 0.5% bupivacaine following musculoskeletal surgery in a rat model

Jasper G. Steverink, Floris R. van Tol, Suzanne Bruins, Andre J. Smorenburg, Marianna A. Tryfonidou, Bas J. Oosterman, Marijke R. van Dijk, Jos Malda, Jorrit-Jan Verlaan

*Published as an Article in: Journal of Experimental Orthopaedics, 2023  
(article in press)*

## **ABSTRACT**

**Purpose:** Various sustained-release formulations incorporate high bupivacaine concentrations but data on local toxicity is lacking. This study explores local toxic effects of highly concentrated (5%) bupivacaine compared to clinically used concentrations *in vivo* following skeletal surgery, to assess the safety of sustained-release formulations with high bupivacaine concentrations.

**Methods:** Sixteen rats underwent surgery, in which screws with catheters affixed were implanted in the spine or femur in a factorial experimental design, allowing single-shot or continuous 72h local administration of 0.5%, 2.5% or 5.0% bupivacaine hydrochloride. During the 30-day follow-up, animal weight was recorded and blood samples were obtained. Implantation sites underwent histopathological scoring for muscle damage, inflammation, necrosis, periosteal reaction/thickening and osteoblast activity. Effects of bupivacaine concentration, administration mode and implantation site on local toxicity scores were analyzed.

**Results:** Chi-squared tests for score frequencies revealed a concentration-dependent decrease in osteoblast count. Moreover, spinal screw implantation led to significantly more muscle fibrosis but less bone damage than femoral screw implantation, reflecting the more invasive muscle dissection and shorter drilling times related to the spinal procedure. No differences between bupivacaine administration modes regarding histological scoring or body weight changes were observed. Weight increased, while CK levels and leukocyte counts decreased significantly during follow-up, reflecting postoperative recovery. No significant differences in weight, leukocyte count and CK were found between interventional groups.

**Conclusion:** This pilot study found limited concentration-dependent local tissue effects of bupivacaine solutions concentrated up to 5.0% following musculoskeletal surgery in the rat study population.

## INTRODUCTION

Musculoskeletal surgeries are perceived as exceptionally painful (4). Currently, postoperative pain is treated with multimodal analgesic protocols that aims to achieve synergistic effects between analgesics by targeting multiple pain pathways.(13) Frequently used analgesics in multimodal protocols include acetaminophen, non-steroidal anti-inflammatory drugs, local anesthetics and alpha-2-antagonists. Still, opioids fulfil a prominent role in analgesia after musculoskeletal surgery. Major drawbacks of opioid use are the frequency of adverse events and risk of dependence or addiction (14). Opioid use and abuse are current societal challenges, with various (inter-)national initiatives being undertaken to limit opioid-related morbidity and mortality (19). Despite treatment with opioids, poorly controlled postoperative pain is reported in up to 75% of patients (12). The limited efficacy of postoperative analgesia and drawbacks of opioids leave a clear unmet need for effective and safe pain treatment following skeletal surgery.

Because sensory nerve fibers are abundant in skeletal tissue, local anesthetics have the potential to decrease opioid consumption following skeletal surgery as part of multimodal analgesic protocols (26). With up to eight hours of analgesia, bupivacaine provides the longest duration of action of all local anesthetics (1). However, eight hours of analgesia is insufficient for most (skeletal) surgeries, driving the development of various new sustained-release formulations of bupivacaine (21). An advantage of local bupivacaine sustained-release formulations is their relatively high drug concentration at the target site, while systemic levels stay low (21). However, multiple *in vitro* studies report concentration-dependent cytotoxicity of musculoskeletal cell types following bupivacaine exposure (24). For example, bupivacaine at subclinical concentrations induces concentration-dependent decreases in mesenchymal stem cell proliferation, osteogenesis and wound healing *in vitro*, three important processes for successful recovery after musculoskeletal surgery (18). The translatability of bupivacaine *in vitro* toxicity to the *in vivo* situation has recently been reviewed (24).

Clinically, bupivacaine is used in concentrations up to 0.5% (5 mg/mL), but novel bupivacaine sustained-release formulations use concentrations ranging from 1.33% to 10.5% (9,10). Such high concentrations are necessary to provide a sufficient dose of local anesthetic for extended durations of analgesia within manageable volumes. One such sustained-release formulation for use in skeletal surgery is currently under development by the authors, for co-implantation with screws (25). However, local toxic effects of bupivacaine concentrations higher than used clinically are largely unknown, and knowledge of these effects is essential to understand the safety of bupivacaine sustained-release formulations (29). To provide insight in the *in vivo* local toxicity of

highly concentrated bupivacaine, this study infused high bupivacaine concentrations in a rat model following musculoskeletal surgery. We hypothesized that bupivacaine induced concentration-dependent toxic effects in musculoskeletal tissue after surgery.

## 2. METHODS

### 2.1 Animals

National Animal Experiments Ethical Committee approval (AVD1150020197225) was obtained before the experiments. Study design and results were reported according to the ARRIVE guideline. Male Wistar rats (Envigo, HsdCpb:WU, 8 weeks old and weighing 250 g upon arrival) were used because of their extensive use in toxicology studies and bupivacaine pharmacokinetics comparable with humans (2,16). Upon arrival, rats were randomly picked from the box upon delivery to receive an ear-marking or not. A predefined schedule was in place to dictate the cage number and ear-marking of a rat, based on the sequence of picking. In each cage, a rat without ear-mark (blank) and a rat with a left ear-mark (left) were placed. The cages were numbered, resulting in animal codes in the format [cage number]-[blank OR left]. Using an online random sequence generator ([www.randomizer.org](http://www.randomizer.org)), animal codes were matched to a treatment (consisting of administration method, administration location and bupivacaine concentration, e.g., D25S: Dosedump – 25mg/mL - Spine). Rats were housed in pairs in standard cages with cage enrichment, a 12-hour light/dark cycle and air conditioning at 23±2°C with 60% humidity. Cages were cleaned at weekly intervals. Standard rodent chow and water were provided *ad libitum*. Animals were allowed one week of acclimatization prior to surgery, with daily handling by the researchers to reduce handling-related stress during experimental procedures. Pre-operative weights were recorded. Following surgery, animals were housed in solitary cages for 72 hours to avoid conflicts between animals, damage to the catheter and wound healing problems. After 72 hours, the catheter was cut at skin level to allow subcutaneous retraction of the catheter and healing of the skin. After the catheter was cut, the rats were housed in pairs again. Each individual rat served as experimental unit.

### 2.2 Surgery

All rats received enrofloxacin (5 mg/kg), carprofen (5 mg/kg) and morphine (2.5 mg/kg) subcutaneously pre-operatively. To broaden generalizability, both a spinal and long bone (femur) application were performed. For spinal applications, rats were placed prone on a prewarmed surgery table under general anesthesia (17). The iliac crest and spinous processes were identified and a midline incision was performed 1 cm cranially from the iliac crest. The paraspinal musculature was dissected laterally to expose the transverse processes of L4-5. A 0.8 mm hole was drilled in the transverse process and a

stainless-steel screw (1\*5 mm), attached via a poly(e-caprolactone) connecting piece to a polyurethane (PU) catheter (internal diameter 0.6 mm, UNO, Zevenaar, Netherlands) was inserted, so that the catheter opening faced the bone surface (Fig. 1). Sterile saline solution was dripped next to the hole during drilling for cooling. The dead volume of catheters was pre-filled with the appropriate bupivacaine solution to ensure infusion of precise volumes. The catheter was tunneled subcutaneously towards an exit-point between the shoulders and fixed to the skin with a suture. Bupivacaine infusion was initiated after confirmed absence of motor deficits (i.e., following observed movement of tail and paws).

For femoral applications, rats were positioned laterally on the surgery table (5). A longitudinal incision was performed lateral to the femur. The vastus lateralis muscle was separated from the femur by blunt dissection. A 0.8 mm hole was drilled in the femoral shaft and a stainless-steel screw attached to a catheter was inserted. The catheter was tunneled as in the spinal application.

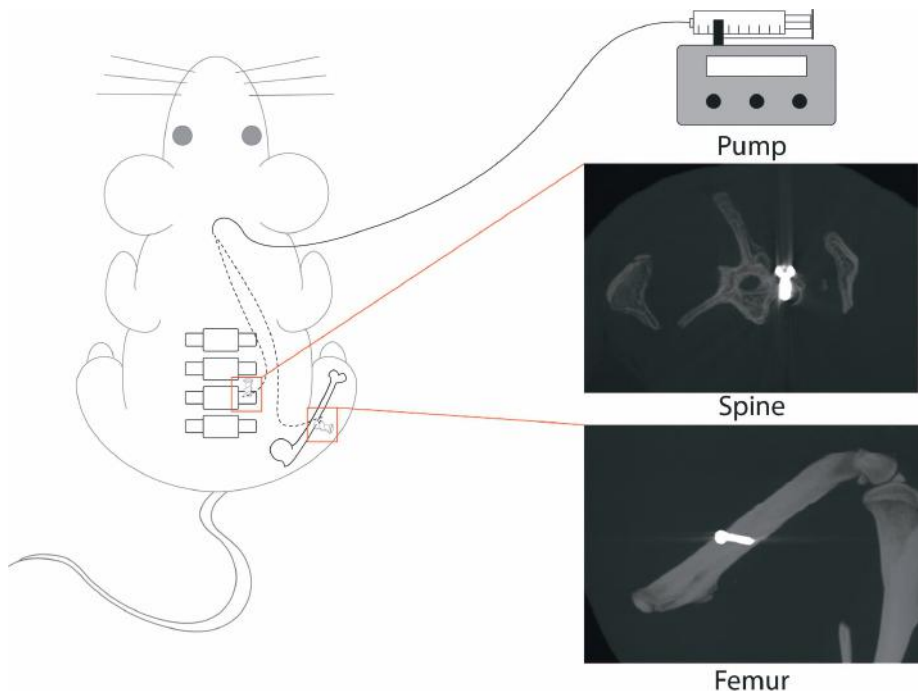


**Figure. 1** Schematic representation of experimental setup. Screws with a catheter attached were implanted in either the spine or femur. Catheters were then tunneled subcutaneously (dotted line) and exited between the shoulders. A pump was connected to the catheter to allow controlled infusion of bupivacaine solutions. Representative MicroCT images for the two surgical locations are shown.

### **2.3 Test Substance**

Clinically used bupivacaine HCl 0.5% was obtained from Aurobindo Pharma (Baarn, Netherlands). Bupivacaine HCl powder was obtained from Siegfried (Evionnaz, Switzerland) and dissolved at 2.5% and 5.0% by a licensed veterinary pharmacy (Utrecht University, Netherlands). Bupivacaine solutions were delivered through the catheter to the surgical site. Potential adsorption of bupivacaine onto the inner lining of the catheter was tested by immersing 5 cm of catheter into a 5.0% bupivacaine solution for 72h at 37°C. Following rinsing to wash away any non-adsorbed drug, bupivacaine content was determined using a previously described UPLC method and expressed as mg drug absorbed per cm of catheter (23). Catheters were attached to a gas chromatography syringe and pump, allowing precise infusion rates. Applying a factorial experimental design, rats underwent either spinal or femoral surgery and received 40 mL of bupivacaine 0.5% (clinically used control), 2.5%, or 5.0%, equating to 0.67, 3.3 and 6.7 mg/kg bodyweight, respectively. The bupivacaine solution was infused within a 10-second window (simulating dose-dumping) or in a sustained fashion (initial 50% of the total volume in the first 2 hours, followed by linear infusion of the remaining 50% over 70 hours), simulating burst release as displayed by various bupivacaine sustained-release formulations (21). This design yielded 12 combinations (Table 1). For every combination, a single rat was allocated. In case of termination of the experiment due to circumstances unrelated to the allocated treatment (e.g., technical failure, surgical complications), additional rats were available to repeat these treatments. To quantify correlations between each independent parameter (i.e., concentration, implantation site and infusion profile) and dependent parameters (i.e., histology scores, weight, leukocytes, CK), rats from the respective independent parameter subcategories were pooled.

### **2.4 Evaluation of Well-Being**

Following surgery, animals were inspected for physical attributes such as appearance, wound healing and general condition. Well-being was scored daily by experienced caretakers. Weight was measured at predetermined intervals. Animals received carprofen and enrofloxacin (5 mg/kg) once daily until 72 hours after surgery. When the clinical condition of an animal caused concern, a veterinarian was consulted and action was taken (and documented) and/or monitoring was adjusted according to dictating circumstances.

### **2.5 Systemic Toxicity: Blood and Serum Analysis**

Blood was sampled from the tail vein at 1, 2, 4, 24 and 72 hours, 11, 18 and 30 days after surgery, and a volume of 100-200mL was collected. Leukocyte counts as a marker for inflammation, and CK levels as a marker for muscle damage were quantified by a blinded veterinary diagnostic laboratory. Bupivacaine serum levels were measured using a commercially available ELISA kit (DEIA-XYL46, Creative Diagnostics, NY, USA).

## 2.6 Local Toxicity: Histological Analysis

Animals were euthanized 30 days after surgery by CO<sub>2</sub> asphyxiation. Gross necropsy was performed according to Registry of Industrial Toxicology Animal data (RITA) and North American Control Animal Database (NACAD) guidelines (20). Screw positioning and surrounding bone quality were imaged directly following euthanasia using computed tomography imaging (MicroCT: Quantum FX, Perkin Elmer, MA, USA). Implantation sites were then resected *en bloc* and stored in 4% buffered formaldehyde. To prevent metal oxidation, screws were removed prior to sample decalcification yet after tissue fixation. Thereafter, samples were decalcified (Rapid Decalcifying Solution, Klinipath, Netherlands) and embedded in paraffin. 4 mm sections were stained using hematoxylin (Haemalun, Fisher Scientific, MA, USA) & eosin (Eosine G(Y), Merck, Germany) stain. Three to five sections were assessed per animal in two locations: at the level of the screw head and in the surgical trajectory. For every animal, two sections containing either the screw hole or trajectory, and visually most extensive damage were scored in a semi-quantitative fashion by a blinded board-certified pathologist using standardized terminology (3). A Nikon Eclipse E900 microscope was used for imaging. All slides were screened for relevant tissue processes and cell types to be included for scoring. Next, the range in which these processes took place was determined on an ordinal scale (0 = absent, 1 = mild, 2 = moderate, 3 = severe). Included categories for scoring were: bone damage, fibrosis, presence of histiocytes, inflammation, necrosis, osteoblasts and periosteal reaction. Muscle tissue was separately scored for atrophy, calcifications, fibrosis, necrosis and inflammation.

## 2.7 Statistical Analysis

As this study aimed to provide a proof-of-principle of bupivacaine-induced toxicity after musculoskeletal surgery, no sample size calculations were performed. Statistical analysis was performed using Rstudio (Boston, USA). Data normality was assessed using Q-Q plots and a Shapiro-Wilk test. All continuous parameters were reported as means  $\pm$  SD. Effect of bupivacaine concentration on local toxicity scores was analyzed using Chi-squared tests, comparing the frequency of category scores (0-3) between groups. In case of significance, Chi-squared tests were combined with a Bonferroni post-hoc test to correct for multiple comparisons. Effects of infusion profile and implantation site on local toxicity scores were analyzed using Chi-squared tests. Sensitivity analyses were performed by employing multivariable ordinal logistic regression analysis (supplementary information). Weight, CK and leukocyte counts were analyzed as dependent parameters using mixed-effects models. Time since surgery, infusion profile, bupivacaine concentration, implantation site and any interactions between these factors were used as fixed effects, while also incorporating a random intercept for each individual rat and a random slope for time since surgery per individual rat. To determine significance,  $p < 0.05$  was used.

### **3. RESULTS**

#### **3.1 Evaluation of Well-Being and Complications**

Sixteen rats underwent surgery. One rat (L5F) died shortly after surgery because of excessive blood loss following femoral drilling and was replaced. Taking into account the blood loss during surgery and evident hypovolemic shock (e.g., pallor), the death was considered unrelated to drug exposure and the treatment was therefore repeated in another rat. All other animals recovered without incidents from surgery. In one rat (L25F), the catheter broke after 8h of infusion, necessitating a reiteration of the experiment to ensure adequate bupivacaine exposure. Following surgery and bupivacaine administration, rat D50F displayed abnormal behavior: gagging, drooling, rhonchi, and tachypnea. The rat received atropine (0.1 mg/kg) treatment and recovered the day after surgery. Because a potential relationship between dose dumping of a high concentration of bupivacaine and these symptoms could not be excluded, the 5.0% bupivacaine dose-dump scenario for both a spinal and femoral administration were repeated in two rats (D50F and D50S). Repeat rats receiving the 5.0% bupivacaine dose-dump scenario did not undergo histological analysis. MicroCT imaging did not display signs of impaired bone healing in any rat (e.g., radiolucent areas around the screws). Furthermore, all screws were tightly anchored in the bone upon post-mortem retrieval. During gross examination following termination, petechia in the thymus were reported in two rats (L5S and L50S).

#### **3.2 Histological Analysis of Local Toxicity**

Cartilaginous new bone formation around the screw, fibrosis, presence of histiocytes, periosteal thickening and varying degrees of inflammation were evident after femoral implantation (Fig. 2A). Following spinal implantation, periosteal reaction, muscle fibrosis, muscle atrophy, and presence of histiocytes were reported (Fig. 2B).



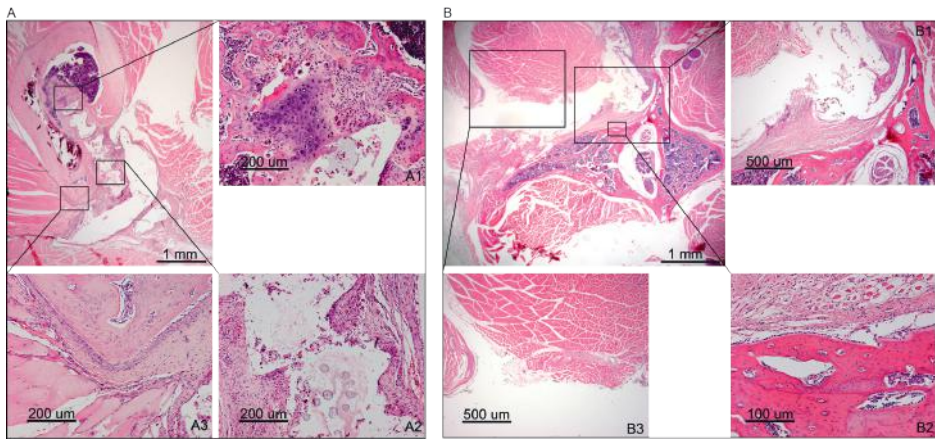


**Figure 2.** Representative histology images. A) Hematoxylin and eosin staining of a femoral implantation site with cartilaginous new bone formation in the screw trajectory (A1), fibrous capsule formation around the screw head (A2) and periosteal thickening (A3). B) Hematoxylin and eosin staining of a spinal implantation site with fibrous capsule formation around the screw head (B1), abundant osteoblasts lining the cortex (B2) and muscle fibrosis (B3).

Individual rat histology scores are displayed in Table 1. Preparation of histology slides failed in rat D5S, as the tissue had been damaged during resection and was no longer suitable for sectioning. Necrosis was absent in all of the samples studied. Fibrosis, histiocyte infiltration, inflammation, muscle atrophy, muscle calcification, muscle inflammation and periosteal reaction scores were not significantly influenced by bupivacaine concentration, administration site or administration profile (Fig. 3). Increasing bupivacaine concentration led to a significant decrease in osteoblast count ( $p = 0.045$ ). Bonferroni post-hoc analysis revealed that the significant difference existed between the clinically used 0.5% concentration and the 5.0% concentration. A significant increase in bone damage ( $p = 0.004$ ) and decrease in muscle fibrosis ( $p = 0.015$ ) was observed when comparing femur with spine. Multivariable sensitivity analysis confirmed these findings (supplementary).

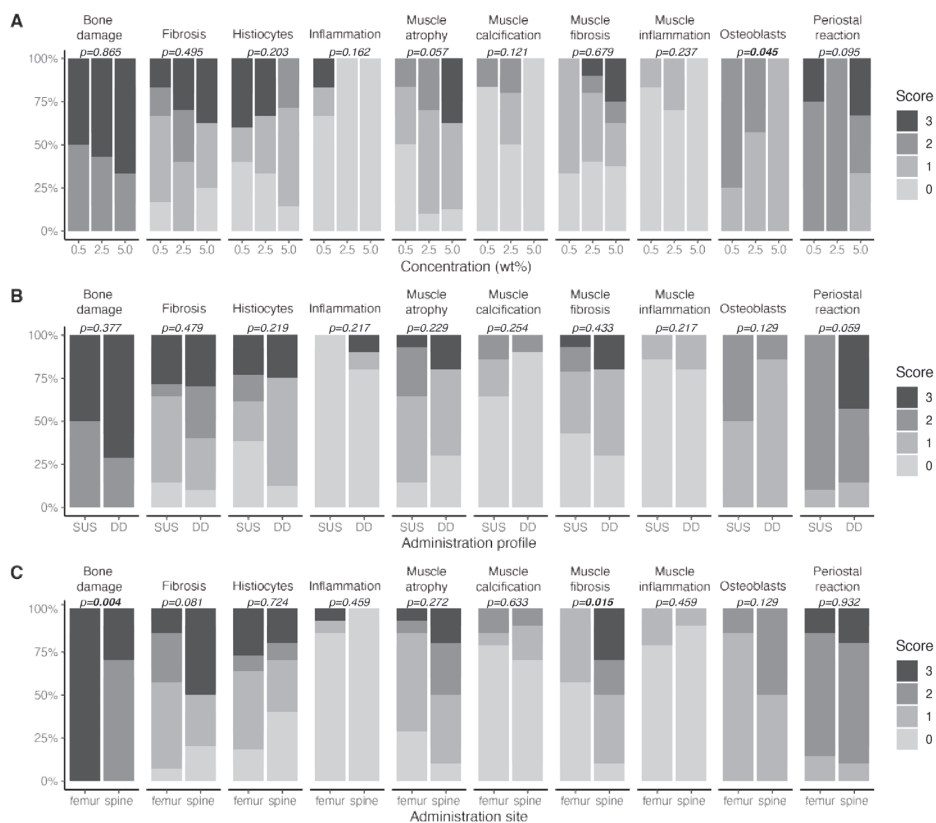


**Figure 3.** Bar charts displaying the frequency of histology scores per histological parameter as a function of A) bupivacaine concentration administered (wt%), B) bupivacaine administration profile (SUS – Sustained administration, DD – Dose Dump administration) and C) administration site (spine and femur). P-values obtained from Chi-squared tests are displayed. In case of a significant Chi-squared test and comparison between >2 groups, a post-hoc Bonferroni testing was performed.

### 3.3 Secondary Outcomes

Body weight was used as indicator for general animal well-being (27). Following an expected initial decrease after surgery, weight increased steadily during postoperative recovery (Fig. 4). Rats undergoing dose-dump administration experienced a steeper decrease in postoperative weight, but recovered as fast as rats receiving continuous infusion. Postoperative leukocyte counts and CK levels are shown in Fig. S1 and Fig. S2, respectively. No delayed or disturbed wound healing was observed in any interventional group. Bupivacaine adsorption per cm of PU catheter was  $2.5 \pm 0.7$  mg, when administering 5.0% bupivacaine. As 1 cm of catheter (diameter 0.6 mm) had a volume of  $2.8 \text{ mm}^3$ , 14 cm of catheter contained 40 mL bupivacaine infused. This led to a potential loss of bupivacaine of  $2.5 \text{ mg/cm} \times 14 \text{ cm} = 35 \text{ mg}$ . Taking the small adsorption values

into account (35 mg on a total dose 2000 mg in the 5.0% bupivacaine group), this effect was presumed minimal.

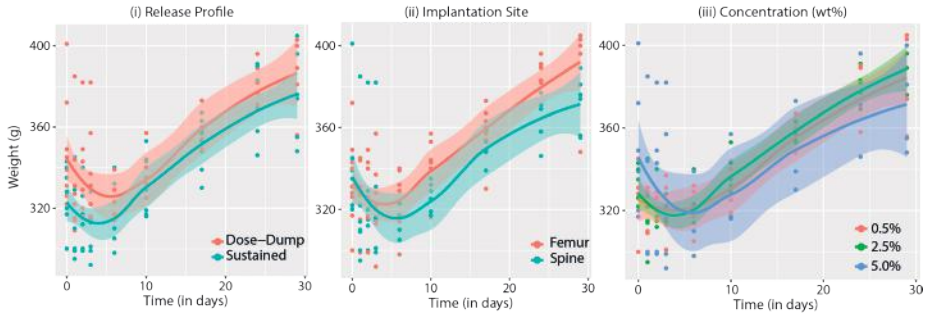


**Figure 4.** Body weight changes in rats undergoing surgery and infusion of bupivacaine. Median body weight and interquartile range (IQR) are shown. (i) Weight changes over time in rats receiving bupivacaine infusion in a dose-dump or sustained fashion. (ii) Weight changes over time in rats undergoing spinal or femoral catheter implantation and bupivacaine infusion. (iii) Weight changes over time in rats receiving infusion of 0.5%, 2.5%, or 5.0% bupivacaine HCl solution.  $T=0$  marks preoperative weight.

Mixed-effect model analysis yielded no significant effects of implantation site, infusion profile or bupivacaine concentration on CK levels or leukocyte counts. Analysis of relations between fixed-effects displayed a positive interaction between time since surgery and weight (regression coefficient 0.91,  $p = 0.012$ ) and negative interactions between time since surgery and CK (regression coefficient -16.354,  $p < 0.001$ ) and time since surgery and leukocyte counts (regression coefficient -0.52,  $p = 0.001$ ). Dose-dump bupivacaine administration led to serum concentrations ranging from below the assay detection limit of 5 ng/mL (when 0.5% bupivacaine was infused) to 170 ng/mL (infusion of 5.0% bupivacaine). All values were an order of magnitude below known systemic toxic values (11,15). Bupivacaine serum levels following sustained administration were below the detection limit of the ELISA kit, regardless of the infused concentration. Gross examination following euthanasia revealed petechiae in the thymus in two rats. This finding can be explained by the employed euthanasia method ( $\text{CO}_2$  asphyxiation), as presence of intrathoracic petechiae has been linked to asphyxiation in previous studies (7).

**Table 1.** Treatment allocation, and histology subcategory scores for individual rats. 0 = None, 1 = Mild, 2 = Moderate, 3 = Severe, x = unable to score. Histology failed in one rat (rat 8 – D5S). DD = dose-dump administration, SUS = sustained administration.

Animal ID	Concentration (%)	Profile	Assessment	Muscle												
				Fibrosis	Atrophy	Calcifications	Necrosis	Inflammation	Inflammation	Bone damage	Periosteal reaction	Osteoblasts	Histiocytes	Necrosis	Fibrosis	
Spine	L5S	0.5	SUS	Trajectory	1	2	2	0	0	0	2	2	2	0	0	1
				Screw head	1	1	0	0	0	0	2	2	2	0	0	1
	D5S	0.5	DD	Trajectory	Histology failed											
				Screw head	Histology failed											
	D25S	2.5	DD	Trajectory	3	1	0	0	1	0	3	2	2	1	0	3
				Screw head	1	1	0	0	0	0	2	2	1	0	0	1
	L25S	2.5	SUS	Trajectory	2	2	1	0	0	0	2	2	2	3	0	3
				Screw head	1	2	1	0	0	0	2	2	2	3	0	3
	D50S	5.0	DD	Trajectory	3	3	0	0	0	0	2	3	1	1	0	3
				Screw head	0	0	0	0	0	0	3	3	1	1	0	3
L50S	5.0	SUS	Trajectory	3	3	0	0	0	0	3	2	1	2	0	0	
			Screw head	2	1	0	0	0	0	2	1	1	0	0	0	
Femur	L5F	0.5	SUS	Trajectory	0	0	0	0	0	0	x	x	x	3	0	1
				Screw head	1	1	0	0	0	0	3	2	2	1	0	3
	D5F	0.5	DD	Trajectory	0	0	0	0	0	1	x	x	x	x	0	0
				Screw head	1	0	0	0	1	3	3	3	1	3	0	2
	L25F	2.5	SUS	Trajectory	0	1	2	0	1	0	x	x	x	x	0	2
				Screw head	0	2	1	0	1	0	3	2	1	1	0	1
	D25F	2.5	DD	Trajectory	1	1	0	0	0	0	x	x	x	1	0	2
				Screw head	0	1	2	0	0	0	3	2	1	3	0	2
	L50F	5.0	SUS	Trajectory	0	1	0	0	0	0	3	2	1	1	0	1
				Screw head	0	1	0	0	0	0	3	2	1	1	0	1
D50F	5.0	DD	Trajectory	1	1	0	0	0	0	x	x	x	x	0	1	
			Screw head	1	3	0	0	0	0	3	1	1	1	0	1	
L25F	2.5	SUS	Trajectory	0	0	0	0	0	0	x	x	x	0	0	1	
			Screw head	1	1	0	0	0	0	3	2	1	0	0	1	

## DISCUSSION

This study explored the local toxicity of highly concentrated bupivacaine in a skeletal surgery rat model, using the current clinical maximum concentration of 0.5% as a control. Bupivacaine is a frequently used local anesthetic in skeletal surgery, and has recently been applied in novel extended-release formulations at concentrations considerably higher than used in clinical practice (6,10). By employing a factorial design, the present study investigated the interaction between the administered concentration, implantation site and infusion profile. In line with *in vitro* reports on concentration-dependent inhibition of osteogenesis by bupivacaine, increasing bupivacaine concentrations significantly decreased osteoblast counts 30 days after spinal or femoral surgery (18). However, no corresponding change in bone damage was found. Moreover, CT-imaging and screw explantation suggested undisturbed bone healing. No concentration-dependent muscle damage was observed, corresponding to previous animal studies showing regeneration of bupivacaine-induced muscle damage after three weeks (30). Significantly more bone damage was observed in rats that underwent femoral surgery compared with spinal surgery. Likely, longer drilling times and subsequent heat generation in the much thicker cortex of the femur can explain this difference. In contrast, significantly more muscle fibrosis was observed in spinal surgery compared with the femur. This can be attributed to the more invasive nature of the spinal procedure: the paraspinal musculature was sharply dissected to expose the transverse processes, while blunt preparation between layers of the lateral vastus muscle was sufficient to obtain exposure of the femur. No significant differences between sustained and dose-dump administration were observed for any histological parameter. Altogether these findings agree with previous studies on 0.25% and 0.5% bupivacaine, indicating that the reported *in vitro* toxicity of bupivacaine does not translate to *in vivo* situations, where regenerative processes can take place (8,24). This conclusion now appears to be extendable to higher concentrations of bupivacaine.

No significant effects of bupivacaine concentration, implantation location or infusion profile on weight, CK or leukocyte counts were present in the mixed-effects model. Weight, CK and leukocyte counts correlated with the elapsed time since surgery, reflecting uncomplicated postoperative recovery. Despite the small study population and group size, the factorial experimental design allowed for exclusion of large effects of highly concentrated bupivacaine on skeletal local toxicity following surgery because of the inherent hidden replication, averaging the results over the levels of the other factors (22). Moreover, multivariable sensitivity analysis yielded results equal to univariable analysis (supplementary). Univariate analyses were retained for clarity and readability. Reported bone healing rate in rats would have allowed assessment of effects of bupivacaine concentrations on bone healing, if present (28). As all rats underwent surgery to receive

bupivacaine infusion, the present results regarding the local toxicity of highly concentrated bupivacaine cannot simply be extrapolated to a non-surgical population. The addition of a control group receiving surgery but not bupivacaine would have further strengthened the conclusion that any local toxicity induced by bupivacaine is minor compared with the tissue damage through surgery, and its absence is a limitation of this study.

In conclusion, this preclinical study underlines the potential of newly developed sustained-release formulations of bupivacaine, as no major concentration-dependent local toxicity of high bupivacaine HCl concentrations was found following musculoskeletal surgery in the rat study population.

### **SUPPLEMENTARY INFORMATION – SENSITIVITY ANALYSIS**

Following parametric testing of histology outcomes, a sensitivity analysis was performed by employing multivariable ordinal logistic regression analysis, setting histology subcategory as dependent variable and infusion profile (dose-dump vs sustained), bupivacaine concentration (0.5% vs 2.5% vs 5.0%) and implantation site (spine vs femur) as independent variables. For all statistical analysis,  $p < 0.05$  was used to determine significance.

Multivariable logistic regression analysis revealed a significant effect of administration site on the severity of muscle fibrosis, corresponding to Chi squared test outcomes in the manuscript. Further, a significant effect of bupivacaine concentration on the severity of muscle atrophy was present. The significant effect of bupivacaine concentration on osteoblast count found in Chi squared testing was not reproduced in multivariable testing. No analysis for necrosis was performed. No other significant effects of concentration or infusion profile were observed in the multivariable logistic regression models.

**Table S1.** Multivariable ordinal logistic regression analysis of the effects of bupivacaine solution concentration, implantation site and infusion profile on cumulative and subdivisions of local toxicity scores. Significant p-values are presented in **bold**.

Administration profile	Concentration (mg/mL)	Necrosis		Fibrosis		Inflammation		Bone damage		Periosteal damage		Osteoblasts		Histocytes		Muscle fibrosis		Muscle atrophy		Muscle necrosis		Muscle calcification		Muscle inflammation				
		Coef (SE)	P-value	Coef (SE)	P-value	Coef (SE)	P-value	Coef (SE)	P-value	Coef (SE)	P-value	Coef (SE)	P-value	Coef (SE)	P-value	Coef (SE)	P-value	Coef (SE)	P-value	Coef (SE)	P-value	Coef (SE)	P-value	Coef (SE)	P-value	Coef (SE)	P-value	
5	25	ref	0.996 (0.300)	ref	-17.09 (72.5)	0.814	5.902 (32.9)	0.858	1.713 (1.52)	0.261 (60.49)	-15.56 (60.49)	0.797	-0.207 (1.13)	0.855 (1.03)	0.148	0.886 (1.04)	1.580 (1.04)	0.128	ref	1.373 (1.29)	0.289 (1.34)	0.854 (1.34)	0.525	ref	1.373 (1.29)	0.289 (1.34)	0.854 (1.34)	0.525
	50	ref	0.024 (1.08)	0.983 (0.983)	-17.35 (79.1)	0.827	7.089 (32.9)	0.829	-1.756 (1.67)	0.293 (106.6)	-38.45 (106.6)	0.718	0.073 (1.10)	0.947 (1.10)	0.800	0.468 (0.89)	2.337 (0.89)	<b>0.0497</b>	0.468 (0.89)	ref	-6.969 (24.5)	0.776 (29.3)	-7.210 (29.3)	0.806	ref	-6.969 (24.5)	0.776 (29.3)	-7.210 (29.3)
Femur	Spine	Not analyzed, no cases of necrosis	ref	0.649 (0.82)	0.428 (0.82)	-0.961 (70.81)	0.989	-14.9 (46.2)	0.747	0.600 (1.17)	22.71 (70.3)	0.609	-0.786 (0.85)	0.353 (1.24)	3.551 (1.24)	<b>0.004</b>	1.642 (0.89)	0.065 (0.89)	ref	0.420 (1.07)	0.696 (1.34)	-0.854 (1.34)	0.525	ref	0.420 (1.07)	0.696 (1.34)	-0.854 (1.34)	0.525
			Not analyzed, no cases of muscle necrosis	ref	0.662 (0.80)	0.408 (0.80)	16.55 (61.7)	0.788	1.187 (1.60)	0.459	2.340 (1.43)	0.101 (49.0)	-14.18 (49.0)	0.772	0.548 (0.86)	0.524 (0.858)	0.979 (0.858)	0.254 (0.86)	-0.852 (0.86)	0.320 (0.86)	ref	-1.435 (1.31)	0.272 (1.20)	0.673 (1.20)	0.575	ref	-1.435 (1.31)	0.272 (1.20)

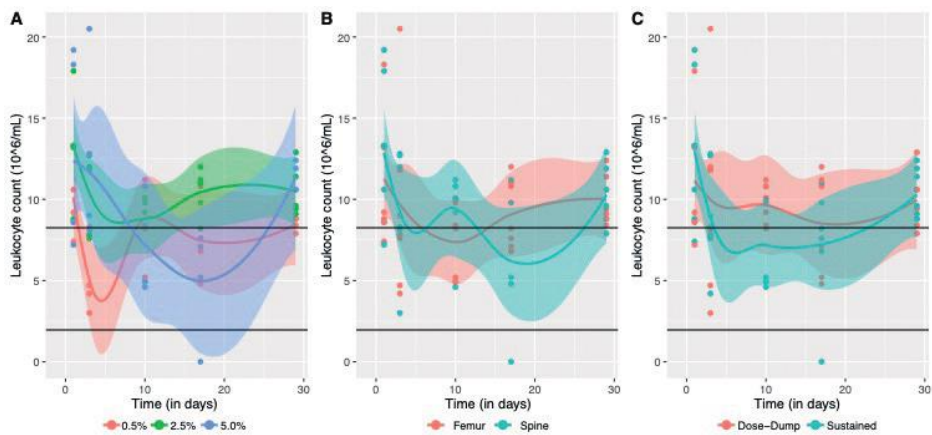


**Figure S1.** Leukocyte counts (in millions per mL) after surgery.  $T=0$  marks the day of surgery. A) Leukocyte counts grouped by bupivacaine concentration. B) Leukocyte counts grouped by administration location. C) Leukocyte counts grouped by administration profile. The horizontal black bars represent the normal limits provided by the laboratory.

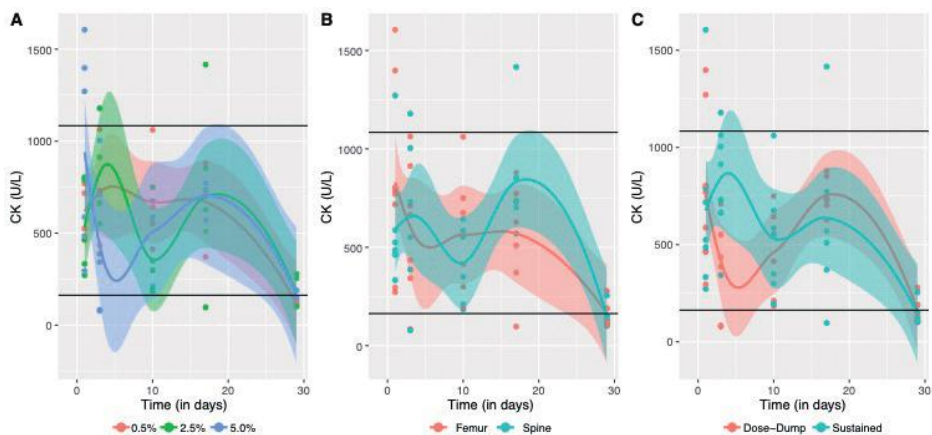
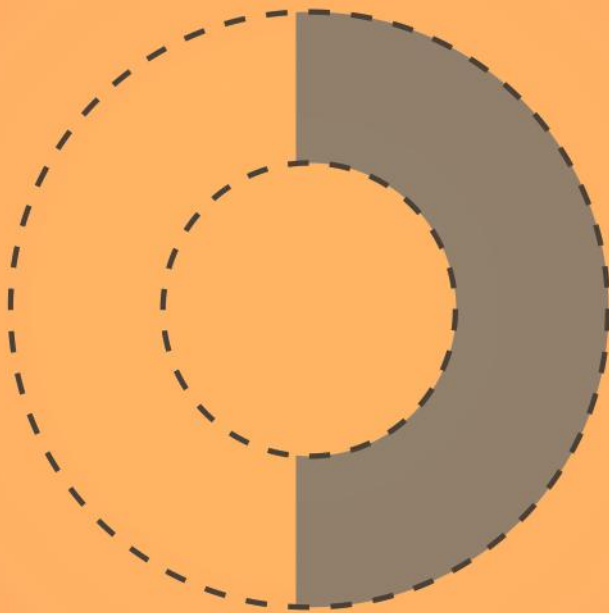


**Figure S2.** Creatine Kinase (CK) levels (in units per L) after surgery.  $T=0$  marks the day of surgery. A) CK levels grouped by bupivacaine concentration. B) CK levels grouped by administration location. C) CK levels grouped by administration profile. The horizontal black bars represent the normal limits provided by the laboratory.







# CHAPTER 6

## Exploratory study into the *ex vivo* conduction properties and local anesthetic susceptibility of nervous tissues

Jasper G. Steverink, Douwe Oostinga, Susanna Piluso, Jos Malda, Jorrit-Jan Verlaan

*In manuscript*

## **ABSTRACT**

Patients undergoing instrumented spinal surgery frequently suffer from severe postoperative pain. Recent histological studies point towards the periosteum as a structure that receives dense sensory innervation and is inevitably damaged during skeletal surgery. Exploratory clinical studies have demonstrated the susceptibility of periosteum to the application of local anesthetics, significantly decreasing the perception of pain after sternotomy. We hypothesized that the periosteum is a major contributor to postoperative pain, which can be treated using local anesthetics. Local anesthetics inhibit action potential conduction in nerve fibers by blocking of voltage-gated sodium channels. However, the concentration needed to inhibit action potential conduction is unknown. This study describes the development and optimization of an *ex vivo* neurophysiological setup to quantify conduction properties of mammalian innervated tissues. Then, bupivacaine is applied in varying concentrations to study its effect on action potential conduction. A reversible bupivacaine-induced block of sheep femoral nerve could be obtained. However, we were not able to record stable measurements in sheep, nor human periosteum. Various suggestions for further optimization of the setup are provided. The results of this exploratory study can contribute to a better understanding of the neurophysiological basis and potential treatment of skeletal pain.

## 1. INTRODUCTION

Severe skeletal pain is a frequently reported symptom by patient suffering from skeletal diseases or following skeletal surgery<sup>12</sup>. This pain severely impacts functional status of these patients<sup>56,114–116,159</sup>. To decrease the sensation of pain, multiple targets can be identified for application of analgesic drugs<sup>6,7</sup>. Each target is susceptible to a certain type of drug, depending on its mode of action. Systemic analgesics, such as morphine, act centrally by blocking mu-opioid receptors in the central nervous system<sup>67</sup>. However, opioid receptors are also present in brain structures associated with respiration. Blocking these receptors can lead to adverse events, such as respiratory depression, associated with the use of opioids<sup>357</sup>.

Regional and local analgesic treatment does not alter pain perception, but rather the conduction of nociceptive stimuli to the central nervous system. Local anesthetics (LA) of the amino-amide type are a class of drugs blocking the conduction of sensory action potentials<sup>358,359</sup>. The mechanism of action of LAs, such as lidocaine and bupivacaine, involves blocking of sodium influx through voltage-gated sodium channels<sup>360,361</sup>. This inhibits any action potential from being conducted through the network of sensory fibers, thereby theoretically eliminating nociception for the duration of action of the respective LA<sup>362</sup>. The pKa of bupivacaine is 8.1 and this means, following the Henderson-Hasselbalch equation that the ionized and non-ionized fraction are equal at a pH of 8.1. Only the non-ionized fraction can cross the phospholipid bilayer of mammalian cells and exert its anesthetic action inside the neuron. The anesthetic potential of local anesthetics hence depends on environmental pH<sup>281,363</sup>. All sensory nerves are susceptible to bupivacaine. Sensory nerves can be classified based on their diameter, myelination and conduction velocity. Erlanger and Gasser have classified nerve fibers into various categories based on these characteristics in 1937, resulting in A-, B- and C-fibers<sup>364</sup>. The susceptibility to LA-induced blockage of conduction is different for each category<sup>361</sup>. This phenomenon, termed differential activity, has been studied in nervous tissue obtained from various animal species, including rat, cat, rabbit and giant squid<sup>361,362,365–367</sup>. These studies reported that large fast-conducting fibers can be blocked with a lower LA concentration compared to smaller slow-conducting fibers<sup>361,362,365</sup>. This suggests that A $\delta$ -fibers (conduction velocity  $\sim$ 20 m/s) are more sensitive to the action of LAs compared to C-fibers (conduction velocity  $\sim$ 1 m/s), as A $\delta$ -fibers are myelinated and their diameters are 1-5  $\mu$ m, and 0.2-1.5  $\mu$ m, respectively<sup>137,139</sup>. For example, Gissen *et al.* found bupivacaine concentrations leading to a 50% action potential amplitude reduction to be four times higher in C-fibers, compared to A-fibers (0.201 vs 0.048 mM, respectively, pH 7.4)<sup>361</sup>. For clinical reference, a 288 mg/L solution of bupivacaine equates to 1 mM, far lower than the concentrations at which bupivacaine is commercially available (2.5, 5.0 and 7.5 mg/mL).

The density of sensory innervation is particularly high in mammalian osseous structures, providing an explanation for the severe pain experienced after skeletal surgery<sup>17,336</sup>. In particular, A $\delta$ -fibers and C-fibers are the types of sensory nerve fibers that predominantly conduct noxious stimuli from the bone<sup>17,137</sup>. The highest innervation densities are reported in the periosteum<sup>17,126,336</sup>. Its dense sensory innervation makes the periosteum a logical target for analgesic therapy. During skeletal surgery, the periosteum is easily accessible for the application of local anesthetics following muscle dissection. In fact, clinical studies have shown potential for the use of LAs in treating periosteum-derived postsurgical pain<sup>34,35</sup>. To this end, bupivacaine solutions are infiltrated into musculoskeletal tissues. However, bupivacaine can induce concentration-dependent toxicity in a variety of musculoskeletal tissue types<sup>339</sup>. Ideally, the bupivacaine dose and concentration administered is sufficient to block action potential conduction but too low to induce toxic effects is applied to nervous tissues. Which dose or concentration is sufficient to obtain analgesia in periosteum is as of yet unknown. For an improved understanding of nervous tissue conduction properties and susceptibility to LA treatment, an *ex vivo* set-up is desirable. *Ex-vivo* setups provide a means to isolated studying of nociceptive stimulation in various sensory fiber types, in their original anatomical configuration. Further, it removes the effects of nociceptive signal conduction and subsequent modulation that results in the sensation of pain in the central nervous system, as occurs in animal studies. To this end, an electrophysiological setup was developed, based on previously reported experiments<sup>361,362</sup>. The present pilot study focuses on the experimental *ex vivo* setup and design of protocols to examine conduction properties of mammalian nervous tissue, and the potential of LAs to inhibit conduction in these tissues. This might provide valuable input on the pathophysiology and treatment of skeletal pain.

## 2. METHODS

### 2.1 Tissue collection and processing

This study used tissue samples from both human patients and cadaveric sheep. All human patients have given prior broad informed consent for anonymized use of excised tissue after surgery. Sheep cadavers were available from prior animal experiments at the Shared Animal Laboratory (GDL) in Utrecht and no prior ethical approval was necessary. None of the sheep included were exposed to systemic treatments or treatments at the site of tissue harvest during the animal experiments. Samples of periosteum (3x1 cm) and samples of femoral nerves (3 cm length) were collected from cadaveric sheep and stored in PBS immediately after harvesting. To prevent interference of joint disease in measurements, periosteum samples were taken from midshaft sections of femur and tibia. Measurements were always performed within 4 hours after the death of the animal.

Human periosteum was harvested from femoral necks that were explanted during total hip replacement surgery. All patients consented to anonymous use of surgical waste tissue for research purposes. Immediately after surgery, the femoral neck was collected, and surgical damage to the periosteum was assessed visually. If the periosteum was substantially damaged due to surgery, the femoral neck was discarded. Before the periosteum was taken off, excess fat, muscle and ligaments were removed using a scissor and a surgical blade No. 20 (Swann-Morton, Sheffield, UK). Approximately 3x1 cm of periosteum was taken off by gentle scraping using the surgical blade. The collected periosteum was hydrated in body-stimulating fluid (Liley solution), and measurements were performed as soon as possible, but always within 4 hours after femoral neck explantation. Liley solution (used for the lateral compartments and as a control before drug perfusion) consisted of NaCl, 136.8 mM; KCl, 5.0 mM; CaCl<sub>2</sub>, 2.0 mM; MgCl<sub>2</sub>, 1.0 mM; C<sub>6</sub>H<sub>12</sub>O<sub>6</sub>, 11.0 mM; and HEPES buffer (4-(2-hydroxyethyl)-1-piperazineethanesulfonic acid), 2.53 mM. The pH was adjusted to 7.4 with the use of NaOH, 0.1 M <sup>361,362</sup>.

### 2.2 Experimental setup: periosteal chamber

The periosteal chamber was made of polydimethylsiloxane (PDMS) (Farnell, Leeds, UK), and consisted of three communicating compartments (Figure 2). Chamber design was based on previous experiments by Wildsmith *et al.*, and Gissen *et al.* <sup>361,362</sup> The dimensions of the periosteal chamber were 70x30x15 mm (LxWxH). The dimensions of the two lateral compartments (stimulating and recording) were 20x20x7.5 mm, and those of the central compartment were 10x20x7.5 mm. The lid contained perfusion ports for all compartments, and two septa of 3 mm wide, which were used to ensure electrical isolation between compartments (Figure 1). The two lateral compartments acted as baths and contained Liley solution, while the middle compartment could be perfused with drug

solution. Platinum-wired stimulating and recording electrodes were fixed in the two lateral compartment walls to ensure consistent positioning between measurements (Figure 1). The stimulating electrodes were placed 2 mm apart and the recording electrodes were situated 5 mm aside. In one lateral compartment corner a reference electrode (part of the recording electrodes) was placed to avoid interference with measurements.

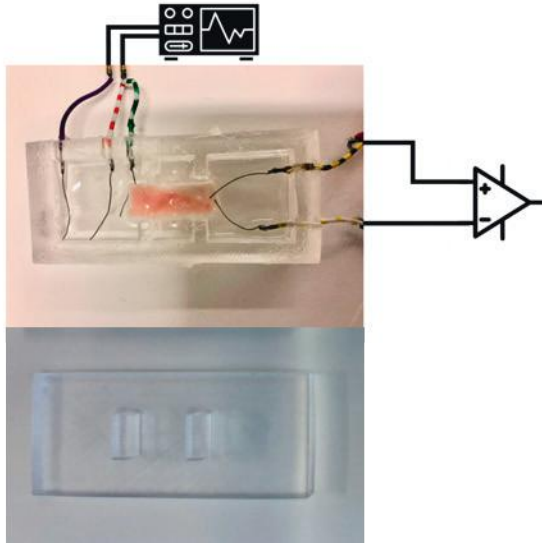


**Figure 1.** The upper image displays a schematic representation of the experimental setup. The middle chamber contains nervous tissue, which is situated across the three compartments. The stimulating electrodes are placed in the right lateral compartment and connected to a pulse generator. The recording electrodes are placed in the left lateral compartment and connected to a recorder. The reference electrode (purple) is placed in the corner of the left lateral compartment. The bottom image displays the lid with the two septa. The locations of the electrodes were altered until a conduction signal with a maximum peak-to-peak amplitude was obtained.

### 2.3 Experimental setup: electrical system

The electrical stimulus was repeated once every second (1 Hz), the duration was set at 0.1 ms (pulse width), and the stimulus intensity was set at 10 mA. The stimulus voltage generated by a stimulus isolator (ADInstruments, Sydney, NSW, AU) was 10 V. Measurements were recorded with the Neuro Amp EX (ADInstruments), and displayed with LabChart 7 Pro (ADInstruments) (Figure 2). Any electrical signal arising at the recording electrodes was led into the recorder, and then transmitted into the PowerLab (ADInstruments) data acquisition device, which was connected to a computer (Figure 2). The electrical stimulus from the stimulator was both sent to the stimulating electrodes and to the data acquisition device to couple the stimulated signal with the recorded signal



(Figure 3). Data was subsequently visualized as the mean and standard deviation (SD) of 10 measurements using Rstudio.

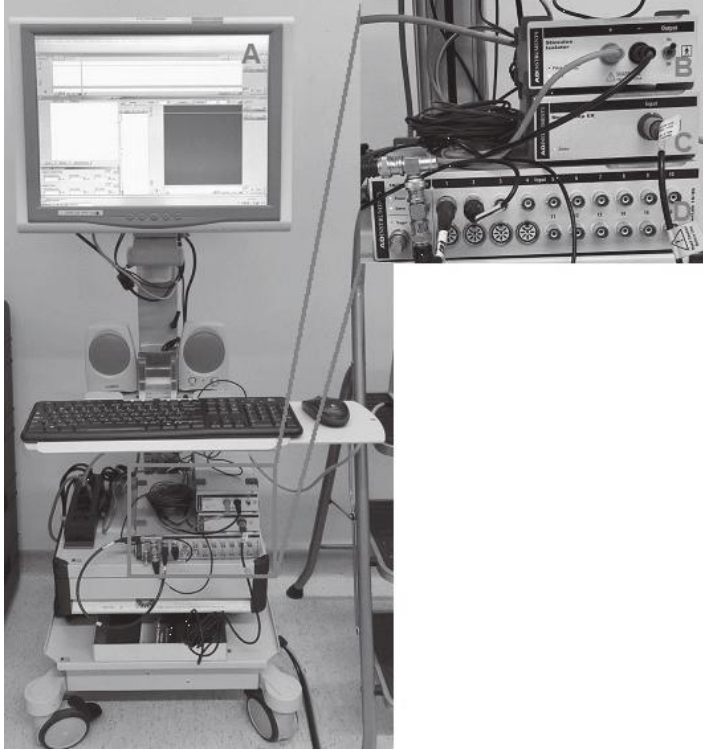


**Figure 2.** The electrical setup containing a computer equipped with LabChart (A), a pulse generator (B), recorder (C), and data acquisition hardware (D). The stimulating electrodes (red and black) were connected to the pulse generator, and the recording electrodes were connected to the recorder.

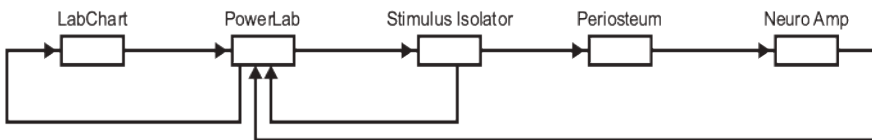


**Figure 3.** A schematic overview of the electrical circuit used in the experimental setup. LabChart was programmed to generate pulses using the data acquisition hardware (PowerLab) and pulse generator (Stimulus Isolator). The electrical pulse was sent to the tissue, and back to the data acquisition hardware and LabChart. The recorder (Neuro Amp) measured any electrical signal at the other end of the tissue, which was sent to the data acquisition hardware and visualized in LabChart.

### 3. RESULTS

#### 3.1 *Ex vivo* conduction measurements

First, three control measurements were performed as a reference for the tissue measurements. The first control was a measurement on an empty tissue chamber to test for signal absence and visualize the amount of noise. The second control was a measurement on the tissue chamber with all three compartments filled with PBS solution. This measurement was used to obtain reference values in the event of compartment leakage. The third control was a measurement on the tissue chamber with all three compartments filled with bupivacaine HCl solution. This measurement was used to visualize the conduction signal in bupivacaine HCl. After the quick control measurements, the nervous tissue (periosteum or nerve) was positioned across the three compartments, and the two septa and outer walls of the middle chamber were sealed with paraffin jelly (Vaseline, Unilever, London, UK). The measurement settings were tuned based on the electrical properties of A $\delta$ -fibers and C-fibers, as these nerve fibers are the most abundant nerve fibers in the periosteum.<sup>17,336</sup>

The first measurement on nervous tissue was with all three compartments filled with simulated body fluid. During these measurements it was tried to deduce an action potential from the nervous tissue conduction curve. Hereafter, fluid from the middle compartment was aspirated and substituted with a 0.5% bupivacaine HCl solution (Aurobindo, Baarn, Netherlands). Measurements were performed for at least 10 min, corresponding to the clinical onset of action of bupivacaine. Hereafter, all three compartments were drained again, and the nervous tissue was discarded.

#### 3.2 Control measurements

Before electrical measurements were performed on nervous tissue, first three control measurements were carried out. The first control consisted of PBS only in all three chambers, which yielded a stable signal without peaks observed, apart from the stimulus artefact at T=0 with a mean peak-to-peak amplitude of 13  $\mu$ V (Figure 4A). The second control consisted of empty chambers. A noisy signal was obtained, with a stimulus artefact at t=0. The peak-to-peak amplitude was 90  $\mu$ V (Figure 4B). The last control consisted of all three chambers filled with bupivacaine HCl solution at 25 mg/mL. Similar to readings in PBS- and air-filled chambers, a noisy signal was obtained. The peak-to-peak amplitude of the stimulus artefact was 26  $\mu$ V, which was slightly higher than the amplitude in PBS (Figure 4C). All measurements on sheep tissue (periosteum and nerve) were performed in PBS, while measurements on human periosteum were performed in Liley solution. Liley solution demonstrated an approximate amplitude of 300 mV. Control readings for Liley solution are shown in Figure S1.

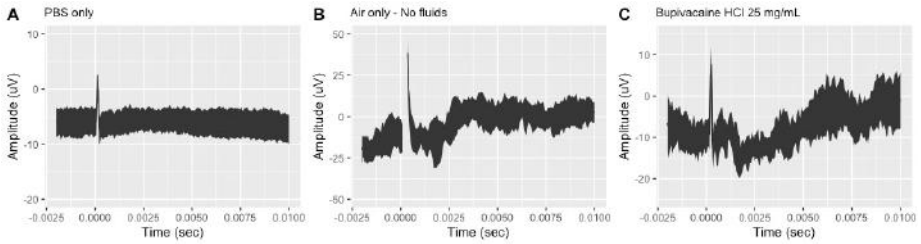


**Figure 4.** Control electrophysiology readings in PBS only (A), air only (B) and bupivacaine HCl solution, 25 mg/mL (C). Noisy signals with varying amplitudes of the stimulus artefact (the peak right after  $t = 0$ ) are obtained.

### 3.3 Sheep femoral nerve measurements

Mammalian large nerves have been used in similar setups before <sup>139,361,368</sup>. For proof-of-concept, and to determine if the current setup was able to detect presence and absence of nervous conduction similar to previous literature, measurements were first performed on sheep femoral nerves. Following control measurements, a section of sheep femoral nerve stretching three centimeters was placed into the electrical setup. Both ends of the nerve section were located in the peripheral chambers. Chambers were isolated from neighboring chambers using paraffine jelly. First, all chambers were filled with PBS and a stable baseline measurement was obtained (Figure 5A). PBS in the central compartment was aspirated and replaced by a 50 mg/mL bupivacaine HCl solution. Measurements were obtained after 5 and 25 minutes (Figure 5B and 5C). After 25 minutes of incubation in bupivacaine solution, the solution was again aspirated and replaced by PBS to wash out bupivacaine. Measurements were recorded 30 seconds and 3 minutes after replacement with PBS (Figure 5D and 5E). Baseline readings displayed a peak after 5-6 milliseconds with an amplitude of approx. 10 uV compared to baseline. This peak disappeared after the application of bupivacaine HCl. Following 3 minutes of bupivacaine washout with PBS, the peak reappeared.

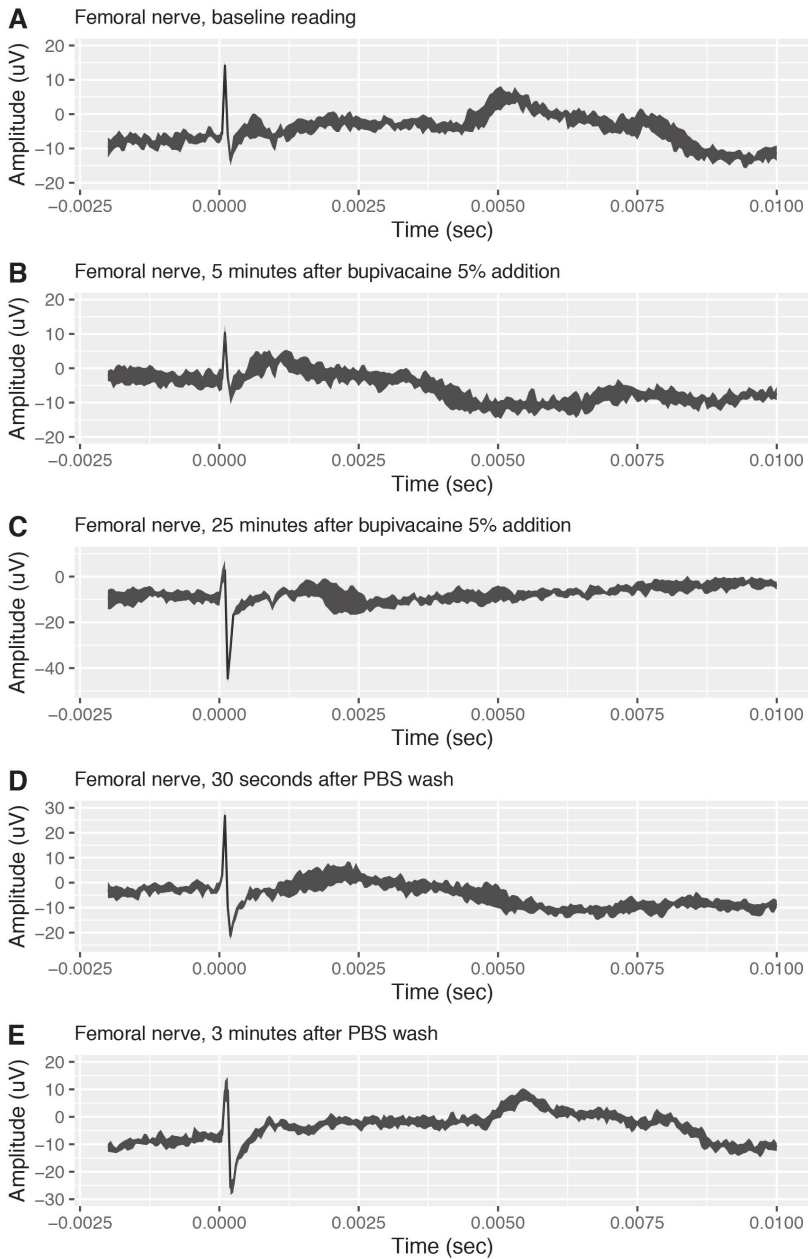


**Figure 5.** Readings from a sheep femoral nerve in the absence and presence of bupivacaine. First, a baseline reading was obtained (A), displaying a sloped peak at  $t = 5\text{--}6$  ms. The nerve was then exposed to bupivacaine 50 mg/mL and incubated for 5 minutes. A second signal was obtained (B), in which the sloped peak at 5–6 ms disappeared. A similar signal was obtained after 25 minutes of bupivacaine exposure (C). Bupivacaine in the central chamber was then replaced by PBS and readings were obtained after 30 seconds (D) and 3 minutes (E). In readings after 3 minutes, the slope at 5–6 ms reappeared.

### 3.4 Human periosteal measurements

To generate stable conduction, the periosteum was situated across the three compartments in Liley solution. The location of the stimulating and recording electrodes was changed until the peak-to-peak amplitude and morphology of the conduction signal were stable (Figure 6). First, the stimulating electrodes were placed in close proximity of the periosteum (Figure 6A). However, placing the electrodes in contact with the periosteum resulted in a higher peak-to-peak amplitude, and additional peaks that might resemble action potentials (Figure 6B). In the other lateral compartments, the recording electrodes were placed in close proximity to the periosteum, but not in contact with the tissue. The stable conduction signal had negative and a positive peak with a peak-to-peak amplitude of approximately 30 mV (Figure 6). Upon reaching a stable conduction signal, Liley solution from the middle compartment was drained, and bupivacaine was applied to the periosteum. The peak-to-peak amplitude of the conduction signal immediately changed to approximately 45 mV, which was higher compared to the conduction signal measured in the control period (Figure 6 and Figure 7A), potentially attributable to leakage. Most measurements did not demonstrate any decrease in peak-to-peak amplitude of the conduction signal. However, one measurement showed a decline in peak-to-peak amplitude from approximately 45 mV to baseline levels within two minutes after addition of bupivacaine to the central compartment (Figure 7). Measurements on sheep periosteum were performed in PBS. Multiple sections of tissue were analyzed, but a stable reference signal was not achieved. A representative signal derived from sheep periosteum is shown in Figure S2.

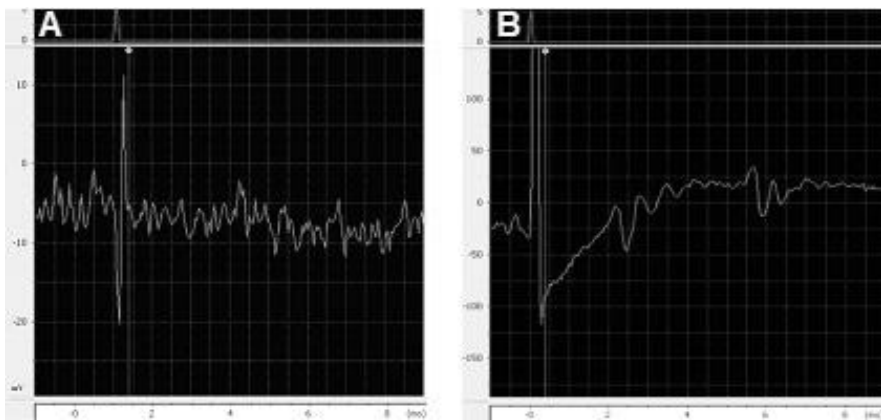


**Figure 6.** LabChart graphs representing the conduction of periosteum in Liley solution. The peak-to-peak amplitude was stable around 30 mV (A). When the stimulating electrodes were placed in contact with the periosteum, the amplitude was higher (B). The noise did not change compared to the measurement with an empty periosteal chamber.

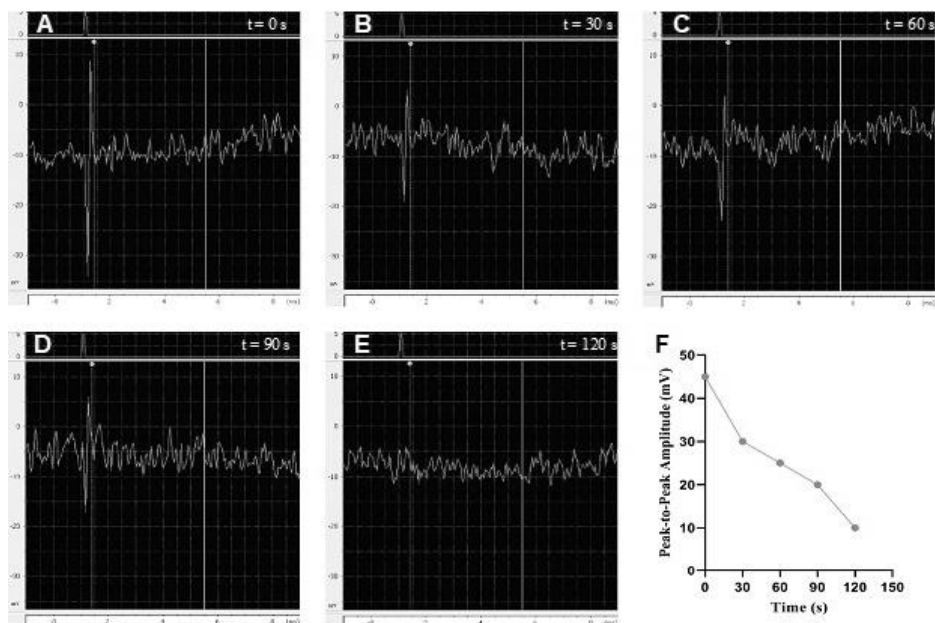


**Figure 7.** LabChart graphs illustrating conduction after application of bupivacaine on periosteum. The peak-to-peak amplitude of the conduction signal first slightly increased with respect to the control (A). After this, the conduction amplitude slowly decreased until only noise remained visible (B-E), as presented in (F).

## 4. DISCUSSION

### Action potential versus conduction

Bupivacaine provides analgesia by blocking the generation and conduction of action potentials in sensory nerve fibers. To better understand the bupivacaine concentrations necessary for inhibition of nociception in nervous tissue, an *ex vivo* electrophysiological setup was developed. With the present experimental setup, we were able to measure conduction in sheep femoral nerve and sheep and human periosteum tissues. This provided some insight in the conduction properties of the tissue; however, we were unable to deduce an action potential in most measurements. To confirm the feasibility of the developed setup and ability to detect the presence and absence of action potentials, measurements were first performed on sheep femoral nerves that were exposed to excessive concentrations of bupivacaine up to 50 mg/mL (Figure 5). A peak following 5-6 ms after the stimulus artefact was observed, which displayed a bupivacaine-dependent reduction in amplitude. Moreover, the block appeared reversible, as peaks reappeared after a bupivacaine wash-out period. The time between stimulus artefact and peak equates to a conduction velocity of 6 m/s, which is in the lower part of the range for A $\delta$ -fibers<sup>369</sup>. As the bupivacaine concentration used was orders of magnitude in

excess of effective concentrations in previous literature (50 mg/mL or 0.17 M vs 0.2 mM, respectively), elimination of action potential conduction was expected<sup>361</sup>. In human periosteum, one measurement (Figure 7B) displayed various sequentially occurring peaks, possibly representing differences in conduction velocity between A $\delta$ -fibers and C-fibers. Conduction velocity could be a potential reason for the challenging distinction between action potentials and the partly overlapping conduction signal. Since the conduction velocity of A $\delta$ -fibers is 6-20 m/s, and the periosteum approximately 3 cm in length, an action potential could reach the recording electrodes as rapidly as in 1.5 ms<sup>137,139,369</sup>. The conduction signal was measured after approximately 1 ms, which might have overlapped an action potential. Furthermore, the conduction velocity of action potentials in C-fibers were  $\sim$  1 m/s, and therefore might have reached the recording electrodes after 30 ms.<sup>137,139</sup> This was outside the recording time, indicating that an action potential from C-fibers might have been missed. Therefore, replicable measurements with post-processing to distinguish an action potential from conduction are necessary. In addition, recording time should be extended, and noise should be suppressed by averaging the measurements.

The lack of stable action potential generation in human periosteum could be related to the presence of disease. The used human periosteum was probably affected by pathology, because the hip from which the periosteum was harvested was replaced in severe cases of osteoarthritis. In addition, a recent study in patients with primary hyperparathyroidism reported that sensory innervation density above bone remodeling surfaces (*e.g.*, the growth of osteophytes in osteoarthritis) was increased.<sup>129</sup> Therefore, the sensory innervation in used periosteum might be different from healthy periosteum, which could have affected the conduction properties. Further studies are needed to study how pathology affects the innervation and conduction of action potentials in periosteum. However, generating a stable signal in sheep periosteum free of any pathology was equally challenging. A possible explanation is the direction of nerve fibers in the periosteal tissue. In a nerve such as the femoral nerve, axons run perpendicular from and to the innervated body part. However, in periosteum, the nerve fibers are organized in a mesh-like structure with no clear directionality.<sup>336</sup> Moreover, the presence of nerve fiber endings in the periosteum could lead to 'dead ends' for stimuli applied to the upstream part of that nerve fiber. A better understanding of the orientation of fibers within the periosteum, and subsequently optimizing the orientation of the periosteum in the experimental setup could enable the generation of stable signals.

### **Future protocol optimization steps**

In addition to the improvements described above, other protocol optimization steps are also necessary. First, temperature should be regulated around body temperature (37°C)

to optimally simulate an *in vivo* environment. The dynamics of sodium channels in sensory neurons are very dependent on local temperature and the amount of used simulated body fluid and bupivacaine<sup>370</sup>. Fluctuations in temperature will affect the sodium influx in sensory neurons, and subsequently the conduction and/or action potential amplitude. Therefore, temperature should be tightly regulated during experiments and during transportation. The experimental setup can be adjusted by incubating the periosteal chamber or by placing it on a hot plate, which allows for temperature control. Another factor that should be controlled is pH, which can be used to modify the non-ionized fraction of bupivacaine and thereby potentiate the drug.

Second, the recorder must perform a minimum number of measurements every second to record an action potential. This so-called sample frequency can be adjusted for the action potential duration of A $\delta$ -fibers ( $\sim$  1 ms), and C-fibers ( $\sim$  2 ms)<sup>371</sup>. Based on the action potential duration of A $\delta$ -fibers and a minimum of ten sample points per action potential, the minimal sample frequency must be set at 10.000 samples/s to obtain a curve. To smoothen this curve, the sample frequency can be increased to the maximum, which was 200.000 samples/s for LabChart. Additional measurements with the highest sample frequency have to be performed.

Third, osteophytes made it in the current experiment sometimes challenging to harvest the periosteum, as these osteophytes grew over the femoral neck. A possible solution for this problem is to use electrical stimulation without removal of the periosteum. This would require an experimental setup that can be attached to the femoral neck with electrodes gently placed on the periosteum. Advantages of such device include earlier measurements after explantation, and no hurdles during periosteum removal. However, this method might make distinction of periosteal conduction from conduction by surrounding tissues more challenging. Another possibility to study the effects of LAs on sensory nerves is the use of an increased intramedullary pressure instead of electrical stimulation. This method was described by Nencini *et al.* in which they increased the intramedullary pressure, and applied LAs to determine the minimal concentration to block action potentials<sup>133,372</sup>. Future studies are needed to study the effects of other LAs (*e.g.*, lidocaine) on periosteum conduction properties.

## 5. CONCLUSION

The present pilot study demonstrated that sheep femoral nerve conducted a stable electrical signal in body-simulating fluid (PBS), which was suppressed following application of bupivacaine. However, obtaining similar readings from sheep or human periosteum remained challenging. Therefore, multiple optimization steps were suggested including



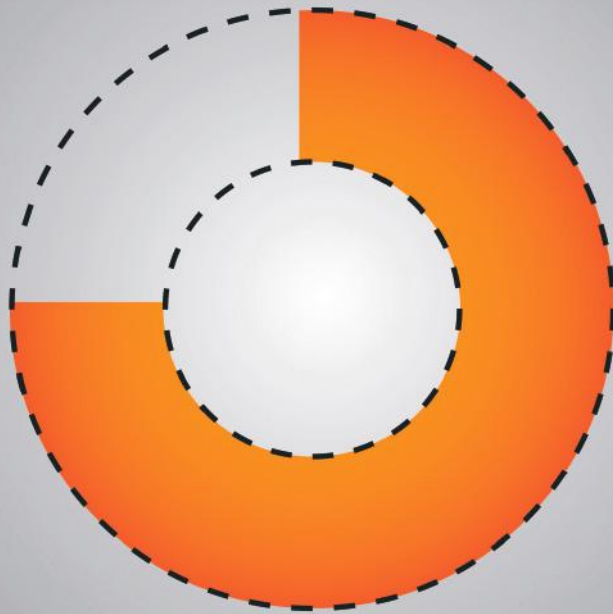
tissue placement in the setup, temperature regulation, noise suppression, sample frequency adjustments, and data post-processing. The presented experimental setup and current pilot study can aid in understanding some of the conduction properties of and nociception in nervous tissues.

## **6. ACKNOWLEDGEMENTS**

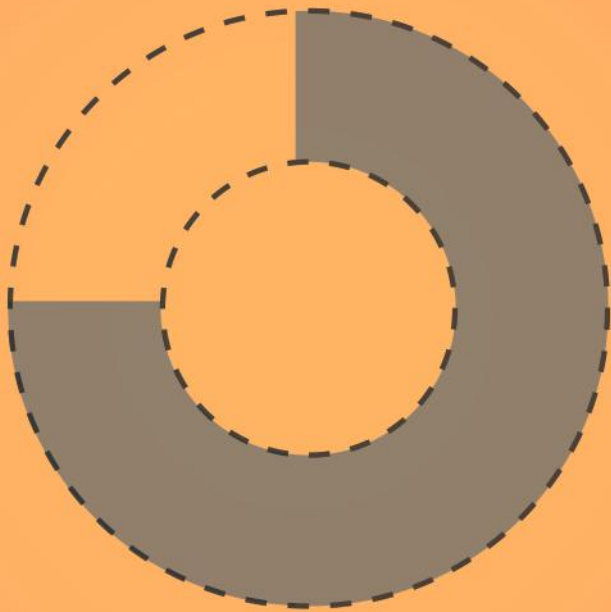
We would like to thank Leonard van Schelven, Ernest Boskovic, and Boudewijn Sleutjes from the Medical Technology and Clinical Physics department of the UMC Utrecht.



# PART III



Robust hydrogel formulation  
for sustained local release of  
bupivacaine



# CHAPTER 7

## Robust gelatin hydrogels for local sustained release of bupivacaine following spinal surgery

Jasper G. Steverink, Floris R. van Tol, Bas J. Oosterman, Tina Vermonden, Jorrit-Jan Verlaan, Jos Malda, Susanna Piluso

## ABSTRACT

Adequate treatment of pain arising from spinal surgery is a major clinical challenge. Opioids are the mainstay of current treatment methods, but the frequency and severity of their side effects display a clear need for opioid-free analgesia. Local anesthetics have been encapsulated into sustained-release drug delivery systems to provide postoperative pain relief. However, these formulations are limited by rapid diffusion out of the surgical site. To overcome this limitation, we synthesized ring-shaped hydrogels incorporating bupivacaine, designed to be co-implanted with pedicle screws during spinal surgery. Hydrogels were prepared by riboflavin-mediated crosslinking of gelatin functionalized with tyramine moieties. Additionally, oxidized  $\beta$ -cyclodextrin was introduced into the hydrogel formulation to form dynamic bonds with tyramine functionalities, which enables self-healing behavior and resistance to shear. Feasibility of hydrogel implantation combined with pedicle screws was qualitatively assessed in cadaveric sheep as a model for instrumented spinal surgery. The *in-situ* crystallization of bupivacaine within the hydrogel matrix provided a moderate burst decrease and sustained release that exceeded 72 hours *in vitro*. The use of bupivacaine crystals decreased drug-induced cytotoxicity *in vitro* compared to bupivacaine HCl. Thus, the presented robust hydrogel formulation provides promising properties to enable the stationary release of non-opioid analgesics following spinal surgery.

## 1. INTRODUCTION

Spinal surgery ranks amongst the most painful interventions overall, and adequate analgesic treatment remains a major clinical challenge<sup>42,373</sup>. Systemic medications, such as opioids, fulfil a central role in the treatment of postoperative pain following spinal surgery, but come at the cost of significant side effects, such as constipation, drowsiness and respiratory depression<sup>76,357</sup>. Furthermore, the use of opioids is associated with the risk of development of opioid dependence or addiction<sup>253,254</sup>. Despite opioid use, high pain scores and inadequate postoperative pain relief are reported in the majority of patients<sup>11,15,373</sup>. The delicate balance between opioid efficacy and side effects displays a clear unmet need for alternative, opioid-free analgesics.

As postoperative pain is a local problem, specifically targeting the surgical site would eliminate most of the side effects of systemically administered analgesics. Local anesthetics (LA), such as lidocaine and bupivacaine, are well-suited to combat local pain, but are hampered by a short duration of action<sup>42,374</sup>. To overcome this limitation, various delivery systems for local anesthetics have been developed<sup>42</sup>. These systems involve mainly the delivery of local anesthetics via microparticles, liposomes and injectable polymer solutions<sup>375</sup>. For example, the incorporation of bupivacaine into polymeric microparticles based on poly (lactic-co-glycolic acid) (PLGA) improved the duration of action in comparison to bupivacaine solutions<sup>376</sup>. Similarly, encapsulation of local anesthetics into liposomes resulted in slow drug release and prolonged duration of the anesthetic effect<sup>377</sup>. Further, preclinical studies confirmed the improvement of bupivacaine safety profile after encapsulation into liposomes<sup>378</sup>. Recently, the incorporation of bupivacaine with meloxicam into a Biochronomer® polymer reduced postoperative pain for 72 hours<sup>260</sup>. Similar results were obtained when using a resorbable bupivacaine-impregnated collagen matrix (Xaracoll, Innocoll Pharmaceuticals) for the management of postoperative pain<sup>337</sup>. The use of these delivery systems can greatly improve the efficacy and duration of bupivacaine. However, all formulations are limited by a high initial burst release and rapid diffusion from the surgical site, thus giving limited analgesic effect beyond 24 hours<sup>40,260,289,320</sup>. Further, some formulations have degradation times well beyond the window of drug release leading to particle debris present at the injection site for weeks<sup>379,380</sup>. Moreover, increased myotoxicity of bupivacaine when combined with polymeric microparticles compared to 0.5% bupivacaine HCl solution has been reported<sup>379</sup>.

Hydrogels provide a unique approach for the delivery of LA at specific sites, with improved efficacy and potential to reduce systemic toxicity. Indeed, they generally exhibit excellent tissue compatibility and tunable drug release profile, mechanical properties and degradation rate<sup>51,52</sup>. Surgical interventions provide an opportunity for administration of

hydrogels by implantation, mitigating the need for injectability of the hydrogel formulation. For optimal performance in patients undergoing spinal surgery, a hydrogel that can simultaneously withstand high compression and shear forces during implantation is needed (Fig. 1A). To this end, we developed a hydrogel formulation for sustained release of bupivacaine based on a dual crosslinked hydrogel, that enables rapid recovery from repeated applications of high strain and shear. The proposed hydrogel system consists mainly of gelatin-tyramine: gelatin functionalized with tyramine moieties (GTA)<sup>381</sup>. Gelatin was selected as it is a natural polymer obtained by hydrolysis of collagen, and gelatin hydrogels have been used frequently in drug delivery as they are well-tolerated in various tissues<sup>50,382</sup>. Further, gelatin contains carboxylic and amino groups that can be used for its functionalization. Its molecular structure and specific amino acid sequence make it susceptible to enzymatic degradation, ensuring rapid clearance from the surgical site<sup>383</sup>. In this study, hydrogels were prepared by combining GTA with oxidized  $\beta$ -cyclodextrin (o $\beta$ -CD) and photo-crosslinked using riboflavin (RB, vitamin B2)/ sodium persulfate (SPS), and exposure to visible light (Fig. 1B)<sup>384</sup>. The riboflavin/SPS photoinitiating system crosslinks two tyramine moieties into di-tyramine adducts. Furthermore, tyramine moieties can form inclusion complexes through interaction with the hydrophobic cavity of  $\beta$ -cyclodextrin, whilst oxidized groups on beta-cyclodextrin allowed for the coupling to amine groups on gelatin *via* imine bond formation<sup>385–387</sup>.

Cyclodextrins ( $\alpha$ -,  $\beta$ - and  $\gamma$ -) are cone-shaped molecules extensively used in drug delivery, with  $\beta$ -cyclodextrin being the most often used<sup>42</sup>. Their main advantage is the capability to encapsulate drugs in the hydrophobic interior, while the hydrophilic exterior ensures water-solubility<sup>388,389</sup>. This inclusion complex formation can lead to increased solubility, and prolonged release of hydrophobic drugs<sup>381,390</sup>. In a hydrogel, cyclodextrins can also provide a means to achieve dynamic crosslinks *via* interactions with suitable moieties on a polymer backbone. Next to self-healing behavior, the inclusion complexes allow for dissipation of energy and thus enhance the mechanical properties of the hydrogel<sup>387</sup>.

Here, we designed a hydrogel to be co-implanted with pedicle screws during instrumented spinal surgery. We hypothesized that these combined crosslink methods could provide the hydrogel with mechanical properties that ensure adequate resistance to the orthopedic implantation procedure, while the biodegradable hydrogel precursor could lead to swift degradation and removal from the surgical site<sup>390,391</sup>. We first evaluated the physical and mechanical properties of the designed hydrogel system.

Next, we investigated whether the proposed hydrogel system could act as a cytocompatible sustained-release formulation for local delivery of bupivacaine following spinal surgery.



## 2. MATERIAL AND METHODS

### 2.1 Synthesis of Gelatin-tyramine

Gelatin-tyramine (GTA) was synthesized as previously reported<sup>381</sup>. Briefly, gelatin (type A, porcine skin, Sigma-Aldrich) was dissolved in 2-(*N*-morpholino)ethanesulfonic acid buffer (MES, Sigma-Aldrich, 50 mM, pH 4.75) at a concentration of 1.67 wt.% and reacted with tyramine HCl (Sigma-Aldrich) in a 4:1 ratio of [Tyramine]:[COOH]. The reaction was performed in presence of 1-ethyl-3-(3-dimethylaminopropyl)carbodiimide hydrochloride (EDC, Sigma-Aldrich) and *N*-hydroxysuccinimide (NHS, Sigma-Aldrich) in a 2:1 ratio at 45°C overnight. The reaction mixture was then dialyzed (MWCO 14 kDa cellulose dialysis membrane, Sigma-Aldrich) against deionized water for 72 hours and subsequently lyophilized. Yield of the reaction following dialysis and freeze drying was 77.3% ( $\pm 6.9\%$ ).

The degree of functionalization (DoF) was determined by measuring the absorbance at 275 nm of 0.1 wt.% gelatin and GTA solutions. Absorbance was interpolated on a tyramine HCl standard curve and corrected for the absorbance of non-functionalized gelatin. The degree of functionalization was expressed as a percentage of the available COOH groups in gelatin (79 mmol/ 100 g)<sup>392</sup>.

### 2.2 Synthesis of oxidized $\beta$ -cyclodextrin ( $\alpha$ B-CD)

$\beta$ -cyclodextrin (B-CD, Sigma-Aldrich) was oxidized by modifying a previously described procedure<sup>381</sup>. B-CD was suspended in MilliQ-water followed by addition of sodium periodate ( $\text{NaIO}_4$ , Sigma-Aldrich) in  $[\text{NaIO}_4]:[\text{B-CD}]$  molar ratios up to 4:1, and stirred at room temperature. Aliquots of the reaction mixture were taken at predetermined time points to assess the degree of oxidation as a function of time. The reaction was quenched by adding glycerol in a 1:1 molar ratio with sodium periodate. The solution was then dialyzed (MWCO 0.5 kDa, VWR) against MilliQ-water in the dark at room temperature for 48 hours. Water was replaced six times daily. The purified solution was then lyophilized to obtain oxidized  $\beta$ -cyclodextrin ( $\alpha$ B-CD). Proton Nuclear Magnetic Resonance ( $^1\text{H}$  NMR) in DMSO- $d_6$  was used to confirm presence of aldehyde groups and quantify the oxidation degree as previously described<sup>386</sup>. Yield following dialysis and freeze drying was 55.8% ( $\pm 5.2\%$ ).

### 2.3 Affinity assay by $^1\text{H}$ NMR of bupivacaine and tyramine for B-CD

To assess affinity of bupivacaine for the cavity of B-CD, a double reciprocal Benesi-Hildebrand plot was constructed using increasing concentrations of bupivacaine (1-8 mM) or tyramine (1-10 mM) in  $\text{D}_2\text{O}$  (Sigma-Aldrich), while the B-CD concentration was kept constant at 11 mM. Samples were analyzed using  $^1\text{H}$ -NMR (400 MHz, Bruker, Leiderdorp,

NL) and an association constant ( $K_a$ ) was calculated<sup>393,394</sup>.  $Dd_{\max}$  was calculated as (1/intercept), after which the  $K_a$  was calculated as  $(1/(\text{slope} * Dd_{\max}))$ .

## 2.4 Preparation of GTA Hydrogels

Stock solutions of GTA, oB-CD, riboflavin 5'-monophosphate sodium salt (RB, Sigma-Aldrich) and sodium persulfate (SPS, Sigma-Aldrich) in deionized water were freshly prepared. Hydrogels were then formed by casting a pre-gel solution of various composition in cylindrical (8 mm diameter x 2 mm height) or ring-shaped (internal diameter 6 mm, external diameter 18 mm, height 6 mm) molds and exposed to visible light (400-700 nm) for 30 minutes. Light intensity at mold level was 60 mW/cm<sup>2</sup>. Hydrogels were hydrated during the photo-crosslinking process to account for evaporation due to heat generated from the lamp. Following crosslinking, gels were washed in excess PBS to remove any unreacted reagents.

## 2.5 Sol fraction and equilibrium swelling of GTA hydrogels

After synthesis, hydrogels were dried in an oven at 37°C ( $m_{d1}$ ) and then incubated in phosphate-buffered saline (PBS, pH 7.4) at 37°C until equilibrium swelling. After 24 hours, the swollen weight was recorded ( $m_s$ ) and the gels were again dried ( $m_{d2}$ ). Swelling ratio was calculated as  $(m_s - m_{d2}) / m_{d2}$ . The sol fraction, representing the non-crosslinked mass fraction in the polymer network, was calculated as  $(m_{d1} - m_{d2}) / m_{d1}$ .

## 2.6 Scanning Electron Microscopy

Hydrogel microstructure was assessed using Scanning Electron Microscopy (SEM, Phenom, Fisher Scientific). Disc-shaped hydrogels were prepared as discussed in section 2.3. After swelling in PBS, hydrogels were flash-frozen in liquid nitrogen. The internal hydrogel structure was exposed by cryofracture, followed by lyophilization. Hydrogels were then fixed on SEM stubs using carbon tape. Following 6 nm gold-sputter coating, imaging was performed.

## 2.7 Mechanical Analysis

Compression modulus of GTA hydrogels was determined using Dynamic Mechanical Analysis (DMA, Q800, TA Instruments, Etten-Leur, NL). A ramp-force protocol was set, increasing force up to 18 N at a rate of 3 N/min. All DMA measurements were performed at room temperature. A stress-strain curve was generated for samples and the coefficient in the linear viscoelastic (LVE) range was retrieved, representing the compression modulus.

## 2.8 Rheological Analysis

Rheological measurements were carried out using a rheometer (Discovery HR-2, TA instruments, Etten-Leur, NL) with a 20 mm parallel plate geometry at RT. Amplitude

sweeps were performed at a frequency of 1 Hz and shear strain from 0.1% to 100%. Frequency sweeps were performed at a strain of 1% and frequency range from 0.1 Hz to 100 Hz. Cyclic strain-recovery was performed by exposing gels to alternating intervals of low strain (2 minutes, 1% strain) and high strain (1 minute, 100% strain).  $G'$  and  $G''$  were recorded to assess viscoelastic behavior of hydrogels. Mesh size calculations based on the rubber elasticity theory were performed using the experimentally determined rheology data according to the following formula<sup>395,396</sup>:

$$\text{mesh size } \xi \text{ (nm)} = \left( \frac{G' \times N_A}{R \times T} \right)^{-\frac{1}{3}}$$

Where  $G'$  is the storage modulus (Pa),  $N_A$  is the Avogadro constant,  $R$  is the molar gas constant and  $T$  is the temperature.

## 2.9 Drug loading and in vitro release

Following washing of crosslinked gels, samples were dried and incubated in a bupivacaine HCl solution at 37°C. In a next step, hydrogels were treated with 0.1 M  $\text{NaHCO}_3$  (pH 8.5) containing glycerol to induce *in situ* alkaline crystallization of bupivacaine. Ring-shaped hydrogel loaded with bupivacaine HCl and crystallized bupivacaine were tested for release in 0.01 M citrate buffer (pH 6) at 37°C. At time points of interest up to 168 hours, aliquots were collected and replaced with the same volume of fresh buffer. After 168 hours the hydrogels were incubated in 0.15% collagenase II solution in 0.01 M citrate buffer (pH 6) until they had completely degraded to determine total drug content.<sup>397</sup>

Bupivacaine content of samples was analyzed using HPLC (Prominence LC20A, Shimadzu Corp, Kyoto, Japan) with Waters Acquity HSS T3 1.8 mm column, 100 mm (Waters Chromatography, Etten-Leur, NL). Mobile phase A and B consisted of 10 mM ammonium formate (pH 2.4) and acetonitrile, formic acid and water in 96:0.2:5 ratio, respectively, utilizing a previously described method<sup>347</sup>. Absorbance was measured at 262 nm. A standard ranging from 5 mg - 5 mg/mL bupivacaine HCl in 0.01 M citrate buffer (pH 6) was used to convert sample absorbance to concentration.

## 2.10. In vitro cytocompatibility

Cytocompatibility of hydrogels (50 mL volume) and drug-loaded hydrogels (50 mL volume) was tested using a direct-contact method. NIH3T3 mouse fibroblasts and human mesenchymal stem cells (hMSCs) were seeded at a density of 8000 cells/ well in a 24-wells plate. Cells were cultured up to 80% confluence in a humidified incubator set at 37°C with 5%  $\text{CO}_2$  using Alpha-Minimum Essential Medium (Alpha-MEM, Gibco,

Fisher Scientific) supplemented with 10% fetal bovine serum (FBS), 1% ascorbic acid and 1% penicillin-streptomycin. Medium was replaced every three days. Hydrogels discs were placed on top of the cells. The control group consisted of cells exposed only to culture medium. After 24 and 48 hours of exposure, cell metabolism was quantified using an Alamar Blue assay. Fluorescence was measured using a Fluoroskan Ascent plate reader (ThermoFisher Scientific) with excitation and emission set at 544 and 570 nm, respectively. Cell viability was assessed using a Live/Dead assay (Invitrogen), staining live cells green with Calcein acetoxymethyl ester (AM) and dead cells red with ethidium homodimer. A stock solution of 2 mM Calcein AM and 4 mM Ethidium homodimer in PBS was prepared. Upon reaching the desired duration of cell exposure to gels, gels and culture medium were removed and cells were washed with PBS. Live/Dead staining stock solution was added to the wells and incubated at 37°C for 30 minutes prior to imaging. Live cell counts were normalized to controls. Imaging was performed using an inverted fluorescence microscope (Olympus BX51, Olympus, Germany). Hydrogels were tested in quintuplicate unless stated otherwise. Three images were taken for each sample to accurately represent cell compatibility. Images were analyzed using ImageJ (NIH, Bethesda, Maryland, USA). All groups were compared to control.

### **2.11 *In vitro* degradation assay**

To assess hydrolytic degradation, the dry mass of disk-shaped hydrogel samples was recorded, after which hydrogels were submerged in 1 mL of PBS containing 0,01% sodium azide to prevent microbiological growth. In the enzymatic degradation assay, hydrogels were submerged in collagenase II at 2 EU/mL (Worthington Biochemical Corp) in PBS with 0,01% sodium azide at 37°C to simulate surgical wound enzyme concentrations<sup>398–400</sup>. The collagenase solution was replaced every three days to maintain constant enzymatic activity. In both the enzymatic and hydrolytic degradation assay, gels were collected at predetermined times and the remaining dry mass was recorded. Mass loss was expressed as (remaining mass/ original mass) \* 100.

### **2.12 *Ex vivo* implantation**

Fresh cadaveric female sheep specimens (age 5-7 years) were obtained for *ex vivo* implantation of twenty ring-shaped hydrogels by a board-certified spine surgeon (JJV). Sheep surgery was performed in the prone position. A midline incision was performed over the spinous processes, paraspinous muscles were dissected and moved laterally to allow for a clear view of lamina, spinous- and transverse processes. A hole was drilled into the pedicle of the lumbar vertebrae. Next, the ring-shaped hydrogel was mounted on a polyaxial pedicle screw and the screw was tightened according to clinical practice. Mechanical performance of the ring was assessed macroscopically. Specific attention was paid to cracks in- or rupturing of the hydrogel. If no damage was observed, the screw

was overtightened and ring performance was scored again. Rings were then explanted and again assessed for signs of failure.

### 2.13 Statistical Analysis

All statistical analysis was performed using Prism 8.0 (GraphPad Software Inc, San Diego, CA, USA). All data are presented as mean  $\pm$  standard deviation. Data was analyzed using a one-way (or two-way when necessary) analysis of variance (ANOVA) combined with Tukey's honestly significant difference to correct for multiple comparisons. A significance level of  $p < 0.05$  was used.

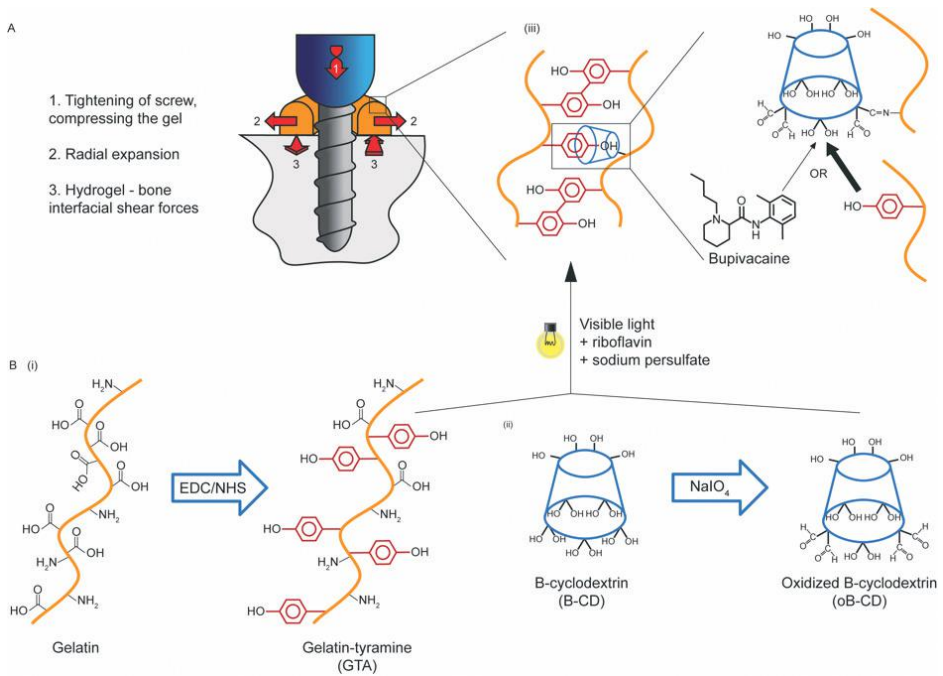


**Figure 1.** Schematic illustration of hydrogel preparation and implantation. **A** Scheme of forces acting on the hydrogel during co-implantation with a pedicle screw. **B (i)** Functionalization of gelatin carboxyl groups with tyramine moieties via EDC/NHS mediated coupling and amide bond formation; **(ii)** oxidation of B-CD secondary hydroxyl groups to aldehyde groups in presence of sodium periodate ( $\text{NaIO}_4$ ). For the sake of clarity only few of the primary and secondary hydroxyl groups of B-CD are shown in the schematic; **(iii)** hydrogel formation achieved by mixing GTA with oB-CD, in presence of riboflavin and sodium persulfate and exposure to visible light with of Schiff-base formation between oB-CD and amine groups present on GTA and tyramine-tyramine photo-crosslinking. The cyclodextrin cavity can form inclusion complexes with both tyramine (high affinity, thick arrow) and bupivacaine (low affinity, thin arrow).

### 3. RESULTS AND DISCUSSION

#### 3.1 Synthesis of Gelatin-Tyramine and Oxidized Beta-Cyclodextrin

Tyramine functionalized gelatin (GTA) was obtained by carbodiimide-mediated coupling of tyramine to the carboxylic groups present on the gelatin backbone (Fig. 1B). The coupling reaction involves the formation of an amine-reactive *N*-hydroxysuccinimide (NHS) ester which is susceptible to hydrolysis<sup>401</sup>. Performing the reaction at low temperature (*e.g.* 4°C) minimizes hydrolysis, increasing the half-life of the active NHS ester and thereby the efficiency of the coupling reaction<sup>401,402</sup>. Because gelatin is soluble at temperatures above 37°C, the coupling reaction cannot be conducted at low temperature. To assess the effect of reaction temperature and time on the degree of functionalization (DoF), the coupling reaction was conducted at three different temperatures, namely 37°C, 45 °C and 55°C. For each temperature, the degree of functionalization was determined at 8 hours and 24 hours of reaction. The amount of tyramine conjugated to gelatin was quantified by measuring the absorbance at 275 nm, as previously described<sup>381</sup>. The DoF of the hydrogels resulting from reactions performed in the temperature range 37-55°C did not significantly differ between temperatures and between 8 and 24 hours of reaction (Fig. 2A). Carboxylic groups are present in gelatin type A at a concentration of 780-800 mmol per gram<sup>392</sup>. A 4:1 excess of tyramine was added during the reaction. Based on these results, the coupling reaction temperature was then set to 45°C and the time to 8 hours, resulting in a degree of functionalization of 22.3% (±1.4%) of the carboxylic groups of gelatin, which equals to 176 mmol tyramine / g GTA.

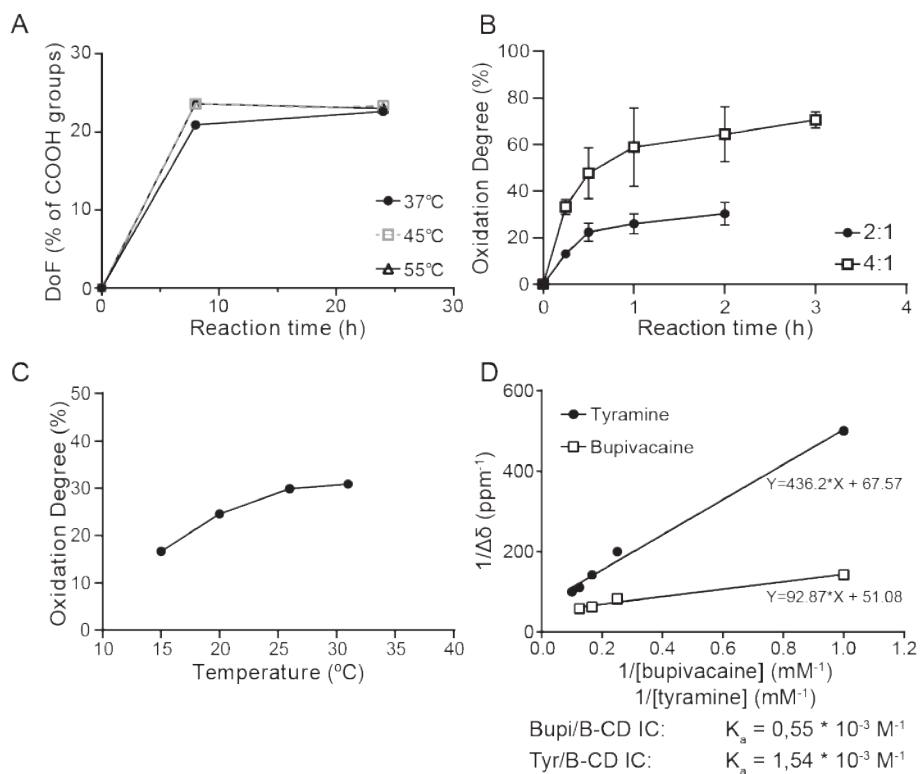


**Figure 2.** Effect of reaction time and temperature on the synthesis of the hydrogel's precursors. **A** Effect of reaction time and temperature on the EDC-mediated coupling of tyramine to gelatin carboxylic groups, using a [tyramine HCl]:[COOH] ratio of 4:1, [EDC]:[NHS] ratio of 2:1 and gelatin at 1.67%. A single reaction per temperature was performed. **B** Effect of [NaIO<sub>4</sub>]:[B-CD] ratio and reaction time on the degree of oxidation degree of B-CD at 25°C. Three reactions per ratio were performed. **C** Effect of temperature on the degree of oxidation of B-CD, using a [NaIO<sub>4</sub>]:[B-CD] ratio of 2:1 and reaction time of 1 hour. A single reaction per temperature was performed. **D** Benesi Hildebrand plot quantifying the association constant ( $K_a$ ) interaction between B-CD and tyramine or bupivacaine in DMSO determined from <sup>1</sup>H NMR spectra. B-CD concentrations were kept constant at 11 mM and combined with increasing bupivacaine concentrations (1-8 mM) or tyramine concentrations (1-10 mM).

Oxidized B-CD (oB-CD) was prepared using sodium periodate (NaIO<sub>4</sub>), which induces the cleavage of vicinal glycols leading to the formation of dialdehyde functionalities. (Fig. 1B-ii). The extent of oxidation was monitored for up to 3 hours using a [NaIO<sub>4</sub>]:[B-CD] ratio of 2:1 and 4:1, and quantified using <sup>1</sup>H NMR (Fig. 2B and Fig. S1). The aldehyde content displayed a fast increase when using a [NaIO<sub>4</sub>]:[B-CD] ratio of 4:1, especially after 1 hour of reaction. A similar curve shape was observed when using a ratio of 2:1, though the aldehyde content was lower in comparison to the one obtained with the ratio 4:1. Because the 2:1 ratio yielded a slower increase in degree of oxidation and a lower

final aldehyde content and thus better control over the reaction, this ratio was selected for further investigations.

To evaluate the effect of temperature on the oxidation degree, the reaction was monitored for 1 hour in a temperature range from 15°C to 35°C (Fig. 2C). When the reaction was conducted at room temperature and at a  $[\text{NaIO}_4]:[\text{B-CD}]$  ratio of 2:1, the oxidation degree was 23.7% ( $\pm 1.5\%$ ), as measured by NMR (Fig. S1). This oxidation degree was chosen to provide sufficient water solubility of oB-CD, while simultaneously allowing a large number of oB-CD molecules to be attached to gelatin chains through Schiff base formation between the amino groups on gelatin and aldehyde functionalities on oB-CD. This way, the main function of oB-CD was to provide additional elasticity to the network *via* guest-host complexation with tyramine moieties grafted on gelatin (Fig. 1B).

### 3.2 Preparation and characterization of GTA / oB-CD hydrogels

As shown in Figure 1, dual-crosslinked hydrogels were prepared by mixing GTA with oB-CD and crosslinked via exposure to visible light, using riboflavin (RB) and sodium persulfate (SPS) as photoinitiating system. Under the influence of visible light, riboflavin and sodium persulfate induce the formation of di-tyramine crosslinks between tyramine moieties grafted onto the gelatin backbone<sup>384</sup>. The exposure of riboflavin to visible light induces photo-excitation of riboflavin, which promotes the formation of tyrosyl radicals from the grafted tyramine moieties and tyrosine residues present on the gelatin backbone. Di-tyramine bonds are then obtained by the coupling of two adjacent tyrosyl radicals<sup>403</sup>. In addition, imine bonds formed through Schiff base reaction between the aldehyde groups on oB-CD with primary amines groups on gelatin, and inclusion complexes formed between the oB-CD cavity and tyramine moieties grafted on the gelatin backbone directly after mixing of stock solutions. Concentration-dependent additional cross-linking by oB-CD was confirmed with dynamic mechanical analysis.

The formation of inclusion complexes of B-CD with a variety of guest molecules (including tyramine) has been previously investigated by  $^1\text{H}$  NMR spectroscopy<sup>404</sup>. Different values of association constants have been reported in the literature for inclusion complexes between B-CD and bupivacaine. The stability of the formed complex depends highly on the pH and the temperature used, and values obtained by different techniques are difficult to compare (*e.g.* HPLC vs NMR)<sup>404,405</sup>. Further, the stability of the complex depends on the type of substituents on the cyclodextrin core. For example, sulphobutylether-B-CD forms a more stable complex with bupivacaine compared to B-CD and bupivacaine<sup>406</sup>. The experiment in our study was performed on B-CD and not oB-CD, as it was hypothesized that aldehyde groups on oB-CD would already have reacted with amine groups present on gelatin at the time of bupivacaine loading.



To assess the stability of complex formed between bupivacaine with B-CD and of tyramine with B-CD, their inclusion into the B-CD cavity was investigated by NMR spectroscopy (Fig. S2 and S3). The association constant ( $K_a$ ) was  $0.55 \times 10^{-3} \text{ M}^{-1}$  for bupivacaine/ B-CD and  $1.54 \times 10^{-3} \text{ M}^{-1}$  for tyramine/ B-CD, as determined using a Benesi-Hildebrand plot (Fig. 2D)<sup>385</sup>. As the  $K_a$  of tyramine exceeds the bupivacaine  $K_a$  almost three-fold, little competition between tyramine and bupivacaine for the B-CD cavity is expected.

Swelling ratio and sol fraction were determined to understand the effect of the hydrogel composition on its physical properties. The swelling ratio is a measure of the amount of water a hydrogel can uptake, expressed as a ratio to the hydrogel's dry weight and is predominantly determined by the crosslinking density of the polymer network. Other factors influencing swelling ratio are temperature, pH, ionic strength of swelling medium and the presence of hydrophilic or hydrophobic groups<sup>407</sup>. With diffusion-based drug loading, the swelling ratio directly influences the amount of drug the hydrogel can encapsulate. We therefore aimed for a crosslinking density that leads to a robust hydrogel but allows for sufficient uptake of solubilized drug. Firstly, the effect of GTA concentration on hydrogel properties was investigated (Fig. 3A-i). To evaluate the effect of GTA concentration, hydrogels were prepared by fixing the concentration of RB and SPS to 2 mM and 20 mM, respectively, and the irradiation time to 30 min. The swelling ratio was significantly lower for hydrogels with a GTA content of 20 wt.% compared to samples with GTA 15 wt.%. No significant difference was observed for hydrogels with a GTA content between 5 and 15 wt.%. Next, we determined the sol fraction of hydrogels with a GTA content from 5 to 20 wt.%, as a measure of the non-crosslinked portion of the polymer mass<sup>408</sup>. Increasing GTA concentration from 5 to 20 wt.% led to significantly lower sol fractions and slightly lower swelling ratio (Fig. 3A-i and 3A-ii). Based on these results, for further experiments GTA concentration was set at 20 wt.% as it

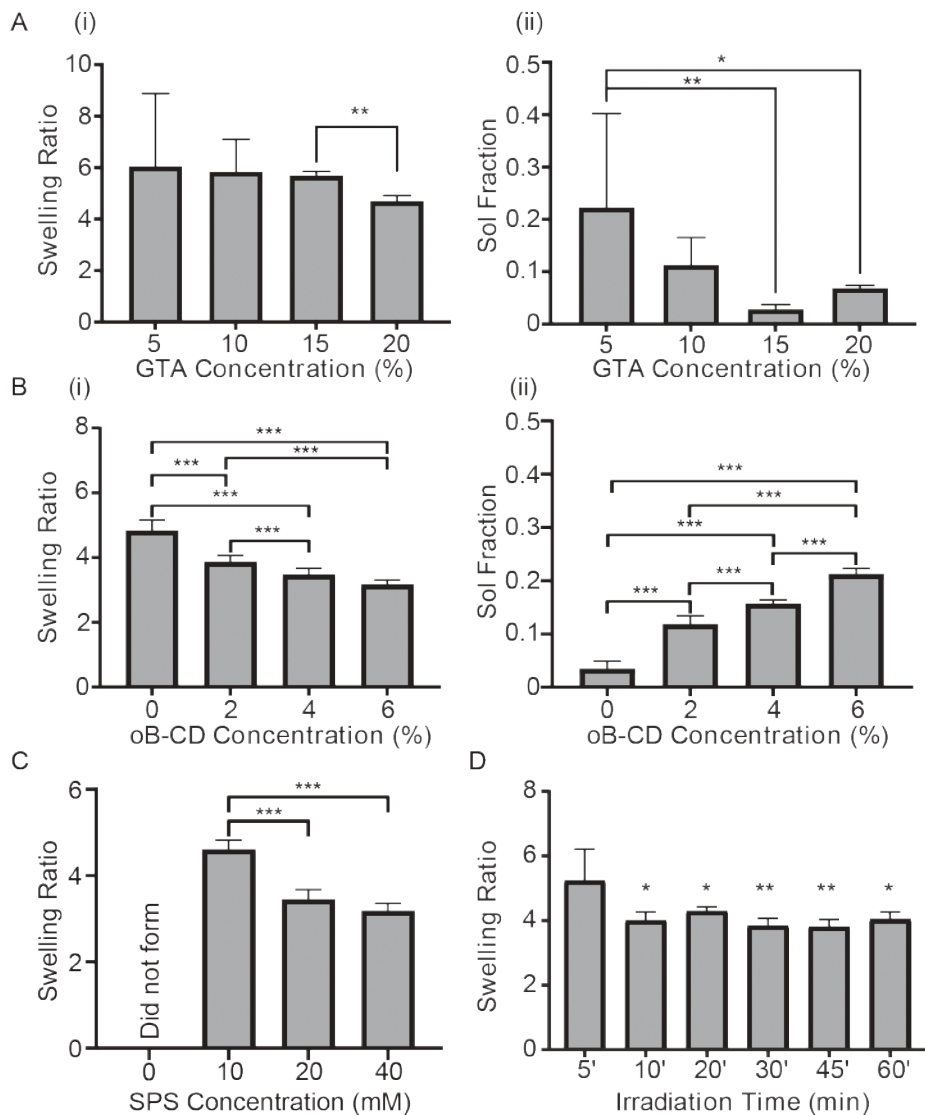


**Figure 3.** Characterization of swelling behavior and sol fraction of GTA/oB-CD hydrogels. **A** Effect of GTA concentration (wt.%) on swelling ratio (i) and sol fraction (ii) of 100  $\mu$ L disc-shaped hydrogels ( $N=6$ ). Hydrogels did not contain oB-CD, irradiation time was set to 30 minutes, SPS concentration at 20 mM and RB at 2 mM. **B** Effect of oB-CD concentration (wt.%) on swelling ratio (i) and sol fraction (ii) of 100  $\mu$ L disc-shaped hydrogels at fixed GTA concentrations of 20 wt.%, RB 2 mM and SPS 20 mM, irradiation time 30 min. **C** Effect of SPS concentration on swelling ratio of disc-shaped hydrogels containing 20% GTA, 4% oB-CD and 2 mM RB. Gels were irradiated for 30 minutes. **D** Effect of irradiation time on hydrogel swelling ratio in disc-shaped hydrogels containing 20% GTA, 4% oB-CD, 20 mM SPS and 2 mM RB.  $N = 4-6$  for all compositions. Data was analyzed using one-way ANOVA, paired with Tukey's test. \*  $p < 0.05$ , \*\*  $p < 0.01$ , \*\*\*  $p < 0.001$ .

displayed low swelling ratio and sol fraction, indicating a more efficient crosslinking compared to the other formulations. To study the effect of oB-CD concentration on the swelling ratio, hydrogels with increasing concentrations of oB-CD up to 6 wt.% were investigated. Increasing the oB-CD concentration led to a decrease in swelling ratio, likely due to the formation of additional crosslinks between oB-CD and GTA (Fig. 3B-i). A significant decrease in swelling ratio was observed for hydrogels with an oB-CD content up to 4 wt.%. Samples containing 4 wt.% and 6 wt.% oB-CD did not exhibit any significant difference in swelling ratio, while the sol fraction significantly increased for oB-CD content from 0-6 wt.%, suggesting a potential saturation of the hydrogel network with oB-CD and subsequent washout of excess oB-CD, resulting in increased sol fraction. (Fig. 3B-ii). Based on the data from swelling ratio and sol fraction, the oB-CD concentration was therefore fixed at 4 wt.%. In a similar fashion, the influence of SPS concentration on gel formation was evaluated. In the absence of SPS, no gels were formed. Increasing the SPS concentration from 10 mM to 40 mM led to significant decreases in swelling ratio (Fig. 3C), as previously described for silk fibroin hydrogels photo-crosslinked using RB/SPS in presence of visible light<sup>384</sup>. Swelling ratio of hydrogels containing 20 mM and 40 mM SPS did not display any significant difference (Fig. 3C). To minimize SPS content yet allowing efficient crosslinking, SPS concentration was therefore fixed at 20 mM. Self-standing hydrogels could be formed following exposure to visible light for 5 minutes. While hydrogels were formed within 5 minutes of irradiation, increasing the irradiation time led to significant decreases in swelling ratio, suggesting that a longer reaction time is required to achieve a complete crosslinking. After 30 minutes of irradiation, no more changes in the swelling ratio were observed (Fig. 3D) and therefore the irradiation time was fixed at 30 minutes for future experiments. These data show that the current photo-crosslinking system allows temporal control of crosslinking, in contrast to systems using enzyme-mediated crosslinking that starts upon mixing hydrogel ingredients together<sup>381</sup>. RB concentration was fixed at 2 mM based on previous investigations<sup>384</sup>. To confirm that this concentration gives the best results with SPS at 20mM and an irradiation time of 30 minutes, hydrogels were prepared by varying RB from 1-4 mM. No significant changes in either swelling ratio or sol fraction were observed when using RB concentrations of 1 mM, 2 mM and 4 mM (Fig. S4). These results show that GTA, oB-CD and SPS concentration as well as irradiation time are important determinants in the network formation. Riboflavin concentration did not affect the crosslinking efficiency in the ranges investigated.

### 3.3 Shear and compressive mechanical properties of GTA / oB-CD hydrogels

Implantation of the hydrogel with a pedicle screw onto a vertebra exerts considerable compressive and shear strain on the hydrogel especially at final tightening of the screw (Fig. 1B). To assess the ability of the GTA / oB-CD hydrogel to withstand shear and compression forces during implantation, we assessed its mechanical properties. The

compressive modulus determined by dynamic mechanical analysis was affected by the oB-CD content and irradiation time (Fig. 4A-i) The compressive modulus increased from 375 kPa ( $\pm 57$ ) to 621 kPa ( $\pm 226$ ) with increasing oB-CD content (*i.e.*, between 0 wt.% and 6 wt.%,  $p < 0.05$ ). Furthermore, as irradiation time is an important determinant in network formation, its effect on compression modulus was tested by varying the exposure time to visible light from 5 to 30 minutes (Fig. 4A-ii) while maintaining the oB-CD content at 4 wt.%. Samples prepared by using an irradiation time of 5 min displayed the lowest compressive modulus (168 kPa  $\pm 30$ ), which is in agreement with the swelling ratio, as shown in Fig. 3D. Samples photo-crosslinked for 10, 20 and 30 minutes exhibited a linear increase of compressive modulus from 328 kPa ( $\pm 29$ ) to 552 kPa ( $\pm 138$ ). The compressive moduli of these hydrogels are considerably higher than other gelatin-based hydrogels, such as gelatin-methacryloyl (GelMA) hydrogels. Indeed, the compressive modulus of GelMA hydrogels varied between 2 kPa for a gelatin content of 5 wt.% up to 180 kPa for hydrogels containing 30 wt.% GelMA, depending on crosslinking agent and degree of substitution<sup>409,410</sup>. This difference is likely due to the mechanism of hydrogel formation, which in the case of GelMA hydrogels occurs via chain growth polymerization of the methacryloyl groups<sup>409</sup>. GTA hydrogels are crosslinked by the formation of dityramine bonds, which lead to a tighter network in comparison to GelMA hydrogels<sup>384,386</sup>. In addition, the present GTA hydrogel contains B-CD which is connected to the gelatin chains via Schiff base formation and guest-host interactions.

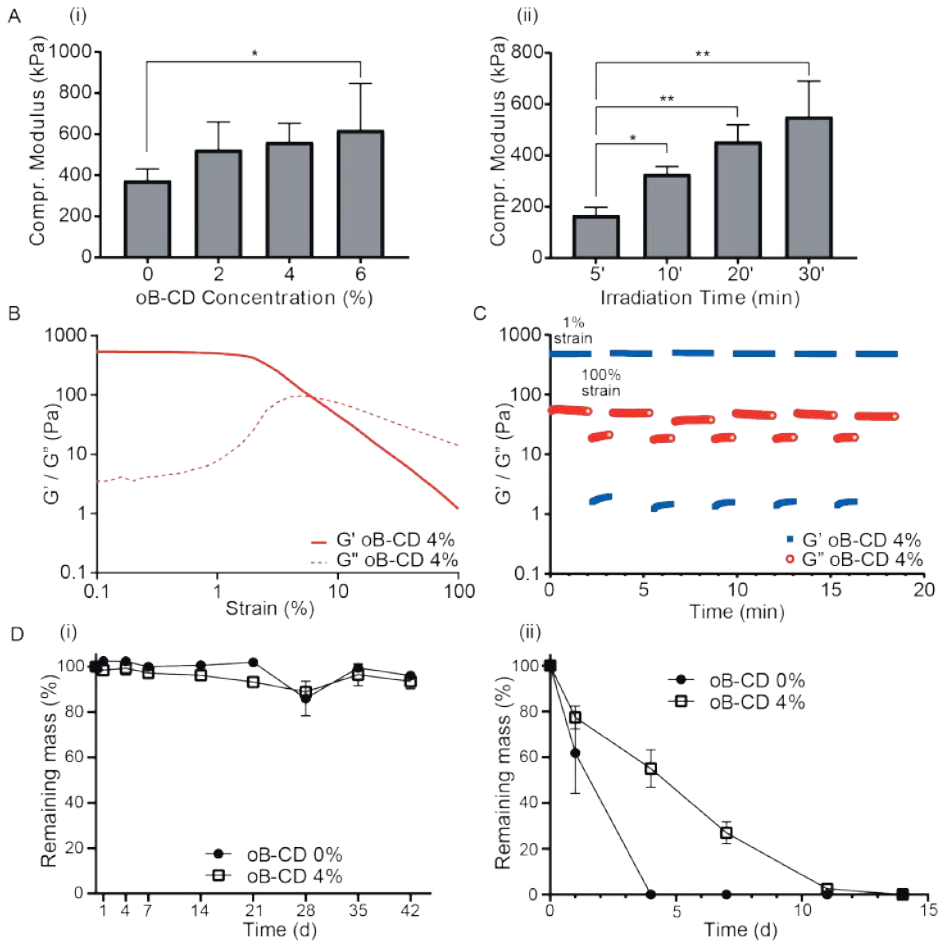


**Figure 4.** Mechanical characterization of GTA/oB-CD hydrogels, and investigation of hydrolytic and enzymatic degradation. A Effects of (i) oB-CD concentration (30 minutes of irradiation) and (ii) irradiation time (gels containing 4% oB-CD) on compression modulus of disc-shaped hydrogels containing 20% GTA, 20 mM SPS and 2 mM RB. B Strain sweep of hydrogels containing 20% GTA and 4% oB-CD hydrogels. A representative sample taken from N=3 is shown. C Rheological properties of hydrogels containing 20% GTA, 4% oB-CD hydrogels during cyclic strain-recovery. Average result of N=5 is shown, standard deviations have been removed for clarity. D Effect of oB-CD content on (i) hydrolytic and (ii) enzymatic degradation. 50  $\mu$ L disc-shaped hydrogels were incubated in PBS or collagenase II 2 EU/mL solution for hydrolytic and enzymatic degradation, respectively. Gels contained 20% GTA, 20 mM SPS, 2 mM RB, 0-4% oB-CD and were irradiated for 30 minutes. \*  $p < 0.05$ , \*\*  $p < 0.01$ .

Next, rheological measurements were conducted to investigate the viscoelasticity of the GTA/oB-CD hydrogels. Strain sweep of GTA/ oB-CD hydrogels displayed a quite broad linear viscoelastic region (LVE) with network breakdown at high strains (Fig. 4B). Further, the shear modulus increased with increasing content of oB-CD in the network;

however, oB-CD content did not impact the amplitude at which the network collapsed (Fig. S5). To assess the recovery of material properties following network breakdown at high strain (100 %), GTA/ oB-CD hydrogels were subjected to shear strain cycles of high (100%) and low (1%) strain (Fig. 4C). At low strain, GTA/ oB-CD hydrogels containing 4% oB-CD exhibited a typical gel behavior with the elastic modulus higher than the viscous modulus ( $G' > G''$ ). In the next cycle, when hydrogels were subjected to a high shear (100%), the elastic modulus decreased from 480 Pa to 1.8 Pa, indicating a transition from a solid-like to a viscous-like behavior. After decreasing the strain to its initial value, a rapid and complete recovery of  $G'$  to the initial levels was observed and it did not change over several cycles. This behavior can be attributed to the combination of the permanent photo-crosslinking with the reversible imine bonds and guest-host interactions, which together contribute to the formation of a strong and self-recovering matrix. We deem these properties desirable for the successful implantation of the hydrogel during musculoskeletal surgery.

### 3.4 Enzymatic and Hydrolytic Degradation

The use of naturally-derived polymers as drug delivery carriers allow shorter *in vivo* degradation time following drug release, a distinct advantage compared to longer degradation times observed when using synthetic polymers such as poly(lactic-co-glycolic) acid and poly(caprolactone) to prepare drug delivery formulations<sup>49,411</sup>. Gelatin can undergo hydrolytic degradation, proceeding *via* the cleavage of amide bonds. Furthermore, its Pro – X – Gly – Pro (where X is a neutral amino acid) sequences make gelatin susceptible to enzymatic degradation. These sequences can be cleaved by matrix metalloproteinases, such as collagenase II, naturally present in the body<sup>412</sup>. To simulate physiological conditions, hydrolytic degradation was investigated by incubation of GTA/oB-CD hydrogels in PBS buffer (pH 7.4) at 37°C. The hydrolytic degradation was monitored by measuring hydrogels' remaining mass at fixed time points over a period of 42 days. As expected, no decrease in hydrogel weight was observed at the physiological conditions used. This resistance of gelatin hydrogels to hydrolytic degradation is in agreement with previously described hydrogels and likely due to the stability of peptide bonds at physiological conditions<sup>413</sup>. The rate of hydrolytic degradation did not differ between hydrogels with and without 4% oB-CD (Fig. 4C-i). As gelatin is susceptible to enzymatic degradation, this was studied at 37°C in a simulated body fluid containing physiological levels of collagenase II (PBS, collagenase II 2 EU/mL)<sup>398</sup>. Hydrogels that did not contain oB-CD were completely degraded in four days, whereas in presence of oB-CD the degradation time increased to eleven days (Fig. 4C-ii). This extended duration of degradation may be due to the presence of bulky oB-CD moieties that might hinder the diffusion of the enzyme within the hydrogel and the accessibility of the enzyme-cleavable sequences in the gelatin chains<sup>414</sup>. With a molecular weight for collagenase of approx.

130 kDa, the molecule's radius is estimated to be at least 3 nm<sup>397,415</sup>. As a result, the enzyme will first cleave the outer gelatin chains, slowly reaching the inner part of the hydrogels leading to a complete degradation. Indeed, calculations based on the rubber elasticity theory showed that the presence of oB-CD leads to a decrease in mesh size, with mesh size of  $11.1 \pm 0.8$  nm and  $8.1 \pm 1.2$  nm for hydrogels without oB-CD and with 6% oB-CD, respectively.

### 3.5 Sustained release of bupivacaine from GTA / oB-CD hydrogels

Following implantation during surgery, the hydrogel was designed to deliver the local anesthetic bupivacaine in a sustained manner. Drug loading was performed by immersing ring-shaped hydrogels in a bupivacaine HCl solution (50 mg/mL) for 24 hours at 37°C. The release profile of bupivacaine from the GTA/oB-CD gels was monitored for 168 hours and displayed a considerable initial burst followed by a fast release beyond 24 hours (Fig. 5A). Decreasing an initial burst of LA from sustained release formulations is a major developmental challenge<sup>42</sup>. Indeed, burst release might lead to sudden high local or serum levels of bupivacaine, putting patients at risk of adverse effects<sup>379</sup>. Conversely, initial burst release inherently decreases the amount of drug available in the hydrogel to provide analgesia after the burst release has been washed out. To decrease this initial burst and achieve a sustained release of bupivacaine, drug crystals were formed inside the hydrogel matrix by pH-induced drug crystallization. This way, crystal dissolution would act as an additional rate-limiting step in the diffusion of the drug from the hydrogel. Previous studies showed that pH-induced drug crystallization enable high drug loading and prolonged release<sup>416</sup>. To induce *in-situ* drug crystals formation, hydrogels were first incubated in a solution of bupivacaine HCl, followed by incubation in a sodium bicarbonate/ glycerol mixture for 2 hours at 37°C. Prior to crystal formation, bupivacaine HCl content per ring was  $55.5 \pm 2.9$  mg. Following alkaline-promoted crystallization, hydrogels contained a bupivacaine dose of  $49.8 \pm 3.5$  mg. The release profile of hydrogels containing crystallized bupivacaine was characterized by a moderate decrease in initial burst release as compared to bupivacaine HCl ( $p < 0.05$ ). The bupivacaine alkaline crystallization procedure led to a formulation with a burst release of  $66.7 \pm 12.9\%$  of total dose after 8 hours, compared to  $90.0 \pm 4.1\%$  of total dose released from hydrogels containing bupivacaine HCl. Release from hydrogels containing crystallized bupivacaine was significantly slower compared to hydrogel containing bupivacaine HCl up to 48 hours after initial drug release. After 168 hours of release, hydrogels were collected and the residual bupivacaine content was determined. Hydrogels subjected to *in situ* crystallization had  $2.6 \pm 2.5\%$  of total drug content left in the matrix (Fig. 5A). No bupivacaine was left in hydrogels containing bupivacaine HCl beyond 24 hours, demonstrating the beneficial effect of bupivacaine crystals in slowing down release. Although hydrogels containing crystallized bupivacaine had only 11% of total dose left

after 24 hours, we believe this concentration might be anesthetically effective as the analgesic effect will likely depend on local concentration and clearance of bupivacaine. As pedicle screws and thus hydrogels will be closely surrounded by muscle tissue following surgery, literature on bupivacaine clearance from muscle might be indicative of in vivo performance. Indeed, in a previous study performed by McDonald et al. muscle tissue concentrations were quantified using microdialysis in rats following administration of bupivacaine HCl infiltration or a bupivacaine microparticle formulation. Despite the in vitro release of the microparticles being limited to 30 hours, tissue concentrations equaling those obtained shortly after bupivacaine HCl infiltration were obtained until four days after administration.<sup>417</sup> Moreover, bupivacaine elimination half-life from swine skeletal muscle was reported to be 82 minutes.<sup>418</sup> Further, in clinical practice, instrumented spinal surgery always involves implantation of four or more pedicle screws which enables the implantation of at least four hydrogels. Taken together, implantation of multiple hydrogel rings, as well as limited local clearance rates that possibly lead to accumulation of bupivacaine at the surgical site, could both increase the likelihood of analgesic effect beyond 24 hours.

Further, to assess the effect of bupivacaine crystals on stiffness, the mechanical properties of hydrogels containing bupivacaine crystals and bupivacaine HCl were investigated by dynamic mechanical analysis. The presence of bupivacaine crystals did not significantly affect the compression modulus of the hydrogel (Fig. 5B). Because bupivacaine is crystallized after the network formation, there is no interference with the crosslinking. As a consequence, bupivacaine crystals can only grow within the space available in the hydrogel matrix. The presence of bupivacaine crystals inside the porous structure of the hydrogel was confirmed using SEM (Fig. 5C).



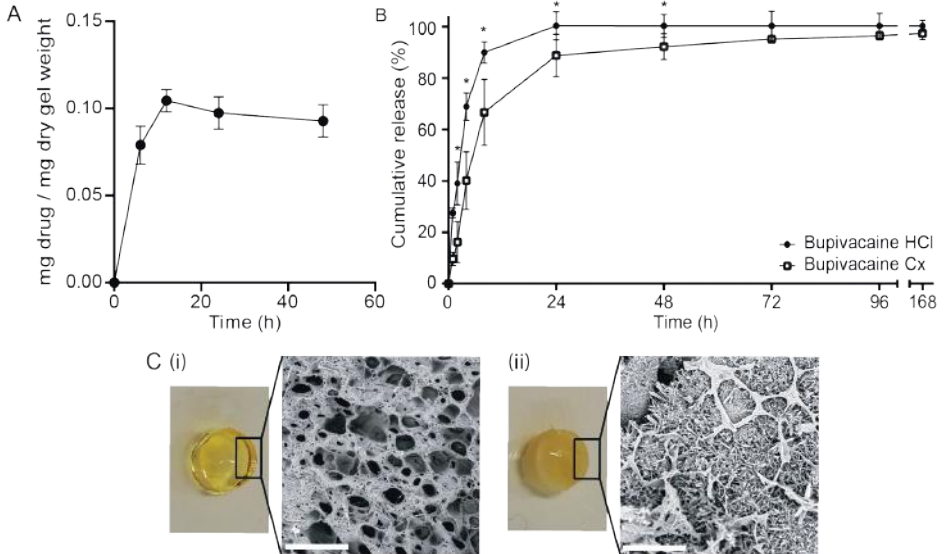


**Figure 5.** Bupivacaine release from GTA/oB-CD hydrogels. *A* Release of bupivacaine HCl and bupivacaine crystals from ring-shaped hydrogels. Release is plotted as the percentage of total bupivacaine content in the hydrogels. Total bupivacaine content was determined by hydrogel degradation after 168 hours of release. Data are presented as mean ( $N=5$ ) with standard deviation as error bars. Data was analyzed using an independent samples t-test at each time point. *B* Effect of bupivacaine crystals on compression modulus. Data was analyzed using an independent-samples T-test ( $p > 0.05$ ). *C* Scanning electron microscope (SEM) images of hydrogels with and without bupivacaine crystals (scale bar 100 mm).

### 3.6 Cytocompatibility of GTA Hydrogels for sustained bupivacaine release

To determine the cytocompatibility of the developed hydrogel formulation, the metabolic activity and viability were determined by culturing human mesenchymal stromal cells (MSCs) and NIH3T3 fibroblasts in presence of GTA hydrogels for 48 hours. MSCs and fibroblasts were selected, as fibroblasts and differentiated MSCs make up the majority of cells present in the orthopedic wound<sup>338</sup>. Indeed, following implantation, the hydrogel for LA delivery comes into contact with various tissues such as bone, muscle, tendon, ligament and fascia. As shown in Fig. 6A, cell metabolic activity was quantified using an Alamar Blue assay on cells cultured in contact with hydrogels contained increasing concentrations of oB-CD. Metabolic activity was quantified after 24 and 48 hours of culture. Significant differences were observed in MSCs and fibroblast metabolic activity compared to controls (Fig. 6A). In all groups exposed to hydrogels, cell metabolism increased compared to controls after 48 hours of culture. This effect could be due to the presence of RB, as RB has been linked to increased cell proliferation<sup>419</sup>. Moreover, RB deficiency has been associated with DNA and protein oxidative damage in liver cells,

inhibiting cell mitosis<sup>420</sup>. Furthermore, the effect of glycerol and sodium bicarbonate on cell metabolism was investigated, as both were used during drug crystallization. As shown in Figure 6A, the presence of glycerol inside the hydrogels did not affect cell metabolism.

Cell viability was assessed using a Live-Dead assay. MSCs and NIH3T3 fibroblasts were seeded in a well plate and cultured in presence of hydrogels. Hydrogel compositions tested contained increasing concentrations of oB-CD with and without glycerol. No significant differences regarding cell viability were observed in NIH3T3 fibroblasts (Fig. 6B-i and Fig. S6) exposed to different concentrations of oB-CD or the presence of glycerol. In the case of MSCs, significant differences in cell viability were observed when compared to control monolayers exposed to culture medium only (Fig. 6B-ii and Fig. S6).

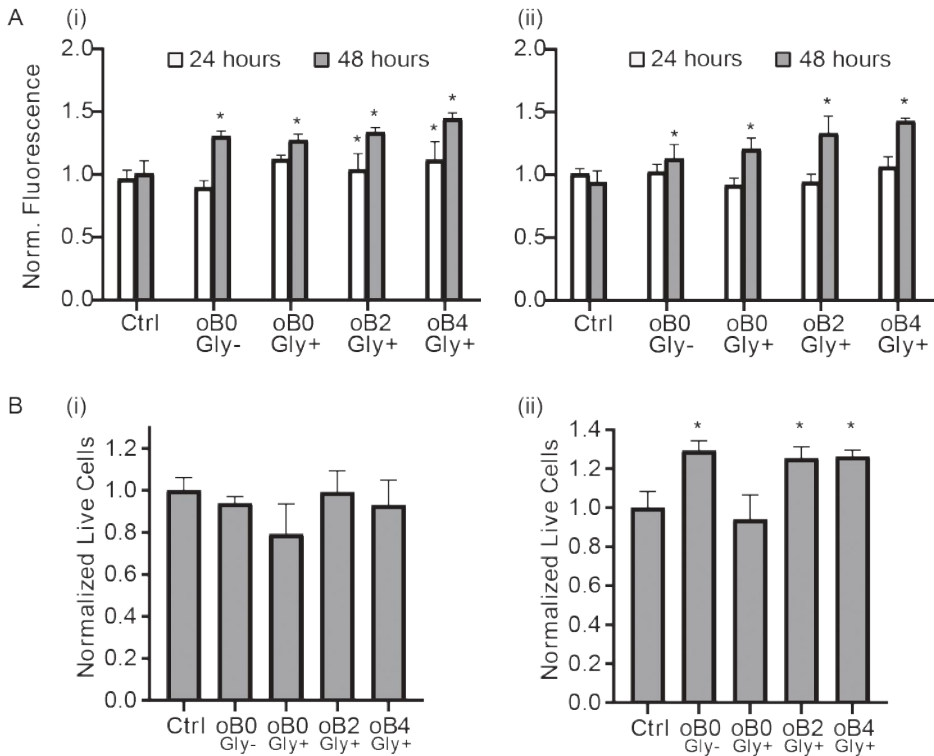


**Figure 6.** Metabolic activity and viability of MSCs and fibroblasts. A Metabolic activity of NIH3T3 fibroblasts (i) and MSCs (ii) determined by Alamar Blue assay after 24 and 48 hours of exposure to GTA hydrogels, with (Gly+) or without (Gly-) glycerol, and containing increasing concentrations of oB-CD (0-4 wt.%). All values have been normalized to controls. B Live/Dead assay of NIH3T3 fibroblasts (i) and MSCs (ii) after 48 hours of exposure to hydrogels with (Gly+) or without (Gly-) glycerol, and containing increasing concentrations of oB-CD (0-4%). Viability is expressed as live cell count normalized to control wells. Controls consisted of monolayer cells exposed to culture medium only in all cases. Data are presented as mean ( $n=4$ ) with standard deviation. Data was analyzed using one-way ANOVA. All groups were compared to controls. \*  $p < 0.05$ .

Next, we evaluated the cytocompatibility of hydrogels loaded with bupivacaine HCl and bupivacaine crystals (Fig. 7). NIH3T3 fibroblasts and MSCs were seeded in well plates and cultured for 24 hours in the presence of hydrogels. Exposing cells to hydrogels containing bupivacaine HCl and bupivacaine crystals caused a significant decrease in viability compared to controls. Hydrogels loaded with crystallized bupivacaine performed significantly better than hydrogels loaded with bupivacaine HCl, when culturing NIH3T3 fibroblasts for 24 hours (Fig. 7B and 7C). To understand whether this effect was due to slower release of bupivacaine from the hydrogels, or to neutralization of acidic bupivacaine following crystal formation, a Live/Dead assay was performed. NIH3T3 fibroblasts and MSCs were cultured in growth medium supplemented with i) bupivacaine HCl (1 mM in

DMSO); ii) bupivacaine crystals (1 mM in DMSO and iii) the equivalent volume of DMSO used for culture i) and ii) for 24 hours (Fig. 7D-i+ii and Fig. S7). After 24 hours, the decrease in cell viability was most extensive in monolayers exposed to bupivacaine HCl dissolved in DMSO, followed by bupivacaine crystals (dissolved in DMSO) and DMSO only. This indicates that cell death induced by bupivacaine HCl is mainly due to the acidic pH. Cells were then further cultured in fresh medium for 48 hours, after which both MSCs and fibroblasts showed recovery following exposure to bupivacaine crystals. In the case of bupivacaine HCl, fibroblasts recovered better than MSCs. Overall, these results show that bupivacaine crystallization enable a sustained release with moderately decreased initial burst and improved cytocompatibility when compared to bupivacaine HCl. These properties might reduce the known myotoxic effects of bupivacaine.<sup>339</sup>

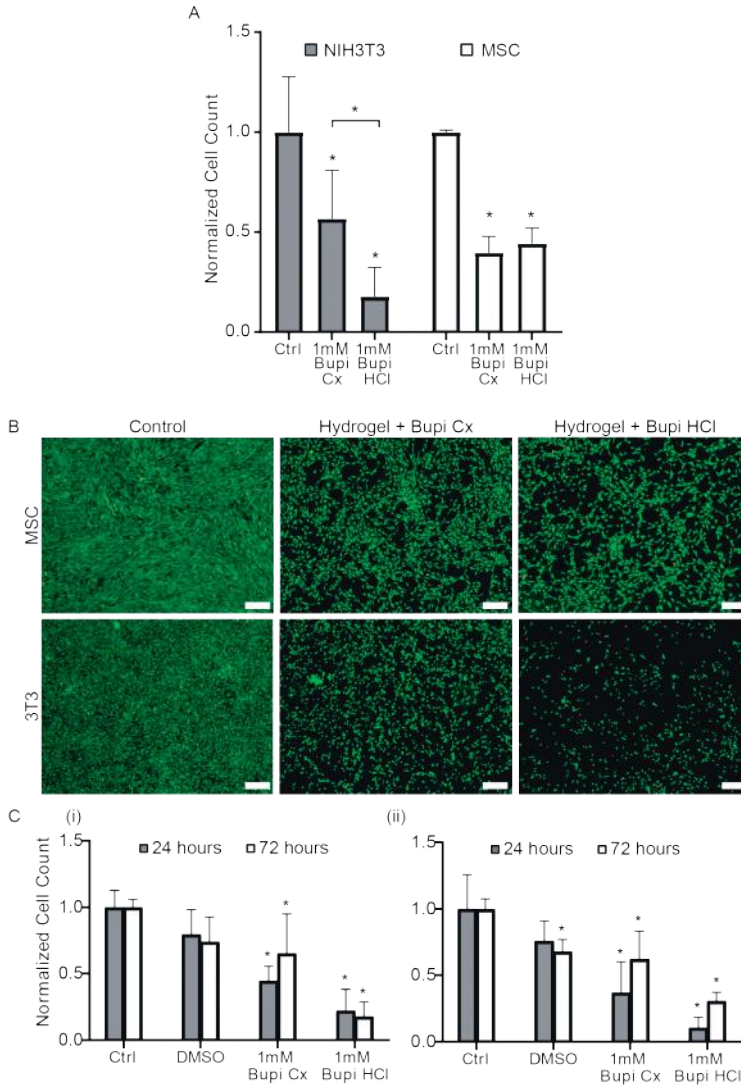


**Figure 7.** Cytocompatibility of GTA/oB-CD hydrogels containing bupivacaine. **A** Live/Dead assay of MSCs and NIH3T3 fibroblasts following 24 hours of exposure to gels loaded with bupivacaine crystals (Cx) or bupivacaine HCl. All values have been normalized to control live cell count. **B** Representative fluorescent microscope images of live/dead staining of MSCs and NIH3T3 fibroblasts, after 24 hours of exposure to gels loaded with bupivacaine crystals (Cx) or bupivacaine HCl (scale bar 200  $\mu$ m). **C** Live/Dead assay of MSCs (i) and NIH3T3 fibroblasts (ii) after 24 hours of exposure to culture medium containing 1 mM bupivacaine HCl in DMSO, 1 mM bupivacaine crystals (Cx) in DMSO, and equivalent volumes of DMSO in culture medium. 72 hours cells were exposed to solutions for 24 hours, followed by 48 hours of recovery. All values have been normalized to control live cell count. Controls consisted of monolayer cells exposed to culture medium only in all cases. Data are presented as mean ( $n=5$ ) with standard deviation as error bars. Statistical analysis was performed using a one-way ANOVA. All groups were compared to controls. \*  $p < 0.05$ .

### 3.7 Ex vivo implantation

To qualitatively assess the suitability of GTA/oB-CD hydrogels for use in instrumented spinal surgery, bupivacaine-loaded hydrogel rings were co-implanted with polyaxial pedicle screws in fresh cadaveric sheep. The ring-shaped hydrogels were resistant to the forces encountered during implantation, as 19 out of 20 hydrogel rings could be implanted successfully and without any macroscopic sign of damage (e.g., cracks, discoloration, tears) (Fig. 8). The design and composition of the hydrogel ring did not interfere with surgical workflow or finding the optimal screw trajectory. Due to its elasticity, the hydrogel could adapt its shape to the surgical environment. Following overtightening of screws, the rings displayed further radial expansion to accommodate the polyaxial screw head. It should be noted that none of the sheep displayed signs of spinal disease. The presence of anatomical malformations, such as scoliosis or fracture in the human patient, might complicate implantation of the screw and subsequently the hydrogel rings.

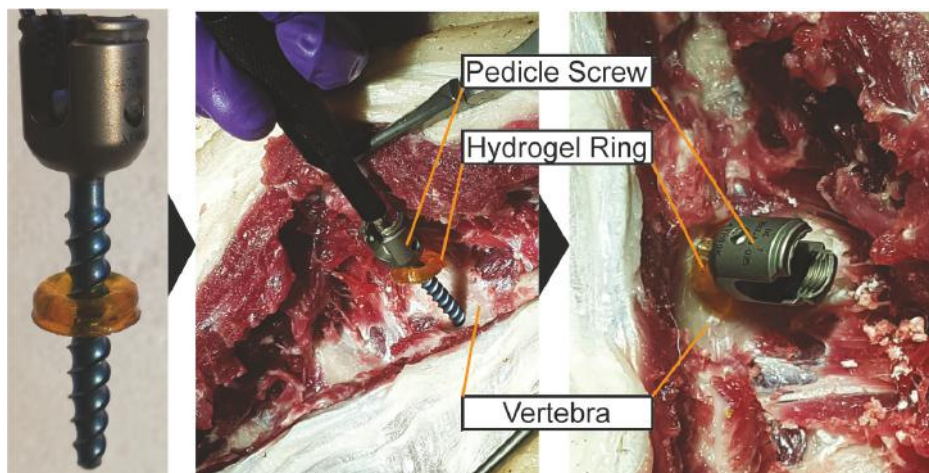


**Figure 8.** Ex vivo implantability of ring-shaped hydrogel. Hydrogel rings were mounted on a 5\*40 mm polyaxial pedicle screw (left). Hydrogel rings being implanted in a sheep spinal column (center). Fully inserted pedicle screw and hydrogel ring. The hydrogel ring radially expands and adapts its shape to the bone surface upon tightening of the screw (right).

## 4. CONCLUSIONS

In summary, our study demonstrates that a GTA/oB-CD photo-crosslinked hydrogel could be a very promising system for the sustained delivery of bupivacaine for pain relief following instrumented spinal surgery. The combination of the riboflavin-mediated photo-crosslinking with the simultaneous Schiff base formation and guest-host interactions provided a tunable hydrogel displaying self-healing properties, capable of withstanding

co-implantation with pedicle screws and providing sustained release for 72 hours. The GTA/oB-CD hydrogel containing *in situ* crystallized bupivacaine is cytocompatible and following release, the hydrogel is susceptible to enzymatic degradation. The moderate decrease in burst release and use of crystallized bupivacaine led to decreased cytotoxicity compared to bupivacaine HCl. This novel photo-crosslinked gelatin-based hydrogel has the potential to reduce opioid consumption following spinal surgery, and provide localized, sustained release of analgesics. In future, the use of this hydrogel formulation can be extended towards other implantation sites and/ or encapsulated drugs.

## **ACKNOWLEDGMENTS**

The authors would like to thank Marko Mihajlovic for help with NMR experiments, Mies van Steenbergen for support and advice in mechanical testing, drug loading and quantification of release, Mattie van Rijen for general support during various stages of this study.

This study was supported by SentryX B.V., Woudenbergseweg 41, 3711AA Austerlitz, Netherlands.

## SUPPLEMENTARY DATA

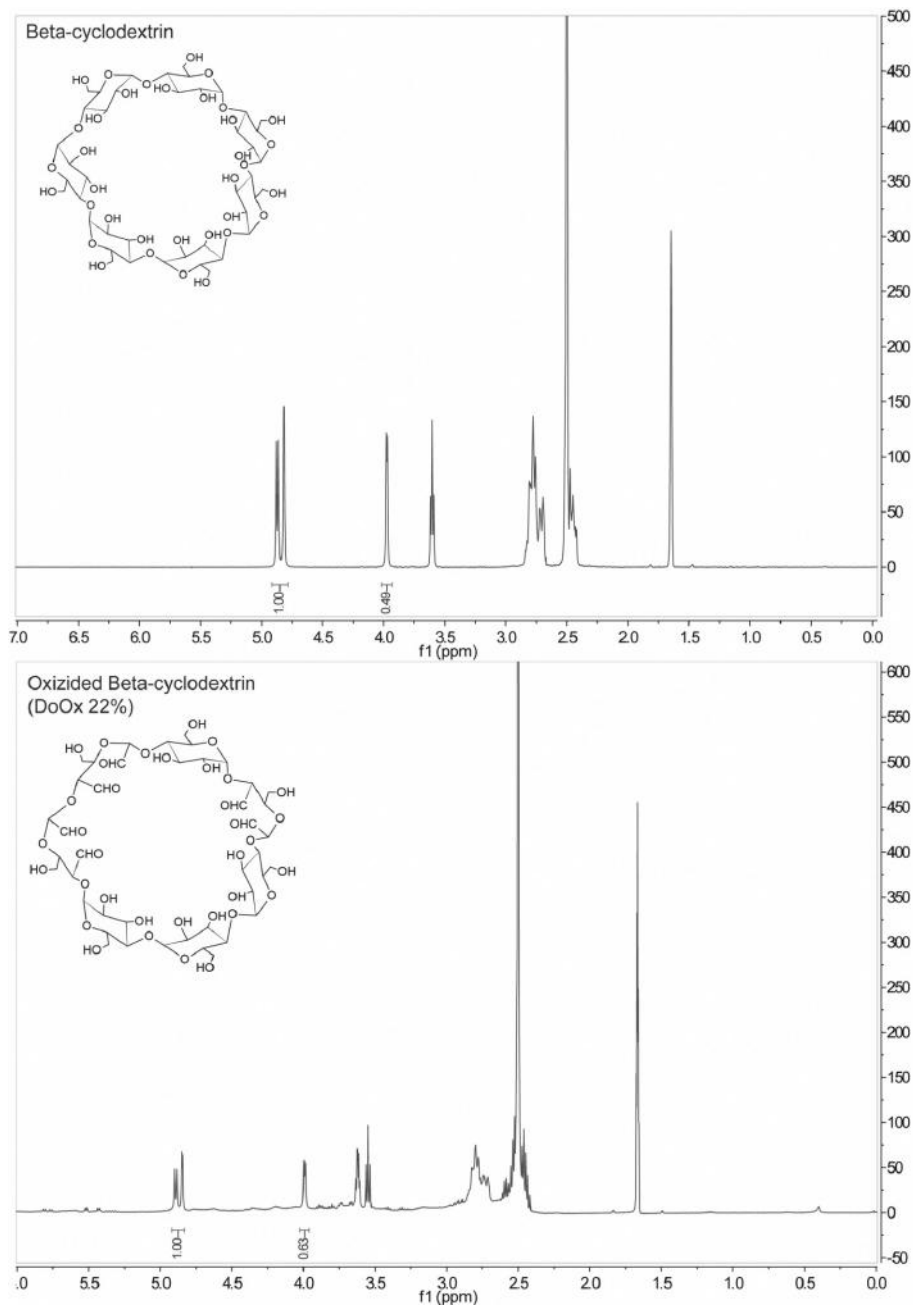


**Figure S1.**  $^1\text{H-NMR}$  Spectra of non-oxidized (top) and oxidized  $\beta$ -cyclodextrin (bottom), used to determine degree of oxidation in DMSO.



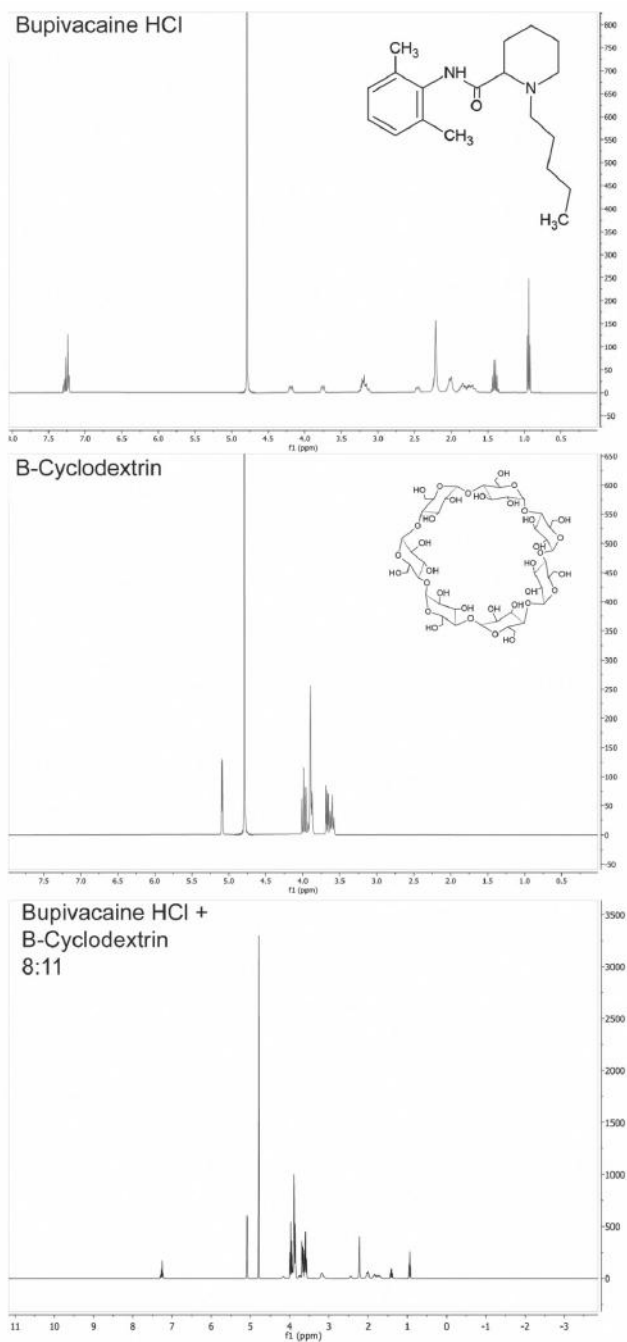


**Figure S2.**  $^1\text{H-NMR}$  spectra of bupivacaine HCl (8 mM), beta-cyclodextrin (11 mM) and beta-cyclodextrin and bupivacaine HCl. All spectra were obtained in  $\text{D}_2\text{O}$ .

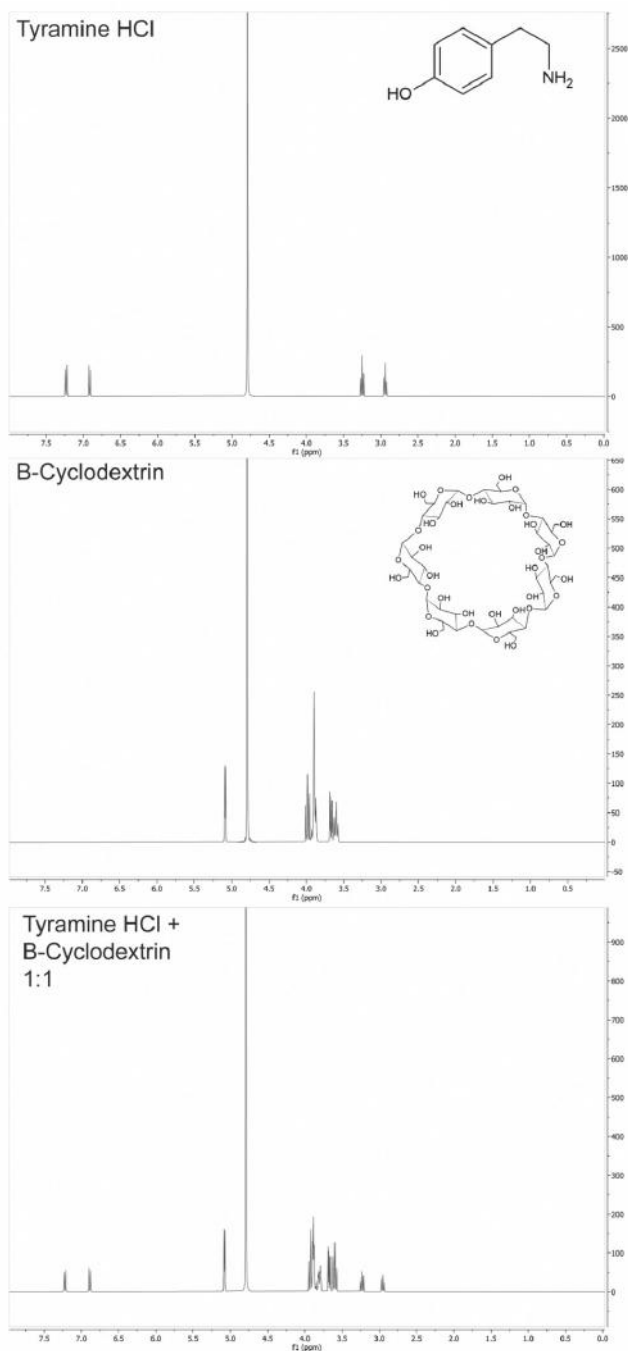


**Figure S3.**  $^1\text{H-NMR}$  spectra of tyramine HCl (10 mM), beta-cyclodextrin (11 mM) and beta-cyclodextrin and tyramine HCl. All spectra were obtained in  $\text{D}_2\text{O}$ .

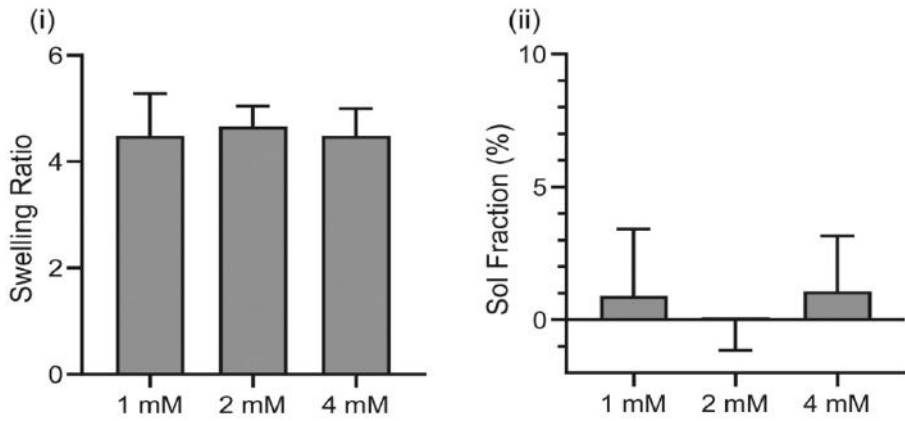


**Figure S4.** Effect of riboflavin concentration on (i) swelling ratio and (ii) sol fraction for hydrogels (100  $\mu$ L) containing 20% GTA, 20 mM SPS, 0% oB-CD and irradiated for 30 minutes.

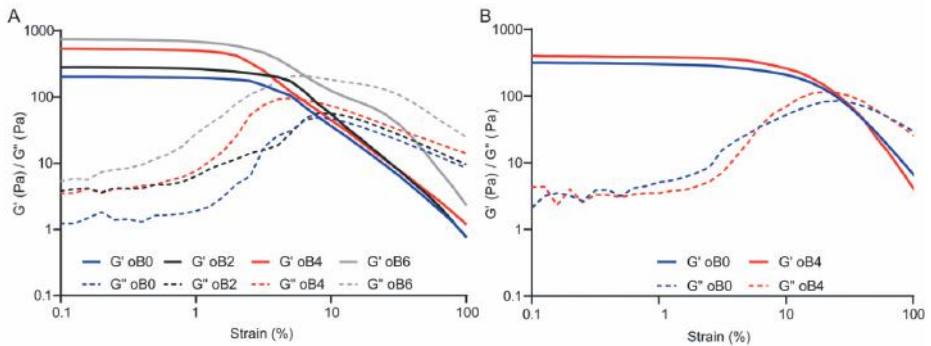


**Figure S5.** A Amplitude sweep of hydrogels containing 20% GTA, 20 mM SPS, 2 mM RB and 0-6% oB-CD. Representative samples are shown,  $N=3$  for all groups. B Amplitude sweep of hydrogels containing 20% GTA, 20 mM SPS, 2 mM RB and 0-4% oB-CD and glycerol. Representative samples are shown,  $N=3$  for all groups.

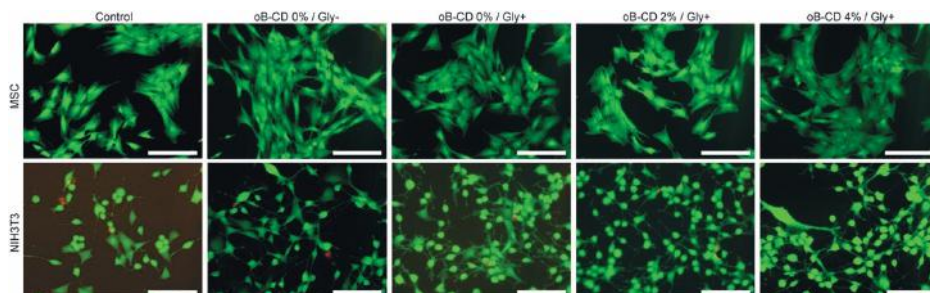


**Figure S6.** Representative fluorescent microscopy images of Live-Dead assay of MSCs and NIH3T3 fibroblasts following 48h of exposure to i) culture medium (control); ii) hydrogels (100 $\mu$ L)- with 20% GTA, 20 mM SPS, 2 mM RB and 0% oB-CD without glycerol (oB-CD 0% / Gly-); iii) 0% oB-CD with glycerol (oB-CD 0% / Gly+); iv) 2% oB-CD with glycerol (oB-CD 2% / Gly+); v) and 4% oB-CD with glycerol (oB-CD 4% / Gly+) in culture medium. Scale bar 200  $\mu$ m.

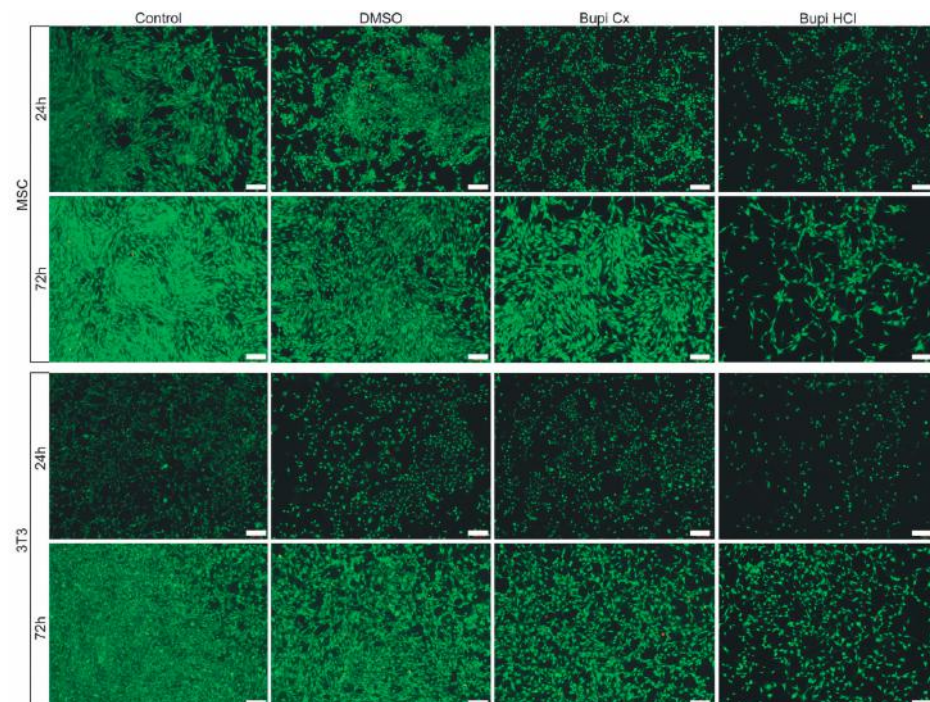
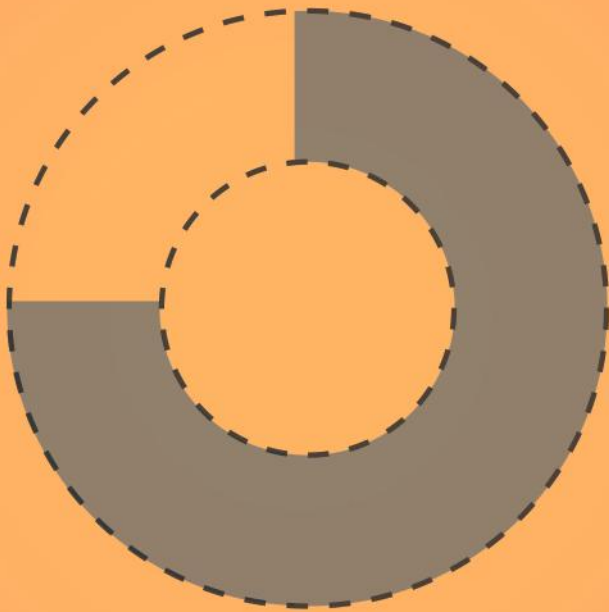


**Figure S7.** Representative fluorescent microscopy images of Live-Dead assay of MSCs and NIH3T3 fibroblasts after 24 hours of exposure to i) culture medium; ii) culture medium supplemented with i) DMSO; iii) 1 mM crystallized bupivacaine in DMSO; iv) 1 mM bupivacaine HCl in DMSO. 72h cells were exposed to conditions I,ii, iii and iv for 24h, followed by 48h of recovery. Scale bar 200  $\mu$ m.





# CHAPTER 8

## Testing a new sustained-release local anesthetic formulation specifically designed for spine surgery in a sheep model

Jasper G. Steverink, Floris R. van Tol, Suzanne Bruins, Kwame B. Amponsah, Jessica Marvela, Andre J. Smorenburg, Hein R. Jonkman, Bas J. Oosterman, Marijke R. van Dijk, Jos Malda, Susanna Piluso, Jorrit-Jan Verlaan

## ABSTRACT

Instrumented spinal surgery is a frequently performed and painful intervention, with severe pain lasting often for three days. Opioids are the cornerstone of treatment of postoperative pain, but can induce severe side effects, dependence and addiction. Novel local anesthetic applications, such as erector spinae plane blocks, and sustained release formulations have the potential to decrease opioid consumption without analgesic compromise, but have limited efficacy beyond 24 hours. A mismatch in duration of pain and duration of non-opioid analgesia is thus present in spine surgery. This study assesses the feasibility of a robust hydrogel for three days of sustained and stationary bupivacaine delivery, designed for co-implantation with pedicle screws, in a sheep model for spinal surgery.

Fifteen sheep received six hydrogel rings loaded with bupivacaine mounted on pedicle screws (total dose 220 mg). Wound and systemic drug levels, hydrogel degradation and histological response were assessed. Moreover, *in vivo* drug release was correlated to *in vitro* release (IVIVC). Rings stayed in place after surgery and displayed a first-order release profile *in vivo* over 72 hours, with excellent IVIVC. Ring intactness after implantation did not affect release. Bupivacaine wound fluid levels exceeded plasma levels 2300-fold, and plasma bupivacaine levels were well below toxic thresholds through 168 hours. Histological analysis of implant sites revealed a conventional foreign-body response that subsided during follow-up. Hydrogels degraded completely in 9 months. The present hydrogel has the potential to provide safe, localized and sustained analgesia following instrumented spinal surgery.



## 1. INTRODUCTION

A large and increasing number of spine surgeries is performed each year, with over 400,000 spinal fusions in the United States alone in 2014.<sup>14</sup> Severe postoperative pain is often experienced for three days or more, and inadequate postoperative pain control is reported by up to 75% of patients.<sup>15,36</sup> Moreover, spinal surgery ranks amongst the most painful interventions overall, despite the use of potent systemic analgesics.<sup>12,15</sup> Postoperative pain has been shown to decrease surgical outcomes and quality of life, and increase the risk of developing chronic pain, thus posing a major health burden for patients undergoing spine surgery.<sup>9,11,15,373</sup> To treat acute and prevent chronic pain, opioids are the mainstay of current analgesic treatment following spinal surgery.<sup>65</sup> Opioids can, however, lead to a plethora of adverse effects with considerable morbidity and mortality.<sup>335</sup> In addition, opioid use is associated with the development of dependence and addiction, to such a degree that national campaigns are organized to combat the so-called 'opioid crisis'.<sup>84</sup> Clinical practice increasingly focuses on enhancing recovery after surgery (ERAS) by optimizing all stages of the perioperative process. This includes improving preoperative patient fitness, minimizing surgical stress, multimodal analgesia and rapid mobilization.<sup>6,7,421</sup> However, recovery after spine surgery is hampered by pain and opioid consumption. Thus, a non-opioid alternative to effectively treat acute pain following instrumented spinal surgery is needed.

Local anesthetics such as bupivacaine are a safe and popular option to provide local pain relief, and have been applied in spinal surgery to establish regional blocks.<sup>102,422</sup> A recently popularized technique is the erector spinae plane (ESP) block for spinal surgery, in which the dorsal rami of the spinal root are anesthetized using local anesthetics. While effective in decreasing postoperative pain, its effective duration of up to 24 hours does not match the duration of severe postoperative pain.<sup>36,103,423,424</sup> Local anesthetics lack the adverse effects of opioids, but are limited in duration of action. In an effort to extend analgesia with local anesthetics, continuous infusion in the wound or near nerves has been tested in various surgical applications. Although this technique comes with several downsides such as the permanent connection of the patient to a pump and uncertainty around the risk of infection, its efficacy highlights the potential of local anesthetics in treatment of acute postoperative pain.<sup>37,425</sup> Therefore, multiple sustained-release formulations of local anesthetics have been developed, mainly incorporating bupivacaine as active pharmaceutical agent. Bupivacaine is listed as WHO essential drug and has been used clinically for over 30 years.<sup>271</sup> Examples of sustained-release formulations are injectable polymer-, microparticle- and liposome formulations of bupivacaine, of which some have reached clinical testing or market approval.<sup>42</sup> Liposome bupivacaine (Exparel®) enabled 24-hour pain relief compared to placebo following bunionectomy surgery and high doses

of liposome bupivacaine were effective in decreasing pain after total knee arthroplasty when compared to bupivacaine HCl infiltration.<sup>320,426</sup> Further, a bupivacaine-impregnated collagen matrix (Xaracoll®) provided reduction in pain intensity and opioid consumption up to 48 hours in open inguinal hernia repair.<sup>427</sup> However, many systems are hampered by high initial burst release, limiting duration of action and leading to correspondingly high bupivacaine plasma levels, which puts patients at risk of local anesthetic systemic toxicity.

In previous work, we have described the development of a robust hydrogel designed for co-implantation with pedicle screws during spinal surgery and demonstrated its *ex vivo* implantability.<sup>428</sup> This hydrogel provided sustained release of bupivacaine *in vitro* up to 72 hours by alkaline crystallization of the active pharmaceutical ingredient. The biodegradable materials displayed excellent cytocompatibility. Here, we report *in vivo* release and degradation results of an improved version of this hydrogel, using a slightly modified approach in raw material functionalization. Further, we describe the *in vitro-in vivo* correlation of release kinetics.

## 2. MATERIALS AND METHODS

### 2.1 Hydrogel preparation

Commercially available gelatin (type A from porcine skin; low endotoxin content) derivatized with 3,4-hydroxyphenylpropionic acid, referred to as GelTyr, with high (HMW) and low molecular weight (LMW) was used for hydrogel synthesis. Ring-shaped hydrogels were prepared as described previously.<sup>428</sup> In short, GelTyr was dissolved in water for injection (WFI) at 45°C. Riboflavin-5-monophosphate (RB) and sodium persulfate (SPS) stock solutions were prepared in WFI. Oxidized beta-cyclodextrin (oB-CD) was prepared as described previously to obtain an oxidation degree of  $\pm 23\%$  and dissolved at 20 wt% in WFI.<sup>428</sup> Stock-solutions were then mixed to obtain a pre-gel solution of 20% GelTyr, 2 mM RB, 20 mM SPS and 4% oB-CD, transferred in ring-shaped molds and irradiated with high-intensity visible white light (400-700 nm) for 30 minutes (figure 1B). The resulting hydrogels were washed to remove any remaining reagents. To load bupivacaine, the hydrogels were submerged in a 5 wt.% bupivacaine HCl solution followed by incubation in sodium bicarbonate buffer/ glycerol (0.1 M, pH 8.5) to induce alkaline crystallization of bupivacaine inside the hydrogels. The bupivacaine loaded hydrogels were then dip coated with poly(lactic-co-glycolic) acid (PLGA, 50:50 ratio) dissolved in acetone at 20 wt.% so that the domed surface of the ring-shaped hydrogel was coated, whilst the flat bone-contact surface remained uncoated. The flat bottom surface of the hydrogel rings, in contact with the bone during surgery, was not coated to allow diffusion of bupivacaine from that surface to the bone. In total, three types of hydrogel rings were prepared using

HMW and LMW gelatin: 1) LMW-GelTyr coated; 2) HMW-GelTyr, uncoated; 3) HMW-GelTyr coated.

Following preparation, hydrogels were sterilized using Gamma-sterilization. To assess endotoxin content of sterilized hydrogels, a quantitative LAL-assay for lipopolysaccharides was performed according to the instruction of the manufacturer (Toxinsensor, Genscript Biotech, Leiden, Netherlands).

### **2.1 *In vitro* release**

*In vitro* release was tested by submerging hydrogels in 20 mL of 0.01 M citrate buffer (pH 6.0) and incubation at 37°C on a shaker plate. At predetermined time points, a 1 mL sample was taken and replaced with 1 mL of fresh buffer. After 168 hours of release, samples were transferred to a 0.1% formic acid in WFI solution at 45°C to extract any remaining bupivacaine in the hydrogel. Bupivacaine concentration in the samples taken was quantified using high-performance liquid chromatography (HPLC) and a cumulative release curve was constructed. Mobile phases consisted of 0.1% formic acid in water and 0.1% formic acid in acetonitrile, and an Agilent Zorbax RRHD column (particle size 1.8  $\mu\text{m}$ , internal diameter 2.1 mm, length 100 mm) was used.

### **2.2 *In vitro* degradation**

To study the rate of hydrogel degradation *in vitro*, three hydrogel rings per type were incubated in 20 mL of collagenase II solution in a simulated body fluid (phosphate-buffered saline, pH 7.4) at 37°C on a shaker plate. Enzymatic activity of the solution was 2 EU\* $\text{mL}^{-1}$  to correspond to *in vivo* conditions.<sup>400</sup> The solution was replaced every three days to maintain enzymatic activity levels. Degradation was monitored visually until the rings had disappeared.

### **2.3 Animal studies**

Approval of the local ethical committee was obtained before the start of animal experiments. Animal experiments were performed according to the ARRIVE 2.0 guideline. The sheep (Swifter ewes, mean preoperative weight  $77.6 \pm 10.1$  (range 56-104) kg, age  $5.8 \pm 1.1$  years) was selected as animal model as body weight, circulating volume and spinal anatomy are similar to humans.<sup>429</sup> Sheep were housed in groups of 5 and allowed 1 week of acclimatization following their arrival at the test facility. After surgery, sheep were housed separately to prevent wound healing complications and conflicts. Animals had unlimited access to hay and water. A 12-hour light-dark cycle was maintained and animal welfare was monitored daily.

## 2.4 Spinal Surgery and Hydrogel Implantation for Release

Twenty-one sheep underwent surgery, in which hydrogel rings were co-implanted with pedicle screws. Each sheep contained 2 rings of each type, leading to six hydrogel rings implanted per sheep. Ring placement on the spine was randomized using the [www.randomized.org](http://www.randomized.org) online randomization tool and is illustrated in **figure 1A**. Surgery was supervised by an experienced spine surgeon (JJV). Sheep were placed in prone position on a heated operation table and received general anesthesia. The dorsal skin was shaved and disinfected using povidone iodine from the pelvis to the thoracolumbar junction. After sterile draping of the surgical field, a midline incision was performed and the fascia was opened. The erector spinae muscle was dissected laterally to expose facet joints and the medial part of transverse processes. The facet joints were partly removed using an osteotome to allow access to the pedicle screw entry point. A single lumbar level was skipped between instrumented levels (L2-4-6) to reduce interference of adjacent hydrogel rings regarding release (figure 1A). A 5 mm hole was drilled through the cortex of the transverse process and into the pedicle and vertebral body. Subsequently, the rings were mounted on polyaxial pedicle screws (6 \* 30 mm, figure 1C) and both were implanted (figure 1D). Screws were tightened until the screw head touched the bony surface and its polyaxial movement decreased. The mechanical performance of the hydrogel ring was assessed by two observers (figure 1E). Following implantation of all six screws and rings, the wound was flushed with 500 mL of pre-warmed 0.9% NaCl solution to simulate rinsing a surgical wound as is regular practice in spine surgery to prevent surgical site infections. Completion of implantation of the last screw was recorded as  $t=0$ . The fascia, subcutaneous tissue, and skin were sutured in layers to close the wound. Sheep were terminated at five different time points after implantation (4, 8, 24, 48, 72 hours). For each time point, three randomly assigned sheep were available.

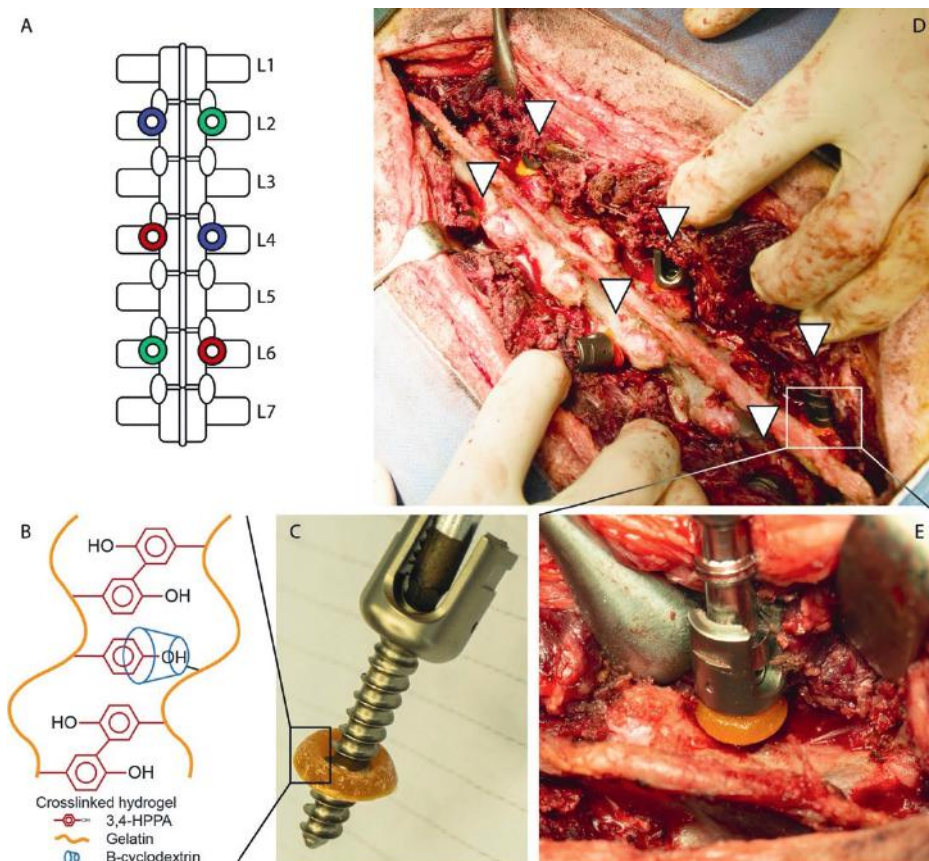


**Figure 1.** Experimental setup. A) Implantation scheme of the various ring compositions tested on the spine, bilaterally at alternating levels. B) Schematic representation of the cross-linking mechanisms involved in forming the hydrogel. 3,4-HPPA: 3,4-hydroxyphenylpropionic acid. C) The hydrogel ring containing bupivacaine mounted on a polyaxial pedicle screw. D) Six hydrogel rings co-implanted with pedicle screws in an ovine model for spinal surgery. E) Close-up of an implanted hydrogel ring, displaying deformability upon tightening of the pedicle screw.

### 2.5 Animal Follow-Up and *In Vivo* Release

Blood was sampled at  $t = 0.5, 1, 2, 4, 8, 24, 48$  and  $72$  hours after the last ring and screw were implanted in the five longest-surviving sheep (48 and 72 hours survival, **table S1**). Blood was centrifuged for 10 min at 3000 rpm, the supernatant plasma aspirated and frozen at  $-20^{\circ}\text{C}$ . At termination, samples of deep (i.e., close to the screws) and superficial (i.e., in the subcutaneous compartment) wound fluid were obtained in selected sheep and centrifuged (table S1). The supernatant was collected and frozen at  $-20^{\circ}\text{C}$ . Analysis of plasma and wound fluid bupivacaine levels was performed by Ardena B.V. (Assen, Netherlands). Sheep terminated after 4 hours were kept under general anesthesia between surgery and termination to reduce animal discomfort. Following termination

at fixed time points, hydrogel rings were explanted and the residual bupivacaine dose was determined by HPLC. Drug was extracted in 0.1% FA and protein precipitation was done by mixing with pure ethanol in 2:1 ethanol: sample ratio. The residual dose in explanted rings was expressed as a percentage of the initial ring dose, as determined per composition during the *in vitro* release testing. Percentual release curves were then obtained by plotting (100% - % left at  $t = X$ ).

## 2.6 *In Vivo* Assessment of Hydrogel Degradation

To assess *in vivo* degradation, hydrogel rings were implanted according to the surgical procedure above in six sheep. Sheep received 8 or 4 hydrogel rings in alternating fashion, to assess the effect of cumulative dose on bupivacaine plasma levels. Plasma samples were obtained  $t = 1, 4, 8, 20, 24, 32, 48, 72, 96, 120, 144$  and 168 hours after the last ring and screw were implanted. An iterative approach was taken (**figure S1**). Hydrogel degradation was assessed by explantation after 28, 56, 168, 252 and 336 days of implantation if hydrogels were present at the previous time point. Remaining hydrogels were then dried, the dry mass was obtained and compared to the initial dry hydrogel mass (without bupivacaine crystals and glycerol). During ring explantation, tissue biopsies were obtained from the direct vicinity of the pedicle screw and hydrogel. Tissue underwent fixation in 4% formaldehyde followed by paraffin embedding and slicing to obtain 4  $\mu\text{m}$  thick histology slides. Next, hematoxylin & eosin staining was performed to allow qualitative evaluation of local tissue response by a board-certified pathologist (MD).

## 2.7 Statistical Analysis

All statistical analysis was performed in Rstudio (Boston, MA, USA). All continuous variables were reported as mean  $\pm$  standard deviation. *In vitro* drug release was fitted to various kinetic models (zero-order, first-order, Higuchi, Korsmeyer-Peppas) to determine the mechanism of drug dissolution.  $R^2$  values and release constants  $k$  were obtained from every model.<sup>430,431</sup> Hydrogels were retrieved from the sheep after predetermined periods of implantation, and drug residues were analyzed using a multivariable linear regression model, setting drug residue as dependent variable and ring type, implantation location, the square root of follow-up time, sheep mobility and ring intactness upon implantation as independent variables. Further, an interaction term between ring type and the square root of follow-up time was added to reduce the effect of start dose on release and improve the model fit. Residuals were saved and Q-Q plots were generated to assess normality.

*In vitro* – *in vivo* correlation was performed by Pearson correlation and linear regression. Pearson *in vitro* – *in vivo* correlation coefficients were obtained for each composition tested. Next, the *in vivo* release was plotted as function of the *in vitro* release at identical

time points (4, 8, 24, 48 and 72 hours). Linear regression was performed and an  $R^2$  value was obtained.

### 3. RESULTS

#### 3.1 Hydrogel preparation

Sixty hydrogels of each type were successfully prepared by photocross-linking, inducing covalent dityrosine bond formation between Phenol groups of the grafted 3,4-hydroxyphenylpropionic acid on GelTyr. In parallel, aldehyde moieties present on oB-CD formed Schiff-bases with the amine groups present on GelTyr. Phenol groups then could form an inclusion complex with the oB-CD cavity, leading to a third method of cross-linking (figure 1B). In the previous report, carboxyl (-COOH) groups present in gelatin were functionalized with tyramine using EDC/NHS chemistry. EDC activation of -COOH groups allowed reacting to amino (-NH<sub>2</sub>) groups on tyramine, but could also yield intramolecular crosslinks between the -NH<sub>2</sub> and -COOH groups present on gelatin. In the present study, -NH<sub>2</sub> groups present on gelatin were with 3,4-hydroxyphenylpropionic acid.<sup>432,433</sup> The improved method of functionalization provides better control of the reaction, easier and scalable purification and yields fewer side products compared to EDC-mediated functionalization.

Bupivacaine dose in hydrogels was quantified using HPLC. Doses per ring were  $43.3 \pm 2.03$  mg for LMW-GelTyr coated,  $41.5 \pm 1.22$  mg for HMW-GelTyr uncoated and  $32.0 \pm 1.47$  mg for HMW-GelTyr coated. To allow application of kinetic models on *in vitro* release profiles, as well *in vitro-in vivo* correlation of release behavior, the *in vitro* release kinetics were determined at physiological conditions. *In vitro*, hydrogels displayed sustained release of bupivacaine up to 96 hours. After 168h, hydrogels had released  $76.4 \pm 3.6\%$  (LMW-GelTyr coated),  $89.6 \pm 0.4\%$  (HMW-GelTyr coated) and  $85.0 \pm 2.0\%$  (HMW-GelTyr uncoated) of total bupivacaine dose. *In vitro* drug release curves were then fitted to various kinetic models for drug release (zero-order, first-order, Higuchi and Korsmeyer-Peppas) using previously described methods to elucidate the driving mechanisms behind drug release.<sup>430,431</sup> High  $R^2$  values were obtained for all models except zero-order (**table 1**). The best-fitting model differed between the hydrogel compositions used.  $n$  exponent values from Korsmeyer-Peppas models ranged between 0.88 and 1.06 for the various compositions tested.

To prevent inflammatory responses once implanted, hydrogel rings were sterilized using gamma sterilization and their endotoxin content was quantified. Endotoxin content of sterilized hydrogel rings was  $1.2 \pm 0.1$  EU per ring on average. To qualitatively study the robustness of the rings, hydrogels were implanted on an anatomical vertebra model

(lumbar spine, sawbones.com, Malmö, Sweden) with a 6\*30 mm pedicle screw. The screw was tightened until the screw head touched the material surface and lost its polyaxial freedom of movement and rings were macroscopically assessed for damage. All rings successfully underwent *ex vivo* implantation. After 28 days of incubation in enzymatic degradation solution, all hydrogels had degraded *in vitro*.

**Table 2.** Fits of kinetic models for *in vitro* release.

Kinetic model		LMW-GelTyr uncoated	HMW-GelTyr coated	LMW-GelTyr coated
Zero-order	R <sup>2</sup>	0,852	0,872	0,877
$x = \text{time}$	$y = a*x \pm b$	0,84*x + 13,64	0,96*x + 11,02	0,80*x + 9,97
$y = \text{drug released (mg)}$	k (=a)	0,84	0,96	0,80
First-order	R <sup>2</sup>	0,955	<b>0,980</b>	0,969
$x = \text{time}$	$y = a*x \pm b$	-0,0084*x + 1,94	-0,0109*x + 1,97	-0,0075*x + 1,98
$y = \log \% \text{ remaining}$	k (=a*ln(10))	0,019	0,025	0,017
Higuchi	R <sup>2</sup>	0,969	0,970	<b>0,975</b>
$x = \text{sqrt time}$	$y = a*x \pm b$	9,01*x + 0,006	10,19*x - 4,09	8,54*x - 2,69
$y = \% \text{ drug released}$	k = a	9,01	10,19	8,54
Korsmeyer-Peppas	R <sup>2</sup>	<b>0,989</b>	0,968	0,971
$x = \log \text{ time}$	$y = a*x \pm b$	0,88*x + 0,61	1,06*x + 0,37	0,94*x + 0,43
$y = \log \% \text{ released}$	k (= e <sup>b</sup> )	1,84	1,44	1,54
	n exponent	0,88	1,06	0,94

### 3.2 Sheep Spinal Surgery

Hydrogel rings were successfully implanted in all 21 sheep. Fifteen sheep, used to determine *in vivo* release, received a mean total bupivacaine dose of (((41.5 ± 1.22) + (32.0 ± 1.47) + (43.3 ± 2.03))\*2 =) 233.6 ± 3.94 mg or 234/77.6 = 3 mg\*kg<sup>-1</sup>. Absence of macroscopic damage was achieved in 85 out of 90 hydrogels following implantation. Five rings developed a radial tear (four rings of LMW-GelTyr coated and one ring of HMW-GelTyr coated). The remaining six sheep, used to study hydrogel degradation, received a dose of either 145.6 mg (4 rings) or 299.6 mg (8 rings). Seventeen out of 21 sheep were able to walk shortly after surgery. Three sheep were kept under general anesthesia until termination after 4 hours and thus did not walk. One sheep displayed immediate and complete paraplegia. Spinal cord injury by pedicle screws breaching the spinal canal was confirmed upon obduction. All other sheep recovered from surgery uneventfully. No wound healing complications were observed.



### 3.3 In vivo release

Upon retrieval of hydrogel rings from the sheep, the residual dose was determined and a release curve was constructed based on six hydrogel rings per composition per time point, implanted across three sheep per time point. Hydrogels displayed sustained release of bupivacaine during 72 hours (**figure 2**). Release was characterized by an initial burst release, which was most pronounced in the HMW-GelTyr non-coated group. LMW-GelTyr coated displayed the most linear release profile of the compositions tested. Multivariable regression analysis (**table 2**) displayed a significantly slower release in LMW-GelTyr coated rings compared to the reference HMW-GelTyr non-coated rings (regression coefficient 7.65,  $p = 0.0025$ ). No significant difference between HMW-GelTyr coated and HMW-GelTyr non-coated rings was present ( $p = 0.1114$ ). As expected, follow-up time after implantation was a significant predictor for drug release from hydrogels (regression coefficient -4.329,  $p < 0.001$ ), indicating longer follow-up leads to decreased residual drug. When incorporating the interaction term between ring type and follow-up time, no significant differences between release of various ring types became apparent, indicating an effect of starting dose on absolute release. The presence of tears in the hydrogel rings after implantation did not affect release *in vivo* ( $p = 0.206$ ). Four sheep remained immobile after surgery, but sheep immobility was not a significant predictor for drug release ( $p = 0.144$ ). No significant effect of implantation location on drug release was present ( $p = 0.35 - 0.97$  for the various locations). In case percentual release was used as outcome (thus correcting for dose differences between rings), release of HMW-GelTyr coated and LMW-GelTyr coated rings was significantly slower compared to LMW-GelTyr uncoated rings (regression coefficient -13.77 ( $p = 0.0347$ ) and regression coefficient -13.61 ( $p = 0.0378$ ), respectively). These differences can be explained by the presence of the coating, effectively decreasing the diffusion surface of the ring.

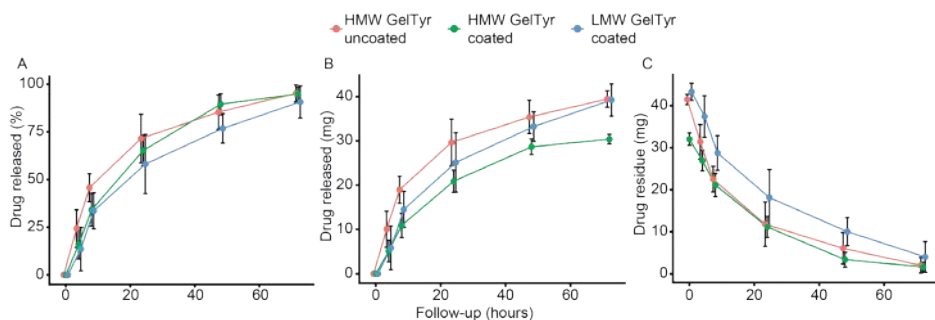


**Figure 2.** *In vivo* drug release from bupivacaine-loaded hydrogel rings. A) Release of bupivacaine expressed as a percentage of starting dose. B) Release of bupivacaine expressed as absolute amount (mg). C) Residual bupivacaine in hydrogel rings at explantation. All data is reported as mean  $\pm$  SD ( $N=6$  per time point).

**Table 3.** Multivariable linear regression of drug release.

Multiple R <sup>2</sup> = 0.8921		Ring residual drug (mg)		Ring percentage released	
Variable	Category	Coeff.	<i>p</i>	Coeff.	<i>p</i>
<b>Intercept</b>		40.804	<b>&lt;0.001</b>	0.8397	0.9121
<b>Ring type</b>	HMW-GelTyr uncoated	<i>Ref</i>		<i>Ref</i>	
	HMW-GelTyr coated	-3.89	0.133	-13.77	<b>0.0347</b>
	LMW-GelTyr coated	7.55	<b>0.004</b>	-13.61	<b>0.0378</b>
<b>Mechanical performance</b>	Broken during implant	<i>Ref</i>		<i>Ref</i>	
	Intact during implant	-2.56	0.206	6.59	0.1925
<b>Mobility</b>	Immobile	<i>Ref</i>		<i>Ref</i>	
	Mobile	-1.48	0.144	3.76	0.1388
<b>Time</b>	Follow-up (square root)	-4.34	<b>&lt;0.001</b>	10.46	<b>&lt;0.001</b>
<b>Implantation location</b>	Bottom-left	<i>Ref</i>		<i>Ref</i>	
	Bottom-right	-0.66	0.674	1.88	0.631
	Middle-left	-1.13	0.469	3.01	0.440
	Middle-right	-1.49	0.348	3.39	0.392
	Top-left	-0.27	0.867	0.66	0.869
	Top-right	-0.05	0.974	0.64	0.869
<b>Interaction ring type – Follow-up</b>	HMW-GelTyr coated	0.38	0.403	1.89	0.100
	LMW-GelTyr coated	-0.60	0.190	0.93	0.413

### 3.4 Plasma and Wound Fluid Analysis

Bupivacaine plasma levels were determined in selected sheep at timepoints 0.5, 1, 2, 4, 8, 24, 48 and 72 hours. Plasma levels gradually rose to a level of  $70.1 \pm 37.9 \text{ ng} \cdot \text{mL}^{-1}$  in 24 hours and remained relatively stable until 72 hours (**figure 3A**). Wound fluid was sampled at  $t=4, 8, 24, 48$  and 72 hours at termination in selected sheep (**figure 3B**). On average, deep wound fluid concentrations were a factor  $2298 \pm 784$  higher than plasma concentrations across time points, while superficial wound concentrations were  $525 \pm 343$  times higher. This indicates a high local concentration with low systemic loads, reducing risk of systemic side effects. The pH of superficial wound fluid was 7.43 after 4h (R1-5) and 7.87 after 72 hours (R1-2), while pH of deep wound fluid was 7.40 after 4 hours and 8.04 after 72 hours, respectively. In the sheep used to study hydrogel degradation, bupivacaine plasma levels were determined up to 168 hours, at which the drug was still present. A dose-dependent increase in AUClast was observed ( $7869 \pm 1798 \text{ ng} \cdot \text{h} \cdot \text{mL}^{-1}$  for 8 rings versus  $3345 \pm 933 \text{ ng} \cdot \text{h} \cdot \text{mL}^{-1}$  for 4 rings). C<sub>max</sub> and T<sub>max</sub> were  $84.3 \pm 14.9 \text{ ng} \cdot \text{mL}^{-1}$  at 32 hours and  $35.2 \pm 10.3 \text{ ng} \cdot \text{mL}^{-1}$  at 24 hours for sheep receiving 8 and 4 rings, respectively. The highest C<sub>max</sub> value recorded in the study was  $130.0 \text{ ng} \cdot \text{mL}^{-1}$ .

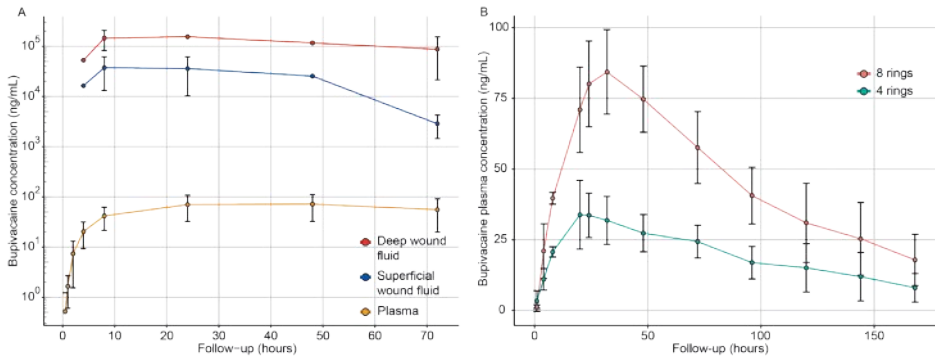


**Figure 3.** Bupivacaine plasma and wound fluid levels obtained in sheep. A) Semi-log plot of bupivacaine plasma and corresponding deep and superficial wound fluid levels in sheep that underwent explantation of hydrogels at predetermined intervals. B) Bupivacaine plasma levels in sheep used to study hydrogel degradation. The sheep received 4 or 8 rings (N=3 sheep each). Data is presented as mean  $\pm$  SD.

### 3.5 In vivo hydrogel degradation

To study the *in vivo* degradation of the hydrogel material, hydrogel rings were explanted at various predetermined intervals after surgery according to the decision tree in figure S1. The residual dry mass of hydrogel rings was obtained and expressed as a percentage of starting dry mass. Results of the *in vivo* degradation study are displayed in **figure 4**. Hydrogels degraded over the course of approximately 9 months, which was confirmed after 336 days of implantation.

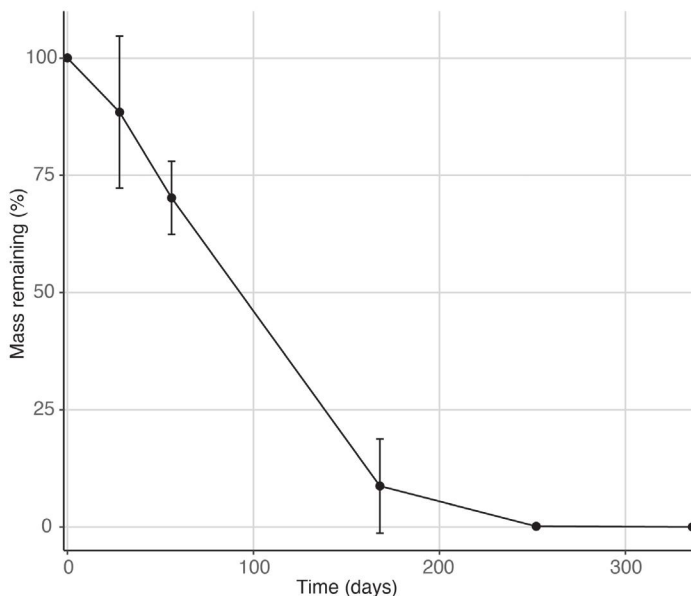


**Figure 4.** *Hydrogel degradation in vivo. Hydrogel mass remaining following explantation was measured at various time points after surgery, as a measure for degradation.*

Tissue samples obtained from the implantation site during explantation displayed a foreign body response with fibrous capsule formation (**figure 5**). Formation of fibrous tissue by active fibroblasts, neovascularization, brown pigmentation compatible with hemosiderin following prior hemorrhage and birefractive foreign body material resembling the hydrogel were observed after 28 days of implantation. Some muscles fibers were atrophic yet vital and no immune cell infiltrate was present. After 56 days, hemosiderin and hydrogel material fragments were encapsulated by multinuclear giant cells. Extensive active fibrosis, rich in fibroblasts was present in all samples. Some macrophages were present as well as areas of atrophic and fibrotic muscle fibers. 168 days after surgery, some giant cells together with fibrosis low in fibroblasts was reported. No clear neovascularization, inflammation or immune cell infiltration was seen. After 252 days, histology consisted of atrophic muscle tissue with interposed mucoid degeneration and fibrosis. Hemosiderin was encapsulated in multinuclear giant cells located in extensive areas of fibrosis and incidental neovascularization. 336 days after implantation, atrophic muscle fibers and fibrosis with low fibroblast counts was present, indicating a subsiding foreign body response.<sup>434</sup>

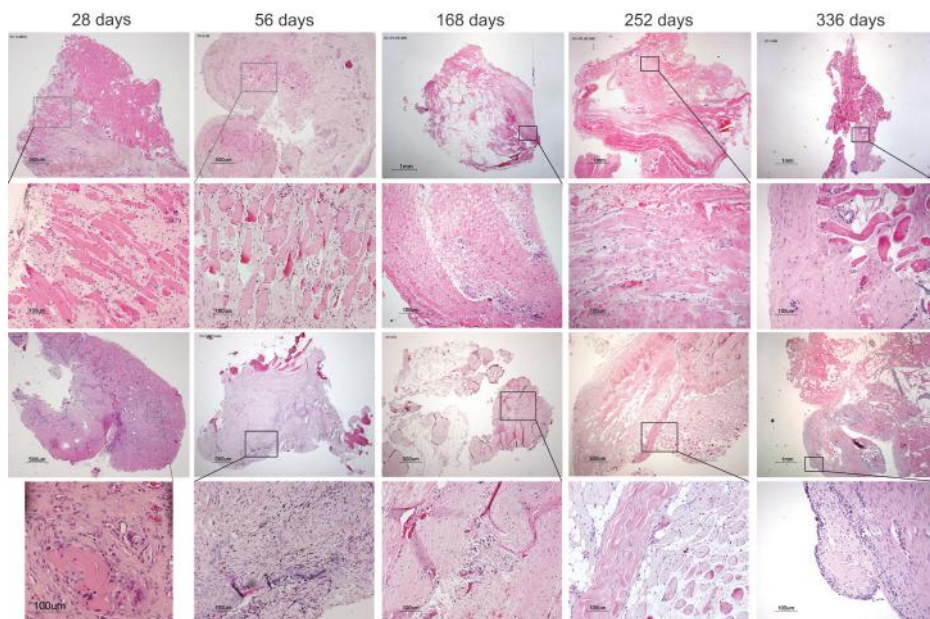


**Figure 5.** Hematoxylin and eosin staining of implant sites. Samples were obtained at 28, 56, 168, 252 and 336 days after implantation. Per time point, two tissue overviews (top and third row) and respective details (second and fourth row) are provided.

### 3.6 Release *In vitro* – *In vivo* correlation

Pearson correlation was performed between *in vitro* and *in vivo* percentual release at similar time points. The Pearson's correlation coefficient was 0.996 for HMW-GelTyr uncoated, 0.998 for HMW-GelTyr coated and 0.994 for LMW-GelTyr coated ( $p < 0.001$  for all compositions). Further, linear regression was performed, setting *in vivo* release as dependent and *in vitro* release as independent variable.  $R^2$  values were  $> 0.99$  for all compositions ( $p < 0.001$ ). The regression coefficient or slope ( $a$  in  $y = ax + b$ ) was between 1.12 and 1.22, indicating that *in vivo* release of bupivacaine from the hydrogel is 12-22% faster compared to *in vitro* (**figure 6**).

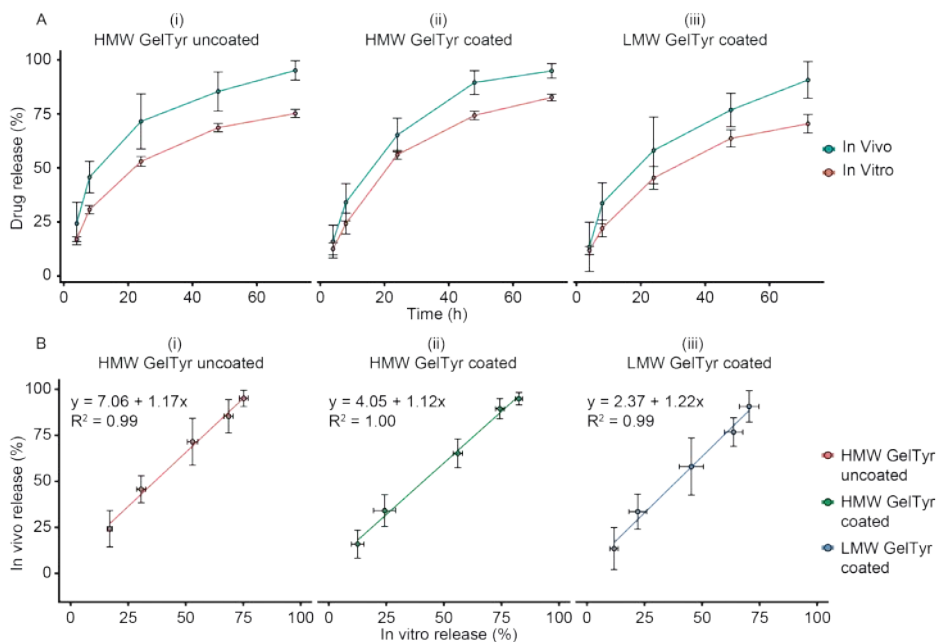


**Figure 6.** *In vitro-in vivo correlation of release. A) plots displaying in vivo and in vitro drug release from the three compositions tested. B) Plots displaying results from linear regression analysis of in vitro versus in vivo release.*

## 4. DISCUSSION

Providing adequate pain treatment following spinal surgery remains a major clinical challenge. Current opioid-based regimes come with a delicate balance between analgesic effect and side effects. Recent developments in the use of local anesthetics, such as ESP blocks and sustained-release formulations, emphasize the potential of LAs in spine surgery but are limited in duration of action.<sup>36,40,103</sup> To provide a non-opioid alternative that effectively and efficiently provides pain relief following instrumented spinal surgery, this study investigated a robust yet deformable ring-shaped hydrogel for sustained and local release of local anesthetic after co-implantation with pedicle screws. This drug delivery formulation was constructed from gelatin functionalized with a tyrosine derivative that allowed photo-crosslinking with the biocompatible photo-initiator riboflavin.<sup>428</sup> Bupivacaine crystals were incorporated as active pharmaceutical ingredient. Upon implantation in a sheep model for spinal surgery, the hydrogels could handle co-implantation with pedicle screws without breaking, provided sustained release of bupivacaine for 72 hours, displayed *in vivo* degradability, and elicited limited local tissue response.

A strength of this study was the experimental setup, that allowed for precise measuring of residual drug in hydrogels and did not rely solely on plasma levels to estimate local release. Explantation of hydrogels further allowed bupivacaine quantification in wound fluids from deep and superficial surgical compartments, giving a better sense of the concentration of analgesic present at relevant sites. The orders-of-magnitude differences between local wound fluid and systemic bupivacaine concentrations underline the localized nature of this novel treatment. As the highest  $C_{max}$  recorded was  $130 \text{ ng} \cdot \text{mL}^{-1}$ , the observed plasma levels stayed well below reported toxic thresholds, even when taking into account the faster elimination of bupivacaine in sheep compared to humans.<sup>435,436</sup> Moreover, time to  $C_{max}$  ( $T_{max}$ ) was considerably longer compared to conventional administration routes of bupivacaine, namely 24-32 hours in the present experiment versus 30 minutes following infiltration by injection.<sup>437</sup> In comparison, a bupivacaine-loaded collagen mesh (Xaracoll, Innocoll) used for analgesia following abdominal hysterectomy yielded a median  $T_{max}$  of 12 hours in humans.<sup>39</sup> Liposome bupivacaine (Exparel, Pacira) has been tested in multiple clinical indications such as inguinal hernia repair, total knee arthroplasty and bunionectomy, leading to median  $T_{max}$  of 12, 24 and 2 hours, respectively. With comparable doses to the present experiment, the obtained  $C_{max}$  of liposome bupivacaine were considerably higher:  $360 \text{ ng} \cdot \text{mL}^{-1}$  for a dose of 266 mg following inguinal hernia repair or total knee arthroplasty.<sup>43-45</sup> Administration of 400 mg of a polymeric injectable formulation of bupivacaine and meloxicam, a non-steroid anti-inflammatory drug (HTX-011, Heron Therapeutics) following total knee arthroplasty yielded a  $C_{max}$  of approximately  $550 \text{ ng} \cdot \text{mL}^{-1}$  after 24 hours, although exact data were not provided.<sup>438</sup> The delay in  $T_{max}$  of the current formulation compared to conventional bupivacaine administration modes indicates the presence of absorption rate-limited elimination, or *flip-flop* kinetics.<sup>439</sup> As elimination half-life in humans is approximately twice as long as in sheep (162 versus 72 minutes), a higher  $C_{max}$  and sustained presence of bupivacaine in human plasma is anticipated.<sup>437,440</sup> As plasma levels were the result of three different ring types implanted in a single sheep, no plasma bupivacaine concentrations could be retrieved for individual ring types.  $C_{max}$  values will likely be slightly higher in case of implantation of six fastest-releasing compositions (i.e., non-coated). *In vivo* release displayed excellent correlation to *in vitro* release results, facilitating prediction of the effects of formulation modification on *in vivo* release characteristics without necessitating additional animal testing.

Kinetic models were fitted to the *in vitro* release data, with good model fits for non-zero order models ( $R^2 > 0.95$ ). The Korsmeyer-Peppas kinetic model yielded  $n$  exponent values of 0.88-1.06, indicating polymer swelling to be a dominant mechanism in drug

release.<sup>431</sup> Indeed, as the hydrogels are implanted in a dried state and subsequently uptake release medium, the pores inside the hydrogel matrix will enlarge, facilitating the transport of drug out of the hydrogel matrix. Considering the high  $R^2$  values obtained when fitting experimental data to both Higuchi and first-order models, drug release is likely a combination of polymer swelling, crystal dissolution and subsequent diffusion of drug from a monolithic matrix. Lastly, although no repeated measures in individual sheep could be obtained, the mean fraction released increased at each consecutive time point, indicating reliable release behavior across individuals.

The main limitation of this study is the lack of pain quantification. Various models to quantify pain in sheep exist.<sup>441</sup> However, as these models frequently rely on left-right differences, application following spinal surgery in the present study was not considered feasible. As frequent blood sampling was performed during the experiment, heart rate measurements and behavioral scores were deemed insufficiently specific and unreliable to measure only postoperative pain in sheep. Co-implantation of the hydrogel and pedicle screw ensures the presence of bupivacaine in an anatomical location similar to ESP blocks, which reduce postoperative pain through 24 hours.<sup>103</sup> Although the analgesic effects of bupivacaine are undisputed, the exact local concentration needed to obtain pain relief in the present application is unknown. Previous work has demonstrated the abundant presence of A-delta and C-fibers in various bone compartments.<sup>120,336</sup> *Ex vivo* studies performed on rabbit sciatic nerves reported bupivacaine concentrations of 0.048 mM and 0.201 mM to be sufficient for a 50% reduction of action potential in myelinated A-delta and unmyelinated C-fibers, respectively.<sup>361</sup> For comparability, wound fluid concentrations of up to 0.72 mM were found in the present experiment. As the nerve sheath was removed from rabbit sciatic nerves but peri- and endoneurium were still present, the concentration needed to provide action potential reduction in individual nerve fibers in musculoskeletal tissue is likely to be lower than the values reported by Gissen *et al.* However, phenomena such as local wound pH (according to the Henderson-Hasselbalch equation, the ionized fraction of drug increases at lower pH, decreasing its capacity to cross cell membranes) could influence the degree of local anesthesia provided. Indeed, bupivacaine has been reported to be less effective at lower pH and in inflamed environments.<sup>363</sup>

Burst release of bupivacaine from hydrogels was most pronounced in the uncoated composition, likely due to the larger diffusion surface available in the absence of a partial coating. However, the differences in bupivacaine dose between hydrogel ring types limited the assessment of effect of molecular weight and presence of a coating on release, as differences in release based on dose could not be ruled out.



Biocompatibility is defined by the FDA as “the ability of a material to perform with an appropriate host response in a specific situation”.<sup>442,443</sup> As such, the present hydrogel adhered to this definition. It performed as expected, releasing bupivacaine over a period of 72 hours. After drug release, the hydrogel elicited a host response resembling a standard foreign body reaction associated with inert materials which subsided over the course of 12 months. Fibrous capsule formation, macrophage infiltration, neovascularization and presence of multinuclear giant cells was observed after 28, 56, 168, 252 and 336 days, corresponding well to the later stages of foreign body response described in previous literature.<sup>434,444–446</sup> No evident lymphocyte immune response was noted. *In vivo* degradation was studied from 28 days onwards but, unexpectedly, far exceeded the *in vitro* degradation time of 28 days. Hydrogel rings had degraded after approximately 9 months *in vivo*. Upon macroscopic examination and histopathological analysis, fibrous capsule formation around the combined ring and screw was observed. Possibly, the presence of this capsule decreased contact between wound fluids and the hydrogel, slowing down the degradation of the hydrogel ring. In the current experimental setup, the foreign body response elicited is a product of both titanium pedicle screw and hydrogel implantation and differentiating between their isolated effects is not possible. Moreover, the severity of foreign body response has been linked to the degree of tissue damage done during surgical implantation. As spinal surgery is a highly invasive procedure, the intervention itself might increase the foreign body response directed against the screw-ring complex.<sup>446</sup>

## CONCLUSION

In conclusion, a robust hydrogel-based drug delivery formulation for sustained release of bupivacaine was designed for co-implantation with pedicle screws. Bupivacaine release from hydrogel rings was sustained for 72 hours *in vivo*, correlated well to *in vitro* release and led to high wound and low systemic concentrations. The hydrogel formulation displayed biodegradability and elicited a conventional foreign body response. This formulation has the potential to improve postoperative analgesia and enhance postoperative recovery following spinal surgery.

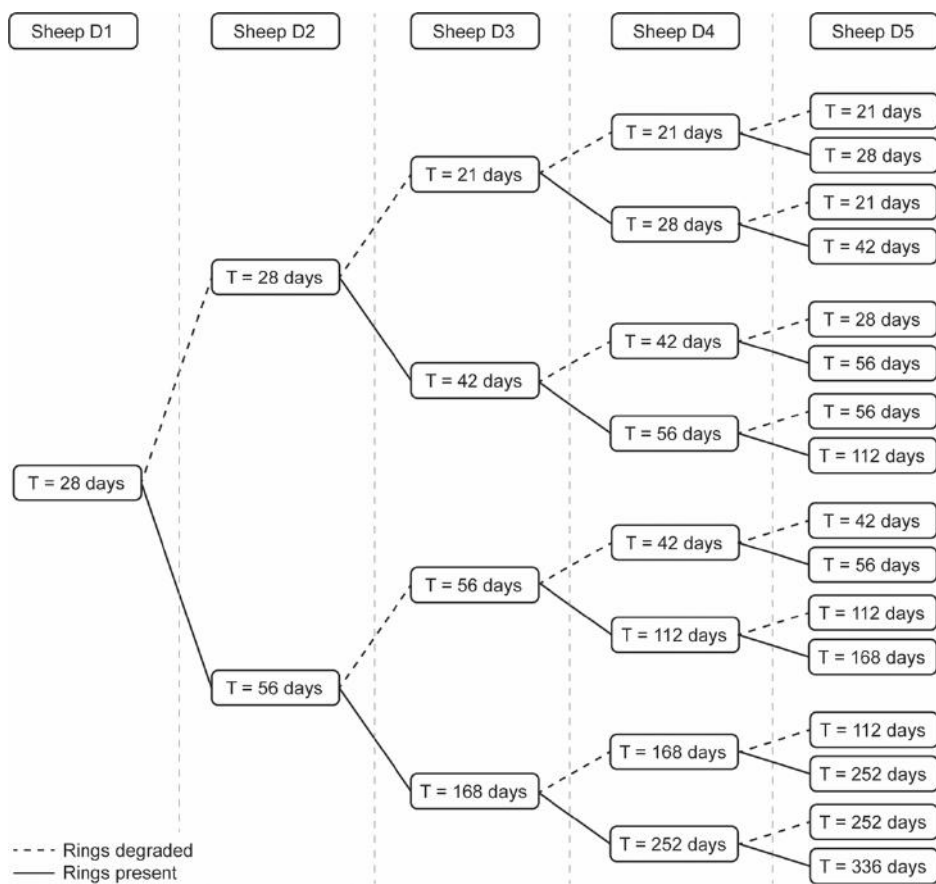
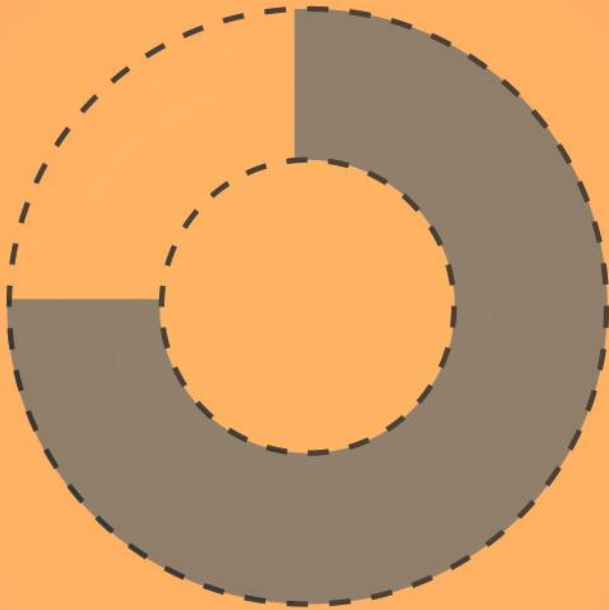


**Figure S1.** Decision tree to study *in vivo* degradation of the bupivacaine-loaded hydrogel. The presence or absence of the hydrogel ring in a prior sheep determined the survival time of the subsequent sheep.





# CHAPTER 9

## Preclinical safety and feasibility of a bupivacaine-loaded hydrogel for drug delivery in spinal surgery

Jasper G Steverink, Suzanne Bruins, Floris R van Tol, Hein R Jonkman, Kwame B Amponsah, Jessica Marvela, Anne-Mare de Vries, Andre J Smorenburg, Bas J Oosterman, Susanna Piluso, Jorrit-Jan Verlaan

*In manuscript*

## ABSTRACT

**Introduction:** Effective postoperative analgesia is an area of active research. Both pain and side-effects of analgesic medication inhibit rapid postoperative recovery of patients undergoing instrumented spine surgery. A focus shift towards localized treatments, employing local anesthetics to minimize the need for systemic analgesics such as opioids is taking place. However, a mismatch between the three-day duration of severe postoperative pain and duration of local anesthetic action is present. Emerging techniques including locoregional nerve blocks and the various sustained-release formulations of local anesthetics in development are promising, but their effects are limited beyond 12-24 hours. An implantable sustained local anesthetic release formulation that is stationary at the target site could be a feasible treatment method for patients undergoing instrumented spine surgery. This GLP-compliant study tests the local and systemic safety of a bupivacaine-loaded hydrogel, designed for co-implantation with pedicle screws, in a sheep model for spine surgery.

**Methods:** Bupivacaine crystals were encapsulated in ring-shaped gelatin hydrogel matrices. Eight sheep underwent implantation of A) eight pedicle-screws only, eight sheep received B) eight pedicle screws and hydrogels without drug (E-matrix), and another eight sheep received C) eight pedicle screws with drug-loaded hydrogels (B-matrix, cumulative dose 256 mg bupivacaine). All sheep underwent plasma sampling for drug levels and systemic safety parameters. The duration of follow-up was 6 days for two sheep per group, and 56 days for six sheep per group, after which histological analysis of implant sites and systemic organs was performed. Host reaction was scored according to the ISO10993-6:2016(E) standard. Additionally, six sheep underwent subcutaneous (SC) infiltration of bupivacaine HCl (dose 133 mg bupivacaine) to allow comparison of pharmacokinetic parameters such as maximum plasma concentration (C<sub>max</sub>), time to C<sub>max</sub> (T<sub>max</sub>), area under the drug plasma curve (AUC), and elimination half-life (T<sub>1/2</sub>) between bupivacaine infiltration and B-matrix implantation.

**Results:** All sheep recovered from surgery uneventfully. C<sub>max</sub> was 138.3±68.5 ng/mL obtained after 1 hour (median T<sub>max</sub>) in group D, and 50.4±24.5 ng/mL obtained after 28 hours (median T<sub>max</sub>) in the B-matrix group (C). T<sub>1/2</sub> was 6.5 times higher in group C compared with D (67.6±15.6 versus 10.7±5.5 hours, respectively). Histological analysis revealed no differences in total host reaction on bone or muscle level between the three surgical groups. Further, blood chemistry, hematological values, and histopathology of systemic organs were comparable between groups.

**Conclusions:** A bupivacaine-loaded ring-shaped hydrogel was designed for co-implantation with pedicle screws, to provide several days of analgesia at the source of pain after instrumented spine surgery. Both B-matrix and E-matrix were well-tolerated in sheep and did not induce additional tissue damage compared with controls. Following administration of B-matrices, lower systemic bupivacaine concentrations were observed compared with SC bupivacaine infiltration. The results indicate both local and systemic safety of the bupivacaine-loaded hydrogel when used in instrumented spine surgery.

## 1. INTRODUCTION

Every day, thousands of spinal surgical interventions are performed.<sup>14</sup> Because of positive effects on patient well-being and increasing healthcare demands, acceleration of the postoperative recovery process is receiving growing attention.<sup>6,421</sup> However, both pain and side effects of analgesic treatment affect the majority of patients undergoing spine surgery, and inhibit swift hospital discharge.<sup>12,65,78,447,448</sup> Severe postoperative pain typically lasts for three days after spine surgery, and can significantly influence surgical outcomes and patient satisfaction.<sup>11,16,36,65</sup> Insufficiently controlled postoperative pain following skeletal surgery is a prevalent clinical problem, putting patients at risk of developing chronic postoperative pain.<sup>10,15,64</sup> Currently, treatment of postoperative pain heavily relies on opioids.<sup>65</sup> The systemic administration of opioids can provide effective analgesia, yet exposes not only the intended target site but also other tissues to the drug. This can lead to side effects such as constipation, ileus, respiratory depression and drowsiness.<sup>24</sup> Moreover, patients consuming opioids are at risk of dependence and addiction.<sup>254</sup> The rapid increase in opioid consumption over the past 25 years and concomitant increase in opioid-related deaths illustrate the magnitude of these risks.<sup>25–29</sup> The existence of insufficiently controlled postoperative pain despite opioid use and the prevalence of opioid-related side effects highlight an unmet clinical need for improved analgesia after skeletal surgery.

Various solutions are in development to provide non-opioid analgesia after surgery, and thus reduce the risk of opioid-related side effects. Wound infiltration with local anesthetics is an effective technique to locally inhibit nociception by blocking action potential conduction, thereby preventing the downstream sensation of pain.<sup>37</sup> However, the duration of action of local anesthetics is limited. An increased duration of analgesia and decreased opioid consumption are obtained when employing regional blocks, such as the erector spinae plane (ESP) block.<sup>102,103,424</sup> Still, these techniques are limited by the duration of action. Systems to continuously infuse local anesthetics into the surgical wound are commercially available (ON-Q Pain Buster<sup>®</sup>, B. Braun, Germany) but require specialized personnel, possibly removal at a later hospital visit and necessitate a constant connection of the patient to the system, disabling patient mobility.<sup>337</sup> Also in ESP block, continuous infusion can be used but with similar downsides and risk of cannula dislodgment.<sup>449</sup>

To provide non-opioid sustained analgesia and overcome the drawbacks of short durations of action and cannulas, we have recently reported on a ring-shaped local anesthetic delivery formulation for co-implantation with pedicle screws during spine surgery.<sup>428</sup> The concept of a ring-shaped, implantable drug delivery formulation yields



several requirements for successful clinical application: i) The formulation should be able to encapsulate and slowly release local anesthetics in sufficient doses to provide analgesia for the duration of severe pain following spine surgery;<sup>36,65</sup> ii) the formulation should be robust enough to withstand orthopedic implantation, yet deformable enough to not interfere with optimal screw positioning and screw head polyaxiality; and iii) the formulation should be composed of a biocompatible and biodegradable material, to prevent local toxic effects or excessive immune system activation that could compromise postoperative recovery.<sup>42</sup>

The present formulation encapsulates bupivacaine in a hydrogel matrix and is designed to work with polyaxial, angular-stable pedicle screws, which are connected with rods following implantation. Polyaxial screw heads can angulate and rotate freely after implantation, for which some space under the screw head is required. Angular-stable screws have good purchase in the bone without complete insertion, preventing pressure of the screw head on bone and periosteal blood vessels with subsequent necrosis.<sup>450</sup> The space under the screw head would allow the placement of a deformable hydrogel ring if it does not compromise screw placement. It is therefore essential that the hydrogel ring is robust enough to remain intact during implantation, but flexible enough to allow optimal screw placement and screw head polyaxiality. The active pharmaceutical ingredient bupivacaine inhibits action potential conduction by blocking voltage-gated sodium channels in sensory neurons, shown to be abundantly present in bony tissues.<sup>120,336,358</sup>

In this study, a sheep model for instrumented spine surgery is employed to quantify the systemic pharmacokinetics of the bupivacaine-loaded hydrogel, and compare with bupivacaine HCl subcutaneous infiltration. In addition, the local and systemic toxicity of both the empty hydrogel matrix (E-matrix) and drug-loaded hydrogel (B-matrix) co-implanted with pedicle screws are investigated by histological comparison with the pedicle screw-only clinical reference situation.

## 2. MATERIALS AND METHODS

### 2.1 Material preparation

Bupivacaine-loaded hydrogel rings (B-matrix) were prepared as described previously.<sup>428</sup> Commercially available gelatin functionalized with a tyrosine derivative (GelTyr), type A from porcine skin, was mixed with oxidized beta-cyclodextrin and photocross-linked in the presence of riboflavin-5-monophosphate and sodium persulfate to obtain the hydrogel matrix. Matrices were then washed, dried and subsequently incubated in bupivacaine solution for drug loading. Following drug loading, matrices were again dried and incubated in a 30% (v/v) glycerol in sodium bicarbonate 0.1 M solution at pH 8.5 to induce bupivacaine crystal formation. After a third drying step, the domed surface of matrices was dip-coated by partial submersion in a 20% (w/v) poly(lactic-co-glycolic acid) solution in ethyl acetate. Excipient hydrogel matrix rings (E-matrix) were prepared in a similar manner, with the exception that the drug-loading step was omitted from production. Two batches of E-matrix (batches 28 and 29) and B-matrix (batches 30 and 31) were manufactured. Both E-matrix and B-matrix were packed in aluminum pouches and underwent  $\geq 25$  kGy gamma sterilization (STERIS, Ede, Netherlands). Bacterial endotoxin content per unit was quantified using Ph. Eur. Method 2.6.14.<sup>451</sup>

### 2.2 Quantification of bupivacaine dose and *in vitro* release

Bupivacaine dose was extracted from B-matrix samples of both batches (N=3) by 24-hour incubation of B-matrix in 0.1% formic acid solution at 45°C. This solution was subsequently analyzed using HPLC to obtain the bupivacaine dose per unit. *In vitro* drug release was studied by submerging B-matrix (N=5 per batch) in 20 mL of 0.01M citrate buffer pH 6.0 at 37°C under continuous agitation.<sup>428</sup> The solution was replaced at predetermined time points, after which residual drug was extracted by 24 hours of incubation in 20 mL of 0.1% formic acid solution at 45°C. At each time point, the bupivacaine concentration was quantified using HPLC and used to construct a cumulative release curve.

### 2.3 Animals

Ethical approval was obtained from the local ethical committee prior to the start of the experiment (dossier number EC MxCl 2021-176), and the experiment and its reporting adhered to the ARRIVE guidelines. All procedures were performed in a GLP-licensed animal facility (Medanex Clinics, Diest, Belgium). All eligible animals underwent parasite monitoring by fecal egg count testing, blood analysis and clinical assessment of health prior to inclusion. Upon arrival at the test facility, animals were allowed a 14-day acclimatization period before the experiment. Before surgery or bupivacaine infiltration, animals were housed in groups. After the procedure, the animals were be individually housed in a small pen, allowing auditory, visual and olfactory contact with other sheep

in the same room. Straw bedding was provided in all housings. Moreover, hay and water were available *ad libitum* except in case of preoperative fasting. All included animals received a temperature chip.

Twenty-four Swifter ewes with a mean preoperative weight of  $75.2 \pm 7.5$  kg and age of  $3.5 \pm 0.9$  years underwent surgical implantation of eight pedicle screws, described in more detail below. Sheep were randomly assigned to either of the three following groups: pedicle screws-only (A), pedicle screws equipped with E-matrix (B), or pedicle screws equipped with B-matrix (C). Prior to surgery, six sheep underwent subcutaneous infiltration of 30 mL bupivacaine HCl 0.5 w/v %, accumulating to a total dose of 150 mg (group D), serving as positive control (Aurobindo Pharma B.V., Baarn, Netherlands). Following 96 hours of plasma samples to quantify bupivacaine levels, a two-week cool-down period to ensure absence of bupivacaine in the plasma and another health assessment, the six sheep were re-used for the surgical part of the experiment. The experimental design is displayed in Figure 1.

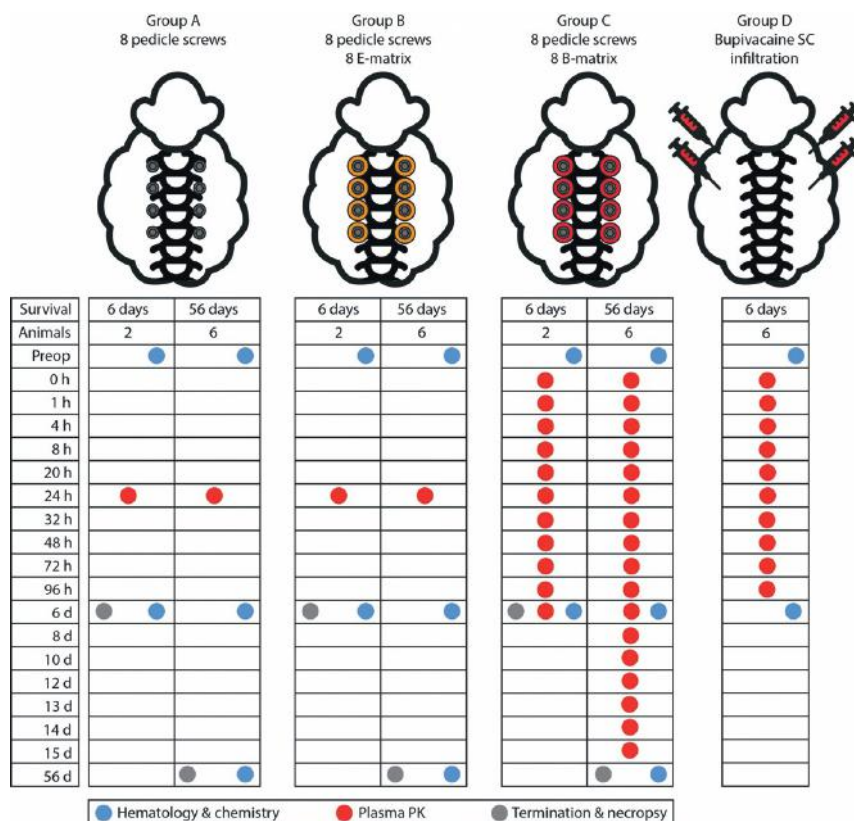


**Figure 1.** Experimental design and sampling scheme of the animal study.

## 2.4 Surgical Intervention

Surgery was performed according to a previously described procedure. In short, general anesthesia was induced using detomidine 0.04 mg/kg IV and propofol 2-5 mg/kg IV. Rocuronium bromide 0.05 mg/kg was administered IV for muscle relaxation. Antibiotic prophylaxis consisted of amoxicillin 1g / clavulanic acid 100 mg IV. Perioperative analgesia was provided by IV buprenorphine (6 ug/kg) and meloxicam (0.5 mg/kg). Blood loss and vital parameters were monitored during surgery. The sheep were positioned in the ventral recumbency position and a midline incision was performed through skin, subcutaneous fat and fascia. The posterior spinal muscles were then dissected laterally to expose the spinous processes, lamina, facet joints and medial part of the transverse process of L1-L6. Bilaterally in vertebra L2 until L5, 5 mm wide holes were drilled in a 45-degree transversal angle where the transverse process meets the lamina. These holes provided access to the pedicles. Following probing of drilling trajectories to ensure integrity of the medial wall, pedicle screws and, if applicable, test items were inserted. Tightening of the last screw was marked as  $t = 0$ . Sheep randomized in group A received eight pedicle screws. Sheep in group B received eight pedicle screws and the same number of E-matrices. Sheep in group C received eight pedicle screws and eight B-matrix, equating to a total dose of 305 mg bupivacaine HCl. In case E-matrices or B-matrices dislodged from their intended location under the screw head, they were replaced. After implantation, the wound was rinsed with 500 mL 0.9% NaCl and closed in layers.

## 2.5 Animal Follow-up

Following SC infiltration of 150 mg bupivacaine HCl, plasma samples were retrieved at predetermined time points up to 96 hours after administration. Sheep were assessed daily for the occurrence of adverse events. In case of blood values within normal ranges, sheep that underwent SC infiltration were included in the surgical groups. After surgery, sheep were monitored daily for clinical well-being, body weight and the occurrence of adverse events and underwent plasma sampling to quantify systemic bupivacaine levels. PK samples were taken 0, 1, 4, 8, 20, 24, 32, 48, 72, 96, and 144 hours post-implantation for all animals included in group C (where 0 hours is the time point when the last screw has been placed). Additional PK sampling was performed at 192, 240, 288, 312, 336 and 360 hours post-implantation for animals with a planned survival time of 56 days. Animals included in group A and B underwent a single PK plasma sampling after 24 hours of follow-up. Plasma samples were analyzed for bupivacaine content by a GLP-licensed facility (Ardena, Assen, Netherlands) and pharmacokinetic data was analyzed by a GLP-accredited contract research organization (DGr Pharma, Oudenbosch, Netherlands) using WinNonLin software. In addition, hematology, biochemistry and coagulation parameters were quantified pre-inclusion as well as 6 and 56 days after infiltration or implantation. When the clinical condition of an animal caused concern, a veterinarian was consulted

and action was taken (and documented) and/or monitoring was adjusted according to dictating circumstances. In groups A, B and C, two sheep per group were terminated after 6 days of follow-up. The remaining six sheep per group were terminated after 56 days of follow-up. Necropsy and macroscopic examination of the surgical site and specified organs was performed directly after termination and any abnormalities were documented.

## 2.6 Histological analysis

In each sheep, two randomly selected screw implantation locations were sent for histopathological processing and analysis by a GLP-licensed contract pathologist (Anapath Services GmbH, Liestal, Switzerland). Two of the four instrumented vertebrae were resected *en bloc* with adjacent muscle attached and intact dorsal fascia. Vertebral levels were fixated in 4% buffered formaldehyde and further trimmed down under fluoroscope guidance after 7 days to improve fixative penetration, resulting in a final slice thickness of  $\pm 2$  cm. After thorough fixation, samples were trimmed in the transversal plane and embedded in poly(methyl methacrylate) resin, sawed by a diamond band saw in transversal sample direction (transversal cut through the E-matrix or B-matrix but longitudinal cut through the pedicle screw). Embedded samples were then ground and polished to a final thickness of approximately 40-60  $\mu\text{m}$  and stained with Paragon (toluidine blue and basic fuchsin).

Additionally, the spinal cords of each animal at implantation site, at thoracic and cervical sites and the tissue samples collected from the spleen, liver, kidneys, lungs, heart, aorta, brain, local lymph nodes (lumbar aortic and medial iliac), sciatic nerve, eyes and skin above implantation site were trimmed and processed by paraffin embedding according to the ISO 10993-11:2016 standard with minor modifications. The spinal cord from implantation sites was trimmed and embedded at three different levels whereas the spinal cords at thoracic and cervical sites was processed and embedded at one level only. The heart was processed following a special five-block scheme. The brain was trimmed following the Bolon's scheme (seven-block scheme). The blocks were sectioned at an approximate thickness of 2-4  $\mu\text{m}$  and stained with hematoxylin and eosin (HE). The slides were quality controlled before being transferred to the study pathologist for histopathological evaluation. An adapted scoring system, described by ISO 10993-6:2016(E), was applied as shown **in supplementary table S1 and S2**.<sup>452</sup> The ISO standard defines a score difference between 0.0 to 2.9 as no or minimal host reaction, 3.0 to 8.9 slight host reaction, 9.0 to 15.0 as moderate host reaction and  $\geq 15.1$  as severe host reaction compared to a reference material. Host reaction was scored both at the muscle and bone level. In addition, device osseointegration, bone resorption and implant degradation at the implant site were evaluated (**supplementary table S3**).

## 2.8 Statistical Analysis

All clinical and histopathological data were collected in Excel (Microsoft Corp, Redmond, WA, USA). All data were reported as mean and standard deviation. Analysis of variance was used to compare clinical outcomes between surgical groups, with *post-hoc* Tukey's test in case of significance. Histological toxicity scores were calculated and analyzed as recommended in the ISO10993-6:2016(E) standards.<sup>452</sup> Statistical analysis was performed using Rstudio version 4.1.2 (Boston, MA, USA).

## 3. RESULTS AND DISCUSSION

### 3.1 Characteristics of test items

Two batches of B-matrix and E-matrix hydrogel rings were produced. Due to the similarities in the preparation process, the presence of drug was the only distinguishing factor between B-matrix and E-matrix. B-matrix batch 30 contained a dose of  $39.7 \pm 2.81$  mg and B-matrix batch 31 a dose of  $24.5 \pm 3.17$  mg bupivacaine base. *In vitro* drug release was similar for both batches, displaying a first-order release profile over 72 hours (**Figure 2**). We have previously shown that obtained *in vitro* curves correspond well to release *in vivo* (chapter 8). Endotoxin content was below the detection limit of 10 EU per matrix.

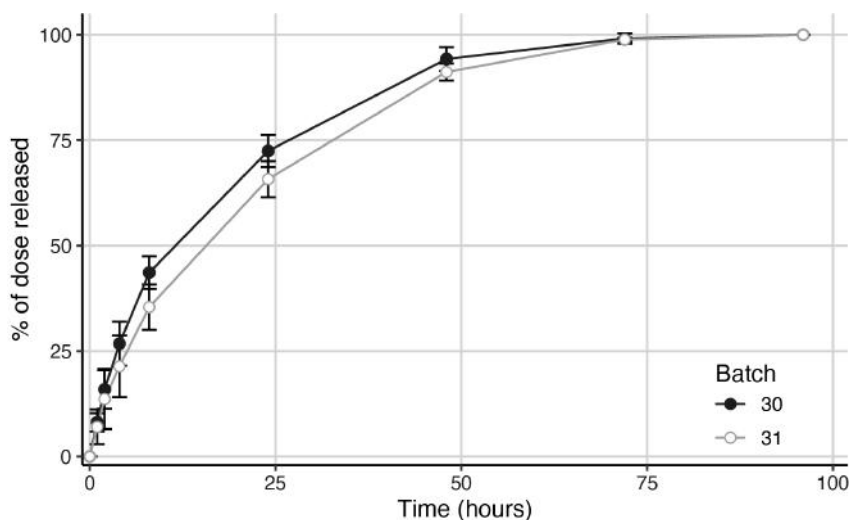


**Figure 2.** *In vitro* release curves of both B-matrix batches used in the animal study. The batches show a near-identical first-order release profile over the course of 72 hours.

### 3.2 Animals

The sheep was selected as animal model, as spinal anatomy, body weight and circulating volume are comparable to humans.<sup>453–459</sup> In addition, the pharmacokinetic properties of bupivacaine in sheep are well-established.<sup>460,461</sup> Postoperative recovery was uncomplicated in most animals. No significant differences regarding blood loss ( $p = 0.487$ ) and duration of surgery ( $p = 0.311$ ) were found between groups. A single animal (animal B4) displayed peroneal nerve paralysis directly after surgery. As the clinical situation did not improve, the animal was removed from the study after three days and replaced. Necropsy revealed a large hematoma between the m. peroneus tertius and m. exterior digitorum longus, and large necrotic and hemorrhagic areas in both m. peroneus tertius and m. exterior digitorum longus. The peripheral part of the peroneal nerve exhibited pink-red discoloration, while the proximal peroneal nerve, sciatic nerve and surgical site did not display abnormalities. The findings were considered most likely due to positioning on the surgery table in combination with a high body weight (91.3 kg). Based on these findings, animal position was changed to ventral recumbency with hind legs extended caudally and hanging from the surgery table for all further surgeries. No signs of pain were reported in any sheep after 2 weeks of follow-up and body weight was stable in all groups. All sheep developed subcutaneous seroma near the surgical wound, which subsided over the course of 2 weeks. Seroma is a commonly reported finding in cattle undergoing surgery, in case of significant space in the subcutaneous compartment after surgery.<sup>462</sup> Four minor AEs occurred in group A (three transient neurological symptoms and one wound infection), six minor (four transient neurological symptoms, one fever and one disturbed wound healing) and one major (persisting neurological deficits, as described above) AEs in group B and three minor AEs in group C (two transient neurological symptoms and one disturbed wound healing). The cases of disturbed wound healing were empirically treated with antibiotics. The incidence of surgical site infection in the present study is within range of the incidence reported in the literature.<sup>463</sup>

### 3.3 Hematology & Clinical Chemistry

To assess overall well-being of animals, and to allow detection of inflammatory processes, blood sampling for quantification of hematological and chemical parameters was performed at baseline and 6 and 56 days after surgery. Outcomes of specific interest were muscle damage markers (CK, LDH and AST) and bone damage markers (Calcium), as toxic effects of bupivacaine on muscle and bone tissue have been reported *in vitro* and *in vivo*.<sup>339</sup> Moreover, as implant infection is a feared potential complication in orthopedic surgery, various innate and adaptive immune system cells were quantified.<sup>464</sup> These included leukocyte, monocyte, neutrophil and lymphocyte counts. As was expected following a surgical intervention with extensive muscle dissection, muscle damage markers significantly increased 6 days after surgery and returned to near-baseline levels

after 56 days of implantation, with similar trends observed in all surgical groups (Figure 3A-C). Serum calcium levels were stable throughout the follow-up period (Figure 3D). Similar trends were observed for immune cells (Figure 3E-H). Leukocyte, monocyte and neutrophil counts showed increases after 6 days of follow-up compared to preoperatively in all groups. These values returned to near-baseline after 56 days of follow-up. Animal B2 was found to have elevated circulating neutrophils after 56 days, without further clinical symptoms. Necropsy revealed a 1-cm abscess in the lumbar region 9 cm laterally from the instrumented vertebrae, possibly explaining the neutrophil counts. No connection between the abscess and the surgical site was present. Further, elevated lymphocyte counts were found in animal B1 after 56 days in the absence of clinical signs of inflammation. Muscle necrosis around pedicle screws was found in this animal which could explain the elevated lymphocytes.<sup>465</sup> However, muscle necrosis was found in many animals in the absence of lymphocytosis, complicating any correlation.



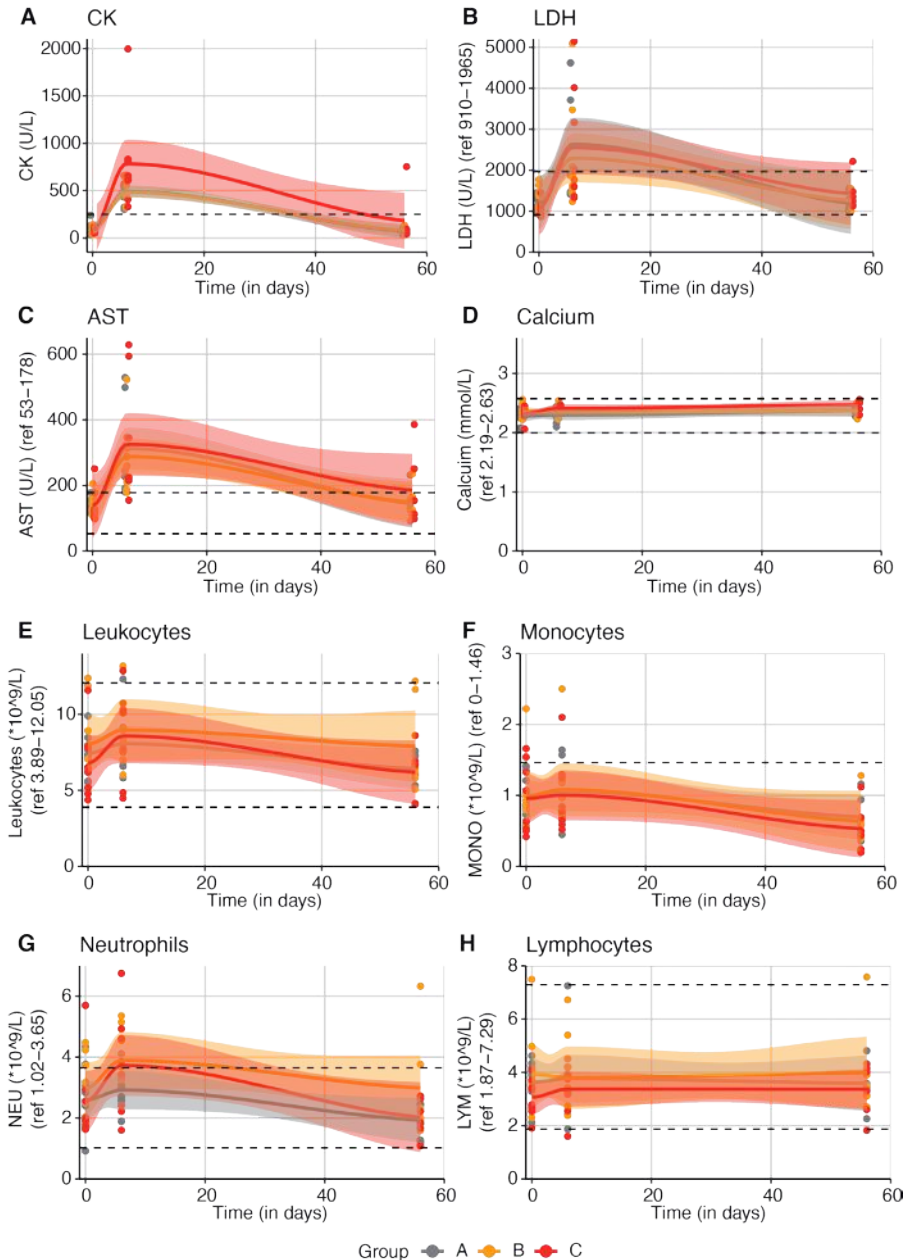


**Figure 3.** Plots displaying hematology and clinical chemistry parameters during post-operative follow-up up to 56 days, split out per surgical group (A – pedicle screws only, B – screws and E-matrix, C – screws and B-matrix). Clinical chemistry parameters include A) creatine kinase, B) lactate dehydrogenase, C) Aspartate aminotransferase and D) calcium. Hematology parameters include E) Total leukocyte count, F) monocytes, G) neutrophils and H) lymphocytes.

### 3.4 Bupivacaine plasma levels

This study evaluated the local and systemic toxicity of B-matrix and excipient matrix according to the principles of Good Laboratory Practice (GLP). GLP is a prerequisite of regulatory authorities such as FDA and EMA in Investigational New Drug Applications (NDA).<sup>466</sup> To reduce duplication of toxicity testing in animals, the FDA 505(b)2 pathway can be used during NDA.<sup>467</sup> In short, this pathway allows the applicant to build on existing knowledge of approved drugs, for example when developing a new strength, formulation or administration mode for that approved drug. By directly comparing the new drug product with a registered use of the reference product, the reference product safety characteristics can be extrapolated, or 'bridged' to the new application. In this study, plasma was sampled in sheep included in group C and D, to determine the pharmacokinetics of B-matrix and bridge with a registered indication for use of bupivacaine HCl solution. In group A and B, a single plasma sample per animal was obtained 24 hours after surgery to confirm the absence of systemic bupivacaine. All such samples contained bupivacaine below the limit of quantification (1.00 ng/mL). The pharmacokinetic results of groups C and D are visualized in **Figure 4** and summarized in **Table 1**.

**Table 1.** Summarized bupivacaine pharmacokinetic parameters for experimental groups C and D.

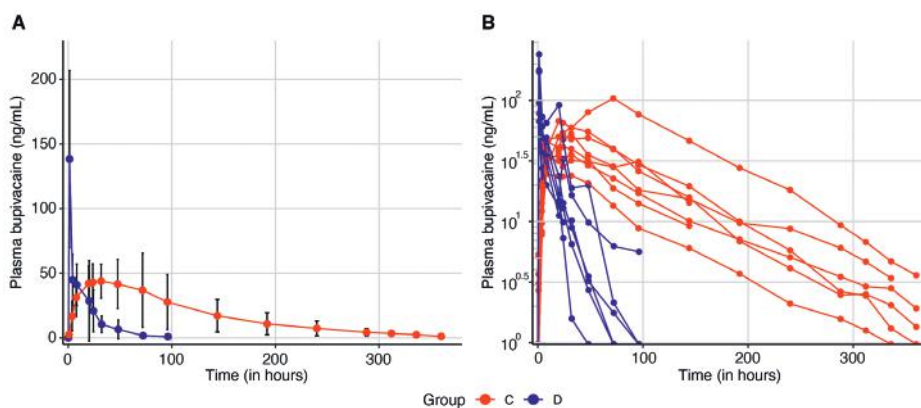
<i>Group C</i>	$C_{max}$ ng/mL	$C_{max}$ DN ng/mL	$AUC_{last}$ ng.h/mL	$AUC_{last}$ DN ng.h/mL	$AUC_{inf}$ ng.h/mL	$AUC_{inf}$ DN ng.h/mL	$t_{1/2}$ h
<i>N</i>	8	8	6	6	7	7	7
<i>Mean</i>	50.43	0.1653	6499	21.31	6287	20.61	67.61
<i>SD</i>	24.51	0.0804	3849	12.62	3741	12.27	15.59
<i>CV%</i>	48.6	48.6	59.2	59.2	59.5	59.5	23.1

<i>Group D</i>	$C_{max}$ ng/mL	$C_{max}$ DN ng/mL	$AUC_{last}$ ng.h/mL	$AUC_{last}$ DN ng.h/mL	$AUC_{inf}$ ng.h/mL	$AUC_{inf}$ DN ng.h/mL	$t_{1/2}$ h
<i>N</i>	6	6	6	6	4	4	4
<i>Mean</i>	138.3	0.9219	1334	8.891	975.7	6.505	10.69
<i>SD</i>	68.5	0.4569	760	5.065	231.1	1.540	5.48
<i>CV%</i>	49.6	49.6	57.0	57.0	23.7	23.7	51.3

Mean  $C_{max}$  in group C was  $50.4 \pm 24.5$  ng/mL, compared to  $138.3 \pm 68.5$  ng/mL in group D ( $p < 0.01$ ). The highest  $C_{max}$  recorded was 104 ng/mL in group C, and 240 ng/mL in group D. All  $C_{max}$  values were thus well below known systemic safety thresholds. In group C, all animals reached this  $C_{max}$  at the first sampling timepoint, 1 hour after surgery ( $t_{max}$ ). This likely indicates that the actual  $C_{max}$  has occurred within one hour after SC infiltration.

Indeed, 30 minutes is reported as  $t_{\max}$  for SC bupivacaine infiltration, meaning that the  $C_{\max}$  values in this study are likely underestimations.<sup>437</sup> Underestimating the  $C_{\max}$  of SC infiltration hampers precise comparison of bupivacaine administration *via* B-matrix *versus* infiltration and is a shortcoming of the present study. Due to the occurrence of a plateau in plasma levels in group C, underestimation of  $C_{\max}$  is far less likely in this group. In group D, median  $t_{\max}$  was 28 (range 8-72 hours).



**Figure 4.** Plots displaying plasma bupivacaine levels in experimental groups C (implantation of 8 B-matrix) and D (subcutaneous infiltration of bupivacaine HCl). A) Mean plasma curves for groups C and D. B) Log-linear plot of individual plasma curves, emphasizing the log-linear elimination phase in both groups.

The elimination half-life  $t_{1/2}$  was  $67.6 \pm 15.6$  hours in group C, and  $10.7 \pm 5.5$  hours in group D ( $p < 0.01$ ). This significant decrease in elimination indicates the presence of absorption rate-limited elimination, or *flip-flop* kinetics.<sup>439</sup> Slow systemic absorption of drugs is a desirable characteristic of a sustained-release formulation, as it indicates the sustained and concentrated presence of drugs at the target site. Bupivacaine was still present in concentrations  $<5$  ng/mL in three out of six surviving sheep after 15 days.

Appreciating the differences in dose between groups C and D (305 mg vs 150 mg), the dose-normalized area-under-the-curve extrapolated to infinity ( $AUC_y$ ) values were  $20.6 \pm 12.3$  and  $6.5 \pm 1.5$   $\text{ng} \cdot \text{h} \cdot \text{mL}^{-1}$  for groups C and D ( $p = 0.053$ ), respectively. Even when taking into account the potential underestimation of  $C_{\max}$  in group D and its resulting underestimation of AUC, the borderline-significant difference is considerable. AUC is defined by (dose \* bioavailability / clearance). As bupivacaine clearance is independent of administration mode, it follows that a difference in dose-normalized AUC is the result of increased bioavailability in arm C compared to arm D. A potential explanation for lower bioavailability could be the formation of a subcutaneous bupivacaine depot in case of SC administration, as the log P value of bupivacaine (3.41) indicates its lipophilicity.<sup>468,469</sup> This locally absorbed fraction of the dose would not appear in the systemic circulation, leading to a lower AUC.

### 3.4 Histopathology of implant site

To study and quantify the tissue effects of both E-matrix and B-matrix in the surgical wound, implantation sites containing a pedicle screw and test item were macro- and microscopically analyzed and compared to the clinical reference situation (i.e., pedicle screw-only). Host reaction was scored according to ISO-standards at both the bone and muscle level. Macroscopically, all samples showed areas of soft tissue focal necrosis and sclerosis around the implant site, which were histologically correlated with necrosis and fibrosis (**Figure 5**). Atrophy of the longissimus muscle was present in almost all cases. The incidence and severity of the macroscopic/histological correlated lesions was similar among the groups, and thus deemed associated with the surgical intervention rather than the presence of B-matrix or E-matrix. All microscopic samples contained a screw inserted into the vertebral body through the pedicle. In groups B and C, the E-matrix or B-matrix were present as black, acellular material. All samples across the groups showed equal histopathological findings at the implantation site, with interindividual variation in severity.

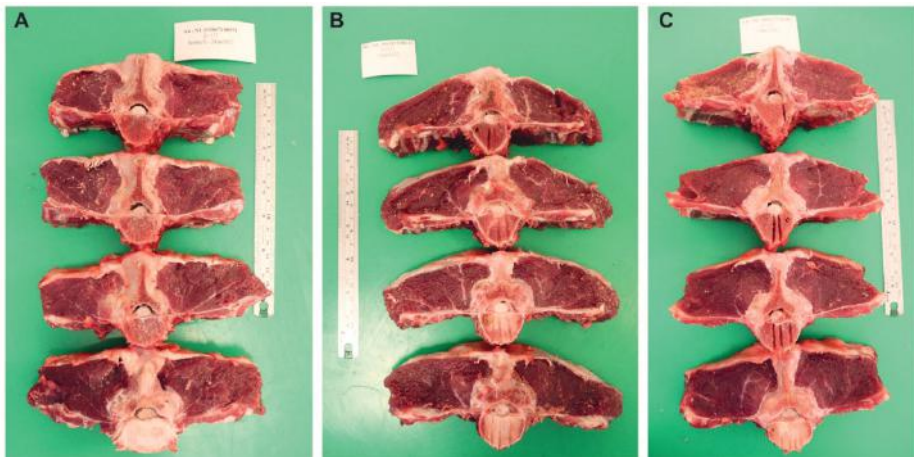


**Figure 5.** Representative macroscopic pathology of the implantation sites, after 56 days of follow-up for group A (image A), B (image B) and C (image C). Vertebral levels are marked by saw cuts I, II, III, and IIII on the cranial face. The side of the vertebra sent for microscopical analysis is marked by a hole.

After six days, the host reaction at muscle level was characterized by a minor inflammatory infiltrate associated with muscle dissection and screw insertion. The muscle around the screws displayed variable degrees of myofibers necrosis and inflammation which was often associated with multifocal hemorrhages. The bone tissue at the implantation site displayed an inflammatory infiltrate at the bone-screw interface, the presence of multifocal hemorrhages and bone fragments sloughed into the bone-screw interface after 6 days. No bone formation, nor osseointegration was detected in any groups at

this time point (Table 4). Employing the criteria stated in ISO 10993-6:2016(E), no to minimal differences in total host reaction score existed between groups after six days.<sup>452</sup>

**Table 2.** Total summarized scores per group from host reaction at muscle level.

MUSCLE Group	6 days			56 days		
	A (control)	B (E-matrix)	C (B-matrix)	A (control)	B (E-matrix)	C (B-matrix)
# Animals	2	2	2	6	6	6
# Samples evaluated	4	4	4	12	12	12
Sum total host reaction	79	68	71	258	234	234
Average total host reaction	19.8	17.0	17.8	21.5	19.5	19.5
PMN cells	2.0	1.3	1.5	1.2	1.0	1.1
Lymphocytes	1.8	1.3	1.3	1.6	1.3	1.6
Plasma cells	0.0	0.0	0.0	0.3	0.1	0.5
Macrophages	1.5	1.3	1.3	1.7	1.7	1.3
Giant cells	0.0	0.0	0.0	0.7	0.3	0.5
Necrosis	3.5	3.5	3.8	2.0	2.1	1.6
Subtotal 1	17.5	14.5	15.5	14.5	12.7	13.2
Neovascular-ization	0.0	0.0	0.0	1.8	2.0	1.9
Hemosiderin	0.0	0.0	0.0	1.0	1.2	1.1
Fibrosis	0.0	0.0	0.0	3.5	3.4	2.8
Hemorrhage	2.3	2.5	2.3	0.7	0.3	0.5
Subtotal 2	2.3	2.5	2.3	7.0	6.8	6.3

**Table 3.** Total summarized scores per group from host reaction at bone level.

BONE Group	6 days			56 days		
	A (control)	B (E-matrix)	C (B-matrix)	A (control)	B (E-matrix)	C (B-matrix)
# Animals	2	2	2	6	6	6
# Samples evaluated	4	4	4	12	12	12
Sum total host reaction	49	39	43	163	109	129
Average total host reaction	12.3	9.8	10.8	13.6	9.1	10.8
PMN cells	1.8	1.5	1.3	1.2	0.8	0.8
Lymphocytes	1.8	1.3	1.5	1.4	1.3	1.4
Plasma cells	0.0	0.0	0.0	0.6	0.1	0.0
Macrophages	1.5	1.0	1.3	1.3	1.1	1.3
Giant cells	0.0	0.0	0.0	0.3	0.0	0.2
Necrosis	0.0	0.0	0.0	0.3	0.0	0.0
Subtotal 1	10.0	7.5	8.0	10.0	6.5	7.3
Neovascular-ization	0.0	0.0	0.0	1.4	0.9	0.9
Hemosiderin	0.0	0.0	0.0	0.3	0.3	0.6
Fibrosis	0.0	0.0	0.0	1.6	1.1	1.3
Hemorrhage	2.3	2.3	2.8	0.3	0.3	0.6
Subtotal 2	2.3	2.3	2.8	3.6	2.6	3.4

After 56 days, the host reaction at muscle level evolved to an inflammatory reaction, consisting mainly of macrophages, incidental giant cells and lymphocytes. The findings are in accordance with reports on different hydrogel formulations encapsulating bupivacaine for sustained release.<sup>470</sup> Heffernan *et al.* encapsulated bupivacaine in a synthetic poly(N-isopropylacrylamide-co-dimethylbutyrolactone acrylamide-co-Jeffamine M-1000 acrylamide) hydrogel at 4 wt%, a drug concentration 8-fold higher than currently used in clinic. The gel was administered to a pig incisional wound and histological analysis was performed after 14 and 49 days. Resembling the histological features in this study, an inflammatory response, characterized by infiltration macrophages and multinuclear giant cells, as well as the formation of fibrous granulation tissue were observed. In the present study, the hydrogel is gelatin-based. Especially hydrogels from natural polymers are generally well-tolerated by the body, as both the polymer molecular structure and hydrogel consistency closely mimic the surrounding tissues.<sup>391,471,472</sup> In addition, the muscle around the screws showed myofiber necrosis and fibrovascular granulation tissue compatible with wound healing, as well as multifocal presence of hemosiderin and scattered hemorrhages at this time point. At the bone level, minor inflammatory infiltrates with a low degree of neovascularization and fibrosis were observed. Hemosiderin and scattered hemorrhages were present, as well as new bone formation towards the screw that multifocally attached to the screw surface (osseointegration) (Table 4). Minor bone resorption was observed in case of direct contact between bone and pedicle screw or ring. No to minimal differences in total host reaction score between groups were present. In accordance with previous animal studies, no additional toxic effects of bupivacaine compared to only an excipient hydrogel were observed.<sup>262</sup> Encapsulation of bupivacaine as crystals, instead of as the hydrochloride salt, has been demonstrated to decrease *in vitro* toxicity, which can provide further explanation for the minimal differences between B-matrix and E-matrix local toxicity.<sup>428</sup> Necrosis decreased between 6 and 56 days, at which time it was least severe in the B-matrix group. In contrast, bone formation at the implant bed was minimally superior in the B-matrix group, while osseointegration was similar. Bone resorption values were similar between 6 and 56 days in all groups. When higher grades of bone resorption were observed, the screw was found to be inserted deeper into the bone, making a mechanical origin for bone resorption likely.

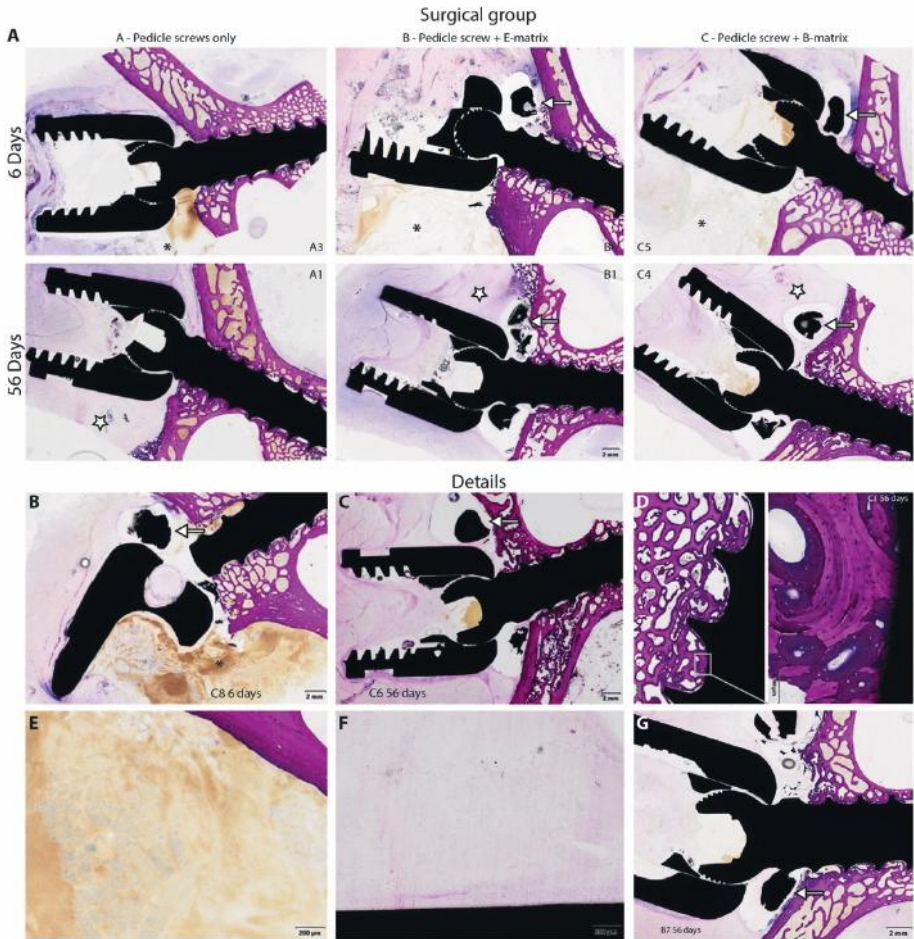


**Figure 6.** Representative histology images of the implant site. A Local host response following implantation of pedicle screws-only, pedicle screws and excipient or pedicle screws and B-matrix after 6 and 56 days of follow-up. All groups display areas of muscle loss, necrosis and hemorrhage after six days (\*). After 56 days, replacement of muscle loss / necrosis by granulation tissue is observed (star). Groups B and C present the E-matrix and B-matrix, respectively (arrow). B Extensive areas of muscle necrosis, 6 days after implantation. E Close-up of B, showing "ghost" myofiber cells. C Replacement of muscle damage by an inflammatory infiltrate, admixed with fibroblastic proliferation and neovascularization. F Close-up of C, showing granulation tissue characterized by fibrosis and a low number of inflammatory cells. D New bone growth is indicated by the darker magenta stain, and osseointegration of the screw is observed after 56 days. G Grade 1 bone resorption is observed in the vicinity of the screw head (circle).

**Table 4.** Summary and differences in average scores for additionally evaluated parameters and host reaction at bone and muscle level after 6 and 56 days.

	Group	# animals	# samples	Avg host reaction bone level	Avg bone formation	Avg osseointegration	Avg bone resorption	Avg host reaction muscle level
6 days	A	2	4	12.3	0.0	0.0	1.0	19.75
	B	2	4	9.8	0.0	0.0	0.0	17.0
	C	2	4	10.8	0.0	0.0	0.8	17.75
	C vs A			-1.5	0.0	0.0	-0.3	-2.0
	C vs B			1.0	0.0	0.0	0.8	0.75
	B vs A			-2.5	0.0	0.0	-1.0	-2.75
	A	6	12	13.6	2.3	1.8	0.4	21.5
	B	6	12	9.1	2.3	2.4	1.0	19.5
	C	6	12	10.8	2.6	2.2	1.0	19.5
56 days	C vs A			-2.8	0.3	0.4	0.6	-2.0
	C vs B			1.7	0.3	-0.3	0.0	0.0
	B vs A			-4.5	0.0	0.7	0.6	-2.0



### 3.5 Histopathology of systemic organs

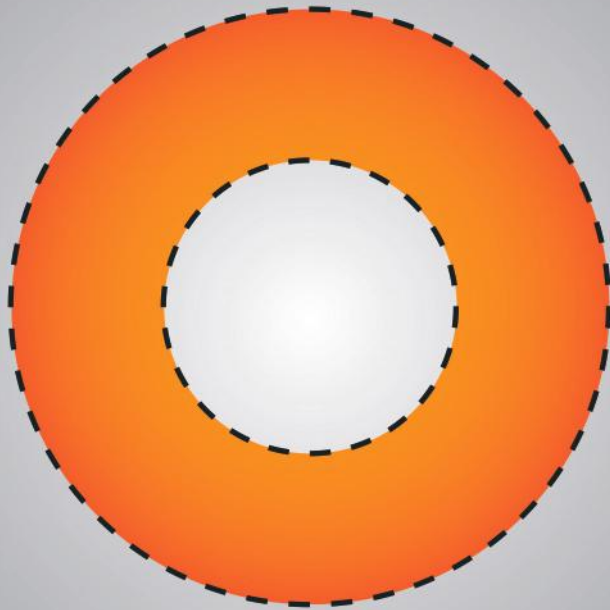
To assess systemic effects of the E-matrix or B-matrix, systemic organs were sampled for histological analysis according to the ISO 10993-11:2016 standard, annex F with minor modifications.<sup>473</sup> Macroscopic findings across the groups included pleural adhesions, calcified liver and lung lesions, white spotted kidneys, abomasal lesions and intra-abdominal hydatid cysts, all compatible with earlier parasitic or bacterial infection.<sup>474–477</sup> In addition, urolithiasis was present in several sheep. All are common findings in farm-derived laboratory animals and without clinical relevance. None of the systemic macroscopic findings recorded during necropsy could be attributed to the E-matrix or B-matrix. Microscopically, the lumbar and iliac lymph nodes displayed multifocal hemosiderin deposits and congestion with similar incidence and severity between groups. The skin directly above the surgical site was histologically characterized by a minor inflammatory infiltrate of mixed cells, most likely associated with the postoperative cutaneous healing process.<sup>478</sup> Minimal inflammatory infiltrates expanding into the Virchow-Robin space were reported in one animal from both the screw-only and E-matrix group at thoracic and cervical level, respectively. A mild unilateral chronic mononuclear neuritis at the dorsal nerve root was observed at lumbar level in one sheep from the E-matrix-group and one from the B-matrix group.

## 4. CONCLUSION

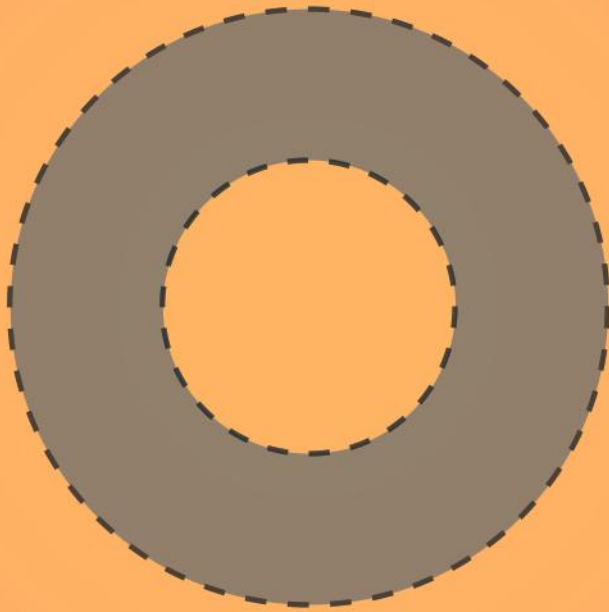
B-matrix provided sustained and low bupivacaine plasma levels compared to the reference subcutaneous bupivacaine infiltration. All plasma levels in this study remained well below toxic thresholds. B-matrix and its excipient material were well-tolerated, and all animals recovered uneventfully from surgery. As tested under GLP, there were none to minimal histological differences in the average total host reaction score at muscle and bone levels among the groups. Therefore, the host reaction at muscle and bone levels were considered associated with the implantation of the screw and non-related to the B-matrix or E-matrix. There were no signs of systemic toxicity that could be attributed to B-matrix or E-matrix. The current findings facilitate clinical testing of B-matrix for safe and effective use in instrumented spine surgery.



# PART IV



Directions for clinical  
application



# CHAPTER 10

Designing a phase Ib clinical trial to assess the safety and preliminary efficacy of a robust hydrogel for sustained bupivacaine release in patients undergoing instrumented spine surgery

## INTRODUCTION

This thesis has focused on better understanding acute postoperative skeletal pain, and the subsequent development of a hydrogel for sustained bupivacaine release (BR-003) after instrumented spine surgery to treat this pain. To reach the ultimate goal of improved postoperative recovery through decreased pain and decreased opioid consumption in patients undergoing spine surgery, BR-003 should become available for clinical use through marketing authorization by regulatory authorities. A prerequisite for marketing authorisation is the demonstration of safety and efficacy in phase I, II and III clinical trials.<sup>479</sup> In parallel, reliable and reproducible manufacturing of the investigational product BR-003 adhering to the principles of Good Manufacturing Practice (GMP) is mandatory. The principles of GMP are enforced by regulatory authorities and aim to ensure a consistently high quality of pharmaceutical products, and prevent harm from occurring to the end user.<sup>480</sup>

Building on the knowledge regarding preclinical safety of the hydrogel obtained in previous chapters, the next step towards clinical implementation is the conduct of a phase Ib clinical trial to investigate its safety and preliminary efficacy. The administration mode of BR-003 (co-implantation with pedicle screws) rules out the inclusion of healthy volunteers in clinical trials, and thus the study population encompasses only patients suffering from spinal disease that warrants surgical intervention. To protect study patients and ensure the quality of the phase Ib clinical trial, ethical and regulatory approval are required prior to patient inclusion. The study protocol presented in this chapter aims to obtain this approval. The protocol is the result of a joint effort involving spine surgeons, anesthesiologists, research nurses, regulatory as well as pharmacokinetic and statistical consultants, and also incorporates advice from the European Medicine Agency.

Considerations for the design of the trial were the selection of end-points to define clinical safety, variations in surgical technique, surgical implants, cumulative dose as a result of the number of BR-003 implanted and the selection of a surgical indication that would make up the first cohort of patients treated with BR-003. The active pharmaceutical ingredient (API) bupivacaine has been used clinically for over 40 years, and data on bupivacaine safety was employed to guide the trial design. The goal was to set up a trial with sufficient precision to accurately study safety with a limited number of patients, while maximizing the generalizability of results to the overall degenerative surgical spinal population.

The strong relation between maximum plasma concentration ( $C_{max}$ ) and the occurrence of Local Anesthetic Systemic Toxicity (LAST) substantiated the choice of  $C_{max}$  as primary

outcome parameter for safety. The present shift towards minimally invasive surgical techniques, as opposed to open implantation of pedicle screws, is represented in the study protocol by inclusion of both techniques. As each hospital typically specializes in a single approach and number of fused levels, inclusion of single- and two-level fusion surgeries through open and percutaneous approach necessitates the selection of multiple hospitals. A typical clinical trial to investigate safety of a new drug would involve a form of dose-escalation. As BR-003 is available in a single dosage strength, dose-escalation in the present clinical trial is realized through the administration of an increasing number of BR-003, equivalent to the number of pedicle screws implanted (four in the first cohort, six in the second cohort). While both cohorts stay within the recommended dosage limits for bupivacaine per 24 hours, the dosage in the second cohort exceeds the recommended maximum single dose. The trial will only proceed to the second cohort in case the safety and safety margin obtained in cohort 1 is deemed sufficient. Patients suffering from degenerative spinal disease, undergoing surgical implantation of four or six pedicle screws were selected as the population for the present clinical trial. The degenerative population allows precise and isolated assessment of BR-003 safety, related events and preliminary efficacy, in contrast to patients suffering from concomitant homeostasis-altering local or systemic disease (e.g., malignant and infectious processes or polytrauma). The rationale for in- and exclusion criteria is further explained in the study protocol.

Once ethical and regulatory approval for the clinical trial have been obtained, patient inclusion can commence. The investigators at participating sites will train their personnel to ensure adequate conduction of the clinical trial, and patients will be informed on the risks associated with trial participation. Patients have to provide written informed consent to participate in the clinical trial, and will undergo screening for eligibility prior to undergoing surgery. During surgery, every pedicle screw is co-implanted with a BR-003 unit. Patients will then be monitored for well-being, drug plasma concentrations, occurrence of adverse events, presence of pain and recovery rate, in order to study the safety and preliminary efficacy of BR-003. Following completion of the first cohort, the data obtained are assessed by an independent Data Safety Monitoring Board (DSMB) and a decision is made on the continuation of the trial with the second cohort. In case of adequate safety in cohorts 1 and 2, the collected preliminary data on efficacy can be employed to estimate an adequate sample size for a phase II clinical trial to study efficacy of BR-003 in treating pain following instrumented spine surgery.

**Study title:** A phaSE Ib study to iNvestigaTe the phaRmacokinetics and safetY of BR-003 in patients undergoing spinal fusion surgery (SENTRY)

**Study design:** An open-label, phase Ib, multi-center, 2-cohort interventional study

**Number of patients:** 6 + 6 (total 12)

### **Indication/study population**

Patients planned for open or percutaneous posterior spinal stabilisation with 4 or 6 pedicle screws with a diameter of 5 to 7.5 mm (inclusive), with or without concomitant posterolateral fusion, vertebral augmentation, intervertebral body fusion devices, osteotomies, and posterior decompression.

### **Product(s) and administration**

BR-003 is an investigational product (IP) presented as an Implantation Matrix (IM) co-implanted with a pedicle screw and providing sustained release of bupivacaine to manage acute postoperative pain, following spinal fusion surgery.

### **Participating study sites**

Elisabeth Twee-Steden Ziekenhuis, Tilburg, Netherlands

Orthopädie Sonnenhof, Inselspital, Bern, Switzerland

### **Study rationale**

The management of postoperative pain after instrumented spine surgery continues to be a major challenge.<sup>12,57</sup> Despite the advent of multimodal analgesia, nearly every patient requires systemic opioids in the first few days after surgery, causing substantial toxicity whilst often providing insufficient pain relief.<sup>67,78,93</sup> Local anaesthetics have long been recognised as promising, non-opioid alternatives for the treatment of postoperative pain, although their effectiveness is limited by a short duration of action. Despite recent efforts to prolong and potentiate the effects of local anaesthetics, a clear unmet medical and societal need remains for even longer lasting, localised, non-opioid pain treatments.<sup>42,93,94</sup>

This study aims to assess the Pharmacokinetic (PK)-parameters and safety of treatment with BR-003 in humans. BR-003 is a pliable, ring-shaped, biocompatible hydrogel that contains 37 mg bupivacaine base, equivalent to 44 mg of bupivacaine HCl, a well-known and approved local anaesthetic. Attached to the shanks of regular polyaxial pedicle screws, BR-003 is co-implanted with each screw without affecting the existing surgical workflow. After placement, BR-003 provides a targeted, sustained release of bupivacaine for at least three days before dissolving within approximately 36 weeks (based on studies in a large animal model).



## Study set-up

The study consists of 2 cohorts with 12 patients in total, according to the scheme below:

	<b>Surgical technique</b>	<b>Number of patients (n)</b>	<b>Instrumented # levels</b>	<b># Screws</b>	<b># BR-003</b>	<b>Cumulative bupivacaine base dose (bupivacaine HCl equiv.)</b>
<b>Cohort I</b>	Open	3	1 level fusion	4	4	148 mg (176 mg)
	Percutaneous	3	1 level fusion	4	4	148 mg (176 mg)
<b>Cohort II</b>	Open	3	2 level fusion	6	6	222 mg (264 mg)
	Percutaneous	3	2 level fusion	6	6	222 mg (264 mg)

In cohort I, six patients undergoing single-level fusion will be included, with 4 pedicle screws and 4 BR-003s with a dose of 37 mg per BR-003. They will receive a cumulative dose of 148 mg bupivacaine. Three patients planned for a percutaneous single-level fusion will be included, as well as three patients planned for an open single-level fusion.

Single-level fusion is selected as the first procedure, since this procedure is frequently performed and utilizes a maximum of 4 pedicle screws. This way, the maximum dose of bupivacaine administered stays within the known tolerated dose of 175 mg, as specified in the summary of product characteristics (SmPC) of Marcaine.<sup>481</sup> In case the resulting systemic bupivacaine concentrations are well below known safety thresholds and BR-003-related adverse events remain absent, the study will proceed to cohort II.<sup>435,436</sup>

In cohort II, six patients undergoing a 2-level fusion will be included, with 6 pedicle screws and 6 BR-003s with a dose of 37 mg per BR-003. They will receive a cumulative dose of 222 mg bupivacaine base. Three patients planned for a percutaneous 2 level fusion will be included, as well as three patients planned for an open 2 level fusion. Together, patients receiving 4 screws and patients receiving 6 screws make up approximately 75% of the population undergoing spinal fusion at the participating study sites.

The dose administered to patients in cohort II exceeds the recommended maximum single dose of Marcaine as stated in the SmPC. However, it remains below the recommended maximum cumulative dose in 24 hours, which is 400 mg.<sup>481</sup> The Marcaine SmPC states that a single dose can be repeated up to every three to four hours. Previous animal studies have shown that BR-003 releases 25% of its dose in the first four hours after surgery. In case of a cumulative dose of 222 mg bupivacaine base, 25% dose release after 4 hours equates to 62.5 mg of bupivacaine HCl released. The release thus does not exceed the maximum dose recommended per four hours.

The high-level visit schedule is displayed in the table below:

<b>Screening</b>	<b>Day of surgery</b>	<b>Day 1 post-op</b>	<b>Day 2 post-op</b>	<b>Day 3 post-op</b>	<b>Day 4 post-op</b>	<i>Every subsequent day until discharge</i>	<b>Day 9 post-op</b>	<b>Day 14 post-op</b>	<b>End of study Day 42 post-op</b>
<b>Outpatient clinic</b>	Admitted	Admitted	Admitted	Admitted	Admitted	Admitted	Outpatient clinic or home visit	Outpatient clinic	Outpatient clinic
<b>Day -90 to Day -1</b>	Day 0	Day 1	Day 2	Day 3	Day 4	Day X	Day 9	Day 14	Day 42

Details about the visits and assessments can be found in section 2 'Study assessment schedule'.

Patients who complete the study will be invited to enter a follow up study, which consists of one additional follow up visit approximately 1 year after the surgery. This will be described in a separate protocol and patients will be asked to sign a separate Informed Consent Form (ICF) for the follow up study.

## Objectives and Endpoints

Objectives	Endpoints
<b>Primary</b>	
Confirm that the $C_{max}$ of BR-003 when co-implanted with pedicle screws onto the spine, stays below the known toxic threshold of 2000 ng/mL <sup>435,436</sup>	Maximum plasma concentration ( $C_{max}$ ) of BR-003
<b>Secondary</b>	
To evaluate additional pharmacokinetic parameters of BR-003 when co-implanted with pedicle screws onto the spine	Time to maximum plasma concentration ( $T_{max}$ ) Area under the curve (AUC) Terminal half-life ( $T_{1/2}$ )
Assess the safety of BR-003 when co-implanted with pedicle screws onto the spine	Incidence, classification and grading of Adverse Events (AEs) Clinical laboratory results (blood chemistry) Electrocardiogram (ECG) data Wound healing Vital signs, neurological assessment Radiological assessment
<b>Exploratory</b>	
Collect efficacy parameters of BR-003 when co-implanted with pedicle screws onto the spine	<u>Pain as assessed by:</u> Numeric Rating Scale (NRS) pain scores International Pain Out (IPO) questionnaire <sup>482</sup>  <u>Mobilisation as assessed by:</u> Functional Ambulation Categories (FAC) scores Energy expenditure in Metabolic equivalent of task (MET) as measured by triaxial accelerometry Activity types as measured by triaxial accelerometry  <u>Opioid use as assessed by:</u> Opioid consumption in Morphine milligram equivalent (MME) Time to first rescue medication  <u>Convalescence as assessed by:</u> Length of hospital stay Discharge location  <u>Gastrointestinal function as assessed by:</u> Oral intake Defecation frequency

**Rationale for selected endpoints**

The maximum plasma concentration ( $C_{\max}$ ) value of bupivacaine is the main determinant of the occurrence of local anaesthetic systemic toxicity (LAST), a condition that is difficult to treat and leads to major cardiovascular and neurological symptoms.<sup>265,266,435,436</sup> It was thus selected as the primary outcome measure for assessment of the safety of a sustained bupivacaine release formulation. To most accurately determine the  $C_{\max}$ , plasma is sampled at multiple time points. Previous animal studies have shown the occurrence of a plateau in bupivacaine plasma levels containing the  $C_{\max}$  between 8 and 48 hours. Plasma sampling is thus intensified in this time window to increase the probability of sampling at  $C_{\max}$ . Further plasma sampling is undertaken to study the pharmacokinetics of BR-003, quantified by the time to  $C_{\max}$  ( $t_{\max}$ ), area-under-the-curve (AUC, a measure for total drug exposure) and elimination half-life ( $t_{1/2}$ ), all functioning as secondary outcome measures.

In addition, various other secondary endpoints are studied. The possible adverse events of bupivacaine are well-described and will be recorded. All adverse events are recorded as defined in the Common Terminology Criteria for Adverse Events (CTCAE). The investigator will grade the severity of the AEs. The severity (mild, moderate, severe, life-threatening and death) is documented according to the CTCAE criteria version 5.0 (grade 1 = mild, grade 2 = moderate, grade 3 = severe, grade 4 = life-threatening and 5 = death)<sup>70</sup>.

At plasma concentrations over 2000 ng/mL, bupivacaine is known to induce cardio- and neurotoxicity, leading to bradycardia, hypotension, paraesthesia, vertigo and convulsions.<sup>435,436</sup> To detect bupivacaine-induced cardiotoxicity, vital signs are tracked and electrocardiography is performed. The occurrence of bupivacaine-induced neurotoxicity is monitored by recording of vital signs and neurological function. Blood chemistry is employed to monitor the effect of BR-003 implantation on body homeostasis and the function of systemic organs. The possible effects of BR-003 on tissue regeneration are studied by wound healing assessment for soft tissues and radiological assessment for bony tissues.

To obtain insight in the potential efficacy of BR-003 for providing analgesia after instrumented spine surgery, various exploratory efficacy outcome parameters are collected. These parameters include pain measurements, employing numeric rating scales (NRS) and the International Pain Outcomes (IPO) questionnaire to quantify the severity and perception of postoperative pain.<sup>482</sup> Moreover, postoperative recovery is studied by mobilisation outcomes such as Functional Ambulation Categories (FAC) scores, accelerometer readings for activity type and energy expenditure and by the convalescence outcomes of length of hospital stay and discharge location. As the delicate balance between analgesia and side effects of current pain treatment is a major incentive

to develop new non-opioid treatments, the effects of BR-003 administration on opioid consumption, time to rescue medication and the occurrence of gastro-intestinal side-effects of opioids are quantified. It is emphasized that all these outcomes are exploratory and do not provide proof for the presence or absence of analgesic effect due to the lack of a control group. However, the outcomes can and will be used for sample size calculations for future efficacy trials.

### **In- and exclusion criteria**

To be eligible for inclusion, patients have to fulfil the following inclusion criteria:

1. Males and females aged between 18 years and 80 years (inclusive).
2. Planned for open or percutaneous posterior spinal stabilisation with 4 (for cohort I), or 6 (for cohort II) pedicle screws with a diameter of 5 to 7.5 mm (inclusive) with or without concomitant posterolateral fusion, vertebral augmentation, intervertebral body fusion devices, osteotomies, and posterior decompression. Only primary instrumented spinal surgery cases can be included.
3. Willing and able to comply with the protocol for the duration of the study.
4. Capable of giving written informed consent prior to any study-related procedure not part of the standard practice, with the understanding that the consent may be withdrawn by the patient at any time without prejudice to his/her (post-)surgery care.
5. Females are eligible only if not currently pregnant, nursing, or planning to become pregnant during the study or within 9 months after study drug administration. Female patients must be surgically sterile, at least 2 years menopausal, or using an acceptable method of birth control. Women of child-bearing potential (WOCBP), must have a documented negative pregnancy test within 24 hours before surgery.

Patients fulfilling one or more of the following criteria are not eligible for participation in the study:

1. Concomitant anterior/lateral procedures (e.g., anteriorly placed vertebral cage, anterior plating, ALIF/XLIF).
2. Use of ilium screws or (additional) pedicle screws with a size < 5 mm or > 7.5 mm.
3. Indication for surgery being:
  - a. Active or previous (para)spinal infection
  - b. Metastatic, malignant or benign tumours of the spine
  - c. Fracture/other traumatic injury
4. Known high risk of surgical complications (e.g., patients having previously undergone more than 2 (non-instrumented) spinal surgeries at the index level)
5. Planned use of a surgical drain

6. Planned use of an epidural catheter
7. Planned use of local amino-amide or amino-ester anaesthetics within 5 days prior to the scheduled surgery (10 days in case of slow-release products), perioperatively and postoperatively for the length of the study
8. Has a pre-existing concurrent acute or chronic painful physical/restrictive condition expected to require analgesic treatment in the postoperative period for pain that is not strictly related to the surgical indication and which may confound the postoperative assessments.
9. Disrupted pain perception according to the treating physician
10. Has a medical condition such that, in the opinion of the Investigator, participating in the study would pose a health risk to the patient or confound the postoperative assessments. Conditions may include, but are not limited to, any of the following:
  - a. History of allergic reactions to bupivacaine or excipients or BR-003, or if the study drug is otherwise contra-indicated
  - b. ASA-classification > 3
  - c. Have clinically significant renal or hepatic abnormalities (defined as an AST or ALT > 3x upper limit of normal (ULN), creatinine > 2x ULN)
  - d. History of clinically significant cardiac abnormality such as myocardial infarction within 6 months prior to study participation, NYHA class III or IV, or clinically significant abnormalities on ECG
  - e. History of coronary artery bypass graft surgery within 12 months prior to study participation
11. Uncontrolled anxiety, schizophrenia, or other psychiatric disorder that, in the opinion of the Investigator, could interfere with study assessments or compliance
12. History of, suspected, or known addiction to or abuse of illicit drug(s), prescription medicine(s), or alcohol
13. Has a body mass index (BMI) > 39 kg/m<sup>2</sup> or patients with a weight below 50 kg
14. As per patient history and/or medical records, has active infection or is currently undergoing treatment for Hepatitis B, Hepatitis C, or human immunodeficiency virus (HIV)
15. Participation in another interventional study

Alternative populations evaluated for inclusion were patients suffering from deformities (such as scoliosis and kyphosis), trauma, infection or malignant disease. However, these populations were deemed unsuitable for the following reasons:

- Scoliosis or kyphosis without underlying malignant, infectious or traumatic cause most frequently occurs in children and adolescents. A first clinical safety study in

- children was considered undesirable. Deformation secondary to degenerative disease is covered in the included patient population;
- Hospital admission of spinal trauma patients cannot be scheduled or planned, and these patients often require acute medical care. This complicates obtaining informed consent and rigorous screening of patients prior to inclusion. Further, patients undergoing non-elective surgical interventions are already at risk of worse postoperative outcomes. Lastly, trauma patients frequently suffer from concomitant injuries, complicating the study of the isolated safety effects of BR-003.
  - Patients suffering from infectious or malignant spinal disease have local and systemic alterations in homeostasis. Although BR-003 is not expected to interfere with infectious or malignant processes, their occurrence complicates the study of isolated safety effects of BR-003, and interactions between BR-003 implantation and infectious or malignant processes cannot be excluded beforehand. The safety and feasibility of BR-003 in patients suffering from spinal infectious or malignant disease is a topic of future clinical studies.
  - To assess long-term safety of BR-003, patients can consent to inclusion in a long-term safety cohort. This cohort provides valuable data on the long-term effects of BR-003 implantation and comprises a hospital visit one year after surgery. However, the limited life expectancy of patients suffering from malignant disease will likely have a large impact on the number of patients available for long-term follow-up in this cohort.

### Sample Size considerations

A total of 12 treated patients (N=12) are planned in this study:

- Cohort I will consist of 6 patients in total, 3 patients per group (open/percutaneous) treated with 4 BR-003s (148 mg bupivacaine base in total)
- Cohort II will consist of 6 patients in total, 3 patients per group (open/percutaneous) treated with 6 BR-003s (222 mg bupivacaine base in total)

Assuming a  $C_{max}$  of approximately 100 ng/mL for a 222 mg dose in humans (twice of what was observed at a comparable dose in sheep) with a standard deviation of 50 ng/mL, sample size calculations show that when the sample size is 3 patients per group the observed 95% confidence interval width (distance from the limit) will not exceed 188.5 ng/mL and will therefore remain well below the toxic threshold of 2000 ng/mL, with a 90% power.<sup>435,436</sup> The planned number of 12 is well above the required number of patients for sufficient statistical power, even if standard deviations are larger.

### **Statistical Analysis**

Study population, demographics, safety, PK and efficacy parameters will be analysed using descriptive statistics only.

### **Nature and extent of the burden and risks associated with participation, benefit, and group relatedness**

All enrolled patients will undergo elective lumbar spine surgery for a degenerative condition and will be treated with a multimodal analgesia protocol in line with evidence based best practices. These surgical procedures and administered medications carry a certain risk profile that is discussed beforehand by the treating physician/spine surgeon. During and after surgery, patients will be monitored for vital functions but also for items related to patient (dis)comfort and perceived changes in well-being in relation to the reason for the surgery. These monitoring activities will also be used to complete most of the activities related to the current study. For the activities required for the current study that cannot be completed during routine examinations, the patient burden and associated risks is considered low and acceptable. The additional assessments are multiple ECG recordings, frequent blood sampling for PK, 3 blood chemistry samples, wearing an accelerometer on one leg from surgery until day 14 and completing one questionnaire about pain management.

By participating in the current study, the patient is exposed to risks associated with bupivacaine and the novel excipient (functionalised gelatin). These can be further divided into local and systemic effects, all of which were studied in a large animal model (sheep) for instrumented spine surgery. The overall risk of local or systemic toxicity for bupivacaine and the novel excipient is estimated as low:

- The **systemic** effects of **bupivacaine** were studied by repeated plasma sampling following BR-003 implantation. In all sheep, drug plasma levels remained orders of magnitude below known toxic thresholds despite administering higher doses than used in the current study.
- The **local** effects of sustained high **bupivacaine** levels in the surgical wound were histologically analysed after 6 and 56 days of follow-up. Surgical site toxicity scores and osseointegration for pedicle screw + BR-003 were similar compared to implantation of pedicle screw-only controls. In addition, overall incidence of wound healing disturbance was low and equally distributed over the groups.
- The **systemic** effects of the **novel excipient** were characterised by histopathological analysis of 35 tissues from 12 organs per animal. No differences between sheep exposed to BR-003 or novel excipient and control sheep were found in any organ. In addition, all sheep recovered uneventfully after surgery.



- The **local** effects of presence of the **novel excipient** in the surgical wound were histologically analysed after 6 and 56 days of follow-up. Surgical site toxicity scores and osseointegration for pedicle screw + novel excipient were similar compared to implantation of pedicle screw-only controls. Overall incidence of wound healing disturbance was low and equally distributed over the groups.

The potential benefits for patients enrolled in the current study are related to the beneficial effects of reduced acute postoperative pain and the associated decrease in consumption of opioid analgesics. It is known from the literature that patients who experience less pain and use fewer opioids after surgery will mobilise sooner, can be discharged earlier, suffer fewer AEs, and score higher on several patient reported outcome measures.

### **Safety overview**

An independent Data Safety Monitoring Board (DSMB) will oversee the safety. The DSMB consists of a spine surgeon, a clinical pharmacologist and a statistician.

#### Safety review after cohort I:

To ensure the safety of the patients in this study, an independent DSMB will assess the reports of all (S)AEs, all clinically relevant lab changes as assessed by the investigators, PK results, abnormal ECG results and abnormal neurological assessment outcomes, after the 6 patients in the first cohort have finished the study. The DSMB will review data to monitor the safety of the study medication and make recommendations to continue with cohort II, to amend cohort II, or to stop the study.

#### Safety review of individual patients:

The DSMB will also be involved in case an unexpected serious adverse drug reaction or death occurs in the study. In case the unexpected serious adverse drug reaction can be found on a predefined list of frequently observed AEs after instrumented spine surgery or systemic opioid use (see appendix 4), this does not immediately lead to (temporary) suspension of the recruitment. Rather, the incidence of these AEs will be assessed on an aggregate level after each cohort. In case an unexpected serious adverse drug reaction not found on this list or death occurs, the recruitment will be suspended, the PK samples of the patient will be analysed ad hoc and shared with the DSMB, together with other safety data of this patient. The members of the DSMB will review the available data and will be asked to make recommendations to continue with the recruitment, to amend the study, or to stop the study.





k: Patient reported pain scores will be obtained using the NRS. On day 0 the NRS is obtained pre-operative and post-operative, during admission it will be obtained 3 times a day (preferably morning, afternoon, evening), and on day 14 and day 42 a single NRS will be obtained. At each time point, the patient will provide a pain score for pain in his/her back and pain in his/her leg (in case of radiated pain). For both locations, the patient will be asked about the pain at rest (PAR), and the pain during movement (PDM). In case multiple assessments will be performed at the same timepoint including the NRS, the NRS should preferably be obtained first before other assessments are being performed.

L: The following parameters will be collected related to mobilisation:

1) FAC score (Appendix 2) at screening visit and subsequently at each time point after surgery, except for day 9 and day 42; 2) Time to the ability to stand next to bed and the ability to ambulate after surgery.

M: The accelerometer will be attached to the upper leg of the patient on the day of surgery, and removed on day 14. The handling and use of the accelerometer will be described in a separate manual.

N: In order to be able to investigate post hoc questions, blood and urine samples will be collected to be stored in the freezer. These could be used for post hoc analysis if needed.

O: The IPO questionnaire will be completed on paper, preferably by the patient him/herself. If not possible, the patient can be interviewed by the research nurse, or delegate. The English version of the IPO can be found in Appendix 1.

P: The patients will be asked daily: 'was oral food intake possible yesterday?'. The answer should be 1 of the following 4 options: 1) No 2) Yes, clear liquids only 3) Yes, solid liquids, 4) Yes, solid food. The patients will be asked daily about their defecation frequency.

q: Adverse events (AEs) will be collected from day of surgery until D42. For each AE the start and stop date will be recorded, as well as the start and stop time (if known). The severity (mild, moderate, severe, life-threatening and death) should be documented according to the Common terminology criteria for adverse events (CTCAE) criteria version 5.0 (grade 1=mild, grade 2=moderate, grade 3=severe, 4 is life-threatening and 5=death). The causality should be documented according to the WHO causality categories.

If a cardiac or neurological AE occurs during the study, a blood sample should be collected at the time that the event is noted to determine the plasma bupivacaine concentration, in addition to collecting the unscheduled vital signs and performing a 12-lead ECG.

r: Screening visit: collect data on current/preoperative medication use, including dose, frequency and start date. For subsequent visits: only document changes compared to the last visit.

s: Patients can only leave the hospital on the day of discharge after the 96 hours PK sample has been drawn. If the patient is discharged prior to the FAC-score and/or second or third NRS score assessment on the day of discharge, these may be omitted.

t: In case a patient is still hospitalised at day 9, the assessments listed under 'every subsequent day until discharge' AND day 9 should all be performed.

u: In case a patient is still hospitalised at day 14, the assessments listed under 'every subsequent day until discharge' AND day 14 should all be performed.

v: If patient withdraws prior to D42, all assessments that are normally collected at D42 are to be collected at the time of the withdrawal visit, if possible.

## PK sampling and ECG schedule:

Screen	0h <sup>a</sup>	2h <sup>c</sup>	4h <sup>c</sup>	8h	12h	24h	36h	48h	72h	96h	D9	D14
Time window	-90 days to day -1	Pre-op	+/- 5 min	+/- 10 min	+/- 25 min	+/- 35 min	+/- 1 hour	+/- 1.5 hour	+/- 2 hour	+/- 3 hour	+/- 4 hour	+/- 2 days
<b>PK sample</b>	+	+	+	+	+	+	+	+	+	+	+	+
<b>ECG</b>	+	+	+	+	+	+	+	+	+	+	+	+

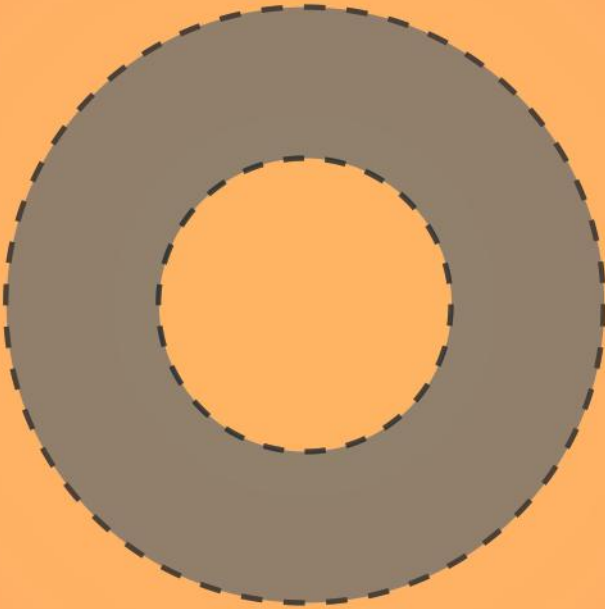
<sup>a</sup>First BR-003 placement will be considered as T0 for all PK and ECG timepoints from the 2h timepoint onwards. To allow for easier logistics, the PK sample at 0h (and ECG if applicable) may be taken just before the surgery instead of the actual 0h timepoint).

<sup>b</sup>In case the screening ECG is taken more than 30 days prior to the day of surgery, the ECG should be repeated prior to the surgery.

<sup>c</sup>Blood samples and ECGs should be collected even if the patient is still in surgery.









# Summary, General Discussion and Dutch Summary

## SUMMARY

Pain after musculoskeletal surgery poses a heavy burden not only on the patient, but also on hospitals and society. Postoperative pain itself, as well as the side effects and addictive potential of opioids used for its treatment can lower the quality of life of patients, lead to increased duration of treatment and thereby tremendously increase healthcare costs. This thesis attempts to better understand the origins of postoperative skeletal pain, quantify its severity and provide directions for its improved treatment. The following paragraphs summarize the main findings of the work conducted.

The **first aim** of this thesis was to understand the origins and severity of postoperative skeletal pain, and effectiveness of current opioid-based treatment. This aim was addressed from multiple perspectives, *i.e.*, a cohort study in patient undergoing spine surgery, an immunohistochemical study analyzing bone innervation patterns and a review of the literature on bone pain. **Chapter 2** described the current clinical practice in patients undergoing spine surgery regarding postoperative pain and its treatment. All 64 patients included required opioids during hospitalization, yet reported moderate to severe pain after major spine surgery. Thirteen patients suffered from such a degree of insufficiently controlled pain that re-admission to the recovery room and administering of a new IV opioid loading dose was necessary. The majority of the 64 patients developed moderate opioid-related adverse drug events (ORADEs), such as nausea. Moreover, severe ORADEs, such as acute respiratory depression were reported in 17 patients. To understand the severity of postoperative skeletal pain, an immunohistochemical study quantifying bone sensory innervation was performed on cadaveric human bone samples from various anatomical locations in **Chapter 3**. The highest sensory innervation density was found in the periosteum, followed by bone marrow and cortical bone. In addition, the anatomical location receiving most sensory innervation was the thoracic spine. Innervation density was similar between genders and decreased with age. Exploring the mechanisms that subsequently convert skeletal nociception to bone pain, **Chapter 4** consists of a review of the literature. This chapter identified four pathways involved in the generation and maintenance of bone pain. These pathways were the activation, sensitization and sprouting of sensory nerve fibers (predominantly A-delta and C-type) as well as central sensitization. Nerve fibers could be activated through mechanical and acidic stimuli. Local neurotrophic factors play a role in peripheral sensitization and nerve sprouting. The intensity of nociceptive signals conducted from bone to brain *via* sensory nerves can be amplified through central sensitization.

The high incidence of postoperative ORADEs illustrated the delicate balance between analgesic and side effects of current postoperative pain treatment. The severity of pain

following skeletal surgery can be explained by dense sensory innervation of osseous structures and especially the periosteum, and the subsequent activation of downstream pathways. Its dense innervation identified the periosteum as a potential target for postoperative analgesia.

The **second aim** was to assess the safety and efficacy of a non-opioid anesthetic (bupivacaine) when applied in high concentrations in musculoskeletal tissues that, when damaged, induce the pain studied in the first aim. Bupivacaine was selected, as it is capable of inhibiting action potential conduction in the sensory nerve types present in bone, and has the longest duration of action of all local anesthetics. The second aim was again approached from three perspectives, by reviewing the literature on bupivacaine toxicity, an animal study investigating toxicity of highly concentrated bupivacaine and the development of an electrophysiological setup to quantify bupivacaine action in nervous tissues.

Across the literature, toxic effects of bupivacaine were reported in bone, muscle and neural tissue, articular cartilage and the intervertebral disc *in vitro*. These effects were reviewed in **Chapter 5**. Bupivacaine delayed osteogenesis and wound healing *in vitro*. However, all reported effects were shown to be reversible in animal and clinical studies, with the exception of chondrotoxicity. Chondrotoxicity following bupivacaine administration is reported clinically, likely because of the limited regenerative capacity of articular cartilage. A similar absence of regenerative capacity in the *in vitro* setting likely limits the translation of laboratory findings to *real-world* toxicity. The musculoskeletal toxicity of bupivacaine reported in literature was limited to clinically used concentrations of 0.5% bupivacaine. However, multiple sustained-release formulations are currently in development that use more concentrated bupivacaine to extend the duration of high local drug levels. To assess the local toxic effects of high bupivacaine concentrations, a rat model for skeletal surgery was used in **Chapter 6**. Rats underwent spinal or femoral implantation of a cannula attached to a screw, to allow bolus administration or sustained infusion of bupivacaine in three concentrations (0.5%, 2.5% and 5.0%) at the surgical site. Following uneventful recovery of all animals, histological analysis of implant sites was performed after 28 days. Significant differences in local toxicity scores existed between spine and femoral surgery, but not between bupivacaine concentrations. To study which bupivacaine concentrations are effective in nervous tissue and surgically damaged periosteum, **Chapter 7** described the development of an electrophysiological setup using freshly excised sheep femoral nerves and periosteum. The electrophysiological setup served as a proof-of-concept that bupivacaine action could be quantified in fresh nervous tissue, but further improvements, such as temperature control and aligning

stimulation direction and fiber orientation, are necessary to allow determination of a minimum inhibitory bupivacaine concentration for periosteal sensory fibers.

The findings indicate the absence of major toxic effects of bupivacaine in musculoskeletal surgery for both conventionally clinically used and experimental higher concentrations, and susceptibility of periosteum to bupivacaine-induced inhibition of action potentials.

The **third aim** builds on the knowledge obtained from the first and second aim, which were to understand the severity and etiology of bone pain and assessment of the safety and efficacy of bupivacaine for its treatment. The third aim concerns the development of a clinically relevant hydrogel-based bupivacaine sustained release formulation for use in musculoskeletal surgery. **Chapter 7** described the development and *in vitro* optimization of a ring-shaped hydrogel, capable of withstanding co-implantation with pedicle screws. The hydrogel displayed tunable mechanical properties and drug-releasing behavior. Drug release was sustained for 72 hours *in vitro*. The material was biodegradable and cytocompatible. Moreover, encapsulation of bupivacaine in the hydrogel as crystals decreased the cytotoxic effects of bupivacaine itself. Employing the hydrogel developed in chapter 7, the *in vivo* drug releasing properties, biocompatibility and -degradability were assessed in a sheep model for spinal surgery in **Chapter 8**. Implantation of up to 8 hydrogel rings yielded sustained but low bupivacaine plasma levels, with correspondingly high surgical site levels for 72 hours. Drug release was quantified by hydrogel explantation and followed a first-order kinetic profile. Hydrogels elicited a mild local foreign body response and degraded *in situ* within approximately 9 months. In **Chapter 9**, a first step towards clinical implantation of the bupivacaine-loaded hydrogel ring from chapters 7 and 8 is taken. To facilitate future endorsement of clinical trial protocols, a toxicokinetic bridging study was performed in sheep according to Good Laboratory Practice (GLP). GLP is a set of rules to ensure the consistency, reliability, reproducibility, quality and integrity of study data and studied products for future use in human health applications, and GLP compliance is a prerequisite for marketing authorization from regulatory authorities. Sheep received either 8 pedicle screws without hydrogel, 8 pedicle screws combined with unloaded hydrogels, or 8 pedicle screws with bupivacaine-loaded hydrogels. Plasma bupivacaine levels remained tenfold below toxic thresholds, and were sustained for a longer period compared to subcutaneous infiltration of bupivacaine. Upon histological evaluation, local tissue reaction and screw osseointegration were found similar between groups.

Taken together, the results indicate biocompatibility, biodegradability, large systemic safety margins and extended drug release of the bupivacaine-loaded hydrogels *in vivo*.

The **final aim** of this thesis was to provide directions for a clinical trial, assessing safety and feasibility of the bupivacaine-loaded hydrogel for use in instrumented spine surgery. In **Chapter 10**, a protocol for a phase 1B dose-escalating clinical trial was presented, in which female and male adult patients suffering from degenerative spinal disease and scheduled for open or percutaneous instrumented spine surgery are included. The patients will receive 4 or 6 hydrogel rings, to be co-implanted with a corresponding number of pedicle screws. The primary outcome of the study is systemic safety of the bupivacaine hydrogel formulation as defined by the  $C_{\max}$  value. In addition, the occurrence of adverse events, analgesic consumption, postoperative pain outcomes and mobility outcomes are recorded to obtain preliminary data on efficacy.

## GENERAL DISCUSSION

The research in this thesis has increased our knowledge on the etiology and severity of postoperative skeletal pain, and has provided a new direction in treatment of this pain. The next paragraphs discuss the findings in light of current literature, and identify remaining challenges in the optimal treatment of postoperative skeletal pain.

### The Unmet Clinical Need

Severe pain after skeletal surgery is frequently reported, especially after spine surgery.<sup>12</sup> Moreover, bone surgery and its resulting postoperative pain are significant predictors of the development of chronic postoperative pain.<sup>64</sup> Adequate treatment of pain after skeletal surgery is thus of vital importance for patients in the short and long term. In our cohort study in patients undergoing instrumented spine surgery (**Chapter 2**), the majority of patients reported severe pain despite considerable opioid consumption. Pain despite opioid use could indicate undertreatment, but it depends on who is asked. Whereas in clinical practice analgesics are prescribed when pain scores exceed 3 out of 10, the majority of patients only desire opioids when pain scores exceed 8 for fear of opioid-related adverse drug events (ORADEs).<sup>85</sup> ORADEs are common and potentially severe. In agreement with previous literature, Chapter 2 found a high incidence of ORADEs, pointing towards a skewed risk-benefit ratio in current analgesic treatment.<sup>78,93,94</sup> In fact, studies have shown that patients would rather experience less pain relief than suffer from ORADEs, such as nausea and vomiting. An improved balance between pain relief and side effects from pain medication is desired by both patients and physicians.<sup>93,94</sup> The results of this study and previous reports in literature identify a clear unmet need for drugs effective at the target site, while not disturbing systemic homeostasis (**Figure 1**). Although the patient cohort originated from a single Dutch tertiary center, the findings can likely be extrapolated to other Western countries as opioid consumption is at least similar and frequently higher, especially in the United States.<sup>91</sup>



**Figure 1.** *Morpheus, the god of dreams and namesake of morphine, is woken by the arrival of Iris, the goddess of the rainbow and divine messenger. This thesis similarly serves as a wake-up call for opioid use after spine surgery. Morpheus et Iris, Pierre-Narcisse Guérin, 1811. Collection of the Hermitage, St. Petersburg, Russia.*

### **Target for Postoperative Analgesia**

A next step is to identify the target site for analgesia after skeletal surgery. The results from the immunohistochemical study performed in **Chapter 3** are a potential explanation for the severe pain arising from skeletal surgery. High densities of sensory nerve fibers were found in osseous tissue, especially in the periosteum. The periosteum is inevitably damaged during instrumented skeletal surgery. Notably, the thoracic vertebra was the most densely innervated bone studied, an observation that matches the painful nature of spinal procedures reported clinically.<sup>12</sup> The results of this study are in line with previous animal research, which identified the periosteum as the most densely innervated bone compartment.<sup>17-19,126</sup> However, the innervation ratio between periosteum, bone marrow and cortex found in animal studies was far greater than we observed in humans (100 : 2 : 0.5 vs 100 : 54 : 8). However, the use of a different species and calculations based on medians instead of means can partially account for these differences. The predominant sensory nerve fibers found in bony tissues were of the A-delta and C-type. In **Chapter 4**, multiple interrelated mechanisms leading to the generation and maintenance of bone pain were identified. These pathways were the activation, sensitization and sprouting of sensory nerve fibers (predominantly A-delta and C-type), as well as central sensitization.

The previously identified A-delta and C-fibers thus play a major role in three of the four pathways described. Although innervation density is not necessarily equal to potential magnitude of pain, it does allow larger orders of nociception.

### **A Mechanism-Based Approach**

The identified mechanisms not only explain the severity of bone pain, but also provide targets for treatment of pain after skeletal surgery and aid in selecting feasible analgesic drug classes. For example, considerable progress in the skeletal application of drugs inhibiting nerve sprouting, such as the anti-nerve growth factor antibody tanezumab, has been made.<sup>233</sup> Ketamine is used in the treatment of acute pain to decrease central sensitization.<sup>484</sup> However, of the mechanisms described in **Chapter 4**, activation of nerve fibers most likely precedes activation of all other pathways. Prevention of peripheral nerve fiber activation thus probably inhibits activation of downstream mechanism. Local anesthetics, such as lidocaine and bupivacaine, are common pharmaceutical agents used to prevent local action potential generation and conduction in sensory nerve fibers.<sup>360</sup> Administration of bupivacaine in the surgical wound would thus treat skeletal pain at its origin, both from an upstream-downstream mechanistic and a peripheral-central sensory perspective. Previous research has shown that the fiber types present in bone-related structures are susceptible to local anesthetics, and have known concentration-dependent sensitivities to bupivacaine-mitigated blocks of action potential generation and conduction.<sup>361,485,486</sup> The analgesic effect of bupivacaine is well-known from years of clinical use. However, no exact local concentration needed to obtain analgesia is reported. In addition, the concentration needed might vary considerably between regional large nerve-blocks (such as femoral blocks) and local blocking of sensory nerve fiber endings. The axons in large nerves are still surrounded by endo-, peri- and epineurium, through which bupivacaine first has to diffuse before reaching its target site on the intracellular membrane of the axon. The concentration of bupivacaine needed locally is thus likely lower than the concentration needed for a regional block. These differences were further explored in **Chapter 7**. Lastly, regional blocks often provide not only sensory, but also motor inhibition, which can impede the accuracy of postoperative neurological examination, as well as delay mobilization.<sup>487,488</sup>

### **Safety of Local Anesthetics in Skeletal Surgery**

Before administering high concentrations of bupivacaine, its safety is to be assessed. In musculoskeletal tissue types, toxic local effects of bupivacaine are reported *in vitro* already at subclinical concentrations, but these findings do not translate well to an *in vivo* setting (**Chapter 5**). Likely, the complexity of an organism, with local drug clearance and regenerative capacity contributes to the absence of severe toxic bupivacaine effects *in vivo*. In one tissue type, articular cartilage, *in vivo* toxic effects of bupivacaine were



reported of similar magnitude to *in vitro* effects.<sup>297,489</sup> Articular cartilage has a known limited healing capacity *in vivo*, as observed in diseases such as focal cartilage defects and osteoarthritis.<sup>490,491</sup> The absence of chondrocyte regenerative capacity in the *in vitro* as well as *in vivo* setting, likely accounts for the similarities found regarding bupivacaine chondrotoxicity between these settings.

Having learned that current *in vitro* models are not representative for bupivacaine toxicity, **Chapter 6** studied the tissue effects of highly concentrated bupivacaine in an *in vivo* rodent model for skeletal surgery. No concentration-dependent toxicity of bupivacaine was observed following spinal or femoral screw implantation with concomitant local bupivacaine infusion. Any differences found between histological toxicity scores in animals were attributable to the surgical intervention. While major tissue effects of concentrated bupivacaine were absent after 28 days, these findings cannot simply be extended to a non-surgical population. Any toxic effects of high bupivacaine concentrations might be more pronounced in the absence of major tissue damage resulting from surgery.

Despite the absence of major toxic effects, patient drug exposure should be limited to the minimum dose of drug needed to obtain a satisfactory effect. The minimum effective concentration for inhibition of regional and local nociceptive signals was studied in a neurophysiological setup, using patient- and animal-derived neural tissues (**Chapter 7**). The setup was designed based on previous electrophysiological reports, and adapted to accommodate periosteum.<sup>361</sup> While this chapter proved the feasibility of bupivacaine-mediated inhibition of nociceptive conduction in large nerves and periosteum, several challenges still remain to be fulfilled before solid conclusions can be drawn from this setup. Controlling temperature, a better understanding of fiber orientation and distinction between readings from different fiber types would benefit reproducibility and render more robust results. Patient-derived tissue was sampled from osteoarthritic femoral necks following total hip arthroplasty. As disease has been shown to impact innervation density, different concentrations or doses of local anesthetic could be necessary in affected tissue.<sup>129</sup> The required dose of local anesthetic in absence and presence of disease, is therefore an interesting and relevant direction for future research.

### **Efficacy of Local Anesthetics in Skeletal Surgery**

Chapter 7 provides *ex vivo* clues for the feasibility of musculoskeletal applications of bupivacaine. Further clinical substantiation of bupivacaine's feasibility in spine surgery is provided by an emerging technique named the erector spinae plane (ESP) block.<sup>103</sup> The ESP block concerns an ultrasound-guided injection of local anesthetic solution in the erector spinae fascia near the lateral tip of the transverse process, in order to block the posterior rami of spinal nerves that innervate dorsal structures. Typically, a single

dose of 50-75 mg bupivacaine is administered, but continuous infusion has also been used. Both approaches have their respective disadvantages; either a short duration of action, or attachment of a cannula to the patient which can dislodge, and which hampers mobility.<sup>337,449</sup> Significant decreases in pain scores and opioid consumption following ESP blocks in spine surgery have been reported up to 24 hours.<sup>103,423,424</sup> Although promising, a mismatch between the duration of ESP block and the duration of severe postoperative pain remains present.<sup>36</sup> As ESP blocks are unilateral procedures, the block has to be repeated contralaterally in the event of bilaterally instrumented spinal surgery. Further, the fascia allows craniocaudal transport of local anesthetic solutions. Especially in open surgical approaches, the intervention directly disrupts the recently deposited reservoir of bupivacaine if administered pre-operatively, making appropriate postoperative localization of bupivacaine solutions uncertain.

Taken together, the discussed literature indicates that bupivacaine can be effective in treating postoperative skeletal pain. However, severe pain after skeletal surgery typically lasts for a few days before subsiding to an acceptable level.<sup>36</sup> As the duration of pain exceeds the duration of action of bupivacaine, sufficient drug that slowly becomes available should thus be present at the target site for a sustained effect to avoid repeated administration. Moreover, as space in the surgical site is limited, high doses of drug should be administered in a limited volume, necessitating an increase in drug concentration. The need for a compact and concentrated local anesthetic reservoir, activated by a single administration and providing sustained analgesia is highlighted by the sheer number of drug release formulations developed in this field.<sup>42</sup> Finding the right formulation and mode of administration for each indication is key. The need for implantation of a drug release formulation is a no-go in many applications, but can be a strength in certain uses, such as instrumented spine surgery. The tissue damage and resulting pain induced by surgical implantation of a drug release formulation for analgesia would obviously counteract its goal of providing pain relief. However, tissue damage is already an inevitable byproduct of instrumented spine surgery, and the implantation of surgical hardware, rather than the drug release formulation, warrants the surgical intervention.

### **Local Treatment of a Local Problem**

Instrumented spine surgery thus provides a window of opportunity for the implantation of a drug release formulation, providing sustained and stationary bupivacaine release (**Chapter 8**). Such a formulation would provide extended analgesia without a cannula, thus eliminating the respective disadvantages of ESP blocks administered by either infiltration or continuous infusion, can easily be applied bilaterally and ensures adequate positioning of the drug reservoir.<sup>37</sup> To this end, the present thesis described the development of a sustained-release formulation of bupivacaine, specifically designed

for co-implantation with pedicle screws. The similarity in anatomical location of ESP block administration and pedicle screw placement in instrumented spinal surgery suggest potential effectiveness of a bupivacaine reservoir near pedicle screws. Patients undergoing spine surgery are a logical first population for application of this sustained release formulation because of a large unmet clinical need, as indicated by high rates of opioid consumption and contradicting high pain scores. For successful application of a bupivacaine delivery formulation in instrumented spine surgery, some conditions should be met: 1) Drug release / analgesia for a clinically meaningful period of time, 2) from a biocompatible and biodegradable carrier, 3) able to withstand orthopedic implantation, and 4) implantation does not interfere with surgical workflow.<sup>42</sup> These requirements are discussed in more detail below.

Firstly, the duration of analgesia should better match the duration of severe pain. Although the target duration of analgesia depends on the application, it should exceed the duration of action of a standard local anesthetic solution. In addition, the delivery formulation should lead to a high sensory : motor block ratio.<sup>42</sup> The occurrence of motor block is undesirable because it could complicate postoperative neurological assessment, as deficits induced by surgery that would warrant surgical re-intervention cannot rapidly be distinguished from bupivacaine-related deficits.<sup>492</sup> Matching the reported duration of severe pain after spine surgery, this thesis considered three days of analgesia a clinically meaningful improvement on current best practice.<sup>36,65,103</sup>

Another requirement for the delivery formulation is biocompatibility, defined by the FDA as “the ability of a material to perform with an appropriate host response in a specific situation”.<sup>442,443</sup> Although biocompatibility is dependent on anatomical location, the combined carrier and drug should be biocompatible, i.e., elicit an acceptable local inflammatory response, and not lead to systemic toxicity.<sup>42,48</sup> Other local anesthetic delivery formulations frequently incorporate high drug doses to ensure sufficiently high local drug levels for extended periods of time.<sup>324</sup> However, such high doses put patients at risk of both local and systemic toxicity induced by local anesthetics. Indeed, rapid initial, or excessive “burst release”, not only leads to a waste of drug payload but can have harmful consequences. For example, higher release rates of bupivacaine have been described to cause more muscle injury.<sup>379</sup> When absorbed into the systemic circulation, spikes in bupivacaine plasma concentration can put patients at risk of Local Anesthetic Systemic Toxicity (LAST), a condition that is difficult to treat and leads to major cardiovascular and neurological symptoms.<sup>265,266</sup> In order to prevent burst release, formulation parameters that dictate release kinetics can be adjusted, such as surface-to-volume ratio, the type of excipient or polymer network density.<sup>48,51</sup> Systemic absorption can be limited by, for example, the addition of vasoconstrictor drugs such as noradrenalin.

This in turn maintains a high local concentration, increasing risks of local toxicity.<sup>48</sup> In fact, market authorization application of a local anesthetic release formulation was withdrawn as a result of local tissue injury in both humans and animals.<sup>48,493</sup>

While the interplay between drug and carrier influences biocompatibility of the formulation, biocompatibility and -degradability is also a requirement for the carrier material itself.<sup>48</sup> Hydrogels are a class of drug carrier that is generally well-tolerated in the body. Their porous structure and thus their mechanical properties are tunable by controlling cross-linking. In addition, their porosity allows drug-loading with subsequent diffusion-dependent release. Moreover, hydrogels closely mimic tissue consistency due to their high water content, likely contributing to biocompatibility. The design of hydrogels can allow *in situ* degradation through enzymatic, hydrolytic or environmental pathways.<sup>51,53</sup> However, challenges still exist for the successful application of hydrogels in drug delivery. First, many hydrogel systems exhibit low tensile strength, potentially resulting in fragmentation and subsequent premature disappearance from the target site. Second, hydrophobic drug loading can be problematic, leading to encapsulation of low doses. Third, small-molecule drugs can rapidly diffuse out due to the hydrogel's high water content and porosity, limiting the gel's potential for sustained release.<sup>51,53</sup> Larger-molecule drugs, or aggregates of small-molecule drugs, generally exhibit a slower release as the mesh size of the hydrogels is smaller than the drug diameter. Such drugs are then released from the hydrogel through network degradation, swelling or mechanical hydrogel deformation.<sup>53</sup>

### **Meeting the Requirements**

In this thesis, a biocompatible and degradable carrier was selected in the form of a gelatin-based hydrogel, with the goal to minimize local tissue response and enable *in situ* biodegradation.<sup>50</sup> Gelatin is a commonly used polymer for hydrogel systems due to its mild tissue response and susceptibility to enzymatic degradation.<sup>50,471</sup> To make the carrier material resistant to implantation, gelatin was functionalized with phenol-containing moieties. This enabled covalent cross-linking of polymer chains under the influence of riboflavin and light, a biocompatible and controllable photocross-linking system. Similar hydrogel systems have been described before, but relied on enzymatic cross-linking. Horseradish peroxidase was employed to induce phenol-phenol cross-links between gelatin chains that were functionalized with tyramine.<sup>386</sup> Enzymatic cross-linking implies that hydrogel formation starts directly after mixing of polymer solutions and enzyme, limiting the time available to process the liquid pre-gel. Although applications exist in which rapid gelation is useful, it is not suitable for the formation of many individual gels from a single pre-gel solution. The increased temporal control of photocross-linking compared to enzymatic cross-linking is a distinct advantage of the system used in this

thesis. Although the obtained covalent bonds following photocross-linking constitute the main mechanism of hydrogel formation, inclusion complex formation was added as a second method of cross-linking to improve hydrogel recovery following the mechanical stress endured at implantation. The cavity of oxidized beta-cyclodextrin, attached to gelatin chains, can host phenolic moieties in a non-covalent manner and so enhances the mechanical properties.<sup>387</sup> In addition, the cyclodextrin cavity could host small-molecule drugs including bupivacaine.<sup>390,494</sup> The resulting hydrogel stiffness could be tuned in the range of 100-600 kPa. Although such values have been described before in literature, high stiffness often also leads to a brittle gel.<sup>495</sup> In contrast, the present hydrogel system displayed shear-thinning properties enhanced by the presence of guest-host interaction between phenolic moieties on gelatin and the cyclodextrin cavity, allowing network interruption and reformation during implantation.<sup>387</sup>

Following implantation, the hydrogel should slowly release the encapsulated bupivacaine. According to the rubber elasticity theory, mesh size is approximately 10 nm in the hydrogel composition (chapter 8).<sup>53,396</sup> In contrast, the diameter of a bupivacaine molecule is approximately a factor 10 lower, and steric hindrance of diffusion will thus be limited.<sup>496</sup> However, increasing cross-linking density to decrease mesh size is undesirable, as this renders very stiff yet brittle hydrogels.<sup>495</sup> To overcome the problem of rapid release, bupivacaine was crystallized *in situ* by alkaline precipitation, effectively increasing drug size and making crystal dissolution the rate-limiting step.<sup>416</sup> Moreover, this technique employs local drug solubility to control maximum local drug concentrations, countering the previously raised concern of excessively high local concentrations that induce toxic effects.<sup>48</sup> The effect of crystallization on rate of drug release is discussed in chapter 8. Control of crystal size would allow further tunability of release rates, as crystal dissolution is dependent on the crystal's surface-to-volume ratio. Pilot experiments revealed pH-dependent increases in crystals size, which constitutes a promising direction of future research to optimize drug release rates.<sup>416</sup> The methods and feasibility of alkaline precipitation of local anesthetic HCl formulations rendering the free base have been reported by others, e.g. for ropivacaine, bupivacaine and mepivacaine.<sup>497,498</sup> The increased non-ionized fraction of local anesthetic available following alkaline precipitation was postulated to enhance efficacy, as the non-ionized fraction readily crosses phospholipid bilayer membranes.<sup>264</sup> However, one study reported significant inflammation following the application of ropivacaine base crystals.<sup>497</sup> Encapsulation of local anesthetic crystals in a biocompatible hydrogel, requiring crystal dissolution for release, could overcome such reactive inflammation.

Three-day release was first optimized *in vitro* and subsequently confirmed in a sheep model for spine surgery (**Chapter 9**). The rationale for selecting the sheep as animal

model is explained in the next paragraph. The experimental setup employed in this chapter allowed for precise assessment of *in vitro-in vivo* correlation (IVIVC) of drug release, as hydrogels could be explanted. Whereas most IVIVCs rely on deconvolution of plasma curves to estimate the local absorption of drug administration, now a point-by-point correlation could be obtained. The use of a scaling factor allows the prediction of *in vivo* release from *in vitro* curves, which are more easily obtained. A good IVIVC can accelerate formulation development by predicting *in vivo* behavior and omitting the need to perform *in vivo* bioequivalence studies in case of minor formulation modifications.<sup>499,500</sup> However, studies validating the predictive performance of the obtained IVIVC still have to be undertaken before the IVIVC is accepted by authorities as a surrogate for *in vivo* testing.<sup>501</sup> Moreover, the currently utilized explantation approach can obviously not be followed in the case of clinical studies, in which one would have to resort to methods employing deconvolution to estimate local release. For oral dosage forms, the FDA requires human data for regulatory consideration of an IVIVC and provides guidelines on its establishment.<sup>502</sup> Guidance and standardization for non-oral extended release-products is still lacking.

### **From the Stables to the Clinic**

Another way in which IVIVC can expedite formulation development, is establishment of a link between *in vitro* release and *in vivo* pharmacokinetic (PK) parameters such as  $C_{max}$  and AUC. Combining the IVIVC with a PK model would allow the determination of such links. Hypothetically, such a model would be able to predict the *in vivo* safety of a drug delivery formulation from its *in vitro* release profile. The IVIVC presented in Chapter 9 predicts the formulation's *in vivo* release profile, after which the released (or Liberated drug) is systemically Absorbed, Distributed, Metabolized and Eliminated (LADME). The processes included in LADME can be viewed as communication rates between physiological compartments such as the administration site (in this case the surgical wound), systemic circulation, high-perfusion (liver, gut) and low-perfusion tissues (fat, skeletal muscle) (**Figure 2**). The parallel occurrence of all these processes results in the drug plasma curves, the compartment most accessible for sampling. The systemic pharmacokinetics of bupivacaine are known for various species including sheep and humans, leaving the systemic absorption rate to be deduced from the plasma curves obtained in animal studies.<sup>503</sup>

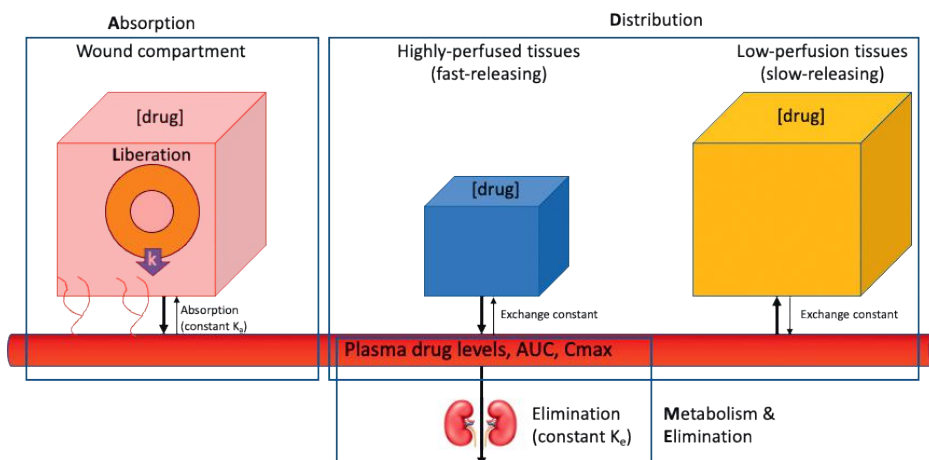


**Figure 2.** Graphical representation of the LADME pharmacokinetic processes taking place following ring implantation and the associated physiological compartments, as can be used in PK models.

As bupivacaine exerts its anesthetic action locally and bupivacaine-induced adverse events are mainly linked to high systemic concentrations, high concentrations at the target surgical site and low circulating drug concentrations are desirable.<sup>266,435,436</sup> The animal study undertaken in Chapter 9 has shown that implantation of six bupivacaine-loaded hydrogels resulted in high local and low systemic drug concentrations. The foreign body response elicited by the combined implantation of pedicle screw and hydrogel was comparable to implantation of only a pedicle screw, indicating biocompatibility of the delivery formulation.<sup>434,445</sup> In addition, hydrogels degraded over the course of 9 months following implantation. As *in vivo* degradation of gelatin hydrogels is dependent on cross-linking density, our high-modulus hydrogel was expected to degrade rather slowly.<sup>504</sup> Considerable differences in degradation rate *in vivo* was observed compared to enzymatic degradation at simulated physiological conditions *in vitro*.<sup>398,400</sup> These enzymes are abundantly present in early tissue-remodeling phases following surgery, but decrease in concentration during the healing process.<sup>398,399</sup> The combined effects of the relatively large size of the hydrogel, the regeneration rate of surgical injury and concomitant events of physiological enzyme concentration and fibrous capsule formation (limiting the enzymes' access to the hydrogel) decrease likely explain the difference between degeneration rates *in vitro* and *in vivo*.

### **The Ovine Spine**

The sheep was selected as large animal model for spine surgery, as sheep compare well to humans regarding weight, circulating volume and gross spinal anatomy.<sup>429</sup> Moreover, the PK properties of bupivacaine in sheep have been well-established, although the sheep as an animal model to study safety and feasibility has some drawbacks.<sup>440</sup> Despite the maximum bupivacaine plasma concentrations being well below systemic safety thresholds in sheep, these findings cannot be simply extrapolated to humans. This also holds true for application of the sheep-derived IVIVC in the human situation, as bupivacaine clearance is twice as fast in sheep compared to humans.<sup>437</sup> This does not mean that maximum plasma concentrations will be twice as high in humans, as the data in sheep indicate the presence of absorption-rate limited elimination (ARLE).<sup>439</sup> In the event of ARLE, the maximum plasma concentration mainly depends on the rate of systemic uptake from the administration site, and thus the comparability of a sheep spinal wound to a human spinal wound. PK modelling could therefore aid in the prediction of safety when translating to humans, and is an interesting direction for future research. This would involve optimization of the model using data obtained in sheep, followed by substitution of sheep pharmacokinetic parameter values for human-derived values available in the literature. As a model is by definition a simplified representation of the truth, which is subsequently used to extrapolate safety data, the modeler should acknowledge its limitations. However, various methods to minimize the error of scaling exist and increasing knowledge on PK models becomes available.<sup>503</sup> To quote statistician George Box: "All models are wrong, but some are useful."<sup>505</sup>



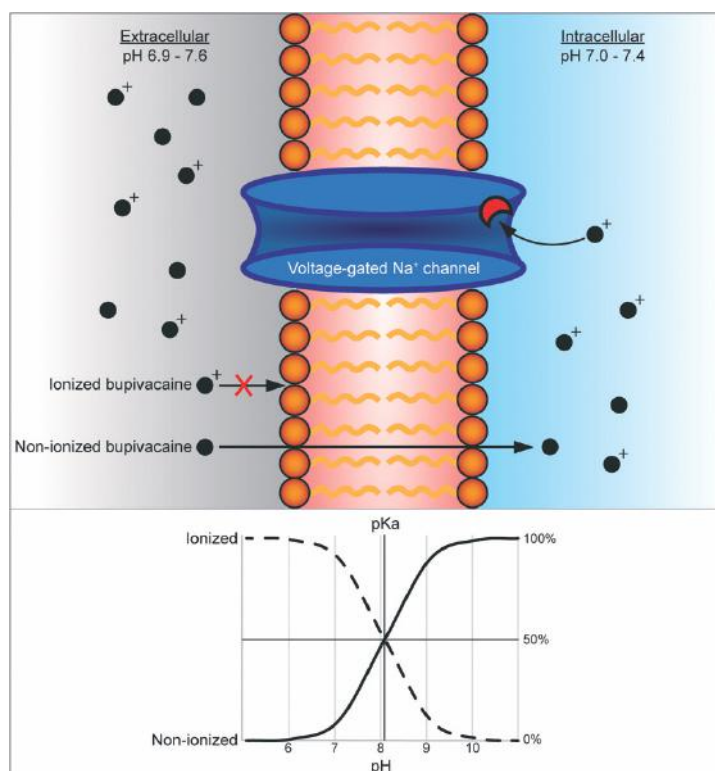


**Figure 3.** Bupivacaine equilibrium across the cellular phospholipid membrane. The Henderson-Hasselbalch equation dictates the ionized drug fraction as function of pH. Only the non-ionized fraction of bupivacaine crosses the membrane. Once intracellular, only the ionized fraction can bind to the sodium channel. Extracellular pH varies between 6.9 and 7.6, while intracellular pH ranges from 7.0 to 7.4.

### Will the concept work?

So far, the pharmacokinetics (*i.e.*, what the body does to the drug) have been discussed, but for estimations of analgesic efficacy of the hydrogel, the focus should shift to pharmacodynamics (*i.e.*, what the drug does to the body), which includes the therapeutic effect of the drug. Pain was not quantified in the animal studies in this thesis, as limited methods for pain quantification in sheep are available and often rely on laterality (*e.g.*, comparing weight bearing on left *versus* right leg). Laterality methods are not applicable in the case of spine surgery, complicating the assessment of analgesic effect of the hydrogel rings.<sup>441</sup> As an alternative, the bupivacaine concentration in the wound was measured. Implantation of six bupivacaine-loaded hydrogel rings led to wound bupivacaine concentrations of up to approximately 200 µg/mL or 720 µM. Previous neurophysiological studies on single sensory neurons reported use-dependent blocks at concentrations

above 30  $\mu\text{M}$  and complete absence of action potential conduction above 300  $\mu\text{M}$  at a pH of 7.4.<sup>485,486</sup> Wound pH varied between 6.9 and 7.6 in the animal studies performed. pH is an important parameter for the efficacy of bupivacaine, as it regulates bupivacaine's ability to enter neurons (**Figure 3**). The Henderson-Hasselbalch equation dictates that at a pH of 8.1, 50% of bupivacaine molecules are non-ionized and thereby able to cross the phospholipid bilayer to exert their intracellular action. Once intracellular, only the ionized fraction can inhibit action potential generation by blocking voltage-dependent sodium channels. Equilibria are constantly restored following diffusion of molecules according to Le Chatelier's principle, which states that a change in concentration results a predictable opposing change in the system to achieve a new equilibrium state. Despite the wound concentrations being above inhibitory thresholds, remaining questions are which part of the bupivacaine is actually quantified in the wound fluid, how large the intracellular non-quantified fraction is, and which part of the total bupivacaine dose is actually effective. In the event of acidic surgical wound conditions, a smaller fraction of the total bupivacaine dose is effective.<sup>506</sup> Events increasing wound pH, such as infection, would enhance the membrane-crossing potential of bupivacaine.<sup>507</sup> Coming back to the question in the title of this paragraph: The local concentrations should be sufficient to inhibit nociception. The next paragraph will explore how inhibition of nociception ultimately translates to the sensation of pain.

### **The Multidimensional Phenomenon that is Pain**

As already discussed in the introduction of this thesis, nociception is the neural process of encoding noxious stimuli, a process influenced by the presence of bupivacaine. Pain is defined as "an unpleasant sensory *and* emotional experience associated with, or resembling that associated with, actual or potential tissue damage". Pain is characterized as a personal experience that is influenced by social, biological and psychological factors and not equal to nociception.<sup>3</sup> Only a weak link exists between pain and extent of tissue injury.<sup>508</sup> Numerous examples exist in literature where supposedly limited nociception generates the sensation of severe pain, and vice versa.<sup>509</sup> The ultimate test for the presence of analgesic effect is a randomized clinical trial, in which the bupivacaine-loaded hydrogel is compared to a placebo intervention and pain scores, analgesic consumption and mobilization are quantified. A protocol for a clinical trial is provided in **Chapter 10**.

Clinical trials studying pain bring various challenges, due to the interrelated efficacy outcome measures of pain, analgesic consumption and patient mobilization.<sup>510</sup> Assuming effect of the hydrogel, a subsequent decrease in analgesic consumption might keep pain scores at a similar level, or similar analgesic consumption can lead to lower pain scores. Lower pain scores could motivate a patient to mobilize earlier, but pain scores are generally higher during mobilization. "Efficacy" of the bupivacaine-loaded hydrogel

could thus be a combined effect on pain scores, analgesic consumption and time to mobilization. As minor improvements on each individual outcome could yield a large cumulative effect on the postoperative recovery process, multiple endpoints or even compound scores are thus preferred in clinical pain trials. This approach further requires strict standardization of analgesics consumption and patient stratification, which both can be difficult to implement in daily clinical practice.<sup>510</sup>

The ambitions of decreased analgesic consumption, earlier mobilization and adequately managed pain reflected in the efficacy outcomes coincide with the principles of the Enhanced Recovery After Surgery (ERAS) philosophy.<sup>6,421</sup> ERAS, as the name suggests, aims to create the optimal environment for rapid postoperative recovery by optimizing the preoperative, perioperative and postoperative processes. Nutrition, wound care, analgesia and mobilization are optimized. The analgesia provided is multimodal and aims to reduce opioid consumption, thereby preventing ORADEs. The present bupivacaine-loaded hydrogel could fit well within this philosophy.

### **Concluding remarks and outlook**

The aim of this thesis was to provide insight in the etiology and severity of postoperative skeletal pain, as well as identify shortcomings in the current treatment of this pain and provide directions for its future treatment. A bupivacaine-loaded hydrogel, suitable for co-implantation with pedicle screws to provide sustained non-opioid pain relief following spine surgery, was developed that fulfills many of the requirements for a successful drug delivery formulation. Building on the proof of the formulation's *in vivo* safety and feasibility, this thesis concludes with the outlines of a clinical trial to study its safety and preliminary efficacy in a real-world setting.

But it does not end there. Future perspectives include the application of the aforementioned bupivacaine-loaded hydrogel in other anatomical locations and surgical indications, such as arthroplasty or soft-tissue surgeries, and loading the same hydrogel composition with different therapeutic agents. In this way, the hydrogel system could function as a platform for multiple applications, which would significantly expand the potential and implications of the presented results. Its tunability, versatility, proven biocompatibility and -degradability, and IVIVC can considerably accelerate the development process of such new applications. Local treatment of local medical conditions, with a high ratio between desired and side effects, can greatly benefit our patients.

## NEDERLANDSE SAMENVATTING

Pijn na skeletoperaties is een last voor de patiënt, maar ook voor het ziekenhuis en de samenleving. De pijn en bijwerkingen van medicijnen om de pijn te stillen verlagen de kwaliteit van leven, verlengen de behandelduur en verhogen zo de gezondheidskosten. Dit proefschrift probeert het ontstaan van pijn na skeletoperaties beter te begrijpen, de ernst van pijn te kwantificeren en richting te bieden voor toekomstige behandelmogelijkheden. De volgende paragrafen vatten de voornaamste bevindingen uit dit proefschrift samen.

**Het eerste doel** van dit proefschrift was om het ontstaan en de ernst van pijn na skeletoperaties, en de effectiviteit van de huidige op opiaten gebaseerde behandeling te begrijpen. Dit doel werd van meerdere kanten benaderd, namelijk een cohortstudie met patiënten die wervelkolomchirurgie ondergaan, een immunohistochemische studie naar botinnervatiepatronen en een review van de literatuur over skeletpijn. **Hoofdstuk 2** beschrijft de huidige stand van zaken wat betreft pijn en pijnstilling voor patiënten die wervelkolomchirurgie ondergaan. Alle 64 patiënten waren opiaatbehoefstig tijdens opname, maar ervoeren ondanks de opiaten toch matige tot ernstige pijn na wervelkolomchirurgie. Bij dertien patiënten was de pijn zodanig ongecontroleerd dat zij op de opnieuw op de verkoeverkamer werden opgenomen, voor een intraveneuze oplaaddosis opiaten. Het merendeel van de patiënten ontwikkelde matig-ernstige opiaat gerelateerde bijwerkingen, zoals misselijkheid. Daarnaast ontwikkelden 17 patiënten ernstige bijwerkingen zoals onderdrukking van de ademhaling. Om de ernst van skeletpijn na operatie beter te begrijpen, is in **Hoofdstuk 3** een immunohistochemische studie naar de dichtheid van sensorische zenuwen in verschillende menselijke botten en botcompartimenten verricht. De hoogste dichtheid van sensorische zenuwen werd gevonden in het botvlies of periost, gevolgd door het beenmerg en de cortex. Het dichtst geïnnerveerde bot was de borstwervel. De dichtheid van vezels was vergelijkbaar tussen mannen en vrouwen, en nam af naarmate donoren ouder werden. Deze zenuwvezels zijn in staat tot nociceptie: het registreren van mogelijk schadelijke externe stimuli. Om te begrijpen hoe nociceptie kan leiden tot de gewaarwording van pijn, is in **Hoofdstuk 4** een review van de literatuur over skeletpijn verricht. Dit hoofdstuk beschrijft vier biologische routes die betrokken zijn in het ontstaan en het onderhoud van skeletpijn. Deze routes zijn de activatie, de sensitatisatie en de nieuwvorming van perifere sensorische vezels (met name van de types A-delta en C), en centrale sensitatisatie. Zenuwvezels kunnen worden geactiveerd door mechanische of chemische stimuli. Lokale zenuwgroeifactoren spelen een rol in zowel perifere sensitatisatie als zenuwnieuwvorming. De intensiteit van nociceptie kan gedurende de geleiding door gevoelszenuwen van bot naar brein worden versterkt door centrale sensitatisatie.

Het vaak voorkomen van opiaat-gerelateerde bijwerkingen bij suboptimale pijnstilling toont een kwetsbare balans tussen werking en bijwerking van huidige pijnbestrijding. De ernst van de pijn na skeletoperaties kan worden verklaard door het dichte zenuwnetwerk in de onvermijdelijk beschadigde botstructuren, met name het botvlies. De vervolgens geactiveerde biologische routes kunnen de pijn moduleren. De zenuwdichtheid van het botvlies maakt het een mogelijk doelwit voor preciezere pijnstilling na operatie.

**Het tweede doel** van dit proefschrift was het analyseren van de veiligheid en werkzaamheid van een geconcentreerde oplossing van een non-opioïde pijnstiller (bupivacaïne) bij toepassing in musculoskeletale weefsels, die bij chirurgische beschadiging leiden tot de pijn besproken onder het eerste doel. Bupivacaïne werd als medicijn gekozen, omdat het in staat is om de geleiding van actiepotentialen in relevante types van gevoelszenuwen te blokkeren, de langste werkingsduur van alle amino-amide lokale anesthetica heeft en wereldwijd gebruikt wordt. Ook het tweede doel van dit proefschrift werd vanuit meerdere perspectieven onderzocht, door de literatuur over de weefseffecten van bupivacaïne te bestuderen, een dierstudie naar de schadelijke weefseffecten van hoge bupivacaïneconcentraties tijdens en na skeletoperatie te verrichten, en een elektrofysiologische onderzoeksofstelling te ontwikkelen om de actie van bupivacaïne in geïnnerveerde weefsels te bestuderen.

Verspreid in de literatuur werden schadelijke effecten van bupivacaïne op bot-, spier-, zenuw-, kraakbeen- en tussenwervelschijfweefsel gevonden in laboratoriumopstellingen. Daarnaast remde bupivacaïne botvorming en wondgenezing in het laboratorium. Deze effecten worden beschreven in **Hoofdstuk 5**. Echter, met uitzondering van kraakbeenschade werden de effecten niet gevonden in dierstudies en klinische studies, of waren ze omkeerbaar. Kraakbeenschade na toediening van bupivacaïne werd ook in patiënten beschreven, waarschijnlijk door de beperkte regeneratiecapaciteit van gewrichtskraakbeen. Een vergelijkbaar gebrek aan regeneratiecapaciteit in het laboratorium leidt waarschijnlijk tot beperkte translatie van toxische effecten naar dieren en mensen. Hierbij moet worden opgemerkt dat alle studies bupivacaïne-concentraties tot 0.5% gebruikten, terwijl momenteel bupivacaïne-formuleringen voor vertraagde afgifte worden ontwikkeld met hogere concentraties. In **Hoofdstuk 6** wordt de rat gebruikt als model om de schadelijke lokale effecten van hoge concentraties bupivacaïne bij skeletoperaties te meten. De ratten ondergingen implantatie van een schroef en canule in de wervelkolom of het bovenbeen. Door de canule kon een bupivacaïne-oplossing in verschillende concentraties (0.5%, 2.5% of 5.0%) gegeven worden als bolus of continue infusie. Na een ongecompliceerd postoperatief beloop van 28 dagen in alle dieren werd de implantatielocatie histologisch onderzocht. Statistisch significante verschillen in scores

voor lokale schade, passend bij de meer invasieve wervelchirurgie, bestonden tussen implantatie op de wervel en het bovenbeen, maar niet tussen bupivacaïne-concentraties.

Om te onderzoeken welke bupivacaïne-concentraties effectief zijn in het blokkeren van actiepotentialen in chirurgisch beschadigd zenuwweefsel en botvlies, beschrijft **Hoofdstuk 7** de ontwikkeling van een elektrofysiologische onderzoekopstelling, waarbij vers afgenomen zenuwen en botvlies uit schapen kunnen worden geanalyseerd. Hoewel de opstelling aantoonde dat de actie van bupivacaïne gemeten kon worden in vers afgenomen zenuwweefsel, zijn nog diverse optimalisatieslagen (zoals temperatuurcontrole en het uitlijnen van stimulusrichting en zenuwvezel oriëntatie) nodig voordat een minimaal effectieve concentratie van bupivacaïne in botvlies vastgesteld kan worden.

Samen wijzen deze bevindingen op de afwezigheid van grote schadelijke effecten van zowel conventionele als hogere concentraties bupivacaïne bij toepassing in skeletchirurgie, en onderschrijven ze de gevoeligheid van het botvlies voor blokkade van actiepotentialen door bupivacaïne.

**Het derde doel** van dit proefschrift borduurt voort op de kennis behaald onder de eerdere twee doelen, namelijk het begrijpen van het ontstaan en de ernst van skeletpijn na operatie, en het bestuderen van de veiligheid en effectiviteit van bupivacaïne ter behandeling van skeletpijn. Het derde doel betreft het ontwikkelen van een klinisch relevante vertraagde-afgifte formulering van bupivacaïne, gebaseerd op een hydrogel en ter gebruik in skeletchirurgie. **Hoofdstuk 7** beschrijft de ontwikkeling van een ringvormige hydrogel in het laboratorium die in staat is om rondom een pedikelschroef geïmplantéerd te worden tijdens wervelkolomchirurgie. De mechanische eigenschappen en medicijnafgifte van de hydrogel konden naar behoefte worden afgestemd en geoptimaliseerd. De medicijnafgifte duurde minstens 72 uur in het laboratorium, daarmee de duur van ernstige pijn na skeletchirurgie evenarend. Het materiaal van de hydrogel was biocompatibel en biologisch afbreekbaar. Bovendien leidde het laden van de ringvormige hydrogel met bupivacaïne in gekristalliseerde vorm tot een afname van de schadelijke effecten ten opzichte van niet-gekrystalliseerde bupivacaïne in celkweken. **Hoofdstuk 8** neemt de hydrogel uit hoofdstuk 7, en bestudeert zijn eigenschappen op het gebied van mechanica, medicijnafgifte, biocompatibiliteit en afbreekbaarheid in schapen als model voor wervelkolomchirurgie. Implantatie van tot 8 ringvormige hydrogels leverde aanhoudend lage bupivacaïne plasmaconcentraties op, met tegelijkertijd hoge lokale concentraties in de chirurgische wond gedurende 72 uur na operatie. Medicijnafgifte uit de hydrogels volgde eerste-orde kinetiek. De hydrogels leidden tot een milde vreemdlichaam reactie en werden in 9 maanden ter plaatse afgebroken door het lichaam. **Hoofdstuk 9** neemt de hydrogel uit hoofdstukken 7 en 8 een eerste stap naar de kliniek.

Om goedkeuring van toekomstige aanvragen voor klinische studies te faciliteren, werd de hydrogel in een toxicokinetische *bridging* studie volgens de principes van "Good Laboratory Practice" (GLP) getest in het schapenmodel voor wervelkolomchirurgie. GLP is een systeem van regelgeving wat als doel heeft om de consistentie, betrouwbaarheid, reproduceerbaarheid, kwaliteit en integriteit van de experimentele data te waarborgen. Voldoen aan GLP is een vereiste voor goedkeuring van medicinale producten door regulatoire autoriteiten. Een directe vergelijking in deze studie met een reeds goedgekeurde toepassing van bupivacaïne, maakt het mogelijk om bestaande data over veiligheid van bupivacaïne over te nemen voor een nieuwe toepassing. In deze studie ondergingen schapen de implantatie van *ofwel* 8 pedikelschroeven zonder hydrogel, *of* 8 pedikelschroeven met een medicijnvrije hydrogel, *of* implantatie van 8 pedikelschroeven met een bupivacaïne-geladen hydrogel. Bupivacaïne concentraties in het bloed bleven een factor 10 onder bekende schadelijke limieten, en hielden langer aan dan na subcutane infiltratie van bupivacaïne. Histologische evaluatie van de implantatielocatie toonde een vergelijkbaar beeld voor alle drie de groepen.

Samengenomen wijzen de resultaten op biocompatibiliteit, biologische afbreekbaarheid, een grote systemische veiligheidsmarge en verlengde medicijnafgifte van de met bupivacaïne geladen ringvormige hydrogels in een diermodel voor wervelkolomchirurgie.

**Het laatste doel** van dit proefschrift was het bieden van toekomstige behandelrichtingen voor pijn na skeletoperatie. Daarom wordt in **Hoofdstuk 10** een studieprotocol voor een fase 1b klinische trial met dosisescalatie gepresenteerd, waarin mannen en vrouwen die ingepland zijn voor open of percutane pedikelschroefplaatsing wegens degeneratie van de wervelkolom worden geïncludeerd. De patiënten zullen 4 of 6 pedikelschroeven ontvangen met een gelijk aantal ringvormige hydrogels. De primaire uitkomstmaat van de studie is de systemische veiligheid van de bupivacaïne-hydrogelformulering, gemeten als de maximale concentratie  $C_{\max}$  in het bloed. Bovendien worden het aantal *adverse events* (nadelige gebeurtenissen tijdens de studie), hoeveelheid benodigde pijnstilling, de ernst van de pijn na operatie en mobilisatie gemeten om data over veiligheid te verkrijgen en de mogelijke effectiviteit te verkennen.

### **Conclusies en vooruitzichten**

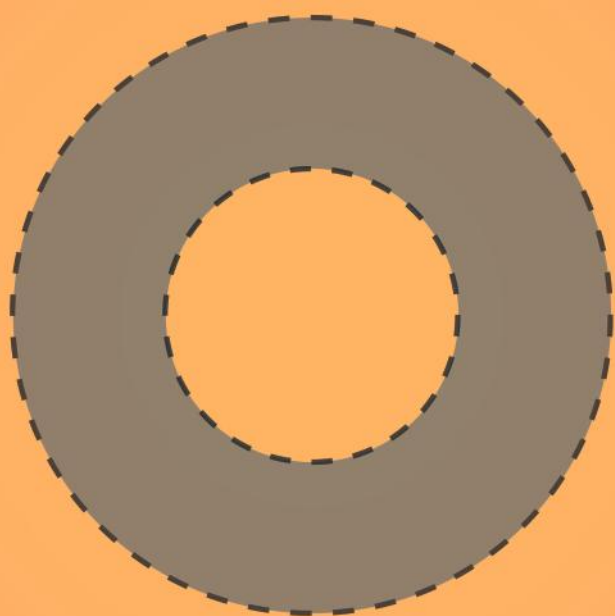
Het doel van dit proefschrift was om inzicht te bieden in het ontstaan en de ernst van pijn na skeletoperaties, het identificeren van tekortkomingen in de huidige pijnbehandeling en richting te bieden voor toekomstige pijnbehandelingen. Het proefschrift beschrijft de ontwikkeling van een met bupivacaïne geladen ringvormige hydrogel, geschikt voor co-implantatie met pedikelschroeven om zo langdurige, lokale en opiaatvrije pijnstilling na wervelkolomchirurgie te bewerkstelligen. Voortbouwend op de aangetoonde veiligheid

en haalbaarheid van de hydrogel in het schaapmodel voor wervelkolomchirurgie, besluit dit proefschrift met een protocol voor een studie om de veiligheid en vroege effectiviteit te testen in de klinische praktijk.

Maar dat is niet het eindstation. Toekomstige richtingen voor onderzoek zijn bijvoorbeeld het toepassen van deze met bupivacaïne geladen hydrogel op andere anatomische locaties of chirurgische indicaties zoals gewrichtsvervanging of weke delenchirurgie, of dezelfde hydrogel laden met een ander medicijn zoals een antibioticum of botgroeistimulator. Zo kan de hydrogel functioneren als een platform voor verschillende toepassingen en de impact van de in dit proefschrift getoonde resultaten verder uitbreiden. De mogelijkheid tot aanpassing van verschillende eigenschappen door verandering van de samenstelling kan de ontwikkeling van nieuwe toepassingen significant versnellen. Een grote ratio tussen gewenste en ongewenste medicijneffecten, door lokale behandeling van ziekten, is een concept waar een grote en diverse groep patiënten van kan profiteren.







## REFERENCES

1. Apfelbaum JL, Chen C, Mehta SS, Gan TJ. 2003. Postoperative pain experience: results from a national survey suggest postoperative pain continues to be undermanaged. *Anesth. Analg.* 97(2):534–540 Available from: <http://www.ncbi.nlm.nih.gov/pubmed/12873949>.
2. Gan TJ, Habib AS, Miller TE, et al. 2014. Incidence, patient satisfaction, and perceptions of post-surgical pain: results from a US national survey. *Curr. Med. Res. Opin.* 30(1):149–60 Available from: <http://www.ncbi.nlm.nih.gov/pubmed/24237004>.
3. International Association for the Study of Pain. 2022. Terminology. [cited 2022 Mar 2] Available from: <https://www.iasp-pain.org/resources/terminology/>.
4. Kirkpatrick DR, McEntire DM, Hamsch ZJ, et al. 2015. Therapeutic Basis of Clinical Pain Modulation. *Clin. Transl. Sci.* 8(6):848–56 Available from: <http://www.ncbi.nlm.nih.gov/pubmed/25962969>.
5. Taylor RS, Ullrich K, Regan S, et al. 2013. The Impact of Early PostOperative Pain on Health-Related Quality of Life. *Pain Pract.* 13(7):515–523 Available from: <https://onlinelibrary.wiley.com/doi/10.1111/papr.12026>.
6. Dietz N, Sharma M, Adams S, et al. 2019. Enhanced Recovery After Surgery (ERAS) for Spine Surgery: A Systematic Review. *World Neurosurg.* 130:415–426 Available from: <https://linkinghub.elsevier.com/retrieve/pii/S1878875019318388>.
7. Wainwright TW, Burgess L. 2020. Enhanced Recovery After Surgery. Cham: Springer International Publishing. 211–217 p. Available from: <http://link.springer.com/10.1007/978-3-030-33443-7>.
8. Chapman CR, Vierck CJ. 2017. The Transition of Acute Postoperative Pain to Chronic Pain: An Integrative Overview of Research on Mechanisms. *J. Pain* 18(4):359.e1-359.e38 Available from: <https://linkinghub.elsevier.com/retrieve/pii/S1526590016303297>.
9. Kehlet H, Jensen TS, Woolf CJ. 2006. Persistent postsurgical pain: risk factors and prevention. *Lancet (London, England)* 367(9522):1618–25 Available from: <http://www.ncbi.nlm.nih.gov/pubmed/16698416>.
10. Mathiesen O, Thomsen BA, Kitter B, et al. 2012. Need for improved treatment of postoperative pain. *Dan. Med. J.* 59(4):A4401 Available from: <http://www.ncbi.nlm.nih.gov/pubmed/22459715>.
11. Joshi GP, Ogunnaik BO. 2005. Consequences of inadequate postoperative pain relief and chronic persistent postoperative pain. *Anesthesiol. Clin. North America* 23(1):21–36.
12. Gerbershagen HJ, Aduckathil S, van Wijck AJM, et al. 2013. Pain intensity on the first day after surgery: a prospective cohort study comparing 179 surgical procedures. *Anesthesiology* 118(4):934–944.
13. Rajae SS, Bae HW, Kanim LEA, Delamarter RB. 2012. Spinal fusion in the United States: analysis of trends from 1998 to 2008. *Spine (Phila. Pa. 1976)*. 37(1):67–76.
14. Sheikh SR, Thompson NR, Benzel E, et al. 2020. Can We Justify It? Trends in the Utilization of Spinal Fusions and Associated Reimbursement. *Neurosurgery* 86(2):E193–E202 Available from: <http://www.ncbi.nlm.nih.gov/pubmed/31574148>.
15. Gan TJ. 2017. Poorly controlled postoperative pain: prevalence, consequences, and prevention. *J. Pain Res.* 10:2287–2298.
16. Svensson I, Sjöström B, Haljamäe H. 2000. Assessment of Pain Experiences after Elective Surgery. *J. Pain Symptom Manage.* 20(3):193–201 Available from: <https://linkinghub.elsevier.com/retrieve/pii/S0885392400001743>.
17. Mach DB, Rogers SD, Sabino MC, et al. 2002. Origins of skeletal pain: Sensory and sympathetic innervation of the mouse femur. *Neuroscience* 113(1):155–166.
18. Jimenez-Andrade JM, Mantyh WG, Bloom AP, et al. 2010. A phenotypically restricted set of primary afferent nerve fibers innervate the bone versus skin: therapeutic opportunity for treating skeletal pain. *Bone* 46(2):306–313.
19. Mantyh PW. 2014. The neurobiology of skeletal pain. *Eur. J. Neurosci.* 39(3):508–519.
20. Nencini S, Ivanusic JJ. 2016. The physiology of bone pain. How much do we really know? *Front. Physiol.* 7(APR):157.
21. Li C, Fennessy P. 2021. The periosteum: a simple tissue with many faces, with special reference to the antler-lineage periosteum. *Biol. Direct* 16(1):17 Available from: <https://biologydirect.biomedcentral.com/articles/10.1186/s13062-021-00310-w>.
22. Krishnamurti C, Rao SC. 2016. The isolation of morphine by Serturmer. *Indian J. Anaesth.* 60(11):861–862 Available from: <http://www.ncbi.nlm.nih.gov/pubmed/27942064>.
23. Booth M. 1999. *Opium: A History*, 1st ed. St. Martin's Griffin. 400 p.

24. Shafi S, Collinworth AW, Copeland LA, et al. 2018. Association of Opioid-Related Adverse Drug Events With Clinical and Cost Outcomes Among Surgical Patients in a Large Integrated Health Care Delivery System. *JAMA Surg.* 153(8):757–763 Available from: <http://www.ncbi.nlm.nih.gov/pubmed/29799927>.
25. DeWeerd S. 2019. Tracing the US opioid crisis to its roots. *Nature* 573(7773):S10–S12 Available from: <http://www.nature.com/articles/d41586-019-02686-2>.
26. Compton WM, Volkow ND. 2006. Major increases in opioid analgesic abuse in the United States: concerns and strategies. *Drug Alcohol Depend.* 81(2):103–7 Available from: <http://www.ncbi.nlm.nih.gov/pubmed/16023304>.
27. Volkow ND, McLellan TA, Cotto JH, et al. 2011. Characteristics of opioid prescriptions in 2009. *JAMA* 305(13):1299–1301.
28. National Safety Council. 2022. Drug overdoses. [cited 2022 Mar 2] Available from: <https://injuryfacts.nsc.org/home-and-community/safety-topics/drugoverdoses/data-details/>.
29. Vowles KE, McEntee ML, Julnes PS, et al. 2015. Rates of opioid misuse, abuse, and addiction in chronic pain. *Pain* 156(4):569–576 Available from: <https://journals.lww.com/00006396-201504000-00003>.
30. Carlson RG, Nahhas RW, Martins SS, Daniulaityte R. 2016. Predictors of transition to heroin use among initially non-opioid dependent illicit pharmaceutical opioid users: A natural history study. *Drug Alcohol Depend.* 160:127–134 Available from: <https://linkinghub.elsevier.com/retrieve/pii/S0376871615018414>.
31. Muhuri P, Gfroerer J, Davies M. 2013. Associations of Nonmedical Pain Reliever Use and Initiation of Heroin Use in the United States. CBHSQ Data Rev (August) Available from: <https://www.samhsa.gov/data/sites/default/files/DR006/DR006/nonmedical-pain-reliever-use-2013.htm>.
32. Maltoni M. 2008. Opioids, pain, and fear. *Ann. Oncol. Off. J. Eur. Soc. Med. Oncol.* 19(1):5–7 Available from: <http://www.ncbi.nlm.nih.gov/pubmed/18073220>.
33. Grandjean P. 2016. Paracelsus Revisited: The Dose Concept in a Complex World. *Basic Clin. Pharmacol. Toxicol.* 119(2):126–132 Available from: <https://onlinelibrary.wiley.com/doi/10.1111/bcpt.12622>.
34. Tageldin ME, Alrashid M, Khoriaty A-A, et al. 2015. Periosteal nerve blocks for distal radius and ulna fracture manipulation—the technique and early results. *J. Orthop. Surg. Res.* 10:134 Available from: <http://www.ncbi.nlm.nih.gov/pubmed/26328789>.
35. Michels T, Ahmadi S, Graf N. 2018. Treatment of peripheral pain with low-dose local anesthetics by epidermal, epithelial and periosteal application. *Local Reg. Anesth.* 11:129–136 Available from: <http://www.ncbi.nlm.nih.gov/pubmed/30588085>.
36. Bianconi M, Ferraro L, Ricci R, et al. 2004. The Pharmacokinetics and Efficacy of Ropivacaine Continuous Wound Instillation After Spine Fusion Surgery. *Anesth. Analg.* :166–172 Available from: <http://journals.lww.com/00000539-200401000-00044>.
37. Huang X-Z, Zhao J-H, Gao P, et al. 2021. Continuous Wound Infiltration with Local Anesthetic Is an Effective and Safe Postoperative Analgesic Strategy: A Meta-Analysis. *Pain Ther.* 10(1):525–538 Available from: <http://www.ncbi.nlm.nih.gov/pubmed/33616874>.
38. Brigham NC, Ji R-R, Becker ML. 2021. Degradable polymeric vehicles for postoperative pain management. *Nat. Commun.* 12(1):1367 Available from: <http://www.nature.com/articles/s41467-021-21438-3>.
39. Cusack SL, Reginald P, Hensen L, Umerah E. 2013. The pharmacokinetics and safety of an intraoperative bupivacaine-collagen implant (XaraColl®) for postoperative analgesia in women following total abdominal hysterectomy. *J. Pain Res.* 6:151–9.
40. Grieff AN, Ghobrial GM, Jallo J. 2016. Use of liposomal bupivacaine in the postoperative management of posterior spinal decompression. *J. Neurosurg. Spine* 25(1):88–93 Available from: <http://www.ncbi.nlm.nih.gov/pubmed/26943250>.
41. McAlvin JB, Reznor G, Shankarappa SA, et al. 2013. Local toxicity from local anesthetic polymeric microparticles. *Anesth. Analg.* 116(4):794–803.
42. Santamaria CM, Woodruff A, Yang R, Kohane DS. 2017. Drug delivery systems for prolonged duration local anesthesia. *Mater. Today (Kidlington)*. 20(1):22–31.
43. Langford R, Chappell G, Karrasch J. [date unknown]. A single administration of DepoBupivacaine intraoperatively results in prolonged detectable plasma bupivacaine and analgesia in patients undergoing inguinal hernia repair. *Present. Annu. Postgrad. Assem. Anesthesiol. New York State Soc. Anesthesiol.* .
44. Golf M, Daniels SE, Onel E. 2011. A phase 3, randomized, placebo-controlled trial of DepoFoam® bupivacaine (extended-release bupivacaine local analgesic) in bunionectomy. *Adv. Ther.* 28(9):776–788 Available from: <http://www.ncbi.nlm.nih.gov/pubmed/21842428>.

45. Gorfine SR, Onel E, Patou G, Krivokapic Z V. 2011. Bupivacaine extended-release liposome injection for prolonged postsurgical analgesia in patients undergoing hemorrhoidectomy: a multicenter, randomized, double-blind, placebo-controlled trial. *Dis. Colon Rectum* 54(12):1552–9 Available from: <http://www.ncbi.nlm.nih.gov/pubmed/22067185>.
46. Cusack SL, Jaros M, Kuss M, et al. 2012. Clinical evaluation of XaraColl(®), a bupivacaine-collagen implant, for postoperative analgesia in two multicenter, randomized, double-blind, placebo-controlled pilot studies. *J. Pain Res.* 5:217–25 Available from: <http://www.ncbi.nlm.nih.gov/pubmed/22792007>.
47. Nguyen TH, Iturriaga C, Verma R. 2021. Efficacy of liposomal bupivacaine in spine surgery: a systematic review. *Spine J.* 21(9):1450–1459 Available from: <http://www.ncbi.nlm.nih.gov/pubmed/33618032>.
48. Kohane DS, Langer R. 2010. Biocompatibility and drug delivery systems. *Chem. Sci.* 1(4):441–446 Available from: <http://xlink.rsc.org/?DOI=C0SC00203H>.
49. Sun H, Mei L, Song C, et al. 2006. The in vivo degradation, absorption and excretion of PCL-based implant. *Biomaterials* 27(9):1735–1740 Available from: <http://www.ncbi.nlm.nih.gov/pubmed/16198413>.
50. Foox M, Zilberman M. 2015. Drug delivery from gelatin-based systems. *Expert Opin. Drug Deliv.* 12(9):1547–1563.
51. Hoare TR, Kohane DS. 2008. Hydrogels in drug delivery: Progress and challenges. *Polymer (Guildf).* 49(8):1993–2007.
52. Bagshaw KR, Hanenbaum CL, Carbone EJ, et al. 2015. Pain management via local anesthetics and responsive hydrogels. *Ther. Deliv.* 6(2):165–76 Available from: <http://www.ncbi.nlm.nih.gov/pubmed/25690085>.
53. Li J, Mooney DJ. 2016. Designing hydrogels for controlled drug delivery. *Nat. Rev. Mater.* 1(12) Available from: <http://www.ncbi.nlm.nih.gov/pubmed/29657852>.
54. 2018. Global, regional, and national incidence, prevalence, and years lived with disability for 354 diseases and injuries for 195 countries and territories, 1990-2017: a systematic analysis for the Global Burden of Disease Study 2017. *Lancet (London, England)* 392(10159):1789–1858.
55. Woolf AD, Erwin J, March L. 2012. The need to address the burden of musculoskeletal conditions. *Best Pract. Res. Clin. Rheumatol.* 26(2):183–224.
56. Woolf AD, Pfleger B. 2003. Burden of major musculoskeletal conditions. *Bull. World Health Organ.* 81(9):646–656.
57. Fisher N, Hooper J, Bess S, et al. 2020. Ninety-day Postoperative Narcotic Use After Hospitalization for Orthopaedic Trauma. *J. Am. Acad. Orthop. Surg.* 28(13):e560–e565.
58. Breivik H. 1998. Postoperative pain management: why is it difficult to show that it improves outcome? *Eur. J. Anaesthesiol.* 15(6):748–751.
59. Ballantyne JC, Carr DB, deFerranti S, et al. 1998. The comparative effects of postoperative analgesic therapies on pulmonary outcome: cumulative meta-analyses of randomized, controlled trials. *Anesth. Analg.* 86(3):598–612.
60. Liu S, Carpenter RL, Neal JM. 1995. Epidural anesthesia and analgesia. Their role in postoperative outcome. *Anesthesiology* 82(6):1474–1506.
61. Kehlet H. 1997. Multimodal approach to control postoperative pathophysiology and rehabilitation. *Br. J. Anaesth.* 78(5):606–617.
62. Carr DB, Goudas LC. 1999. Acute pain. *Lancet (London, England)* 353(9169):2051–2058.
63. Peters ML, Sommer M, de Rijke JM, et al. 2007. Somatic and psychologic predictors of long-term unfavorable outcome after surgical intervention. *Ann. Surg.* 245(3):487–494.
64. van Driel MEC, van Dijk JFM, Baart SJ, et al. 2022. Development and validation of a multivariable prediction model for early prediction of chronic postsurgical pain in adults: a prospective cohort study. *Br. J. Anaesth.* Available from: <https://linkinghub.elsevier.com/retrieve/pii/S0007091222002495>.
65. Bajwa SJS, Haldar R. 2015. Pain management following spinal surgeries: An appraisal of the available options. *J. craniovertebral junction spine* 6(3):105–110 Available from: <http://www.ncbi.nlm.nih.gov/pubmed/26288544>.
66. Crofford LJ. 2010. Adverse effects of chronic opioid therapy for chronic musculoskeletal pain. *Nat. Rev. Rheumatol.* 6(4):191–197.
67. Colvin LA, Bull F, Hales TG. 2019. Perioperative opioid analgesia—when is enough too much? A review of opioid-induced tolerance and hyperalgesia. *Lancet* .
68. Dorn S, Lembo A, Cremonini F. 2014. Opioid-induced bowel dysfunction: epidemiology, pathophysiology, diagnosis, and initial therapeutic approach. *Am. J. Gastroenterol. Suppl.* 2(1):31–37.
69. Benson JL, Campbell HE, Phillips CN. 2015. Opioid-induced pruritus. *Consult. Pharm. J. Am. Soc. Consult. Pharm.* 30(4):221–227.
70. Dahan A, Aarts L, Smith TW. 2010. Incidence, Reversal, and Prevention of Opioid-induced Respiratory Depression. *Anesthesiology* 112(1):226–238.

71. Barletta JF, Asgeirsson T, Senagore AJ. 2011. Influence of intravenous opioid dose on postoperative ileus. *Ann. Pharmacother.* 45(7–8):916–923.
72. Goettsch WG, Sukel MPP, van der Peet DL, et al. 2007. In-hospital use of opioids increases rate of coded postoperative paralytic ileus. *Pharmacoepidemiol. Drug Saf.* 16(6):668–674.
73. Smith HS, Laufer A. 2014. Opioid induced nausea and vomiting. *Eur. J. Pharmacol.* 722:67–78.
74. Bell TJ, Panchal SJ, Miaskowski C, et al. 2009. The prevalence, severity, and impact of opioid-induced bowel dysfunction: results of a US and European Patient Survey (PROBE 1). *Pain Med.* 10(1):35–42.
75. Oderda GM, Gan TJ, Johnson BH, Robinson SB. 2013. Effect of opioid-related adverse events on outcomes in selected surgical patients. *J. Pain Palliat. Care Pharmacother.* 27(1):62–70.
76. Kessler ER, Shah M, Gruschkus SK, Raju A. 2013. Cost and quality implications of opioid-based postsurgical pain control using administrative claims data from a large health system: opioid-related adverse events and their impact on clinical and economic outcomes. *Pharmacotherapy* 33(4):383–391.
77. Jain N, Sharma M, Wang D, et al. 2021. Burden of preoperative opioid use and its impact on healthcare utilization after primary single level lumbar discectomy. *Spine J.* 21(10):1700–1710.
78. Pizzi LT, Toner R, Foley K, et al. 2012. Relationship Between Potential Opioid-Related Adverse Effects and Hospital Length of Stay in Patients Receiving Opioids After Orthopedic Surgery. *Pharmacother. J. Hum. Pharmacol. Drug Ther.* 32(6):502–514 Available from: <https://onlinelibrary.wiley.com/doi/10.1002/j.1875-9114.2012.01101.x>.
79. Bedene A, Lijfering WM, Niesters M, et al. 2019. Opioid Prescription Patterns and Risk Factors Associated With Opioid Use in the Netherlands. *JAMA Netw. open* 2(8):e1910223.
80. Kolodny A, Courtwright DT, Hwang CS, et al. 2015. The prescription opioid and heroin crisis: a public health approach to an epidemic of addiction. *Annu. Rev. Public Health* 36:559–574.
81. Scholl L, Seth P, Kariisa M, et al. 2018. Drug and Opioid-Involved Overdose Deaths - United States, 2013-2017. *MMWR. Morb. Mortal. Wkly. Rep.* 67(5152):1419–1427.
82. Bohnert ASB, Valenstein M, Bair MJ, et al. 2011. Association between opioid prescribing patterns and opioid overdose-related deaths. *JAMA* 305(13):1315–1321.
83. Rudd RA, Seth P, David F, Scholl L. 2016. Increases in Drug and Opioid-Involved Overdose Deaths - United States, 2010-2015. *MMWR. Morb. Mortal. Wkly. Rep.* 65(50–51):1445–1452.
84. Kuehn B. 2017. NIH Strategy to Combat Opioid Crisis. *JAMA* .
85. van Dijk JFM, Kappen TH, Schuurmans MJ, van Wijck AJM. 2015. The Relation Between Patients' NRS Pain Scores and Their Desire for Additional Opioids after Surgery. *Pain Pract.* 15(7):604–9 Available from: <http://www.ncbi.nlm.nih.gov/pubmed/24735082>.
86. Breivik EK, Björnsson GA, Skovlund E. 2000. A comparison of pain rating scales by sampling from clinical trial data. *Clin. J. Pain* 16(1):22–28.
87. [Date unknown]. WHO's cancer pain ladder for adults.
88. Shaheen PE, Walsh D, Lasheen W, et al. 2009. Opioid equianalgesic tables: are they all equally dangerous? *J. Pain Symptom Manage.* 38(3):409–417.
89. Schober P, Boer C, Schwarte LA. 2018. Correlation Coefficients: Appropriate Use and Interpretation. *Anesth. Analg.* 126(5):1763–1768 Available from: <http://www.ncbi.nlm.nih.gov/pubmed/29481436>.
90. Minkowitz HS, Gruschkus SK, Shah M, Raju A. 2014. Adverse drug events among patients receiving postsurgical opioids in a large health system: risk factors and outcomes. *Am. J. Heal. Pharm. AJHP Off. J. Am. Soc. Heal. Pharm.* 71(18):1556–1565.
91. Lindenhovius ALC, Helmerhorst GTT, Schnellen AC, et al. 2009. Differences in prescription of narcotic pain medication after operative treatment of hip and ankle fractures in the United States and The Netherlands. *J. Trauma* 67(1):160–4 Available from: <http://www.ncbi.nlm.nih.gov/pubmed/19590328>.
92. Wheeler M, Oderda GM, Ashburn MA, Lipman AG. 2002. Adverse events associated with postoperative opioid analgesia: A systematic review. *J. Pain* 3(3):159–180 Available from: <https://linkinghub.elsevier.com/retrieve/pii/S1526590002000007>.
93. Gregorian RS, Gasik A, Kwong WJ, et al. 2010. Importance of side effects in opioid treatment: a trade-off analysis with patients and physicians. *J. pain* 11(11):1095–108 Available from: <http://www.ncbi.nlm.nih.gov/pubmed/20452835>.
94. Gan TJ, Lubarsky DA, Flood EM, et al. 2004. Patient preferences for acute pain treatment. *Br. J. Anaesth.* 92(5):681–8 Available from: <http://www.ncbi.nlm.nih.gov/pubmed/15003986>.
95. Soffin EM, Wetmore DS, Beckman JD, et al. 2019. Opioid-free anesthesia within an enhanced recovery after surgery pathway for minimally invasive lumbar spine surgery: a retrospective matched cohort study. *Neurosurg. Focus* 46(4):E8.
96. Martinez L, Ekman E, Nakhla N. 2019. Perioperative Opioid-sparing Strategies: Utility of Conventional NSAIDs in Adults. *Clin. Ther.* 41(12):2612–2628.

97. Mathiesen O, Dahl B, Thomsen BA, et al. 2013. A comprehensive multimodal pain treatment reduces opioid consumption after multilevel spine surgery. *Eur. spine J. Off. Publ. Eur. Spine Soc. Eur. Spinal Deform. Soc. Eur. Sect. Cerv. Spine Res. Soc.* 22(9):2089–2096.
98. Gabriel RA, Swisher MW, Sztain JF, et al. 2019. State of the art opioid-sparing strategies for postoperative pain in adult surgical patients. *Expert Opin. Pharmacother.* 20(8):949–961.
99. Andersen LJ, Poulsen T, Krogh B, Nielsen T. 2007. Postoperative analgesia in total hip arthroplasty: a randomized double-blinded, placebo-controlled study on peroperative and postoperative ropivacaine, ketorolac, and adrenaline wound infiltration. *Acta Orthop.* 78(2):187–192.
100. Titman S, Hommel A, Dobrydnjov I, et al. 2018. The efficacy of high volume of local infiltration analgesia for postoperative pain relief after total hip arthroplasty under general anaesthesia - A randomised controlled trial. *Int. J. Orthop. TRAUMA Nurs.* 28:16–21.
101. Tsukada S, Wakui M, Hoshino A. 2014. Postoperative epidural analgesia compared with intraoperative periarticular injection for pain control following total knee arthroplasty under spinal anesthesia: a randomized controlled trial. *96(17):1433-1438.*
102. van den Broek RJC, van de Geer R, Schepel NC, et al. 2021. Evaluation of adding the Erector spinae plane block to standard anesthetic care in patients undergoing posterior lumbar interbody fusion surgery. *Sci. Rep.* 11(1):7631 Available from: <http://www.nature.com/articles/s41598-021-87374-w>.
103. Oh SK, Lim BG, Won YJ, et al. 2022. Analgesic efficacy of erector spinae plane block in lumbar spine surgery: A systematic review and meta-analysis. *J. Clin. Anesth.* 78:110647 Available from: <https://linkinghub.elsevier.com/retrieve/pii/S0952818022000034>.
104. Thomas EJ, Studdert DM, Newhouse JP, et al. 1999. Costs of medical injuries in Utah and Colorado. *Inquiry* 36(3):255–264.
105. Linton SJ, Shaw WS. 2011. Impact of Psychological Factors in the Experience of Pain. *Phys. Ther.* 91(5):700–711 Available from: <https://academic.oup.com/ptj/article-lookup/doi/10.2522/ptj.20100330>.
106. Peters ML. 2015. Emotional and Cognitive Influences on Pain Experience. p 138–152 Available from: <https://www.karger.com/Article/FullText/435938>.
107. Stanton AL, Snider PR. 1993. Coping with a breast cancer diagnosis: A prospective study. *Heal. Psychol.* 12(1):16–23 Available from: <http://doi.apa.org/getdoi.cfm?doi=10.1037/0278-6133.12.1.16>.
108. Hoy D, Bain C, Williams G, et al. 2012. A systematic review of the global prevalence of low back pain. *Arthritis Rheum.* 64(6):2028–2037.
109. Lubeck DP. 2003. The costs of musculoskeletal disease: health needs assessment and health economics. *Best Pract. Res. Clin. Rheumatol.* 17(3):529–539.
110. Leigh JP, Seavey W, Leistikow B. 2001. Estimating the costs of job related arthritis. *J. Rheumatol.* 28(7):1647–1654.
111. Brooks PM. 2006. The burden of musculoskeletal disease--a global perspective. *Clin. Rheumatol.* 25(6):778–781.
112. Murray CJL, Lopez AD, Organization WH, et al. 1996. The Global burden of disease : a comprehensive assessment of mortality and disability from diseases, injuries, and risk factors in 1990 and projected to 2020 : summary / edited by Christopher J. L. Murray, Alan D. Lopez.
113. St Sauver JL, Warner DO, Yawn BP, et al. 2013. Why patients visit their doctors: assessing the most prevalent conditions in a defined American population. *Mayo Clin. Proc.* 88(1):56–67.
114. Rosemann T, Laux G, Kuehlein T. 2007. Osteoarthritis and functional disability: results of a cross sectional study among primary care patients in Germany. *BMC Musculoskelet. Disord.* 8:79.
115. Dominick KL, Ahern FM, Gold CH, Heller DA. 2004. Health-related quality of life and health service use among older adults with osteoarthritis. *Arthritis Rheum.* 51(3):326–331.
116. Sawatzky R, Liu-Ambrose T, Miller WC, Marra CA. 2007. Physical activity as a mediator of the impact of chronic conditions on quality of life in older adults. *Health Qual. Life Outcomes* 5:68.
117. Cimmino MA, Ferrone C, Cutolo M. 2011. Epidemiology of chronic musculoskeletal pain. *Best Pract. Res. Clin. Rheumatol.* 25(2):173–183.
118. McCarthy EF. 2011. Genetic diseases of bones and joints. *Semin. Diagn. Pathol.* 28(1):26–36.
119. Mantyh PW. 2019. Mechanisms that drive bone pain across the lifespan. *Br. J. Clin. Pharmacol.* 85(6):1103–1113.
120. Oostinga D, Steverink JG, van Wijck AJM, Verlaan J-J. 2020. An understanding of bone pain: A narrative review. *Bone* 134.
121. Edgar MA. 2007. The nerve supply of the lumbar intervertebral disc. *J. Bone Joint Surg. Br.* 89(9):1135–9 Available from: <http://www.ncbi.nlm.nih.gov/pubmed/17905946>.
122. Miyagi M, Millecamps M, Danco AT, et al. 2014. ISSLS Prize winner: Increased innervation and sensory nervous system plasticity in a mouse model of low back pain due to intervertebral disc degeneration. *Spine (Phila. Pa. 1976).* 39(17):1345–54 Available from: <http://www.ncbi.nlm.nih.gov/pubmed/24718079>.

123. Thurston TJ. 1982. Distribution of nerves in long bones as shown by silver impregnation. *J. Anat.* 134(Pt 4):719–28 Available from: <http://www.ncbi.nlm.nih.gov/pubmed/7130036>.
124. RALSTON HJ, MILLER MR, KASAHARA M. 1960. Nerve endings in human fasciae, tendons, ligaments, periosteum, and joint synovial membrane. *Anat. Rec.* 136:137–47 Available from: <http://www.ncbi.nlm.nih.gov/pubmed/14435991>.
125. Martin CD, Jimenez-Andrade JM, Ghilardi JR, Mantyh PW. 2007. Organization of a unique net-like meshwork of CGRP+ sensory fibers in the mouse periosteum: implications for the generation and maintenance of bone fracture pain. *Neurosci. Lett.* 427(3):148–152.
126. Castaneda-Corral G, Jimenez-Andrade JM, Bloom AP, et al. 2011. The majority of myelinated and unmyelinated sensory nerve fibers that innervate bone express the tropomyosin receptor kinase A. *Neuroscience* 178:196–207.
127. Chartier SR, Mitchell SAT, Majuta LA, Mantyh PW. 2018. The Changing Sensory and Sympathetic Innervation of the Young, Adult and Aging Mouse Femur. *Neuroscience* 387:178–190.
128. Thai J, Kyloh M, Travis L, et al. 2020. Identifying spinal afferent (sensory) nerve endings that innervate the marrow cavity and periosteum using anterograde tracing. *J. Comp. Neurol.* :10.1002/cne.24862.
129. Sayilekshmy M, Hansen RB, Delaissé J-M, et al. 2019. Innervation is higher above Bone Remodeling Surfaces and in Cortical Pores in Human Bone: Lessons from patients with primary hyperparathyroidism. *Sci. Rep.* 9(1):5361.
130. Bataille C, Mauprivez C, Hay E, et al. 2012. Different sympathetic pathways control the metabolism of distinct bone envelopes. *Bone* 50(5):1162–1172.
131. Eimar H, Tamimi I, Murshed M, Tamimi F. 2013. Cholinergic regulation of bone. *J. Musculoskelet. Neuronal Interact.* 13(2):124–132.
132. Longo G, Osikowicz M, Ribeiro-da-Silva A. 2013. Sympathetic fiber sprouting in inflamed joints and adjacent skin contributes to pain-related behavior in arthritis. *J. Neurosci.* 33(24):10066–10074.
133. Nencini S, Ivanusic J. 2017. Mechanically sensitive Adelta nociceptors that innervate bone marrow respond to changes in intra-osseous pressure. *J. Physiol.* 595(13):4399–4415.
134. Chartier SR, Thompson ML, Longo G, et al. 2014. Exuberant sprouting of sensory and sympathetic nerve fibers in nonhealed bone fractures and the generation and maintenance of chronic skeletal pain. *Pain* 155(11):2323–2336.
135. Nencini S, Ringuet M, Kim D-H, et al. 2017. Mechanisms of nerve growth factor signaling in bone nociceptors and in an animal model of inflammatory bone pain. *Mol. Pain* 13:1744806917697011.
136. Cao J, Zhang S, Gupta A, et al. 2019. Sensory Nerves Affect Bone Regeneration in Rabbit Mandibular Distraction Osteogenesis. *Int. J. Med. Sci.* 16(6):831–837.
137. Ivanusic JJ, Mahns DA, Sahai V, Rowe MJ. 2006. Absence of large-diameter sensory fibres in a nerve to the cat humerus. *J. Anat.* 208(2):251–255.
138. Ivanusic JJ. 2009. Size, neurochemistry, and segmental distribution of sensory neurons innervating the rat tibia. *J. Comp. Neurol.* 517(3):276–283.
139. Mahns DA, Ivanusic JJ, Sahai V, Rowe MJ. 2006. An intact peripheral nerve preparation for monitoring the activity of single, periosteal afferent nerve fibres. *J. Neurosci. Methods* 156(1–2):140–144.
140. Jimenez-Andrade JM, Bloom AP, Mantyh WG, et al. 2009. Capsaicin-sensitive sensory nerve fibers contribute to the generation and maintenance of skeletal fracture pain. *Neuroscience* 162(4):1244–1254.
141. Brown MF, Hukkanen M V, McCarthy ID, et al. 1997. Sensory and sympathetic innervation of the vertebral endplate in patients with degenerative disc disease. *J. Bone Joint Surg. Br.* 79(1):147–53.
142. Koeck FX, Schmitt M, Baier C, et al. 2016. Predominance of synovial sensory nerve fibers in arthrofibrosis following total knee arthroplasty compared to osteoarthritis of the knee. *J. Orthop. Surg. Res.* 11:25.
143. Lawson SN, Waddell PJ. 1991. Soma neurofilament immunoreactivity is related to cell size and fibre conduction velocity in rat primary sensory neurons. *J. Physiol.* 435:41–63.
144. Schou WS, Ashina S, Amin FM, et al. 2017. Calcitonin gene-related peptide and pain: a systematic review. *J. Headache Pain* 18(1):34.
145. Chen L-J, Zhang F-G, Li J, et al. 2010. Expression of calcitonin gene-related peptide in anterior and posterior horns of the spinal cord after brachial plexus injury. *J. Clin. Neurosci. Off. J. Neurosurg. Soc. Australas.* 17(1):87–91.
146. Gervasi NM, Scott SS, Aschrafi A, et al. 2016. The local expression and trafficking of tyrosine hydroxylase mRNA in the axons of sympathetic neurons. *RNA* 22(6):883–895.
147. Thompson RJ, Doran JF, Jackson P, et al. 1983. PGP 9.5--a new marker for vertebrate neurons and neuroendocrine cells. *Brain Res.* 278(1–2):224–228.



148. Lundberg LM, Alm P, Wharton J, Polak JM. 1988. Protein gene product 9.5 (PGP 9.5). A new neuronal marker visualizing the whole uterine innervation and pregnancy-induced and developmental changes in the guinea pig. *Histochemistry* 90(1):9–17.
149. Doran JF, Jackson P, Kynoch PA, Thompson RJ. 1983. Isolation of PGP 9.5, a new human neurone-specific protein detected by high-resolution two-dimensional electrophoresis. *J. Neurochem.* 40(6):1542–7.
150. Bernal Sierra YA, Haseleu J, Kozlenkov A, et al. 2017. Genetic Tracing of Cav3.2 T-Type Calcium Channel Expression in the Peripheral Nervous System. *Front. Mol. Neurosci.* 10:70.
151. Cleypool CGJ, Schurink B, van der Horst DEM, Bleys RLAW. 2020. Sympathetic nerve tissue in milky spots of the human greater omentum. *J. Anat.* 236(1):156–164 Available from: <http://www.ncbi.nlm.nih.gov/pubmed/31498441>.
152. Rots ML, de Borst GJ, van der Toorn A, et al. 2019. Effect of bilateral carotid occlusion on cerebral hemodynamics and perivascular innervation: An experimental rat model. *J. Comp. Neurol.* 527(14):2263–2272 Available from: <http://www.ncbi.nlm.nih.gov/pubmed/30840325>.
153. Haskins W, Benitez S, Mercado JM, Acosta CG. 2017. Cutaneous inflammation regulates TH1K1 expression in small C-like nociceptor dorsal root ganglion neurons. *Mol. Cell. Neurosci.* 83:13–26.
154. Lawson SN, Perry MJ, Prabhakar E, McCarthy PW. 1993. Primary sensory neurones: neurofilament, neuropeptides, and conduction velocity. *Brain Res. Bull.* 30(3–4):239–243.
155. Viehöfer AF, Shinohara Y, Sprecher CM, et al. 2015. The molecular composition of the extracellular matrix of the human iliolumbar ligament. *Spine J.* 15(6):1325–31 Available from: <http://www.ncbi.nlm.nih.gov/pubmed/24139866>.
156. Yen LD, Bennett GJ, Ribeiro-da-Silva A. 2006. Sympathetic sprouting and changes in nociceptive sensory innervation in the glabrous skin of the rat hind paw following partial peripheral nerve injury. *J. Comp. Neurol.* 495(6):679–690.
157. Koo TK, Li MY. 2016. A Guideline of Selecting and Reporting Intraclass Correlation Coefficients for Reliability Research. *J. Chiropr. Med.* 15(2):155–63 Available from: <http://www.ncbi.nlm.nih.gov/pubmed/27330520>.
158. Amaya F, Izumi Y, Matsuda M, Sasaki M. 2013. Tissue injury and related mediators of pain exacerbation. *Curr. Neuropharmacol.* 11(6):592–7 Available from: <http://www.ncbi.nlm.nih.gov/pubmed/24396335>.
159. Santy J, Mackintosh C. 2001. A phenomenological study of pain following fractured shaft of femur. *J. Clin. Nurs.* 10(4):521–527.
160. Luger NM, Mach DB, Sevcik MA, Mantyh PW. 2005. Bone cancer pain: from model to mechanism to therapy. *J. Pain Symptom Manage.* 29(5):S32–46.
161. Ivanusic JJ. 2017. Molecular Mechanisms That Contribute to Bone Marrow Pain. *Front. Neurol.* 8:458.
162. Benerini Gatta L, Cadei M, Balzarini P, et al. 2012. Application of alternative fixatives to formalin in diagnostic pathology. *Eur. J. Histochem.* 56(2):e12.
163. Shi S-R, Liu C, Pootrakul L, et al. 2008. Evaluation of the value of frozen tissue section used as “gold standard” for immunohistochemistry. *Am. J. Clin. Pathol.* 129(3):358–66 Available from: <http://www.ncbi.nlm.nih.gov/pubmed/18285257>.
164. Eftekhari S, Warfvinge K, Blixt FW, Edvinsson L. 2013. Differentiation of nerve fibers storing CGRP and CGRP receptors in the peripheral trigeminovascular system. *J. pain* 14(11):1289–303 Available from: <http://www.ncbi.nlm.nih.gov/pubmed/23958278>.
165. Iyengar S, Ossipov MH, Johnson KW. 2017. The role of calcitonin gene-related peptide in peripheral and central pain mechanisms including migraine. *Pain* 158(4):543–559 Available from: <http://www.ncbi.nlm.nih.gov/pubmed/28301400>.
166. 2003. The burden of musculoskeletal conditions at the start of the new millennium. Switzerland. i–x, 1–218, back cover p.
167. Stovitz SD, Pardee PE, Vazquez G, et al. 2008. Musculoskeletal pain in obese children and adolescents. *Acta Paediatr.* 97(4):489–493.
168. Peltonen M, Lindroos AK, Torgerson JS. 2003. Musculoskeletal pain in the obese: a comparison with a general population and long-term changes after conventional and surgical obesity treatment. *Pain* 104(3):549–557.
169. Mercadante S. 1997. Malignant bone pain: pathophysiology and treatment. *Pain* 69(1):1–18.
170. Portenoy RK, Payne D, Jacobsen P. 1999. Breakthrough pain: characteristics and impact in patients with cancer pain. *Pain* 81(1–2):129–134.
171. Chrischilles EA, Butler CD, Davis CS, Wallace RB. 1991. A model of lifetime osteoporosis impact. *Arch. Intern. Med.* 151(10):2026–2032.
172. Bonar SK, Tinetti ME, Speechley M, Cooney LM. 1990. Factors associated with short- versus long-term skilled nursing facility placement among community-living hip fracture patients. *J. Am. Geriatr. Soc.* 38(10):1139–1144.

173. Popping DM, Elia N, Marret E, et al. 2008. Protective effects of epidural analgesia on pulmonary complications after abdominal and thoracic surgery: a meta-analysis. *Arch. Surg.* 143(10):990–9; discussion 1000.
174. Frost CO, Hansen RR, Heegaard A-M. 2016. Bone pain: current and future treatments. *Curr. Opin. Pharmacol.* 28:31–37.
175. Bjorkman D. 1998. Nonsteroidal anti-inflammatory drug-associated toxicity of the liver, lower gastrointestinal tract, and esophagus. *Am. J. Med.* 105(5A):17S-21S.
176. Savage SR. 1996. Long-term opioid therapy: assessment of consequences and risks. *J. Pain Symptom Manage.* 11(5):274–286.
177. Sullivan MD, Howe CQ. 2013. Opioid therapy for chronic pain in the United States: promises and perils. *Pain* 154 Suppl:S94-100.
178. Helmerhorst GTT, Vranceanu A-M, Vrahas M, et al. 2014. Risk factors for continued opioid use one to two months after surgery for musculoskeletal trauma. *J. Bone Joint Surg. Am.* 96(6):495–499.
179. Pountos I, Georgouli T, Calori GM, Giannoudis P V. 2012. Do nonsteroidal anti-inflammatory drugs affect bone healing? A critical analysis. *ScientificWorldJournal.* 2012:606404.
180. Chrastil J, Sampson C, Jones KB, Higgins TF. 2013. Postoperative opioid administration inhibits bone healing in an animal model. *Clin. Orthop. Relat. Res.* 471(12):4076–4081.
181. Bielby R, Jones E, McGonagle D. 2007. The role of mesenchymal stem cells in maintenance and repair of bone. *Injury* 38 Suppl 1:S26-32.
182. Hutmacher DW, Sittinger M. 2003. Periosteal cells in bone tissue engineering. *Tissue Eng.* 9 Suppl 1:S45-64.
183. Ivanusic JJ, Sahai V, Mahns DA. 2009. The cortical representation of sensory inputs arising from bone. *Brain Res.* 1269:47–53.
184. Zhao J, Levy D. 2014. The sensory innervation of the calvarial periosteum is nociceptive and contributes to headache-like behavior. *Pain* 155(7):1392–1400.
185. Haegerstam GA. 2001. Pathophysiology of bone pain: a review. *Acta Orthop. Scand.* 72(3):308–317.
186. Rundel CH, Wang H, Yu H, et al. 2006. Microarray analysis of gene expression during the inflammation and endochondral bone formation stages of rat femur fracture repair. *Bone* 38(4):521–529.
187. Inglis JJ, Nissim A, Lees DM, et al. 2005. The differential contribution of tumour necrosis factor to thermal and mechanical hyperalgesia during chronic inflammation. *Arthritis Res. Ther.* 7(4):R807–R816.
188. Schweizerhof M, Stösser S, Kurejova M, et al. 2009. Hematopoietic colony-stimulating factors mediate tumor-nerve interactions and bone cancer pain. *Nat. Med.* 15(7):802–807.
189. Gold MS, Gebhart GF. 2010. Nociceptor sensitization in pain pathogenesis. *Nat. Med.* 16(11):1248–1257.
190. Chen H, Hu B, Lv X, et al. 2019. Prostaglandin E2 mediates sensory nerve regulation of bone homeostasis. *Nat. Commun.* 10(1):181.
191. Yoneda T, Hiasa M, Nagata Y, et al. 2014. Acidic extracellular microenvironment in myeloma colonized bone contributes to bone pain. *Blood* 124(21).
192. T. Y. 2009. Involvement of osteoclast-released protons in bone cancer pain. *Bone* 44:S209.
193. Yoneda T, Hiasa M, Nagata Y, et al. 2015. Contribution of acidic extracellular microenvironment of cancer colonized bone to bone pain. *Biochim. Biophys. Acta* 1848(10):2677–2684.
194. Ringe JD, Body J-J. 2007. A review of bone pain relief with ibandronate and other bisphosphonates in disorders of increased bone turnover. *Clin. Exp. Rheumatol.* 25(5):766–774.
195. Boyce AM. 2017. Denosumab: an Emerging Therapy in Pediatric Bone Disorders. *Curr. Osteoporos. Rep.* 15(4):283–292.
196. Hiasa M, Okui T, Allette YM, et al. 2017. Bone Pain Induced by Multiple Myeloma Is Reduced by Targeting V-ATPase and ASIC3. *Cancer Res.* 77(6):1283–1295.
197. Nagae M, Hiraga T, Yoneda T. 2007. Acidic microenvironment created by osteoclasts causes bone pain associated with tumor colonization. *J. Bone Miner. Metab.* 25(2):99–104.
198. Ikeuchi M, Kolker SJ, Sluka KA. 2009. Acid-sensing ion channel 3 expression in mouse knee joint afferents and effects of carrageenan-induced arthritis. *J. Pain* 10(3):336–342.
199. Olson TH, Riedl MS, Vulchanova L, et al. 1998. An acid sensing ion channel (ASIC) localizes to small primary afferent neurons in rats. *Neuroreport* 9(6):1109–1113.
200. Morgan M, Nencini S, Thai J, Ivanusic JJ. 2019. TRPV1 activation alters the function of Aδ and C fiber sensory neurons that innervate bone. *Bone* 123:168–175.
201. Kowada T, Kikuta J, Kubo A, et al. 2011. In vivo fluorescence imaging of bone-resorbing osteoclasts. *J. Am. Chem. Soc.* 133(44):17772–17776.
202. Sevcik MA, Luger NM, Mach DB, et al. 2004. Bone cancer pain: the effects of the bisphosphonate alendronate on pain, skeletal remodeling, tumor growth and tumor necrosis. *Pain* 111(1–2):169–180.

203. Body J-J, Diel IJ, Bell R, et al. 2004. Oral ibandronate improves bone pain and preserves quality of life in patients with skeletal metastases due to breast cancer. *Pain* 111(3):306–312.
204. Cook AD, Christensen AD, Tewari D, et al. 2018. Immune Cytokines and Their Receptors in Inflammatory Pain. *Trends Immunol.* 39(3):240–255.
205. Richter F, Natura G, Ebbinghaus M, et al. 2012. Interleukin-17 sensitizes joint nociceptors to mechanical stimuli and contributes to arthritic pain through neuronal interleukin-17 receptors in rodents. *Arthritis Rheum.* 64(12):4125–4134.
206. Richter F, Natura G, Loser S, et al. 2010. Tumor necrosis factor causes persistent sensitization of joint nociceptors to mechanical stimuli in rats. *Arthritis Rheum.* 62(12):3806–3814.
207. Brenn D, Richter F, Schaible H-G. 2007. Sensitization of unmyelinated sensory fibers of the joint nerve to mechanical stimuli by interleukin-6 in the rat: an inflammatory mechanism of joint pain. *Arthritis Rheum.* 56(1):351–359.
208. Sevcik MA, Ghilardi JR, Peters CM, et al. 2005. Anti-NGF therapy profoundly reduces bone cancer pain and the accompanying increase in markers of peripheral and central sensitization. *Pain* 115(1–2):128–141.
209. Zhang X, Huang J, McNaughton PA. 2005. NGF rapidly increases membrane expression of TRPV1 heat-gated ion channels. *EMBO J.* 24(24):4211–4223.
210. Enomoto M, Mantyh PW, Murrell J, et al. 2019. Anti-nerve growth factor monoclonal antibodies for the control of pain in dogs and cats. *Vet. Rec.* 184(1):23.
211. Mamet J, Baron A, Lazdunski M, Voilley N. 2002. Proinflammatory mediators, stimulators of sensory neuron excitability via the expression of acid-sensing ion channels. *J. Neurosci.* 22(24):10662–10670.
212. Denk F, Bennett DL, McMahon SB. 2017. Nerve Growth Factor and Pain Mechanisms. *Annu. Rev. Neurosci.* 40:307–325.
213. Obreja O, Rukwied R, Nagler L, et al. 2018. Nerve growth factor locally sensitizes nociceptors in human skin. *Pain* 159(3):416–426.
214. Howe CL, Valletta JS, Rusnak AS, Mobley WC. 2001. NGF signaling from clathrin-coated vesicles: evidence that signaling endosomes serve as a platform for the Ras-MAPK pathway. *Neuron* 32(5):801–814.
215. Papatoutian A, Reichardt LF. 2001. Trk receptors: mediators of neurotrophin action. *Curr. Opin. Neurobiol.* 11(3):272–280.
216. Julius D, Basbaum AI. 2001. Molecular mechanisms of nociception. *Nature* 413(6852):203–210.
217. Gould HJ 3rd, Gould TN, England JD, et al. 2000. A possible role for nerve growth factor in the augmentation of sodium channels in models of chronic pain. *Brain Res.* 854(1–2):19–29.
218. Xue Q, Jong B, Chen T, Schumacher MA. 2007. Transcription of rat TRPV1 utilizes a dual promoter system that is positively regulated by nerve growth factor. *J. Neurochem.* 101(1):212–222.
219. Amaya F, Shimosato G, Nagano M, et al. 2004. NGF and GDNF differentially regulate TRPV1 expression that contributes to development of inflammatory thermal hyperalgesia. *Eur. J. Neurosci.* 20(9):2303–2310.
220. Li J, Ahmad T, Spetea M, et al. 2001. Bone reinnervation after fracture: a study in the rat. *J. Bone Miner. Res.* 16(8):1505–1510.
221. Li Z, Meyers CA, Chang L, et al. 2019. Fracture repair requires TrkA signaling by skeletal sensory nerves. *J. Clin. Invest.* 129(12):5137–5150.
222. Yasui M, Shiraishi Y, Ozaki N, et al. 2012. Nerve growth factor and associated nerve sprouting contribute to local mechanical hyperalgesia in a rat model of bone injury. *Eur. J. Pain* 16(7):953–965.
223. Hukkanen M, Konttinen YT, Santavirta S, et al. 1993. Rapid proliferation of calcitonin gene-related peptide-immunoreactive nerves during healing of rat tibial fracture suggests neural involvement in bone growth and remodelling. *Neuroscience* 54(4):969–979.
224. Tomlinson RE, Li Z, Li Z, et al. 2017. NGF-TrkA signaling in sensory nerves is required for skeletal adaptation to mechanical loads in mice. *Proc. Natl. Acad. Sci. U. S. A.* 114(18):E3632–E3641.
225. Jimenez-Andrade JM, Bloom AP, Stake JJ, et al. 2010. Pathological sprouting of adult nociceptors in chronic prostate cancer-induced bone pain. *J. Neurosci.* 30(44):14649–14656.
226. Jimenez-Andrade JM, Ghilardi JR, Castaneda-Corral G, et al. 2011. Preventive or late administration of anti-NGF therapy attenuates tumor-induced nerve sprouting, neuroma formation, and cancer pain. *Pain* 152(11):2564–2574.
227. Jimenez-Andrade JM, Mantyh PW. 2012. Sensory and sympathetic nerve fibers undergo sprouting and neuroma formation in the painful arthritic joint of geriatric mice. *Arthritis Res. Ther.* 14(3):R101.
228. Mantyh WG, Jimenez-Andrade JM, Stake JJ, et al. 2010. Blockade of nerve sprouting and neuroma formation markedly attenuates the development of late stage cancer pain. *Neuroscience* 171(2):588–598.

229. Walsh DA, McWilliams DF, Turley MJ, et al. 2010. Angiogenesis and nerve growth factor at the osteochondral junction in rheumatoid arthritis and osteoarthritis. *Rheumatology (Oxford)*. 49(10):1852–1861.
230. Bloom AP, Jimenez-Andrade JM, Taylor RN, et al. 2011. Breast cancer-induced bone remodeling, skeletal pain, and sprouting of sensory nerve fibers. *J. Pain* 12(6):698–711.
231. Jimenez-Andrade JM, Martin CD, Koewler NJ, et al. 2007. Nerve growth factor sequestering therapy attenuates non-malignant skeletal pain following fracture. *Pain* 133(1–3):183–196.
232. Koewler NJ, Freeman KT, Buus RJ, et al. 2007. Effects of a monoclonal antibody raised against nerve growth factor on skeletal pain and bone healing after fracture of the C57BL/6J mouse femur. *J. Bone Miner. Res.* 22(11):1732–1742.
233. Lane NE, Schnitzer TJ, Birbara CA, et al. 2010. Tanezumab for the Treatment of Pain from Osteoarthritis of the Knee. *N. Engl. J. Med.* 363(16):1521–1531 Available from: <http://www.nejm.org/doi/abs/10.1056/NEJMoa0901510>.
234. Hochberg MC. 2015. Serious joint-related adverse events in randomized controlled trials of anti-nerve growth factor monoclonal antibodies. *Osteoarthr. Cartil.* 23 Suppl 1:S18–S21.
235. Williams MC, Ivanusic JJ. 2008. Evidence for the involvement of the spinoparabrachial pathway, but not the spinothalamic tract or post-synaptic dorsal column, in acute bone nociception. *Neurosci. Lett.* 443(3):246–250.
236. Honore P, Rogers SD, Schwei MJ, et al. 2000. Murine models of inflammatory, neuropathic and cancer pain each generates a unique set of neurochemical changes in the spinal cord and sensory neurons. *Neuroscience* 98(3):585–598.
237. Sikandar S, West SJ, McMahon SB, et al. 2017. Sensory processing of deep tissue nociception in the rat spinal cord and thalamic ventrobasal complex. *Physiol. Rep.* 5(14).
238. Arendt-Nielsen L, Nie H, Laursen MB, et al. 2010. Sensitization in patients with painful knee osteoarthritis. *Pain* 149(3):573–581.
239. Yanagisawa Y, Furue H, Kawamata T, et al. 2010. Bone cancer induces a unique central sensitization through synaptic changes in a wide area of the spinal cord. *Mol. Pain* 6:38.
240. Ivanusic JJ. 2008. The pattern of Fos expression in the spinal dorsal horn following acute noxious mechanical stimulation of bone. *Eur. J. Pain* 12(7):895–899.
241. Schwei MJ, Honore P, Rogers SD, et al. 1999. Neurochemical and cellular reorganization of the spinal cord in a murine model of bone cancer pain. *J. Neurosci.* 19(24):10886–10897.
242. Shi X, Guo T-Z, Wei T, et al. 2015. Facilitated spinal neuropeptide signaling and upregulated inflammatory mediator expression contribute to postfracture nociceptive sensitization. *Pain* 156(10):1852–1863.
243. Vanderah TW, Laughlin T, Lashbrook JM, et al. 1996. Single intrathecal injections of dynorphin A or des-Tyr-dynorphins produce long-lasting allodynia in rats: blockade by MK-801 but not naloxone. *Pain* 68(2–3):275–281.
244. Lai J, Luo M-C, Chen Q, et al. 2006. Dynorphin A activates bradykinin receptors to maintain neuropathic pain. *Nat. Neurosci.* 9(12):1534–1540.
245. Shen W, Hu X-M, Liu Y-N, et al. 2014. CXCL12 in astrocytes contributes to bone cancer pain through CXCR4-mediated neuronal sensitization and glial activation in rat spinal cord. *J. Neuroinflammation* 11:75.
246. Chessell IP, Hatcher JP, Bountra C, et al. 2005. Disruption of the P2X7 purinoceptor gene abolishes chronic inflammatory and neuropathic pain. *Pain* 114(3):386–396.
247. Tsuda M, Shigemoto-Mogami Y, Koizumi S, et al. 2003. P2X4 receptors induced in spinal microglia gate tactile allodynia after nerve injury. *Nature* 424(6950):778–783.
248. Gong Q-J, Li Y-Y, Xin W-J, et al. 2009. ATP induces long-term potentiation of C-fiber-evoked field potentials in spinal dorsal horn: the roles of P2X4 receptors and p38 MAPK in microglia. *Glia* 57(6):583–591.
249. Ulmann L, Hatcher JP, Hughes JP, et al. 2008. Up-regulation of P2X4 receptors in spinal microglia after peripheral nerve injury mediates BDNF release and neuropathic pain. *J. Neurosci.* 28(44):11263–11268.
250. Trang T, Beggs S, Wan X, Salter MW. 2009. P2X4-receptor-mediated synthesis and release of brain-derived neurotrophic factor in microglia is dependent on calcium and p38-mitogen-activated protein kinase activation. *J. Neurosci.* 29(11):3518–3528.
251. Coull JAM, Beggs S, Boudreau D, et al. 2005. BDNF from microglia causes the shift in neuronal anion gradient underlying neuropathic pain. *Nature* 438(7070):1017–1021.
252. Wang L-N, Yang J-P, Zhan Y, et al. 2012. Minocycline-induced reduction of brain-derived neurotrophic factor expression in relation to cancer-induced bone pain in rats. *J. Neurosci. Res.* 90(3):672–681.

253. Cicero TJ, Ellis MS, Kasper ZA. 2017. Psychoactive substance use prior to the development of iatrogenic opioid abuse: A descriptive analysis of treatment-seeking opioid abusers. *Addict. Behav.* 65:242–244.
254. Madras BK. 2017. The Surge of Opioid Use, Addiction, and Overdoses: Responsibility and Response of the US Health Care System. *JAMA psychiatry* 74(5):441–442.
255. Substance Abuse and Mental Health Services Administration, Rockville MD. 2013. Results from the 2012 National Survey on Drug Use and Health: Summary of National Findings. Available from: <https://www.samhsa.gov/data/sites/default/files/NSDUHresults2012/NSDUHresults2012.pdf>.
256. Accord Healthcare Limited. 2015. Bupivacaine 0.5%w/v solution for injection.
257. Becker DE, Reed KL. 2012. Local anesthetics: review of pharmacological considerations. *Anesth. Prog.* 59(2):90–101; quiz 102–3 Available from: <http://www.ncbi.nlm.nih.gov/pubmed/22822998>.
258. Casati A, Putzu M. 2005. Bupivacaine, levobupivacaine and ropivacaine: are they clinically different? *Best Pract. Res. Clin. Anaesthesiol.* 19(2):247–68 Available from: <http://www.ncbi.nlm.nih.gov/pubmed/15966496>.
259. Chahar P, Cummings KC. 2012. Liposomal bupivacaine: A review of a new bupivacaine formulation. *J. Pain Res.* 5:257–264.
260. Viscusi E, Minkowitz H, Winkle P, et al. 2019. HTX-011 reduced pain intensity and opioid consumption versus bupivacaine HCl in herniorrhaphy: results from the phase 3 EPOCH 2 study. *Hernia* .
261. Ellis D, Verity N, Lissin D, Wendicke-Lophaven K. 2013. Treatment of postoperative pain in shoulder surgery with SABER-Bupivacaine. *J. Pain* 14(4):S84.
262. Hutchins J, Taylor W. 2017. An evaluation of the analgesic effect of AnestaGel on mechanical allodynia in a rat model of postoperative incisional pain. *J. Pain Res.* Volume 10:2807–2813.
263. World Health Organization. 2017. WHO Model List of Essential Medicines, 20th edition.:1 [cited 2019 Apr 26] Available from: <https://apps.who.int/iris/bitstream/handle/10665/273826/EML-20-eng.pdf?ua=1>.
264. Shafiei FT, Lopez J. 2020. Bupivacaine. Available from: <http://www.ncbi.nlm.nih.gov/pubmed/30422478>.
265. Rubin DS, Matsumoto MM, Weinberg G, Roth S. 2018. Local Anesthetic Systemic Toxicity in Total Joint Arthroplasty: Incidence and Risk Factors in the United States From the National Inpatient Sample 1998-2013. *Reg. Anesth. Pain Med.* 43(2):131–137.
266. Mörwald EE, Zubizarreta N, Cozowicz C, et al. [date unknown]. Incidence of Local Anesthetic Systemic Toxicity in Orthopedic Patients Receiving Peripheral Nerve Blocks. *Reg. Anesth. Pain Med.* 42(4):442–445.
267. Møiniche S, Mikkelsen S, Wetterslev J, Dahl JB. [date unknown]. A systematic review of intra-articular local anesthesia for postoperative pain relief after arthroscopic knee surgery. *Reg. Anesth. Pain Med.* 24(5):430–437.
268. Andersen L Øand Kehlet H. 2014. Analgesic efficacy of local infiltration analgesia in hip and knee arthroplasty: a systematic review. *Br. J. Anaesth.* 113(3):360–374.
269. Cardone DA, Tallia AF. 2003. Diagnostic and therapeutic injection of the hip and knee. *Am. Fam. Physician* 67(10):2147–2152.
270. Pfizer. 2015. Bupivacaine HCl injection, USP.:1–14 [cited 2019 Apr 30] Available from: <http://labeling.pfizer.com/ShowLabeling.aspx?id=4377>.
271. National Institute of Health. 2006. Bupivacaine HCl Archived Drug Label - NIH. [cited 2019 Apr 30] Available from: <https://dailymed.nlm.nih.gov/dailymed/archives/fdaDrugInfo.cfm?archiveid=1828>.
272. 2017. bupivacaine hydrochloride (Bupivacaine Hydrochloride) injection, solution. [cited 2017 Dec 20] Available from: <https://dailymed.nlm.nih.gov/dailymed/archives/fdaDrugInfo.cfm?archiveid=1828>.
273. Williams DJ, Walker JD. 2014. A nomogram for calculating the maximum dose of local anaesthetic. *Anaesthesia* 69(8):847–853.
274. Hussain N, McCartney CJL, Neal JM, et al. 2018. Local anaesthetic-induced myotoxicity in regional anaesthesia: a systematic review and empirical analysis. *Br. J. Anaesth.* 121(4):822–841.
275. Zink W, Graf BM. 2004. Local anesthetic myotoxicity. *Reg. Anesth. Pain Med.* 29(4):333–340.
276. Hall-Craggs EC. 1980. Early ultrastructural changes in skeletal muscle exposed to the local anaesthetic bupivacaine (Marcaine). *Br. J. Exp. Pathol.* 61(2):139–149.
277. Nonaka I, Takagi A, Ishiura S, et al. 1983. Pathophysiology of muscle fiber necrosis induced by bupivacaine hydrochloride (Marcaine). *Acta Neuropathol.* 60(3–4):167–174.
278. Horiguchi T, Shibata M-A, Ito Y, et al. 2002. Macrophage apoptosis in rat skeletal muscle treated with bupivacaine hydrochloride: possible role of MCP-1. *Muscle Nerve* 26(1):79–86.
279. Zink W, Graf BM, Sinner B, et al. 2002. Differential effects of bupivacaine on intracellular Ca<sup>2+</sup> regulation: potential mechanisms of its myotoxicity. *Anesthesiology* 97(3):710–6.

280. Zink W, Missler G, Sinner B, et al. 2005. Differential effects of bupivacaine and ropivacaine enantiomers on intracellular Ca<sup>2+</sup> regulation in murine skeletal muscle fibers. *Anesthesiology* 102(4):793–8.
281. Hogan Q, Dotson R, Erickson S, et al. 1994. Local anesthetic myotoxicity: a case and review. *Anesthesiology* 80(4):942–947.
282. Zink W, Seif C, Bohl JRE, et al. 2003. The acute myotoxic effects of bupivacaine and ropivacaine after continuous peripheral nerve blockades. *Anesth. Analg.* 97(4):1173–9, table of contents.
283. Irwin W, Fontaine E, Agnolucci L, et al. 2002. Bupivacaine myotoxicity is mediated by mitochondria. *J. Biol. Chem.* 277(14):12221–12227.
284. Öz Gergin Ö, Yildiz K, Bayram A, et al. 2015. Comparison of the myotoxic effects of levobupivacaine, bupivacaine, and ropivacaine: an electron microscopic study. *Ultrastruct. Pathol.* 39(3):169–176.
285. Hofmann P, Metterlein T, Bollwein G, et al. 2013. The myotoxic effect of bupivacaine and ropivacaine on myotubes in primary mouse cell culture and an immortalized cell line. *Anesth. Analg.* 117(3):634–640.
286. Yildiz K, Efesoy SN, Ozdamar S, et al. 2011. Myotoxic effects of levobupivacaine, bupivacaine and ropivacaine in a rat model. *Clin. Invest. Med.* 34(5):E273.
287. Plant DR, Colarossi FE, Lynch GS. 2006. Notexin causes greater myotoxic damage and slower functional repair in mouse skeletal muscles than bupivacaine. *Muscle Nerve* 34(5):577–585.
288. Zhao P, Hoffman EP. 2006. Musculin isoforms and repression of MyoD in muscle regeneration. *Biochem. Biophys. Res. Commun.* 342(3):835–842.
289. McAlvin JB, Padera RF, Shankarappa SA, et al. 2014. Multivesicular liposomal bupivacaine at the sciatic nerve. *Biomaterials* 35(15):4557–64.
290. Jehan FS, Hagan JC, Whittaker TJ, Subramanian M. 2001. Diplopia and ptosis following injection of local anesthesia without hyaluronidase. *J. Cataract Refract. Surg.* 27(11):1876–1879.
291. Rhee S-M, Chung NY, Jeong HJ, Oh JH. 2018. Subacromial Local Anesthetics Do Not Interfere With Rotator Cuff Healing After Arthroscopic Repair. *Am. J. Sports Med.* 46(5):1097–1105.
292. Jayaram P, Kennedy DJ, Yeh P, Dragoo J. 2018. Chondrotoxic Effects of Local Anesthetics on Human Knee Articular Cartilage: A Systematic Review. *PM R* 11(4):379–400.
293. Gungor I, Yilmaz A, Ozturk AM, et al. 2014. Bupivacaine and levobupivacaine induce apoptosis in rat chondrocyte cell cultures at ultra-low doses. *Eur. J. Orthop. Surg. Traumatol.* 24(3):291–295.
294. Cobo-Molinos J, Poncela-Garcia M, Marchal-Corrales JA, Delgado-Martinez AD. 2014. Effect of levobupivacaine on articular chondrocytes: an in-vitro investigation. *Eur. J. Anaesthesiol.* 31(11):635–9.
295. Werdehausen R, Braun S, Fazeli S, et al. 2012. Lipophilicity but not stereospecificity is a major determinant of local anaesthetic-induced cytotoxicity in human T-lymphoma cells. *Eur. J. Anaesthesiol.* 29(1):35–41.
296. Kreuz PC, Steinwachs M, Angele P. 2018. Single-dose local anesthetics exhibit a type-, dose-, and time-dependent chondrotoxic effect on chondrocytes and cartilage: a systematic review of the current literature. *Knee Surg. Sports Traumatol. Arthrosc.* 26(3):819–830.
297. Piper SL, Kramer JD, Kim HT, Feeley BT. 2011. Effects of local anesthetics on articular cartilage. *Am. J. Sports Med.* 39(10):2245–2253.
298. Baker JF, Mulhall KJ. 2012. Local anaesthetics and chondrotoxicity: What is the evidence? *Knee Surg. Sports Traumatol. Arthrosc.* 20(11):2294–2301.
299. Shaw KA, Moreland C, Jacobs J, et al. 2018. Improved Chondrotoxic Profile of Liposomal Bupivacaine Compared With Standard Bupivacaine After Intra-articular Infiltration in a Porcine Model. *Am. J. Sports Med.* 46(1):66–71.
300. Gomoll AH, Yanke AB, Kang RW, et al. 2009. Long-term effects of bupivacaine on cartilage in a rabbit shoulder model. *Am. J. Sports Med.* 37(1):72–77.
301. Chu CR, Coyle CH, Chu CT, et al. 2010. In vivo effects of single intra-articular injection of 0.5% bupivacaine on articular cartilage. *J. Bone Joint Surg. Am.* 92(3):599–608.
302. Gulihar A, Robati S, Twaij H, et al. 2015. Articular cartilage and local anaesthetic: A systematic review of the current literature. *J. Orthop.* 12(Suppl 2):S200–10.
303. Lee H, Sowa G, Vo N, et al. 2010. Effect of bupivacaine on intervertebral disc cell viability. *Spine J.* 10(2):159–166.
304. Quero L, Klawitter M, Nerlich AG, et al. 2011. Bupivacaine--the deadly friend of intervertebral disc cells? *Spine J.* 11(1):46–53 Available from: <http://www.ncbi.nlm.nih.gov/pubmed/21168098>.
305. Wang D, Vo N V, Sowa GA, et al. 2011. Bupivacaine decreases cell viability and matrix protein synthesis in an intervertebral disc organ model system. *Spine J.* 11(2):139–146.
306. Cai X-Y, Xiong L-M, Yang S-H, et al. 2014. Comparison of toxicity effects of ropivacaine, bupivacaine, and lidocaine on rabbit intervertebral disc cells in vitro. *Spine J.* 14(3):483–490.

307. Chee A V, Ren J, Lenart BA, et al. 2014. Cytotoxicity of local anesthetics and nonionic contrast agents on bovine intervertebral disc cells cultured in a three-dimensional culture system. *Spine J.* 14(3):491–498.
308. Cai X-Y, Xia Y, Yang S-H, et al. 2015. Ropivacaine- and bupivacaine-induced death of rabbit annulus fibrosus cells in vitro: involvement of the mitochondrial apoptotic pathway. *Osteoarthr. Cartil.* 23(10):1763–1775.
309. Iwasaki K, Sudo H, Yamada K, et al. 2014. Effects of single injection of local anesthetic agents on intervertebral disc degeneration: ex vivo and long-term in vivo experimental study. *PLoS One* 9(10):e109851.
310. Iwasaki K, Sudo H, Yamada K, et al. 2014. Cytotoxic effects of the radiocontrast agent iotrolan and anesthetic agents bupivacaine and lidocaine in three-dimensional cultures of human intervertebral disc nucleus pulposus cells: identification of the apoptotic pathways. *PLoS One* 9(3):e92442.
311. Ohtori S, Inoue G, Orita S, et al. 2013. No acceleration of intervertebral disc degeneration after a single injection of bupivacaine in young age group with follow-up of 5 years. *Asian Spine J.* 7(3):212–217.
312. Carragee EJ, Don AS, Hurwitz EL, et al. 2009. 2009 ISSLS Prize Winner: Does discography cause accelerated progression of degeneration changes in the lumbar disc: a ten-year matched cohort study. *Spine (Phila. Pa. 1976).* 34(21):2338–2345.
313. Gruber HE, Rhyne AL, Hansen KJ, et al. 2012. Deleterious effects of discography radiocontrast solution on human annulus cell in vitro: changes in cell viability, proliferation, and apoptosis in exposed cells. *Spine J.* 12(4):329–35.
314. Strube P, Pfitzner BM, Streitparth F, et al. 2017. In vivo effects of bupivacaine and gadobutrol on the intervertebral disc following discoblock and discography: a histological analysis. *Eur. Radiol.* 27(1):149–156.
315. Lucchinetti E, Awad AE, Rahman M, et al. 2012. Antiproliferative effects of local anesthetics on mesenchymal stem cells: potential implications for tumor spreading and wound healing. *Anesthesiology* 116(4):841–856.
316. Henry BJ, Kenison M, McVay C, et al. 2002. The effect of local hematoma blocks on early fracture healing. *Orthopedics* 25(11):1259–1262.
317. Huss MK, Felt SA, Pacharisak C. 2019. Influence of Pain and Analgesia on Orthopedic and Wound-healing Models in Rats and Mice. *Comp. Med.* .
318. Dimopoulou I, Anagnostou TL, Prassinou NN, et al. 2017. Effect of intrafracture bupivacaine (haematoma block) on analgesic requirements in dogs undergoing fracture repair. *Vet. Anaesth. Analg.* .
319. Herrera JA, Wall EJ, Foad SL. 2004. Hematoma Block Reduces Narcotic Pain Medication after Femoral Elastic Nailing in Children. *J. Pediatr. Orthop.* .
320. Golf M, Daniels SE, Onel E. 2011. A phase 3, randomized, placebo-controlled trial of DepoFoam® bupivacaine (extended-release bupivacaine local analgesic) in bunionectomy. *Adv. Ther.* 28(9):776–88.
321. Guo S, Dipietro LA. 2010. Factors affecting wound healing. *J. Dent. Res.* 89(3):219–29.
322. Abrão J, Fernandes CR, White PF, et al. 2014. Effect of local anaesthetic infiltration with bupivacaine and ropivacaine on wound healing: a placebo-controlled study. *Int. Wound J.* 11(4):379–385.
323. Waite A, Gilliver SC, Masterson GR, et al. 2010. Clinically relevant doses of lidocaine and bupivacaine do not impair cutaneous wound healing in mice. *Br. J. Anaesth.* 104(6):768–773.
324. Baxter R, Bramlett K, Onel E, Daniels S. 2013. Impact of local administration of liposome bupivacaine for postsurgical analgesia on wound healing: a review of data from ten prospective, controlled clinical studies. *Clin. Ther.* 35(3):312–320.e5.
325. Campbell I, Cavanagh S, Creighton J, et al. 2015. To infiltrate or not? Acute effects of local anaesthetic in breast surgery. *ANZ J. Surg.* 85(5):353–357.
326. Perez-Castro R, Patel S, Garavito-Aguilar Z V, et al. 2009. Cytotoxicity of local anesthetics in human neuronal cells. *Anesth. Analg.* 108(3):997–1007.
327. Malet A, Faure M-O, Deletage N, et al. 2015. The comparative cytotoxic effects of different local anesthetics on a human neuroblastoma cell line. *Anesth. Analg.* 120(3):589–596.
328. Damjanovska M, Cvetko E, Kuroda MM, et al. 2019. Neurotoxicity of intraneural injection of bupivacaine liposome injectable suspension versus bupivacaine hydrochloride in a porcine model. *Vet. Anaesth. Analg.* 46(2):236–245.
329. Yamashita A, Matsumoto M, Matsumoto S, et al. 2003. A comparison of the neurotoxic effects on the spinal cord of tetracaine, lidocaine, bupivacaine, and ropivacaine administered intrathecally in rabbits. *Anesth. Analg.* 97(2):512–9, table of contents.

330. Barrington MJ, Watts SA, Gledhill SR, et al. [date unknown]. Preliminary results of the Australasian Regional Anaesthesia Collaboration: a prospective audit of more than 7000 peripheral nerve and plexus blocks for neurologic and other complications. *Reg. Anesth. Pain Med.* 34(6):534–41.
331. Brull R, McCartney CJL, Chan VWS, El-Beheiry H. 2007. Neurological complications after regional anesthesia: contemporary estimates of risk. *Anesth. Analg.* 104(4):965–974.
332. Verlinde M, Hollmann MW, Stevens MF, et al. 2016. Local Anesthetic-Induced Neurotoxicity. *Int. J. Mol. Sci.* 17(3):339.
333. Urban MK, Urquhart B. [date unknown]. Evaluation of brachial plexus anesthesia for upper extremity surgery. *Reg. Anesth.* 19(3):175–182.
334. Kendall MC, Castro Alves LJ, De Oliveira G. 2018. Liposome Bupivacaine Compared to Plain Local Anesthetics to Reduce Postsurgical Pain: An Updated Meta-Analysis of Randomized Controlled Trials. *Pain Res. Treat.* 2018:5710169.
335. Madras BK. 2018. The President’s Commission on Combating Drug Addiction and the Opioid Crisis: Origins and Recommendations. *Clin. Pharmacol. Ther.* .
336. Steverink JG, Oostinga D, van Tol FR, et al. 2021. Sensory innervation of human bone: an immunohistochemical study to further understand bone pain. *J. pain* Available from: <http://www.ncbi.nlm.nih.gov/pubmed/33964414>.
337. Cusack SL, Minkowitz HS, Kuss M, et al. 2012. A randomized, multicenter, pilot study comparing the efficacy and safety of a bupivacaine-collagen implant (XaraColl®) with the ON-Q PainBuster® Post-op Pain Relief System following open gynecological surgery. *J. Pain Res.* 5:453–461.
338. Caplan AI. 1991. Mesenchymal stem cells. *J. Orthop. Res.* 9(5):641–650 Available from: <http://doi.wiley.com/10.1002/jor.1100090504>.
339. Steverink JG, Puluso S, Malda J, Verlaan J-J. 2021. Comparison of in vitro and in vivo Toxicity of Bupivacaine in Musculoskeletal Applications. *Front. Pain Res.* 2 Available from: <https://www.frontiersin.org/articles/10.3389/fpain.2021.723883/full>.
340. Hu D, Onel E, Singla N, et al. 2013. Pharmacokinetic profile of liposome bupivacaine injection following a single administration at the surgical site. *Clin. Drug Investig.* 33(2):109–15 Available from: <http://www.ncbi.nlm.nih.gov/pubmed/23229686>.
341. Danielsson BR, Danielson MK, Böö EL, et al. 1997. Toxicity of bupivacaine and ropivacaine in relation to free plasma concentrations in pregnant rats: a comparative study. *Pharmacol. Toxicol.* 81(2):90–96 Available from: <http://www.ncbi.nlm.nih.gov/pubmed/9298506>.
342. Bruguerolle B, Attolini L, Roucoules X, Lorec AM. 1994. Cigarette smoke increases bupivacaine metabolism in rats. *Can. J. Anaesth.* 41(8):733–737 Available from: <http://www.ncbi.nlm.nih.gov/pubmed/7923523>.
343. Levy RH, Rowland M. 1974. Absorption kinetics of a series of local anesthetics from rat subcutaneous tissue. I. *J. Pharmacokinet. Biopharm.* 2(4):313–335 Available from: <https://doi.org/10.1007/BF01061405>.
344. Patel IH, Levy RH. 1974. Absorption kinetics of local anesthetics from rat subcutaneous tissue. II. Effects of vasodilators. *J. Pharmacokinet. Biopharm.* 2(4):337–346 Available from: <https://doi.org/10.1007/BF01061406>.
345. Li W, Lee M, Whang J, et al. 2010. Delivery of lyophilized Nell-1 in a rat spinal fusion model. *Tissue Eng. Part A* 16(9):2861–2870 Available from: <http://www.ncbi.nlm.nih.gov/pubmed/20528102>.
346. Glatt V, Matthys R. 2014. Adjustable stiffness, external fixator for the rat femur osteotomy and segmental bone defect models. *J. Vis. Exp.* (92):e51558.
347. Siddareddy K, Reddy MAU, Suresh B, Sreeramulu J. 2017. Development and Validation of Analytical Method for Simultaneous Estimation of Bupivacaine and Meloxicam in Human Plasma Using UPLC-MS/MS. *Pharm. Methods* .
348. Söderberg L, Dyhre H, Roth B, Björkman S. 2002. In-vitro release of bupivacaine from injectable lipid formulations investigated by a single drop technique--relation to duration of action in-vivo. *J. Pharm. Pharmacol.* 54(6):747–55 Available from: <http://www.ncbi.nlm.nih.gov/pubmed/12078990>.
349. Ruehl-Fehlert C, Kittel B, Morawietz G, et al. 2003. Revised guides for organ sampling and trimming in rats and mice--part 1. *Exp. Toxicol. Pathol.* 55(2–3):91–106 Available from: <http://www.ncbi.nlm.nih.gov/pubmed/14620530>.
350. Kittel B, Ruehl-Fehlert C, Morawietz G, et al. 2004. Revised guides for organ sampling and trimming in rats and mice--Part 2. A joint publication of the RITA and NACAD groups. *Exp. Toxicol. Pathol.* 55(6):413–31 Available from: <http://www.ncbi.nlm.nih.gov/pubmed/15384248>.
351. Morawietz G, Ruehl-Fehlert C, Kittel B, et al. 2004. Revised guides for organ sampling and trimming in rats and mice--Part 3. A joint publication of the RITA and NACAD groups. *Exp. Toxicol. Pathol.* 55(6):433–49 Available from: <http://www.ncbi.nlm.nih.gov/pubmed/15384249>.
352. Fossey S, Vahle J, Long P, et al. 2016. Nonproliferative and Proliferative Lesions of the Rat and Mouse Skeletal Tissues (Bones, Joints, and Teeth). *J. Toxicol. Pathol.* .



353. Turner P V, Pang DS, Lofgren JL. 2019. A Review of Pain Assessment Methods in Laboratory Rodents. *Comp. Med.* .
354. Rosenblatt JD. 1992. A time course study of the isometric contractile properties of rat extensor digitorum longus muscle injected with bupivacaine. *Comp. Biochem. Physiol. -- Part A Physiol.* .
355. Selwyn MR. 1996. Chapter 5 - Common Designs in Biological Experimentation. In: *Principles of Experimental Design for the Life Sciences, Illustrate*. CRC Press. p 53–58.
356. Utvåg SE, Grundnes O, Reikerås O. 1994. Healing of segmental and simple fractures in rats. *Acta Orthop. Scand.* 65(5):559–63 Available from: <http://www.ncbi.nlm.nih.gov/pubmed/7801763>.
357. Barletta JF. 2012. Clinical and economic burden of opioid use for postsurgical pain: focus on ventilatory impairment and ileus. *Pharmacotherapy* 32(9 Suppl):12S–8S.
358. Butterworth JF, Strichartz GR. 1990. Molecular Mechanisms of Local Anesthesia. *Anesthesiology* 72(4):711–734.
359. Docherty RJ, Farmer CE. 2009. The pharmacology of voltage-gated sodium channels in sensory neurones. *Handb. Exp. Pharmacol.* (194):519–61.
360. SHANDLER L. 1965. MECHANISM OF ACTION OF LOCAL ANESTHETICS. *J. Am. Dent. Soc. Anesthesiol.* 12:62–66.
361. Gissen AJ, Covino BG, Gregus J. 1980. Differential sensitivities of mammalian nerve fibers to local anesthetic agents. *Anesthesiology* 53(6):467–74 Available from: <http://www.ncbi.nlm.nih.gov/pubmed/7457962>.
362. Wildsmith JA, Gissen AJ, Gregus J, Covino BG. 1985. Differential nerve blocking activity of amine-ester local anaesthetics. *Br. J. Anaesth.* 57(6):612–620.
363. Hargreaves KM, Keiser K. 2002. Local anesthetic failure in endodontics: *Endod. Top.* 1(1):26–39 Available from: <http://doi.wiley.com/10.1034/j.1601-1546.2002.10103.x>.
364. Erlanger J, Gasser H, Solandt DY. 1937. *Electrical Signs Of Nervous Activity*. By Joseph Erlanger and Herbert S. Gasser . (Philadelphia: University of Pennsylvania Press; London: Humphrey Milford, Oxford University Press, 1937). *Am. J. Psychiatry* 93(6):1472-a-1473 Available from: <http://psychiatryonline.org/doi/abs/10.1176/ajp.93.6.1472-a>.
365. Bekkers JM, Greeff NG, Keynes RD. 1986. The conductance and density of sodium channels in the cut-open squid giant axon. *J. Physiol.* 377:463–486.
366. Gissen AJ, Covino BG, Gregus J. 1982. Differential sensitivity of fast and slow fibers in mammalian nerve. III. Effect of etidocaine and bupivacaine on fast/slow fibers. *Anesth. Analg.* 61(7):570–575.
367. Rosenberg PH, Heinonen E. 1983. Differential sensitivity of A and C nerve fibres to long-acting amide local anaesthetics. *Br. J. Anaesth.* 55(2):163–167.
368. Ford DJ, Raj PP, Singh P, et al. 1984. Differential peripheral nerve block by local anesthetics in the cat. *Anesthesiology* 60(1):28–33.
369. Obi T, Takatsu M, Yamazaki K, et al. 2007. Conduction velocities of A-delta-fibers and C-fibers in human peripheral nerves and spinal cord after CO<sub>2</sub> laser stimulation. *J. Clin. Neurophysiol.* 24(3):294–7 Available from: <http://www.ncbi.nlm.nih.gov/pubmed/17545835>.
370. Collins CA, Rojas E. 1982. Temperature dependence of the sodium channel gating kinetics in the node of Ranvier. *Q. J. Exp. Physiol.* 67(1):41–55.
371. Villiere V, McLachlan EM. 1996. Electrophysiological properties of neurons in intact rat dorsal root ganglia classified by conduction velocity and action potential duration. *J. Neurophysiol.* 76(3):1924–1941.
372. Nencini S, Ringuet M, Kim D-H, et al. 2018. GDNF, Neurturin, and Artemin Activate and Sensitize Bone Afferent Neurons and Contribute to Inflammatory Bone Pain. *J. Neurosci.* 38(21):4899–4911.
373. Polanco-García M, García-Lopez J, Fàbregas N, et al. 2017. Postoperative Pain Management in Spanish Hospitals: A Cohort Study Using the PAIN-OUT Registry. *J. Pain* 18(10):1237–1252 Available from: <http://www.ncbi.nlm.nih.gov/pubmed/28619696>.
374. McLure HA, Rubin AP. 2005. Review of local anaesthetic agents. *Minerva Anesthesiol.* (71):59–74.
375. Holgado MA, Arias JL, Cózar MJ, et al. 2008. Synthesis of lidocaine-loaded PLGA microparticles by flow focusing. *Int. J. Pharm.* 358(1–2):27–35 Available from: <https://linkinghub.elsevier.com/retrieve/pii/S037851730800121X>.
376. Ohri R, Wang JC-F, Blaskovich PD, et al. 2013. Inhibition by Local Bupivacaine-Releasing Microspheres of Acute Postoperative Pain from Hairy Skin Incision. *Anesth. Analg.* 117(3):717–730 Available from: <http://journals.lww.com/0000539-201309000-00025>.
377. Viscusi ER, Sinatra R, Onel E, Ramamoorthy SL. 2013. The Safety of Liposome Bupivacaine, A Novel Local Analgesic Formulation. *Clin. J. Pain* :1 Available from: <http://journals.lww.com/00002508-900000000-99622>.
378. Boogaerts J, Declercq A, Lafont N, et al. 1993. Toxicity of Bupivacaine Encapsulated into Liposomes and Injected Intravenously. *Anesth. Analg.* 76(3):553–555 Available from: <http://journals.lww.com/0000539-199303000-00018>.

379. Padera R, Bellas E, Tse JY, et al. 2008. Local myotoxicity from sustained release of bupivacaine from microparticles. *Anesthesiology* 108(5):921–928 Available from: <http://www.ncbi.nlm.nih.gov/pubmed/18431129>.
380. Kohane DS, Lipp M, Kinney RC, et al. 2002. Biocompatibility of lipid-protein-sugar particles containing bupivacaine in the epineurium. *J. Biomed. Mater. Res.* 59(3):450–9 Available from: <http://www.ncbi.nlm.nih.gov/pubmed/11774302>.
381. Hoang Thi TT, Lee Y, Ryu SB, et al. 2017. Oxidized cyclodextrin-functionalized injectable gelatin hydrogels as a new platform for tissue-adhesive hydrophobic drug delivery. *RSC Adv.* 7(54):34053–34062 Available from: <http://xlink.rsc.org/?DOI=C7RA04137C>.
382. Young S, Wong M, Tabata Y, Mikos AG. 2005. Gelatin as a delivery vehicle for the controlled release of bioactive molecules. *J. Control. Release* 109(1–3):256–274 Available from: <https://linkinghub.elsevier.com/retrieve/pii/S0168365905004979>.
383. Zhu M, Wang Y, Ferracci G, et al. 2019. Gelatin methacryloyl and its hydrogels with an exceptional degree of controllability and batch-to-batch consistency. *Sci. Rep.* .
384. Piluso S, Flores Gomez D, Dokter I, et al. 2020. Rapid and cytocompatible cell-laden silk hydrogel formation via riboflavin-mediated crosslinking . *J. Mater. Chem. B* .
385. Roy MN, Saha S, Kundu M, et al. 2016. Exploration of inclusion complexes of neurotransmitters with  $\beta$ -cyclodextrin by physicochemical techniques. *Chem. Phys. Lett.* 655–656:43–50 Available from: <https://linkinghub.elsevier.com/retrieve/pii/S0009261416303323>.
386. Hoang Thi TT, Lee Y, Ryu SB, et al. 2017. Oxidized cyclodextrin-functionalized injectable gelatin hydrogels as a new platform for tissue-adhesive hydrophobic drug delivery. *RSC Adv.* 7(54):34053–34062.
387. Feng Q, Wei K, Lin S, et al. 2016. Mechanically resilient, injectable, and bioadhesive supramolecular gelatin hydrogels crosslinked by weak host-guest interactions assist cell infiltration and in situ tissue regeneration. *Biomaterials* 101:217–228.
388. Gidwani B, Vyas A. 2015. A Comprehensive Review on Cyclodextrin-Based Carriers for Delivery of Chemotherapeutic Cytotoxic Anticancer Drugs. *Biomed Res. Int.* 2015:198268 Available from: <http://www.ncbi.nlm.nih.gov/pubmed/26582104>.
389. Davis ME, Brewster ME. 2004. Cyclodextrin-based pharmaceuticals: Past, present and future. *Nat. Rev. Drug Discov.* .
390. Cereda CMS, Tofoli GR, Maturana LG, et al. 2012. Local neurotoxicity and myotoxicity evaluation of cyclodextrin complexes of bupivacaine and ropivacaine. *Anesth. Analg.* 115(5):1234–1241.
391. Lai J-Y. 2010. Biocompatibility of chemically cross-linked gelatin hydrogels for ophthalmic use. *J. Mater. Sci. Mater. Med.* 21(6):1899–911 Available from: <http://www.ncbi.nlm.nih.gov/pubmed/20238149>.
392. Sigma-Aldrich. 2020. Gelatin Product Information.:3 [cited 2020 Nov 17] Available from: [https://www.sigmaaldrich.com/content/dam/sigma-aldrich/docs/Sigma/Product\\_Information\\_Sheet/2/g9382pis.pdf](https://www.sigmaaldrich.com/content/dam/sigma-aldrich/docs/Sigma/Product_Information_Sheet/2/g9382pis.pdf).
393. Kuntz ID, Gasparro FP, Johnston MD, Taylor RP. 1968. Molecular Interactions and the Benesi-Hildebrand Equation. *J. Am. Chem. Soc.* .
394. Sarkar K, Barman BK, Nath Roy M. 2018. Study to explore inclusion complexes of A- and B-cyclodextrin molecules with 3-octyl-1-methylimidazolium bromide with the manifestation of hydrophobic and hydrophilic interactions. *Chem. Phys. Lett.* .
395. Lohmann N, Schirmer L, Atallah P, et al. 2017. Glycosaminoglycan-based hydrogels capture inflammatory chemokines and rescue defective wound healing in mice. *Sci. Transl. Med.* 9(386) Available from: <http://www.ncbi.nlm.nih.gov/pubmed/28424334>.
396. Hasturk O, Jordan KE, Choi J, Kaplan DL. 2020. Enzymatically crosslinked silk and silk-gelatin hydrogels with tunable gelation kinetics, mechanical properties and bioactivity for cell culture and encapsulation. *Biomaterials* 232:119720 Available from: <http://www.ncbi.nlm.nih.gov/pubmed/31896515>.
397. Worthington Corporation. 2021. Collagenase product information. [cited 2021 Nov 3] Available from: <https://worthington-biochem.com/CLS/default.html>.
398. Ågren MS, Taplin CJ, Woessner JF, et al. 1992. Collagenase in wound healing: Effect of wound age and type. *J. Invest. Dermatol.* .
399. ÅGREN MS. 1994. Gelatinase activity during wound healing. *Br. J. Dermatol.* .
400. Zhao X, Lang Q, Yildirim L, et al. 2016. Photocrosslinkable Gelatin Hydrogel for Epidermal Tissue Engineering. *Adv. Healthc. Mater.* 5(1):108–18 Available from: <http://www.ncbi.nlm.nih.gov/pubmed/25880725>.
401. Madison SA, Carnali JO. 2013. pH Optimization of Amidation via Carbodiimides. *Ind. Eng. Chem. Res.* 52(38):13547–13555 Available from: <https://pubs.acs.org/doi/10.1021/ie401724m>.

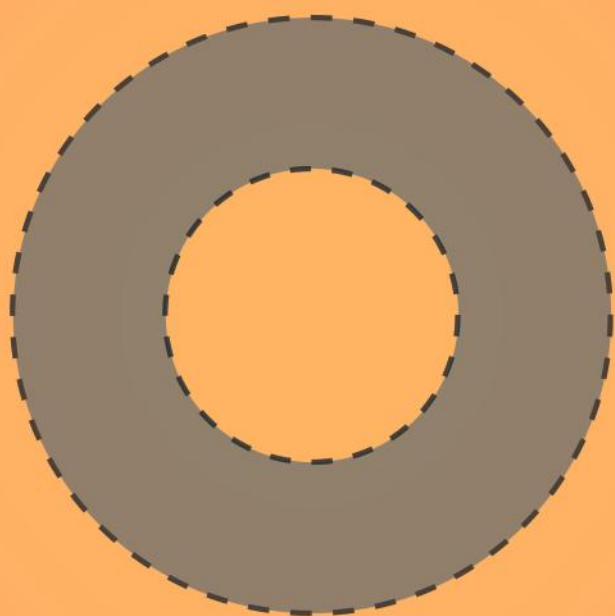
402. Lewis MR, Kao JY, Anderson A-LJ, et al. 2001. An Improved Method for Conjugating Monoclonal Antibodies with N-Hydroxysulfosuccinimidyl DOTA. *Bioconjug. Chem.* 12(2):320–324 Available from: <https://pubs.acs.org/doi/10.1021/bc0000886>.
403. Redmond RW, Kochevar IE. 2019. Medical Applications of Rose Bengal- and Riboflavin-Photosensitized Protein Crosslinking. *Photochem. Photobiol.* 95(5):1097–1115 Available from: <http://www.ncbi.nlm.nih.gov/pubmed/31111489>.
404. Mura P. 2014. Analytical techniques for characterization of cyclodextrin complexes in aqueous solution: a review. *J. Pharm. Biomed. Anal.* 101:238–50 Available from: <http://www.ncbi.nlm.nih.gov/pubmed/24680374>.
405. MORAES C, ABRAMI P, DEPAULA E, et al. 2007. Study of the interaction between S(-) bupivacaine and 2-hydroxypropyl- $\beta$ -cyclodextrin. *Int. J. Pharm.* 331(1):99–106 Available from: <https://linkinghub.elsevier.com/retrieve/pii/S0378517306007897>.
406. Jug M, Mennini N, Melani F, et al. 2010. Phase solubility, <sup>1</sup>H NMR and molecular modelling studies of bupivacaine hydrochloride complexation with different cyclodextrin derivatives. *Chem. Phys. Lett.* 500(4–6):347–354 Available from: <https://linkinghub.elsevier.com/retrieve/pii/S0009261410014272>.
407. Peppas NA, Bures P, Leobandung W, Ichikawa H. 2000. Hydrogels in pharmaceutical formulations. *Eur. J. Pharm. Biopharm.* 50(1):27–46 Available from: <http://www.ncbi.nlm.nih.gov/pubmed/10840191>.
408. Park H, Guo X, Temenoff JS, et al. 2009. Effect of Swelling Ratio of Injectable Hydrogel Composites on Chondrogenic Differentiation of Encapsulated Rabbit Marrow Mesenchymal Stem Cells In Vitro. *Biomacromolecules* 10(3):541–546 Available from: <https://pubs.acs.org/doi/10.1021/bm801197m>.
409. Yue K, Trujillo-de Santiago G, Alvarez MM, et al. 2015. Synthesis, properties, and biomedical applications of gelatin methacryloyl (GelMA) hydrogels. *Biomaterials* 73:254–271 Available from: <https://linkinghub.elsevier.com/retrieve/pii/S014296121500719X>.
410. Wu Y, Xiang Y, Fang J, et al. 2019. The influence of the stiffness of GelMA substrate on the outgrowth of PC12 cells. *Biosci. Rep.* 39(1) Available from: <https://portlandpress.com/biosci/rep/article/doi/10.1042/BSR20181748/240/The-influence-of-the-stiffness-of-GelMA-substrate>.
411. Grayson ACR, Voskerician G, Lynn A, et al. 2004. Differential degradation rates in vivo and in vitro of biocompatible poly(lactic acid) and poly(glycolic acid) homo- and co-polymers for a polymeric drug-delivery microchip. *J. Biomater. Sci. Polym. Ed.* 15(10):1281–1304 Available from: <https://www.tandfonline.com/doi/full/10.1163/1568562041959991>.
412. Sigma Aldrich. [date unknown]. Collagenase from C. histolyticum Product Information.:1–3 [cited 2020 Dec 18] Available from: <https://www.sigmaaldrich.com/content/dam/sigma-aldrich/docs/Sigma/Datasheet/3/c9891dat.pdf>.
413. Xing Q, Yates K, Vogt C, et al. 2014. Increasing mechanical strength of gelatin hydrogels by divalent metal ion removal. *Sci. Rep.* .
414. Piluso S, Lendlein A, Neffe AT. 2017. Enzymatic action as switch of bulk to surface degradation of clicked gelatin-based networks. *Polym. Adv. Technol.* 28(10):1318–1324.
415. Erickson HP. 2009. Size and shape of protein molecules at the nanometer level determined by sedimentation, gel filtration, and electron microscopy. *Biol. Proced. Online* 11:32–51 Available from: <http://www.ncbi.nlm.nih.gov/pubmed/19495910>.
416. Ci T, Shen Y, Cui S, et al. 2017. Achieving High Drug Loading and Sustained Release of Hydrophobic Drugs in Hydrogels through In Situ Crystallization. *Macromol. Biosci.* .
417. McDonald S, Faibushevich AA, Garnick S, et al. 2002. Determination of local tissue concentrations of bupivacaine released from biodegradable microspheres and the effect of vasoactive compounds on bupivacaine tissue clearance studied by microdialysis sampling. *Pharm. Res.* 19(11):1745–52 Available from: <http://www.embase.com/search/results?subaction=viewrecord&from=export&id=L35305528>.
418. Feldman HS, Hartvig P, Wiklund L, et al. 1997. Regional distribution of <sup>11</sup>C-labeled lidocaine, bupivacaine, and ropivacaine in the heart, lungs, and skeletal muscle of pigs studied with positron emission tomography. *Biopharm. Drug Dispos.* 18(2):151–64 Available from: <http://www.ncbi.nlm.nih.gov/pubmed/9099451>.
419. Nakano E, Mushtaq S, Heath PR, et al. 2011. Riboflavin depletion impairs cell proliferation in adult human duodenum: Identification of potential effectors. *Dig. Dis. Sci.* .
420. Manthey KC, Rodriguez-Melendez R, Hoi JT, Zemleni J. 2006. Riboflavin deficiency causes protein and DNA damage in HepG2 cells, triggering arrest in G1 phase of the cell cycle. *J. Nutr. Biochem.* 17(4):250–256 Available from: <https://linkinghub.elsevier.com/retrieve/pii/S0955286305001282>.
421. Debono B, Wainwright TW, Wang MY, et al. 2021. Consensus statement for perioperative care in lumbar spinal fusion: Enhanced Recovery After Surgery (ERAS®) Society recommendations. *Spine J.* 21(5):729–752 Available from: <https://linkinghub.elsevier.com/retrieve/pii/S1529943021000024>.
422. Tulgar S, Ahiskalioglu A, De Cassai A, Gurkan Y. 2019. Efficacy of bilateral erector spinae plane block in the management of pain: current insights. *J. Pain Res.* 12:2597–2613 Available from: <http://www.ncbi.nlm.nih.gov/pubmed/31695476>.

423. Singh S, Choudhary NK, Lalin D, Verma VK. 2020. Bilateral Ultrasound-guided Erector Spinae Plane Block for Postoperative Analgesia in Lumbar Spine Surgery: A Randomized Control Trial. *J. Neurosurg. Anesthesiol.* 32(4):330–334 Available from: <http://www.ncbi.nlm.nih.gov/pubmed/31033625>.
424. Yayik AM, Cesur S, Ozturk F, et al. 2019. Postoperative Analgesic Efficacy of the Ultrasound-Guided Erector Spinae Plane Block in Patients Undergoing Lumbar Spinal Decompression Surgery: A Randomized Controlled Study. *World Neurosurg.* 126:e779–e785 Available from: <http://www.ncbi.nlm.nih.gov/pubmed/30853517>.
425. Marques EMR, Jones HE, Elvers KT, et al. 2014. Local anaesthetic infiltration for peri-operative pain control in total hip and knee replacement: systematic review and meta-analyses of short- and long-term effectiveness. *BMC Musculoskelet. Disord.* 15:220 Available from: <http://www.ncbi.nlm.nih.gov/pubmed/24996539>.
426. Bramlett K, Onel E, Viscusi ER, Jones K. 2012. A randomized, double-blind, dose-ranging study comparing wound infiltration of DepoFoam bupivacaine, an extended-release liposomal bupivacaine, to bupivacaine HCl for postsurgical analgesia in total knee arthroplasty. *Knee* 19(5):530–6 Available from: <http://www.ncbi.nlm.nih.gov/pubmed/22285545>.
427. Velanovich V, Rider P, Deck K, et al. 2019. Safety and Efficacy of Bupivacaine HCl Collagen-Matrix Implant (INL-001) in Open Inguinal Hernia Repair: Results from Two Randomized Controlled Trials. *Adv. Ther.* 36(1):200–216 Available from: <http://www.ncbi.nlm.nih.gov/pubmed/30467808>.
428. Steverink JG, van Tol FR, Oosterman BJ, et al. 2022. Robust gelatin hydrogels for local sustained release of bupivacaine following spinal surgery. *Acta Biomater.* Available from: <https://linkinghub.elsevier.com/retrieve/pii/S1742706122002768>.
429. Wilke HJ, Kettler A, Claes LE. 1997. Are sheep spines a valid biomechanical model for human spines? *Spine (Phila. Pa. 1976).* 22(20):2365–74 Available from: <http://www.ncbi.nlm.nih.gov/pubmed/9355217>.
430. Dash S, Murthy PN, Nath L, Chowdhury P. [date unknown]. Kinetic modeling on drug release from controlled drug delivery systems. *Acta Pol. Pharm.* 67(3):217–23 Available from: <http://www.ncbi.nlm.nih.gov/pubmed/20524422>.
431. Siepmann J, Siepmann F. 2008. Mathematical modeling of drug delivery. *Int. J. Pharm.* 364(2):328–343 Available from: <https://linkinghub.elsevier.com/retrieve/pii/S0378517308006169>.
432. Elvin CM, Vuocolo T, Brownlee AG, et al. 2010. A highly elastic tissue sealant based on photopolymerised gelatin. *Biomaterials* 31(32):8323–31 Available from: <http://www.ncbi.nlm.nih.gov/pubmed/20674967>.
433. Bolton AE, Hunter WM. 1973. The labelling of proteins to high specific radioactivities by conjugation to a 125I-containing acylating agent. *Biochem. J.* 133(3):529–39 Available from: <http://www.ncbi.nlm.nih.gov/pubmed/4733239>.
434. Anderson JM. 2001. Biological Responses to Materials. *Annu. Rev. Mater. Res.* 31(1):81–110 Available from: <http://www.annualreviews.org/doi/10.1146/annurev.matsci.31.1.81>.
435. Jorfeldt L, Löfström B, Pernow B, et al. 1968. The effect of local anaesthetics on the central circulation and respiration in man and dog. *Acta Anaesthesiol. Scand.* 12(4):153–69 Available from: <http://www.ncbi.nlm.nih.gov/pubmed/4896937>.
436. Knudsen K, Beckman Suurkula M, Blomberg S, et al. 1997. Central nervous and cardiovascular effects of i.v. infusions of ropivacaine, bupivacaine and placebo in volunteers. *Br. J. Anaesth.* 78(5):507–14 Available from: <http://www.ncbi.nlm.nih.gov/pubmed/9175963>.
437. Farmacotherapeutisch kompas. 2022. Bupivacaine.
438. Lachiewicz PF, Lee G-C, Pollak RA, et al. 2020. HTX-011 Reduced Pain and Opioid Use After Primary Total Knee Arthroplasty: Results of a Randomized Phase 2b Trial. *J. Arthroplasty* 35(10):2843–2851 Available from: <http://www.ncbi.nlm.nih.gov/pubmed/32561266>.
439. Yáñez JA, Remsberg CM, Sayre CL, et al. 2011. Flip-flop pharmacokinetics--delivering a reversal of disposition: challenges and opportunities during drug development. *Ther. Deliv.* 2(5):643–72 Available from: <http://www.ncbi.nlm.nih.gov/pubmed/21837267>.
440. Mather LE, Rutten AJ, Plummer JL. 1994. Pharmacokinetics of bupivacaine enantiomers in sheep: Influence of dosage regimen and study design. *J. Pharmacokinet. Biopharm.* 22(6):481–498 Available from: <http://link.springer.com/10.1007/BF02353791>.
441. Stubbsjøn SM, Flø AS, Moe RO, et al. 2009. Exploring non-invasive methods to assess pain in sheep. *Physiol. Behav.* 98(5):640–648 Available from: <https://linkinghub.elsevier.com/retrieve/pii/S0031938409003187>.
442. Food and Drug Administration. 2016. Use of International Standard ISO 10993-1, Biological evaluation of medical devices - Part 1: Evaluation and testing within a risk management process. *Dep. Heal. Hum. Serv. Food Drug Adm.* :68 Available from: <https://www.fda.gov/downloads/medicaldevices/deviceregulationandguidance/guidancedocuments/ucm348890.pdf>.

443. Black J, Black J. 2005. *Biological Performance of Materials*. CRC Press. Available from: <https://www.taylorfrancis.com/books/9781420057843>.
444. Bryers JD, Giachelli CM, Ratner BD. 2012. Engineering biomaterials to integrate and heal: the biocompatibility paradigm shifts. *Biotechnol. Bioeng.* 109(8):1898–911 Available from: <http://www.ncbi.nlm.nih.gov/pubmed/22592568>.
445. Anderson JM, Rodriguez A, Chang DT. 2008. Foreign body reaction to biomaterials. *Semin. Immunol.* 20(2):86–100 Available from: <https://linkinghub.elsevier.com/retrieve/pii/S1044532307000966>.
446. Klopffleisch R, Jung F. 2017. The pathology of the foreign body reaction against biomaterials. *J. Biomed. Mater. Res. Part A* 105(3):927–940 Available from: <https://onlinelibrary.wiley.com/doi/10.1002/jbm.a.35958>.
447. Chan JJI, Thong SY, Tan MGE. 2018. Factors affecting postoperative pain and delay in discharge from the post-anaesthesia care unit: A descriptive correlational study. *Proc. Singapore Healthc.* 27(2):118–124 Available from: <http://journals.sagepub.com/doi/10.1177/2010105817738794>.
448. Gerbershagen HJ, Pogatzki-Zahn E, Aduckathil S, et al. 2014. Procedure-specific Risk Factor Analysis for the Development of Severe Postoperative Pain. *Anesthesiology* 120(5):1237–1245 Available from: <https://pubs.asahq.org/anesthesiology/article/120/5/1237/13793/Procedure-specific-Risk-Factor-Analysis-for-the>.
449. Oezel L, Hughes AP, Arzani A, et al. 2022. Surgeon-Placed Erector Spinae Plane Catheters for Multilevel Lumbar Spine Fusion: Technique and Outcomes Compared With Single-Shot Blocks. *Int. J. Spine Surg.* :8300 Available from: <http://ijssurgery.com/lookup/doi/10.14444/8300>.
450. Magerl F. 1982. External Skeletal Fixation of the Lower Thoracic and the Lumbar Spine. In: *Current Concepts of External Fixation of Fractures*. Berlin, Heidelberg: Springer Berlin Heidelberg. p 353–366 Available from: [http://link.springer.com/10.1007/978-3-642-68448-7\\_40](http://link.springer.com/10.1007/978-3-642-68448-7_40).
451. European Directorate for the Quality of Medicines & HealthCare (EDQM). 2019. 2.6.14 Bacterial Endotoxins. *Eur. Pharmacopoeia* .
452. International Organization for Standardization. 2016. ISO 10993-6:2016. *Biological Evaluation of Medical Devices - Test for Local Effects after Implantation*. Geneva, Switzerland.
453. Wilke H-J et al. 1997. Are Sheep Spines a Valid Biomechanical Model for Human Spines? *Spine (Phila. Pa. 1976)*. 22(20):2365–2374.
454. Wilke HJ, Kettler A, Wenger KH, Claes LE. 1997. Anatomy of the sheep spine and its comparison to the human spine. *Anat. Rec.* 247(4):542–555 Available from: <https://pubmed.ncbi.nlm.nih.gov/9096794>.
455. Sheng SR, Wang XY, Xu HZ, et al. 2010. Anatomy of large animal spines and its comparison to the human spine: A systematic review. *Eur. Spine J.* 19(1):46–56.
456. Rehman I, Smith R, Hench LL, Bonfield W. 1995. Structural evaluation of human and sheep bone and comparison with synthetic hydroxyapatite by FT-Raman spectroscopy. *J. Biomed. Mater. Res.* 29(10):1287–1294 Available from: <https://pubmed.ncbi.nlm.nih.gov/8557731>.
457. Aerssens J. 1998. Interspecies Differences in Bone Composition, Density, and Quality: Potential Implications for in Vivo Bone Research. *Endocrinology* 139(2):663–670 [cited 2020 Feb 24] Available from: <https://academic.oup.com/endo/article-lookup/doi/10.1210/en.139.2.663>.
458. Martini L, Fini M, Giavaresi G, Giardino R. 2001. Sheep model in orthopedic research: a literature review. *Comp. Med.* 51(4):292–299 Available from: <https://pubmed.ncbi.nlm.nih.gov/11924786>.
459. Mills LA, Simpson AHRW. 2012. In vivo models of bone repair. *J. Bone Joint Surg. Br.* 94(7):865–874 Available from: <https://pubmed.ncbi.nlm.nih.gov/22733938>.
460. Feldman HS, Dvoskin S, Halldin MH, et al. 1997. Comparative local anesthetic efficacy and pharmacokinetics of epidurally administered ropivacaine and bupivacaine in the sheep. *Reg. Anesth.* 22(5):451–460 Available from: <https://pubmed.ncbi.nlm.nih.gov/9338908>.
461. Huang YF, Pryor ME, Mather LE, Veering BT. 1998. Cardiovascular and central nervous system effects of intravenous levobupivacaine and bupivacaine in sheep. *Anesth. Analg.* 86(4):797–804.
462. Fubini SL, Ducharme N. 2016. *Farm Animal Surgery*, 2nd ed. Elsevier Health Sciences. 664 p.
463. Chahoud J, Kanafani Z, Kanj SS. 2014. Surgical Site Infections Following Spine Surgery: Eliminating the Controversies in the Diagnosis. *Front. Med.* 1 Available from: <http://journal.frontiersin.org/article/10.3389/fmed.2014.00007/abstract>.
464. Zimmerli W. 2014. Clinical presentation and treatment of orthopaedic implant-associated infection. *J. Intern. Med.* 276(2):111–9 Available from: <http://www.ncbi.nlm.nih.gov/pubmed/24605880>.
465. Abramson N, Melton B. 2000. Leukocytosis: basics of clinical assessment. *Am. Fam. Physician* 62(9):2053–60 Available from: <http://www.ncbi.nlm.nih.gov/pubmed/11087187>.
466. Andrade EL, Bento AF, Cavalli J, et al. 2016. Non-clinical studies in the process of new drug development - Part II: Good laboratory practice, metabolism, pharmacokinetics, safety and dose translation to clinical studies. *Brazilian J. Med. Biol. Res. = Rev. Bras. Pesqui. medicas e Biol.* 49(12):e5646 Available from: <http://www.ncbi.nlm.nih.gov/pubmed/27982281>.

467. US FDA. 1999. Applications Covered by Section 505(b)(2). Rockville, MD. Available from: <https://www.fda.gov/regulatory-information/search-fda-guidance-documents/applications-covered-section-505b2>.
468. Deadman CM, Kellaway IW, Yasin M, et al. 2007. An investigation into the influence of drug lipophilicity on the in vivo absorption profiles from subcutaneous microspheres and in situ forming depots. *J. Control. Release* 122(1):79–85 Available from: <http://www.ncbi.nlm.nih.gov/pubmed/17638603>.
469. National Center for Biotechnology Information (NCBI). 2022. PubChem Compound Summary for CID 2474, Bupivacaine. [cited 2022 Jul 26] Available from: <https://pubchem.ncbi.nlm.nih.gov/compound/Bupivacaine>.
470. Heffernan JM, McLaren AC, Glass CM, Overstreet DJ. 2022. Extended Release of Bupivacaine from Temperature-Responsive Hydrogels Provides Multi-Day Analgesia for Postoperative Pain. *Pain Med.* Available from: <http://www.ncbi.nlm.nih.gov/pubmed/35944219>.
471. Jaipan P, Nguyen A, Narayan RJ. 2017. Gelatin-based hydrogels for biomedical applications. *MRS Commun.* 7(03):416–426.
472. Koshy ST, Desai RM, Joly P, et al. 2016. Click-Crosslinked Injectable Gelatin Hydrogels. *Adv. Healthc. Mater.* 5(5):541–547 Available from: <https://onlinelibrary.wiley.com/doi/10.1002/adhm.201500757>.
473. International Organization for Standardization. 2016. ISO 10993-11:2016. Biological Evaluation of Medical Devices - Tests for Systemic Toxicity. Geneva, Switzerland. Available from: [www.iso.org](http://www.iso.org).
474. Dorjee S, Heuer C, Jackson R, et al. 2009. Are white-spot lesions in sheep associated with leptospirosis? *N. Z. Vet. J.* 57(1):28–33 Available from: <http://www.ncbi.nlm.nih.gov/pubmed/19252540>.
475. Abosse JS, Terefe G, Teshale BM. 2022. Comparative study on pathological changes in sheep and goats experimentally infected with *Haemonchus contortus*. *Surg. Exp. Pathol.* 5(1):14 Available from: <https://surgeppathol.biomedcentral.com/articles/10.1186/s42047-022-00116-8>.
476. Abdulhameed MF, Habib I, Al-Azizz SA, Robertson I. 2018. Cystic echinococcosis in marketed offal of sheep in Basrah, Iraq: Abattoir-based survey and a probabilistic model estimation of the direct economic losses due to hydatid cyst. *Parasite Epidemiol. Control* 3(1):43–51 Available from: <http://www.ncbi.nlm.nih.gov/pubmed/29774298>.
477. Khanjari A, Bahunar A, Fallah S, et al. 2014. Prevalence of fasciolosis and dicrocoeliosis in slaughtered sheep and goats in Amol Abattoir, Mazandaran, northern Iran. *Asian Pacific J. Trop. Dis.* 4(2):120–124 Available from: <https://linkinghub.elsevier.com/retrieve/pii/S2222180814603273>.
478. Gantwerker EA, Hom DB. 2012. Skin: histology and physiology of wound healing. *Clin. Plast. Surg.* 39(1):85–97 Available from: <http://www.ncbi.nlm.nih.gov/pubmed/22099852>.
479. Food and Drug Administration. 2018. The Drug Development Process. Step 3 Clinical Research.
480. World Health Organization [WHO]. 2007. Quality Assurance of Pharmaceuticals: A Compendium of Guidelines and Related Materials. Good manufacturing practices and inspection, Volume 2, Revised. 409 p.
481. Food and Drug Administration, Hospira Inc. 2009. Bupivacaine Hydrochloride Injection, USP. [cited 2022 Aug 22] Available from: [https://www.accessdata.fda.gov/drugsatfda\\_docs/label/2010/071165s020lbl.pdf](https://www.accessdata.fda.gov/drugsatfda_docs/label/2010/071165s020lbl.pdf).
482. Rothaug J, Zaslansky R, Schwenkglens M, et al. 2013. Patients' perception of postoperative pain management: validation of the International Pain Outcomes (IPO) questionnaire. *J. Pain* 14(11):1361–70 Available from: <http://www.ncbi.nlm.nih.gov/pubmed/24021577>.
483. Kirshblum SC, Waring W, Biering-Sorensen F, et al. 2011. Reference for the 2011 revision of the International Standards for Neurological Classification of Spinal Cord Injury. *J. Spinal Cord Med.* 34(6):547–554.
484. Bell RF, Kalso EA. 2018. Ketamine for pain management. *PAIN Reports* 3(5):e674 Available from: <https://journals.lww.com/01938936-201810000-00007>.
485. Scholz A, Vogel W. 2000. Tetrodotoxin-resistant action potentials in dorsal root ganglion neurons are blocked by local anesthetics. *Pain* 89(1):47–52 Available from: <http://www.ncbi.nlm.nih.gov/pubmed/11113292>.
486. Scholz A, Kuboyama N, Hempelmann G, Vogel W. 1998. Complex blockade of TTX-resistant Na<sup>+</sup> currents by lidocaine and bupivacaine reduce firing frequency in DRG neurons. *J. Neurophysiol.* 79(4):1746–54 Available from: <http://www.ncbi.nlm.nih.gov/pubmed/9535944>.
487. Garreau de Loubresse C. 2014. Neurological risks in scheduled spinal surgery. *Orthop. Traumatol. Surg. Res.* 100(1):S85–S90 Available from: <https://linkinghub.elsevier.com/retrieve/pii/S1877056813002570>.
488. Polley LS, Columb MO, Naughton NN, et al. 2003. Relative analgesic potencies of levobupivacaine and ropivacaine for epidural analgesia in labor. *Anesthesiology* 99(6):1354–1358.
489. Dragoo JL, Braun HJ, Kim HJ, et al. 2012. The in vitro chondrotoxicity of single-dose local anesthetics. *Am. J. Sports Med.* 40(4):794–799.

490. Malda J, Groll J, van Weeren PR. 2019. Rethinking articular cartilage regeneration based on a 250-year-old statement. *Nat. Rev. Rheumatol.* 15(10):571–572 Available from: <http://www.ncbi.nlm.nih.gov/pubmed/31367006>.
491. Steinert AF, Ghivizzani SC, Rethwilm A, et al. 2007. Major biological obstacles for persistent cell-based regeneration of articular cartilage. *Arthritis Res. Ther.* 9(3):213 Available from: <http://www.ncbi.nlm.nih.gov/pubmed/17561986>.
492. LACASSIE H, HABIB A, LACASSIE H, COLUMB M. 2007. Motor Blocking Minimum Local Anesthetic Concentrations of Bupivacaine, Levobupivacaine, and Ropivacaine in Labor. *Reg. Anesth. Pain Med.* 32(4):323–329 Available from: <https://rapm.bmj.com/lookup/doi/10.1016/j.rapm.2007.05.003>.
493. Castillo J, Curley J, Hotz J, et al. 1996. Glucocorticoids prolong rat sciatic nerve blockade in vivo from bupivacaine microspheres. *Anesthesiology* 85(5):1157–66 Available from: <http://www.ncbi.nlm.nih.gov/pubmed/8916834>.
494. Kost B, Brzeziński M, Socka M, et al. 2020. Biocompatible Polymers Combined with Cyclodextrins: Fascinating Materials for Drug Delivery Applications. *Molecules* 25(15):3404 Available from: <https://www.mdpi.com/1420-3049/25/15/3404>.
495. Chimene D, Kaunas R, Gaharwar AK. 2020. Hydrogel Bioink Reinforcement for Additive Manufacturing: A Focused Review of Emerging Strategies. *Adv. Mater.* 32(1):1902026 Available from: <https://onlinelibrary.wiley.com/doi/10.1002/adma.201902026>.
496. Nanocomposix. 2022. Molecular Weight to Size Calculator. [cited 2022 Jul 27] Available from: <https://nanocomposix.com/pages/molecular-weight-to-size-calculator#target>.
497. Foley PL, Ulery BD, Kan HM, et al. 2013. A chitosan thermogel for delivery of ropivacaine in regional musculoskeletal anesthesia. *Biomaterials* 34(10):2539–46 Available from: <http://www.ncbi.nlm.nih.gov/pubmed/23321347>.
498. Bigeleisen PE, Wempe M. 2001. Identification of the precipitate in alkalized solutions of mepivacaine and bupivacaine at 37 oC. *J. Clin. Pharm. Ther.* 26(3):171–173 Available from: <http://doi.wiley.com/10.1046/j.1365-2710.2001.00339.x>.
499. Cardot J-M, Beyssac E, Alric M. 2007. In Vitro–In Vivo Correlation: Importance of Dissolution in IVIVC. *Dissolution Technol.* 14(1):15–19 Available from: [http://www.dissolutiontech.com/DTresour/200702Articles/DT200702\\_A02.pdf](http://www.dissolutiontech.com/DTresour/200702Articles/DT200702_A02.pdf).
500. Lu Y, Kim S, Park K. 2011. In vitro-in vivo correlation: perspectives on model development. *Int. J. Pharm.* 418(1):142–8.
501. Shen J, Burgess DJ. 2015. In vitro–in vivo correlation for complex non-oral drug products: Where do we stand? *J. Control. Release* 219:644–651 Available from: <https://linkinghub.elsevier.com/retrieve/pii/S0168365915301528>.
502. US FDA. 1997. Guidance for Industry: Extended Release Oral Dosage Forms: Development, Evaluation, and Application of In Vitro In Vivo Correlations.
503. Zou H, Banerjee P, Leung SSY, Yan X. 2020. Application of Pharmacokinetic-Pharmacodynamic Modeling in Drug Delivery: Development and Challenges. *Front. Pharmacol.* 11 Available from: <https://www.frontiersin.org/article/10.3389/fphar.2020.00997/full>.
504. Ozeki M, Tabata Y. 2005. In vivo degradability of hydrogels prepared from different gelatins by various cross-linking methods. *J. Biomater. Sci. Polym. Ed.* 16(5):549–561 Available from: <https://www.tandfonline.com/doi/full/10.1163/1568562053783731>.
505. Box GEP. 1979. Robustness in the Strategy of Scientific Model Building. In: *Robustness in Statistics*. Elsevier. p 201–236 Available from: <https://linkinghub.elsevier.com/retrieve/pii/B9780124381506500182>.
506. Lr B, Cn M, Rj S, et al. 2017. The pH of wounds during healing and infection : A descriptive literature review. *Wound Pract. Res. J. Aust. Wound Manag. Assoc.* 25(2):63–69.
507. Metcalf DG, Haalboom M, Bowler PG, et al. 2019. Elevated wound fluid pH correlates with increased risk of wound infection. *Wound Med.* 26(1):100166 Available from: <https://linkinghub.elsevier.com/retrieve/pii/S2213909519300217>.
508. Wall PD. 1979. On the relation of injury to pain. The John J. Bonica lecture. *Pain* 6(3):253–264 Available from: <http://www.ncbi.nlm.nih.gov/pubmed/460933>.
509. Loeser JD, Melzack R. 1999. Pain: an overview. *Lancet* 353(9164):1607–1609 Available from: <https://linkinghub.elsevier.com/retrieve/pii/S0140673699013112>.
510. Gilron I, Carr DB, Desjardins PJ, Kehlet H. 2019. Current methods and challenges for acute pain clinical trials. *PAIN Reports* 4(3):e647 Available from: <https://journals.lww.com/01938936-201906000-00035>.





List of Publications, Manuscripts,  
Acknowledgements and Curriculum Vitae

## LIST OF PUBLICATIONS AND MANUSCRIPTS

This thesis is based upon the following publications and manuscripts:

Oostinga D, **Steverink JG**, van Dijk JFM, van Wijck AJM, Verlaan JJ. Balancing postoperative pain relief with the risk of developing ORADEs in patients undergoing major spine surgery. *Submitted*.

**Steverink JG**, Oostinga D, van Tol FR, van Rijen MHP, Mackaaij C, Verlinde-Schellekens SAMW, Oosterman BJ, Van Wijck AJM, Roeling TAP, Verlaan JJ. Sensory Innervation of Human Bone: An Immunohistochemical Study to Further Understand Bone Pain. *J Pain*. 2021 Nov;22(11):1385-1395.

Oostinga D, **Steverink JG**, van Wijck AJM, Verlaan JJ. An understanding of bone pain: A narrative review. *Bone*. 2020 May;134:115272.

**Steverink JG**, Piluso S, Malda J, Verlaan JJ. Comparison of *in vitro* and *in vivo* Toxicity of Bupivacaine in Musculoskeletal Applications. *Front Pain Res (Lausanne)*. 2021 Aug 20;2:723883.

**Steverink JG**, van Tol FR, Bruins S, Smorenburg AJ, Tryfonidou MA, Oosterman BJ, van Dijk MR, Malda J, Verlaan JJ. Lack of concentration-dependent local toxicity of highly concentrated (5%) versus conventional 0.5% bupivacaine following musculoskeletal surgery in a rat model. *J Exp Orthop*, 2023, in press.

**Steverink JG**, van Tol FR, Oosterman BJ, Vermonden T, Verlaan JJ, Malda J, Piluso S. Robust gelatin hydrogels for local sustained release of bupivacaine following spinal surgery. *Acta Biomater*. 2022 Jul 1;146:145-158.

**Steverink JG**, van Tol FR, Bruins S, Amponsah KB, Marvela J, Smorenburg AJ, Jonkman HR, Oosterman BJ, van Dijk MR, Malda J, Piluso S, Verlaan JJ. Testing a new sustained-release local anesthetic formulation specifically designed for spine surgery in a sheep model. *Submitted*.

**Steverink JG**, Bruins S, van Tol FR, Jonkman HR, Amponsah KB, Marvela J, de Vries AM, Smorenburg AJ, Oosterman BJ, Piluso S, Verlaan JJ. Preclinical safety and feasibility of a bupivacaine-loaded hydrogel for drug delivery in spinal surgery. *In preparation*.

Not included in this thesis:

**Steuerink JG**, Willems SM, Philippens MEP, Kasperts N, Eppinga WSC, Versteeg AL, van der Velden JM, Faruqi S, Sahgal A, Verlaan JJ. Early Tissue Effects of Stereotactic Body Radiation Therapy for Spinal Metastases. *Int J Radiat Oncol Biol Phys.* 2018 Apr 1;100(5):1254-1258.

**Steuerink JG**, Wisse RPL. Intraoperative optical coherence tomography in descemet stripping automated endothelial keratoplasty: pilot experiences. *Int Ophthalmol.* 2017 Aug;37(4):939-944.

## ACKNOWLEDGEMENTS - DANKWOORD

Promoveren is een teamsport, en de leden van dat team hebben dit traject een onvergetelijke en leerzame ervaring gemaakt.

Prof. Dr. Ir. Malda, beste Jos, bedankt voor je begeleiding van mijn promotietraject en het opnemen in je Biofab group, ook al voldeed mijn traject niet helemaal aan kraakbeen en bioprinten. Ik heb veel geleerd van je open blik en kritische houding, en het zien van mogelijke nieuwe onderzoeksrichtingen of samenwerkingen. Die kritische blik heeft zeker gezorgd voor een hogere wetenschappelijke kwaliteit van de studies. Fijn ook dat je de academische voortgang in het oog hield. Ik bewonder hoe jij ondanks je grote onderzoeksgroep de tijd vindt voor het begeleiden van al je PhD's.

Prof. Dr. Verlaan, beste Jorrit-Jan, zo'n 5 jaar geleden stuurde je een mysterieus mailtje of ik eens wilde 'komen praten'. Wie had durven denken dat het hiertoe zou leiden. Dank voor de kans die jij me hebt gegeven op dit promotietraject buiten de gebaande paden. Ik heb veel van je geleerd qua creativiteit, klinische relevantie van labonderzoek en besluitvorming. En dan laat ik diverse tegelwijsheden over vingers in dijken of nimmer bange chirurgen en kennis over obscure jaren-80 hits nog buiten beschouwing. *Shoot it up.*

Dr. Piluso, dear Susanna, *grazie* for taking the chance of supervising a lab novice. When I started in the lab, I had never seen a hydrogel, nor held a pipette. Under your supervision, it was easy to become accustomed to the daily business in the lab. Our two-weekly meetings were very helpful to maintain momentum in working towards this thesis. As a bonus, I learned a lot on the *dos and don'ts* of Italian culture and cuisine. I am glad our collaboration continues at SentryX.

Dr. Oosterman, beste Bas, samen met Jorrit-Jan gaf jij me de kans om bij SentryX te beginnen. Ik bewonder hoe jij binnen enkele vragen tot de kern van elk probleem kan komen en het probleem vervolgens helder en bondig weet te formuleren. Inspirerend om te zien hoe jij en Jorrit-Jan ondanks alle *unknown unknowns* SentryX vooruit leiden en daarbij de balans vinden tussen wetenschap, funding en het menselijk aspect.

Geachte leden van de leescommissie, Prof. Dr. M.R. van Dijk, Prof. Dr. P. Robe, Prof. Dr. A. Dahan, Prof. Dr. R. Schiffelers en Prof. Dr. F.C. Öner, hartelijk dank voor het lezen en beoordelen van mijn proefschrift.

Aan alle co-auteurs, dank voor jullie tijd en bijdrage aan dit proefschrift. Douwe, dank voor de fijne samenwerking. Jouw werklust heeft een flinke bijdrage geleverd aan dit proefschrift, en ik ben blij dat je een fijne plek in Nijmegen hebt gevonden. GDL: afdeling Klein (Trudy en Anja) én Groot (Koen, Helma, Hester, Tamara, Nico, Jeroen en Evelien), veel dank voor jullie ondersteuning bij de dierproeven en het pampieren van onze eerste wollige patiënten.

Collega's van de orthopedie (in het bijzonder labmaatjes Margot, Margo, Mattie en Jasmijn, en van Q Anneli, Bas, Bruce, Casper, Chella, Chien, Erin, Floris, Jelle, Joëll, Jonneke, Justin, Koen, Lorenzo, Rob, Steven, WP), dank voor alle gezelligheid, borrels, bruin fruit, onvergetelijke congresbezoeken, orthoski's, Oktoberfests en natuurlijk de 24 uur in Keulen, ondanks mijn mysterieuze baan bij 'the X'. Dear Biofabulous, thank you for letting me be part of your group and activities.

Collega's van SentryX (Alain, Andre, Anne-Mare, Carlijne, Danni, Floris, Frances, Hein, Jessica, Kwame, Rana, Roos, Susanna en Suzanne), dank voor de fijne samenwerking en gezamenlijke drive om een zo goed mogelijke pijnstillers neer te zetten die door alle regulatoire hoepels heen weet te springen. Dank ook voor de gezelligheid, pingpong lunches en leuke team-uitjes.

Diesty Boys / Dukes of Hasselt Floris en Hein, super dat jullie mijn paranimfen willen zijn. Met jullie valt er altijd wel wat te lachen, we delen het enthousiasme voor nerd-achtige zaken (method of cylindrical shells, modelleren, R-code) en bijna niks is te gek (Foute Uur non-stop, semi-spontane deelname Egmond, gewoon twee smoskes crusty boulette p.p., Dikke Duvel Donderdag). Ik ben benieuwd naar jullie eigen promotie!

Lieve vrienden, dank voor de interesse in en afleiding tijdens dit promotietraject, maar vooral voor de oprechte en ongecompliceerde vriendschap. Of het nou een etentje, borrel, spelletje, fietstocht, feestje, weekend weg (met sportieve nadruk of juist niet) of telefoontje is, door de gegarandeerde gezelligheid kijk ik altijd alweer uit naar de volgende. Surfboyz en -Girlz + aanstaande uitbreiding, omdat het altijd goed zit. Heeren 1, omdat het dak er sowieso vanaf gaat. MORAAAAL, met de ideale balans tussen in- en ontspanning. Dirk, Fabrice en Joep, voor gekke fietsplannen en het vaste piekmoment in het voorjaar. Arjan, Diederik, Kevin en Klaske, voor de sociale ladder en de Top-2000. LIC, voor de potjes Carcassonja. Huize Homerusbewoners, voor de fijne tijd daar.

Lieve schoonfamilie (met ongewoon hoog percentage Dr.), dank voor de altijd warme ontvangst en interesse in mijn onderzoek en andere bezigheden. Ik geniet van jullie nieuwsgierige houding en onze theoretische discussies over de ideale onderzoeksopzet om de meest alledaagse fenomenen eens kritisch te bestuderen inclusief analyse in programmeertaal naar keuze, maar ook van blokkentorens bouwen met Liam. Na vandaag wéér een Dr. erbij.

Lieve familie, bedankt voor jullie steun en geduld in met name het eerste jaar, toen alles nog een beetje geheimzinnig was. Inmiddels zijn jullie goed op de hoogte, en door alle kritische vragen op verjaardagen en aan de eettafel kon ik mooi al voorbereiden op mijn verdediging. Lieve Niels en Anne Fleur, dank voor een vriendschap met levenslange garantie, en fijn dat de lijntjes zo kort zijn. Lieve pa en ma, dank voor jullie ondersteuning, adviezen, vrijheid om mijn eigen keuzes te maken en doorgeven van jullie kritische blik. Het eindresultaat van mijn promotietraject is denk ik een product van jullie gecombineerde sterke punten: analytisch waar het moet en creatief waar het kan.

Lieve Lisa, dank voor je onvoorwaardelijke steun en liefde. Door toeval op dezelfde verdieping van het RMCU terecht gekomen. Binnenkort ga je promoveren op een prachtig proefschrift over organoids binnen taaislijmziekte, en ik ben hartstikke trots op je! Fijn om elkaars bezigheden zo goed te begrijpen, zonder dat dit ten koste van de romantiek gaat. Je bent mijn maatje in alles wat ik belangrijk vind. Ik kijk er enorm naar uit om samen te ontdekken wat de toekomst ons brengt.

## CURRICULUM VITAE

Jasper Gerard Steverink was born in Zwijndrecht, the Netherlands on the 26<sup>th</sup> of October 1993. After graduating high school in 2011 (Johan de Witt-gymnasium, Dordrecht) with distinction, he studied medicine at Utrecht University in the Netherlands. Jasper performed his pediatric rotation in Tygerberg Hospital, Cape Town, South Africa. During his study and rotations, he became interested in orthopedic surgery, leading to extracurricular research on patient-reported outcomes after meniscus surgery at the department of Orthopedic Surgery in the University Medical Center Utrecht (UMCU).



In his last year of medical school, he did a research internship under supervision of Dr. J.J. Verlaan on the early tissue effects of stereotactic irradiation of vertebral metastases. The study was awarded the Prof. Dr. Ir. Rik Huiskes award for best fundamental orthopedic research at the Dutch Orthopedic Society (NOV) annual meeting in 2018. In addition, he performed his senior clinical rotation at the department of Orthopedic Surgery, UMCU, under supervision of Dr. J.J. Verlaan. Jasper temporarily paused his final year of medical school to coordinate the orthopedic track of the Selective Utrecht Medical Master (SUMMA).

After graduation in April 2018, he started his PhD project at both SentryX B.V. and the department of Orthopedic Surgery, UMCU, under supervision of Prof. Dr. Ir. J. Malda, Prof. Dr. J.J. Verlaan and Dr. S. Piluso. The main goals of the project were to better understand pain after skeletal surgery and the development of a non-opioid bupivacaine sustained release formulation for use in spine surgery. This research resulted in several oral presentations at international conferences and collaboration with a broad spectrum of experts, including chemists, biologists, orthopedic surgeons, pathologists and pharmacologists. Following the completion of his PhD thesis in 2023, Jasper continues to work on the development and clinical translation of opioid-free pain treatment after skeletal surgery.

